Safety in Mines Research Advisory Committee

Final Project Report

The impact of soft loading conditions on the performance of elongate support elements

A. Daehnke, B.P. Watson, D. Roberts,
E. Acheampong and M. van Zyl

Research Agency: **CSIR: Division of Mining Technology**
Project Number: **GAP 613**
Date: **March 2000**

Executive Summary

Rock mass instabilities represent the single largest cause of injuries and fatalities suffered by the workforce in South African gold and platinum mines. Stope support systems, which typically consist of elongates and packs, are used to stabilise the rock mass surrounding the mining excavations and reduce the risk of rockfalls.

In a discontinuous, jointed rock mass, loose blocks can, under certain conditions, rotate and move obliquely, thereby subjecting elongate support elements to different loading conditions than those experienced under conventional axial loading. Since many panels of Bushveld and shallow gold mines are supported by elongates only, it is vital to understand and quantify the elongate interaction with rotating and obliquely moving blocks of rock. An assessment is required to determine if elongates are suitable and the optimum support type to stabilise such unstable blocks.

This project investigates the mechanisms of the rotation and oblique movement of blocks, and analyses the capabilities of elongates to support such unstable blocks. To this end, theoretical, laboratory and underground studies are conducted to ensure meaningful and practically relevant insights and solutions.

It was found that the most significant factor contributing to failure of support units by rotation of keyblocks is the support spacing. The reason for this is that the centroid of the potentially rotating block and the resultant reaction force from the support units are brought closer together by increasing the support density (i.e. reducing the support spacing). The probability of blocks failing by rotating out of the hangingwall of a stope depends on the shape of the block. Blocks with shallow dipping sides rotate more readily than blocks with steeply dipping sides. An important output of the project is a computer program to quantify optimum support spacing in geotechnical areas where keyblock rotation is likely.

A laboratory press was modified to simulate the loading conditions induced by rotating and obliquely moving blocks. The press was used to investigate and quantify the performance characteristics of mine poles and Profile Props subjected to non-axial loading. It was found that installing elongates at an oblique angle to the loading surface has little effect on the elongate performance. A modified (empirically based) relationship is proposed to determine the anticipated underground mine pole performance from the performance of mine poles quantified by means of laboratory compression tests. The relationship downgrades the laboratory curves in terms of (i) initial mine pole stiffness, and (ii) peak mine pole load.

The work conducted as part of this project has led to the conclusion that, in general, elongate support is considered suitable for use in Bushveld and shallow gold mines. To ensure rock mass stability, however, the rock engineer needs to determine if block rotation is likely (guidelines for determining if block rotation is possible are given in the report). If block rotation is likely, the tributary area design methodology needs to be modified and the software developed as part of this project should be used to optimise support spacing. Furthermore, if block rotation is likely, the elongates should always be pre-stressed (preferably to 200 kN). If block rotation is kinematically impossible, the standard tributary area method for support design is appropriate.

In geotechnical areas where the hangingwall is intensely jointed (i.e. between one and three support units per block), mine poles with a diameter of at least 170 mm should be used. A

comparatively continuous hangingwall can be supported by mine poles with diameters of 140 mm – 170 mm.

Finally, a video was produced, giving details of the salient findings of the project. It is recommended to distribute the video to the relevant rock mechanics practitioners on the platinum mines to increase the awareness of the hazard and special support requirements associated with hangingwall keyblocks with a propensity for rotation and oblique movement.

Acknowledgements

Table of Contents

List of Figures

14

14

14

14

List of Tables

Glossary of Abbreviations and Terms

Abbreviations

SABS   South African Bureau of Standards

FOG   Fall Of Ground

SDA   Support Design Analysis

Symbols

r Distance between a fulcrum and a point (radius of a circle)

ε Enclosed angle

β Discontinuity angle

V_I, V_{II} Vertical components of shear resistance

W Weight of a keyblock

$SRSF$ Support resistance safety factors

SR_s Support resistance provided by support units

SR_r Support resistance required to hold a block

F_{req} Support force required to maintain equilibrium

l_1 Distance from the point of rotation

L Length of keyblock, Length of block

l_2 Length of lever-arm

F_{max} Maximum force transmitted by support unit

F Support force

l_{req} Length of lever-arm to ensure equilibrium

P Probability of location of force

f_1, f_2 Spacing between sets of fractures

A_b Base area of keyblock

l_{max} Maximum perpendicular distance of force from an edge

l_{rl}	Required lever-arm to prevent support from rotating
l	Lever-arm of weight about which rotation is possible
k	Factor of rotational increment
F_R	Resultant support force
d	Perpendicular distance between edge of keyblock and resultant support force
δ	Perpendicular distance between edge of keyblock and closest support unit
S	Support spacing
N	Number of support units per length of keyblock
n	Number of full spans between support units per length of keyblock, support units
d_{min}	Minimum lever-arm length of support force about the edge of a keyblock
α	Orientation of support system relative to keyblock.
M	Number of support units per keyblock
Δ	Distance through which a support is displaced
M_A, M_B	Bedding moments at a support
E	Elasticity modulus of timber
d	Diameter of beam
P	Axial load
ϕ	Resistance factor
γ_1	Partial material factor for moisture content
γ_2	Partial material factor for pressure treatment
L_e	Effective length of compression element
K	Effective length factor
r	Radius of gyration
λ_d	Slenderness of gyration
C_r	Maximum load carried by a compression member (axial capacity).
f_c	Characteristic compressive strength
γ_1, γ_2	Material factors
λ_{dcr}	Critical slenderness value

C_u	Applied axial load
M_u	Applied moment (bending moment generated by displacement/ride)
M_r	Moment resistance (bending capacity)
U_1	Moment magnification factor for a beam-column
W_a	Weight of material in beam per metre in the dip direction
b	Unit length of beam in strike direction
h	Height of beam, height of instability
$F_{u/g}$	Force corrected for underground loading rates
F_{lab}	Force obtained (e.g. from a laboratory test)
$v_{u/g}$	Underground closure velocity
v_{lab}	Laboratory test velocity
m	Empirical factor, slope of graph
μ	Mean value
σ	Standard deviation
y	Load value at displacement
I	Displacement interval
K_{su}	Overall stiffness of a support unit
K_m	Stiffness of a Minepole
K_p	Stiffness of a pre-stressing unit
K_c	Equivalent stiffness of an uneven hangingwall contact
K_f	Stiffness of a footwall
F	Load carried by a single support unit (N)
$W_{T.A.}$	Weight of hangingwall associated with a tributary area
ρ	Rock density (kg/m^3),
g	Acceleration due to gravity ($\approx$10 m/s^2)
A	Tributary area (m^2)

1   Introduction

1.1 Background

Rock mass instabilities represent the single largest cause of injuries and fatalities suffered by the workforce in South African platinum mines. Most of the rock related fatalities in platinum mines are associated with rockfalls. Stope support systems, which typically consist of elongates and packs, are used to stabilise the rock mass surrounding the mining excavations and reduce the risk of rockfalls.

The present support design methodology commonly applied in South African platinum mines is based upon the tributary area concept. Here a given weight of rock, determined by an area in the plane of the reef and the fall-out height, is divided by a fixed number of support units according to the attributable area. The area is determined by the face layout and the fall-out height is presumed to be known from previous observations. This simple concept takes care of the equilibrium requirements in a rudimentary sense, but it does not adequately address the fact that the rock being supported is likely to be discontinuous. Clearly, in these circumstances, the distribution of the support elements may be of paramount importance.

In a discontinuous, jointed rock mass, loose blocks can, under certain conditions, rotate and move obliquely, thereby subjecting elongate support elements to different loading conditions than those experienced under conventional axial loading. Since many panels of Bushveld and shallow gold mines are supported by elongates only, it is vital to understand and quantify the elongate interaction with rotating and obliquely moving blocks of rock. An assessment is required to determine if elongates are suitable and the optimum support type to stabilise such unstable blocks.

This project investigates the mechanisms of the rotation and oblique movement of blocks, and investigates the capabilities of elongates to support such unstable blocks. To this end, theoretical, laboratory and underground studies are conducted to ensure meaningful and practically relevant insights and solutions.

Analytical techniques are used to quantify the kinematics and degrees of freedom of a jointed rock mass. The two- and three-dimensional theoretical studies result in design charts, which, based upon the (i) *in situ* hangingwall stress, (ii) intersecting fracture and joint set angles and (iii) bedding heights, quantify the block geometry prone to rotation and/or oblique movement. The design charts are calibrated and verified by underground observations and measurements.

Further theoretical and underground studies give insights into the interaction of elongates with rotating and obliquely moving blocks. Case studies of actual collapses and back-analyses thereof are used to identify various elongate deformation and failure mechanisms (for example, buckling, toppling) related to geotechnical area, block geometry and block size.

Laboratory tests, using various elongate types and simulated loading conditions, which are induced by rotating and obliquely moving blocks, form an important part of the project. For this

purpose a special loading plate was constructed to simulate off-centre and lateral loading, as well as induce bending moments, which are induced by block rotation. CSIR loading presses are utilised in conjunction with the loading platen to quantify the elongate performance when loaded by rotating blocks. The work builds on expertise gained from GAP 330 (Stope Face Support Systems), where preliminary tests making use of stepped and inclined platens indicated the buckling potential of various elongates in use by the platinum mines. A major output of the work is a critical assessment of the suitability of elongates to support a discontinuous rock mass, where non-axial loading, block rotation and oblique movement are likely.

The new technology developed by this project is transferred to the industry by means of discussions with rock engineers from the platinum mining industry, seminars (SAIMM Industry Seminar, October 1999), a technical report supported by photographs of laboratory and underground tests, and a video showing outcomes of the elongate tests.

1.2 Scope of project

SIMRAC Project GAP 613, titled "*The impact of soft loading conditions on the performance of elongate support elements*", is managed and co-ordinated by the CSIR: Division of Mining Technology. The project provides a confirmation as to whether or not it is kinematically possible for jointed blocks to rotate or move obliquely downwards, and gives an assessment of the capability of elongates to support such unstable blocks and their suitability for use in most Bushveld mines.

Five enabling outputs (EOs) have contributed towards this objective. These were defined in the project proposal, and are addressed in the relevant sections of this report, as follows:

EO 1   Determine under which conditions it is kinematically possible for jointed blocks to rotate and move obliquely downwards.

(Addressed in Chapter 2 of this report)

Step 1.1   Using analytical and numerical methods, quantify the movement and degrees of freedom of jointed hangingwall blocks and the influence on the stability of standard and pre-stressed units.
(Addressed in Section 2.1)

Step 1.2   Using underground observations and investigations, quantify block rotation mechanisms taking into account relevant support criteria (for example, support position and spacing, support stiffness, support load resistance and pre-stressing).
(Addressed in Section 2.2)

EO 2 **Utilise CSIR loading presses to simulate loading conditions, which result from block rotation and oblique block movement.**

(Addressed in Chapter 3 of this report)

Step 2.1   Design and manufacture a loading device to simulate off-centre loading and bending moments induced by rotating and obliquely moving blocks.
(Addressed in Section 3.1)

Step 2.2   Utilise the loading device and CSIR loading presses to simulate loading conditions, which result from block rotation.
(Addressed in Section 3.2)

EO 3 **Test and evaluate various elongates with off-centre loading to simulate block rotation and oblique rock movement.**

(Addressed in Chapter 4 of this report)

Step 3.1   Conduct laboratory tests to evaluate various elongates loaded by rotating blocks and oblique block movement.
(Addressed in Sections 4.2 and 4.3)

Step 3.2   Compare test results to previous tests conducted as part of SIMRAC Project GAP 330 on elongates loaded in a conventional press (i.e. axial loading only).
(Addressed in Sections 4.4 and 4.5)

EO 4 **Evaluate the suitability of elongate support systems for use in Bushveld mines.**

(Addressed in Chapter 5 of this report)

Step 4.1   Assess the suitability of elongates to support a discontinuous rock mass where non-axial loading, block rotation and oblique movement are likely.
(Addressed in Sections 5.1 to 5.5)

EO 5 **Communicate test results and rotational/oblique movement of blocky rock masses by means of videos.**

(Addressed in Chapter 6 of this report)

Step 5.1   Visualise the interaction of elongate support with rotating and obliquely moving blocks by means of videos.
(Addressed in Sections 6.1 and 6.2)

It is emphasised that the research conducted as part of this project is particularly relevant to shallow gold and platinum mines, i.e. up to a mining depth of typically 1000 m. Most of the underground work reported here was conducted on platinum mines. The results are, however, equally applicable to shallow gold mines.

A final chapter synthesises the main outcomes and new knowledge gained, and makes recommendations for further research work. For a brief overview and summary of the principal findings of this project, it is recommended that the reader focus his/her attention on Chapters 5 and 7.

2 Analysis of keyblock kinematics in Bushveld mines

2.1 Introduction

Rock mass instabilities represent the single largest cause of injuries and fatalities suffered by the workforce in South African platinum mines. Most of the rock related fatalities in platinum mines are associated with rockfalls. Stope support systems, which usually consist of packs and props, are used to stabilise the rock mass surrounding the mining excavations and reduce the risk of rockfalls.

The present design methodology in South Africa is based upon the tributary area concept. Here a given weight of rock, determined by an area in the plane of the reef and the fall-out height, is divided by a fixed number of support units according to the attributable area. The area is determined by the face layout and the fall-out height is presumed to be known from previous observations. This simple concept takes care of the equilibrium requirements in a rudimentary sense, but it does not adequately address the fact that the rock being supported is likely to be fractured and jointed. Clearly, in these circumstances, the distribution of the support elements may be of paramount importance. Relatively little progress has been made in quantifying the effects of support spacing on the stability of the rock mass.

In a jointed rock mass, it is possible for loose blocks to rotate and slide obliquely, thereby subjecting elongate support elements to oblique (non-axial) loading. In many of the stopes in the Bushveld mines, elongates are the only means of support, and thus it is considered necessary to evaluate the potential for rotational failure.

The objectives of this chapter are to investigate the conditions under which it is kinematically possible for jointed blocks to rotate and move obliquely downwards. A theoretical investigation is presented to quantify the movement and degrees of freedom of jointed hangingwall blocks and determine the influence on stability of standard and pre-stressed units. This is followed by an underground study to determine under which conditions keyblock rotation is likely.

2.2 Theoretical evaluation of keyblock kinematics

Unstable blocks of rock in the hangingwall may be identified using the keyblock approach (Goodman & Shi, 1985). A keyblock is defined as a block of rock, bounded by discontinuities, which may be removed from the rock mass without interference from the surrounding rock. Keyblocks are typically the first rocks to fall from the hangingwall, allowing other non-keyblocks to follow. If keyblocks are held in position by support, failure of the hangingwall should not take place.

In this section, the results of a study of keyblock rotation (Esterhuizen, 1999) are presented. The objective of the study is to make use of the keyblock approach to assess the potential for keyblocks to rotate, and thus cause elongate support units to fail.

The program JBlock (Esterhuizen, 1996) is used to conduct the analyses. The program is able to evaluate the stability of individual blocks and support units. It is also able to generate many thousands of blocks, using the joint properties (length, spacing and orientation) in the hangingwall and testing each generated block for stability. The program was modified to evaluate potential edge rotation of keyblocks and to calculate the effect of block rotation on elongate stability.

A number of basic block shapes are analysed to determine their ability to rotate and their effect on support units. Furthermore, actual hangingwall jointing from three different Bushveld areas is modelled and checked for rotational failure. The results are presented below.

2.2.1 Failure of support units by keyblock rotation

Edge rotation of keyblocks is considered for the purposes of this study. If an excavation is over-hanging, such as a stope hangingwall, keyblock rotation is only possible if support forces, acting in the opposite direction, are present – otherwise the block would simply fall out. It is further assumed that if the block weight exceeds the capacity of the support, the support will fail anyway, and rotation is not evaluated.

Since rotation is only considered when the support capacity exceeds the weight of the block, the keyblock can only fail the support by the "leverage" provided by rotation. The leverage effect is calculated by comparing rotational moments about the pivot line of the block. The support fails if the downward rotational moment, which is due to the weight of the block, is greater than the upward moment provided by the support force. This is illustrated in Figure 2.2.1
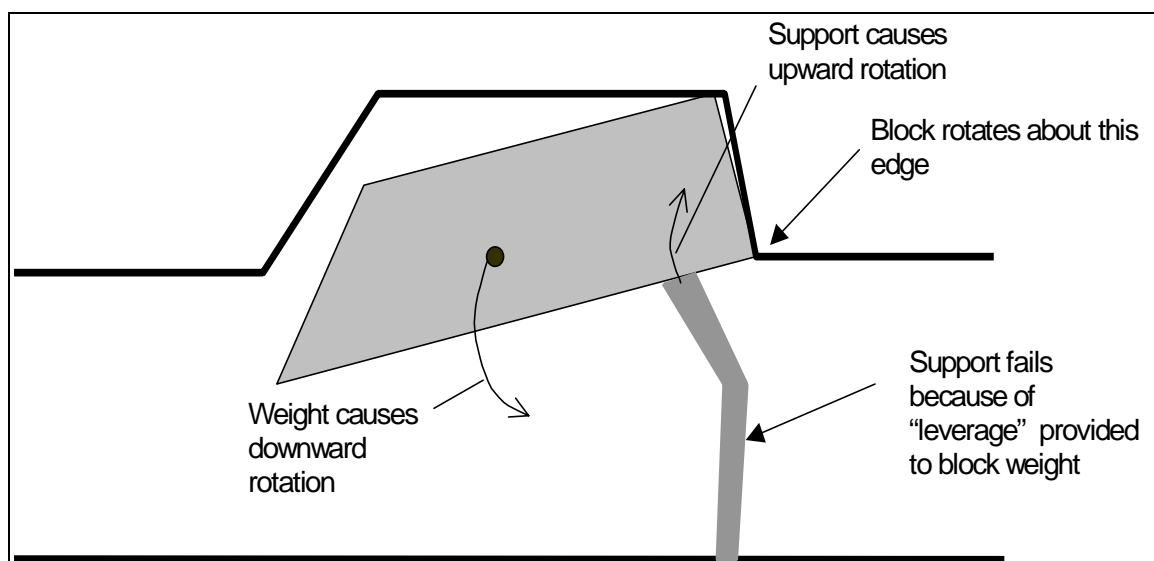
Figure 2.2.1   ***Rotational failure occurs when the block weight is less than the support capacity. The support is failed by the leverage of the weight when rotation occurs.***

2.2.2 Method of evaluating keyblock rotation

All keyblocks cannot necessarily rotate out of the surrounding rock mass. The possibility of a block rotating depends on the geometry of the block and the pivot point. In this discussion, the corners of a block, which are inside the rock mass, are called inner corners and the corners on the excavation surface are referred to as surface corners. In two dimensions, it is only possible for a keyblock to rotate if the radii, from the pivot point to the inner corners of the block, are shorter than the radius to the surface corner, as illustrated in Figure 2.2.2

Rotation about A is not possible because R_2 is greater than R_3

Rotation about B is possible because R_1 and R_2 are both shorter than R_3
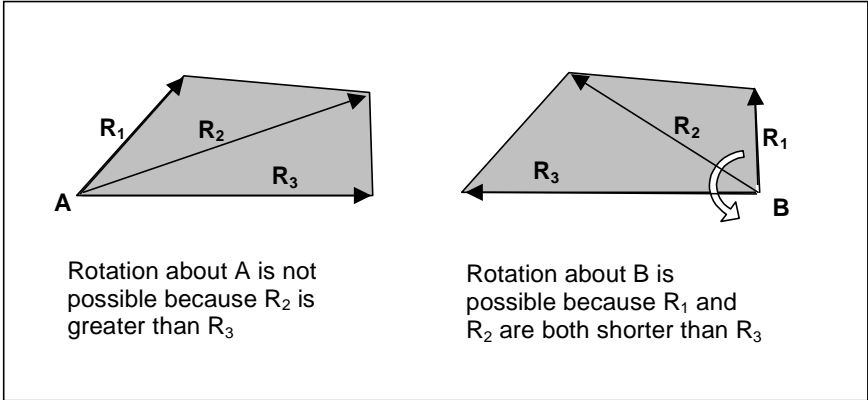
Figure 2.2.2   ***Criterion for checking the possibility of block rotation in two dimensions (after Esterhuizen, 1999).***

A more mathematical description of the criteria that prevent rotation follows. As an example, postulate that the block, if it rotates, will pivot around its furthermost hangingwall corner point on the left (see Figure 2.2.3). Let this point of fulcrum be A. Denote by r the distance between the fulcrum and point B, the furthest point on the right of the top plane of the block. Rotation can occur only if point B can move past the next block to the right.

Let C be the point where the fracture at the right end of the block intersects the hangingwall. Clearly, the limiting geometry is when the block can start to pivot around its fulcrum, that is, around point A. This can occur when the line $\overline{BC}$ (in section) is tangent to the circle of radius r with its centre at point A. If we denote the angle enclosed by lines $\overline{AC}$ and $\overline{AB}$ by ε, then this criterion is satisfied if $\varepsilon + \beta = \frac{1}{2}\pi$. Thus if $\varepsilon + \beta \leq \frac{1}{2}\pi$, the keyblock can rotate around its fulcrum and, if $\varepsilon + \beta > \frac{1}{2}\pi$, keyblock rotation is kinematically impossible.
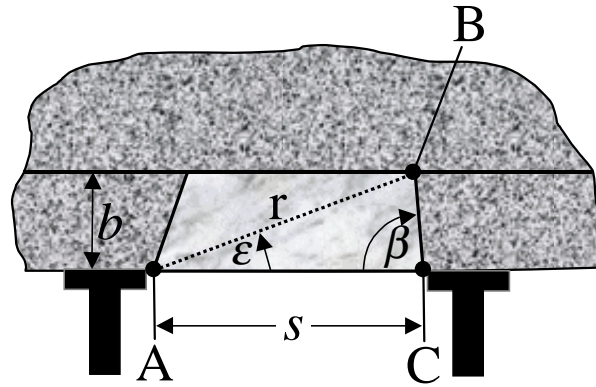
Figure 2.2.3   Geometry parameters governing the rotational stability of hangingwall blocks.

Now introduce the ratio $\kappa = b/s$. It is simple to show that

$$\varepsilon = \arctan\left(\frac{\kappa}{1 - \kappa \cot(\beta)}\right).$$

(2.2.1)

These two relationships are sufficient to obtain the following results:

$$\kappa(\beta) = \frac{1}{2}\sin(2\beta) \text{ or alternatively } \beta(\kappa) = \frac{1}{2}\arcsin(2\kappa).$$

(2.2.2)

The first of these relationships is depicted graphically in Figure 2.2.4. In this illustration, rotation is prevented for cases that fall above the curve, therefore, the block is *stable*. In instances that plot on or under the curve rotation can occur, and hence the block is *unstable*.

Since the value of the sine function does not exceed unity, it is obvious from the first of these expressions that instability cannot occur when $\kappa > \frac{1}{2}$ or $b > \frac{1}{2} s$.

It is evident from Figure 2.2.4 that $\kappa(\beta)$ is a double valued function. If we denote the two solutions by β_1 and β_2 ($0 < \beta_1 \leq \frac{\pi}{4}$ and $\frac{\pi}{4} \leq \beta_2 \leq \frac{\pi}{2}$), the stability conditions concerning the block can be summarised as follows:

Stable: a) If $\kappa \leq \frac{1}{2}$ and $\beta < \beta_1$ or $\beta > \beta_2$

b) If $\kappa > \frac{1}{2}$

(2.2.3)

Unstable: If $\kappa \leq \frac{1}{2}$ and $\beta_1 \leq \beta \leq \beta_2$

77
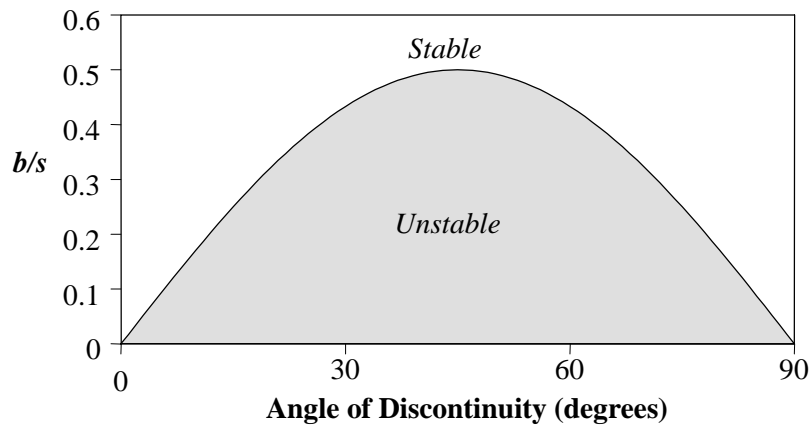
***Figure 2.2.4   Stability envelopes characterised by the ratio of b over s versus
discontinuity angle (the angle of discontinuity is taken opposite
the potential pivot point).***
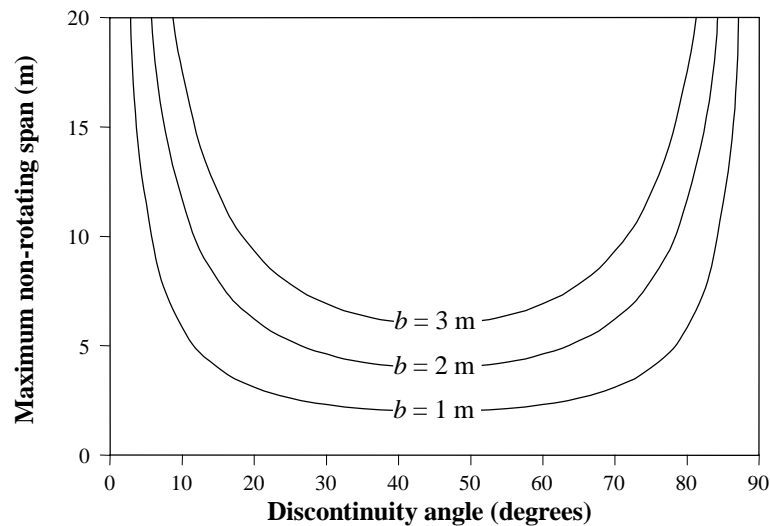
Figure 2.2.5   Upper limit of stable spans (based on Equations 2.2.1 and 2.2.2).

It is obvious from Figure 2.2.5 that the upper bound of the span that will not rotate increases (for a fixed beam thickness) as the value of angle β (or α) departs, up or down, from 45 degrees. It is also noteworthy that for situations where the thickness b is greater than 2 m, rotation is unlikely to cause instability in the hangingwall.

The above discussion is valid for keyblocks having a geometry as shown in Figure 2.2.3. For certain keyblocks delineated by shallow dipping discontinuities and/or small spans, however, the geometry could be of the form shown in Figure 2.2.6. In this case keyblock rotation is kinematically impossible if $\alpha + \beta > \frac{1}{2}\pi$.

77
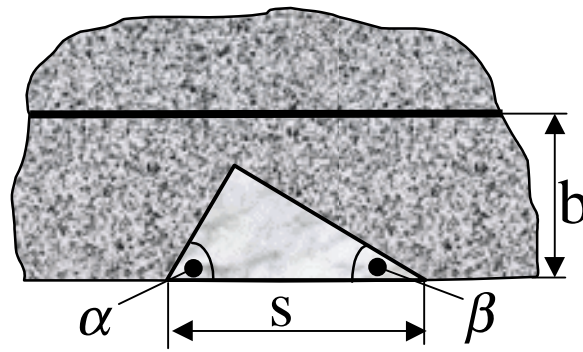
Figure 2.2.6   Keyblock geometry delineated by shallow dipping discontinuities and/or small spans.

An interesting case occurs when all fractures are parallel. Postulate that the face is on the left-hand side. In this case $\alpha = \pi - \beta$ and the expression for the vertical component of the shear resistance on the left becomes:

$$V_I = \sigma_x b \cot(\beta - \varphi),$$ (2.2.4)

(note the change in sign) and φ is the friction angle. The formula for V_{II} (for the right-hand-side fracture) remains unaltered. This expression remains positive as long as

$$\varphi < \beta < \tfrac{1}{2}\pi + \varphi.$$ (2.2.5)

It is obvious from these expressions that $V_I > V_{II}$ as long as $\beta > \varphi$. Since this criterion is almost always satisfied in practice, it can be concluded that this block is unconditionally stable in most cases, provided $V_{II} > \tfrac{1}{2}W$, where W is the block weight.

In three dimensions a similar method is followed. Each surface edge of a keyblock is considered as a possible candidate for rotation. Planes are constructed perpendicular to the edge of rotation through each inner corner of the block. Each plane represents a two dimensional section through the block. Each section is tested for rotation, using the two-dimensional test. If all the sections pass the test, the block is able to rotate about that edge. The principle is illustrated in Figure 2.2.7, where a section through one of the inner corners is shown.
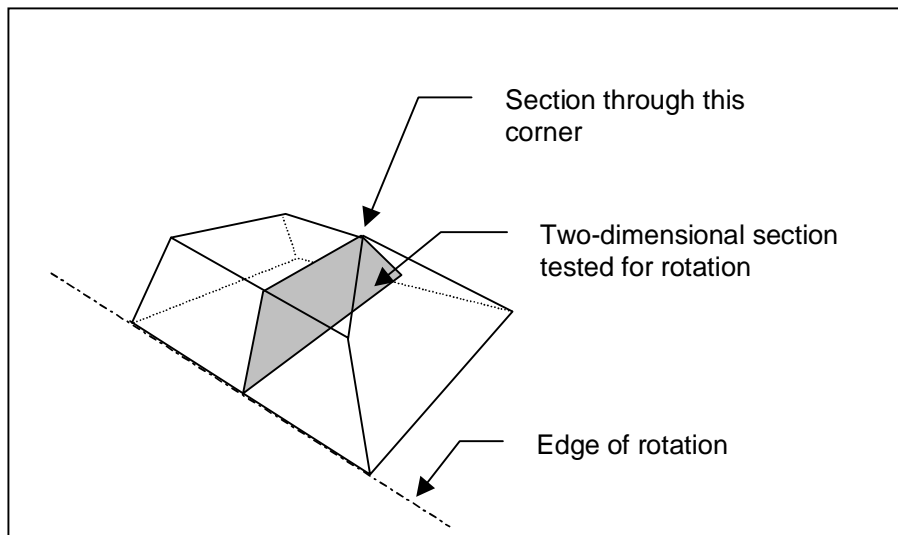
Figure 2.2.7   Sketch showing principle of testing for rotation about an edge.

2.2.3 Method of evaluating support failure by rotation

The principle of support failure by rotation has been presented briefly in Section 2.2. The method of calculation is as follows:

(i)   Find the centroid of the keyblock:

- Triangulate the keyblock into a number of tetrahedra and find the centroid of each.

- Find the weighted centroid of the tetrahedra.

(ii)   The moment arm of the weight is determined as the perpendicular distance between the weight vector and the edge of rotation (assume that the weight of the block works through the centroid of the keyblock).

(iii)   The centroid of the support forces is determined and the moment arm is similarly calculated.

(iv)   Do a simple moment calculation to determine in which direction the keyblock will rotate under the influence of its weight and the support forces.

(v)   If the rotation is downwards, the support unit is assumed to fail.

(vi)   If the rotation is upwards, the support forces hold the block in position.

The method is schematically illustrated in Figure 2.2.8.
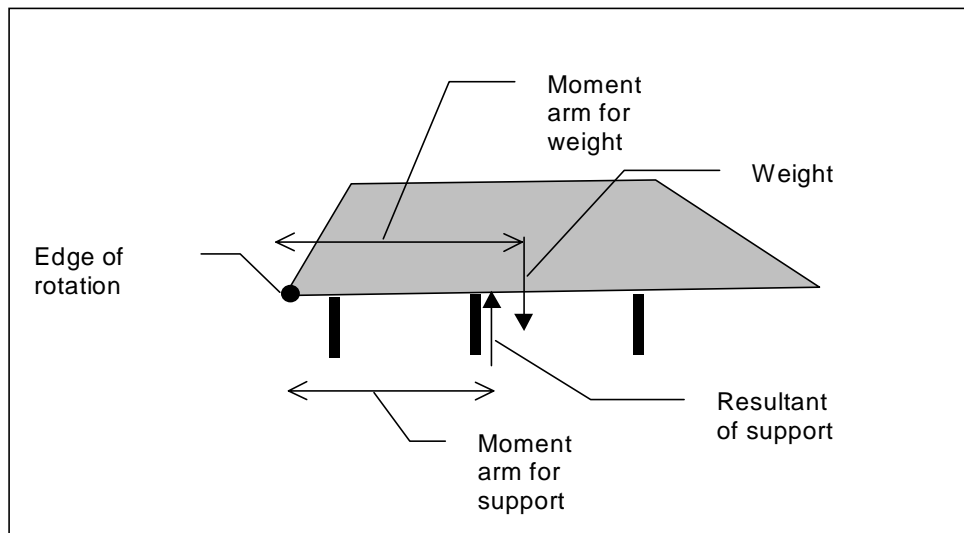
Figure 2.2.8   Schematic illustrating the calculation procedure (after Esterhuizen, 1999).

2.2.4 Analysis of basic block types

The initial part of the study is aimed at understanding the potential for rotation of a number of basic block shapes. Variations of a pyramid shaped block are selected. The shapes are illustrated in Figure 2.2.9, where it can be seen that the blocks have different degrees of freedom for rotation. Block A has three steep edges and can only rotate about the edge marked with an arrow. Similarly, Block B can only rotate about the two marked edges, and so on.
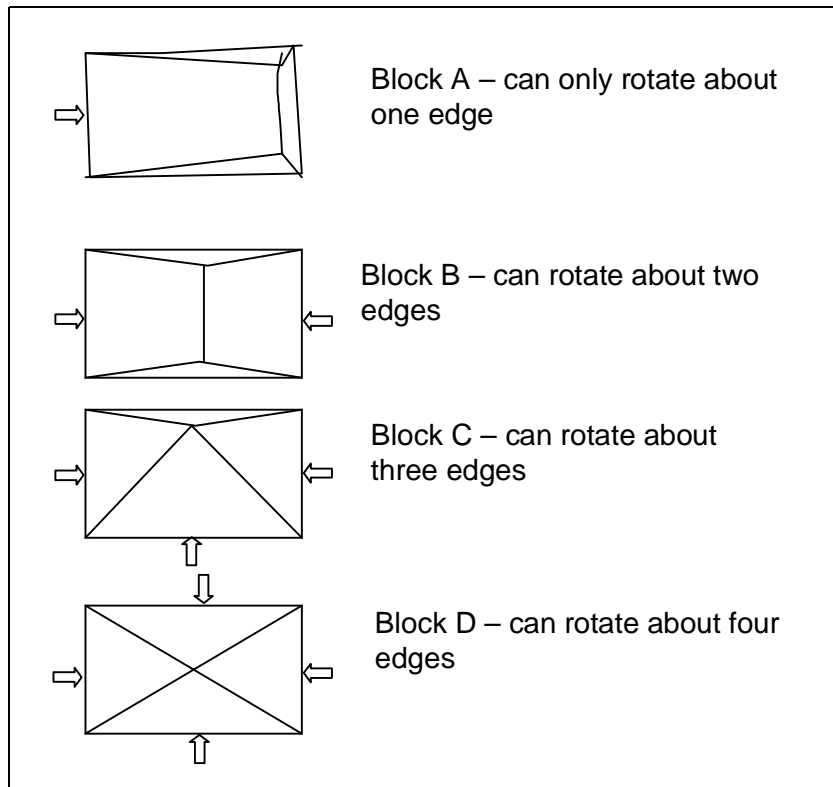
Figure 2.2.9   Plan views of basic block shapes.

2.2.5 Effect of support capacity on rotational failure probability

It is now necessary to determine how the block weight to support capacity ratio affects the rotational potential of the different block shapes. Analyses were conducted in which one thousand of each block type were randomly placed over a single elongate support unit. The blocks all had hangingwall surface areas (face areas) of 2 m x 1 m. The potential for rotation about each edge of the block was tested. The support capacity was increased from 1,1 times the block weight to five times the block weight. The results are summarised in Figure 2.2.10, which shows that the probability of rotational failure is significantly different for the different block shapes. As the support capacity increases, the potential for rotational failure decreases rapidly. However, even when the support capacity is five times the block weight, the probability of rotational failure is between 10 and 30 percent for the different block shapes. If the support capacity exceeds the block weight by a factor of two (factor of safety of 2,0), the probability of rotational failure could be as high as 80 percent.

Note that the above results were obtained for a single support unit. The next step was to use the same block shapes, but use an array of support units. The support units were placed in a square pattern at different distances apart, ranging from 0,9 m x 0,9 m to 3 m x 3 m. The blocks all had face dimensions of 2 m by 1 m so that with the 0,9 m spacing each block was supported by up to six support units. The blocks were again paced at random positions over the support array and tested for rotational failure. The results are presented in Figure 2.2.11, which shows that, when the support spacing is smaller than the block face dimensions, the rotational failure probability becomes very small. This is probably due to the fact that the resultant support force and the centroid of the block are closer to one another and the combined support capacity exceeds the block weight by a large factor.
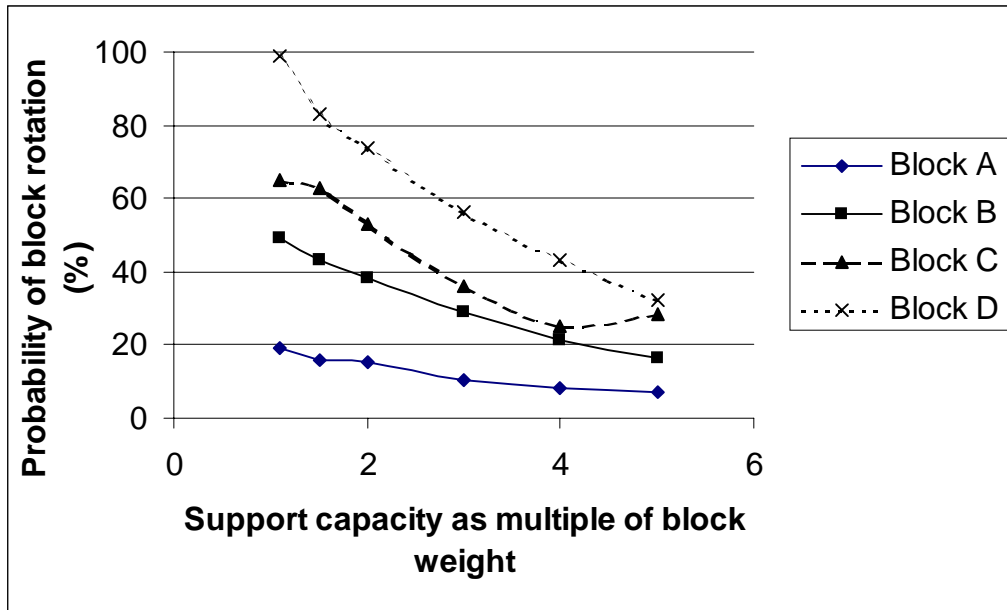
Figure 2.2.10   Effect of block type and support capacity on probability of rotational failure.
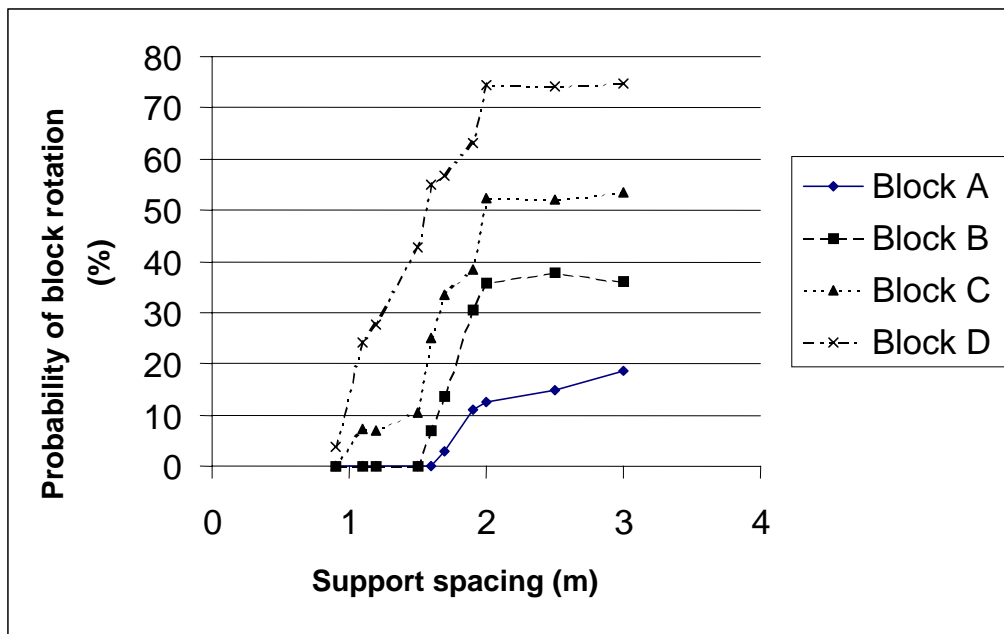
Figure 2.2.11   Effect of support spacing on failure probability of blocks, support capacity is twice the block weight, the block face is 2m x 1m.

When the support spacing is much larger than the block face dimensions, the failure probabilities revert to similar values as those obtained with a single support unit. However, in these runs the support resistance changed as the spacing was varied.

2.2.6 Effect of multiple support units on the probability of rotational failure

To further investigate the effect of rotational failure of blocks supported by multiple support units, a number of runs were set up in which the support resistance was modified. The blocks were made large, with face areas of 3 m x 5 m and the support spacing was kept at 1 m x 1 m. This meant that about 15 support units supported each keyblock. The support capacity was modified so that the support resistance varied between 1,1 and 1,6 times the required resistance to hold the block in position (carry the deadweight). The results, presented in Figure 2.2.12, show that if the support resistance is more than about 1,5 times the required resistance (i.e. a factor of safety of 1,5), keyblock rotation is no longer possible for the block shapes tested. This result is only valid if the keyblocks are supported by a large number of support units.

The practical effect of the above findings is that smaller keyblocks require a higher support resistance than large keyblocks to prevent rotational failure. In this context, small implies the face of the keyblock is in the same order as the support spacing and large means the face area of the block is several times the support spacing.
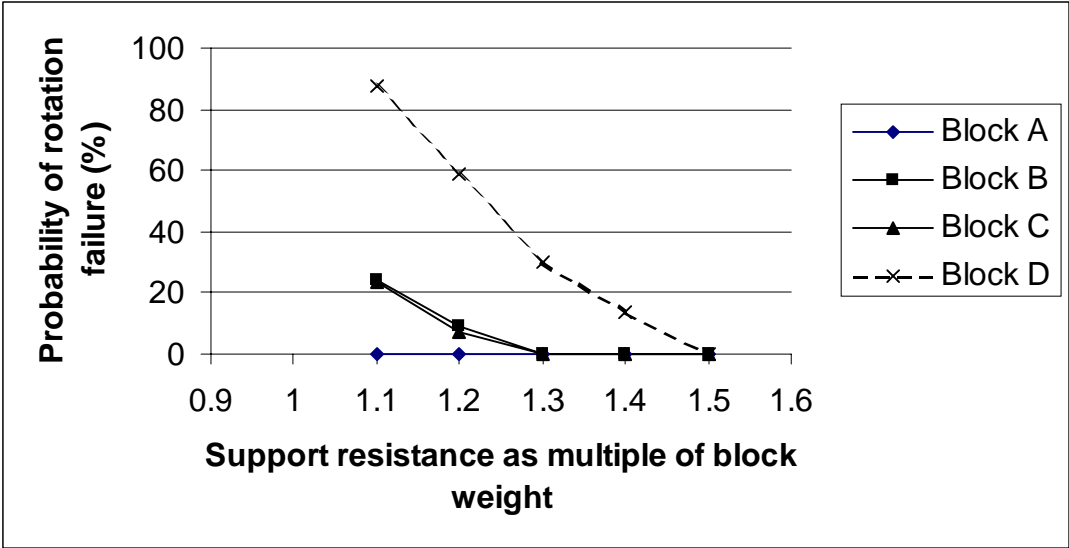
Figure 2.2.12   Effect of support resistance on rotational failure of large keyblocks, which are supported by multiple support units.

2.2.7 Failure modes for keyblocks

In a supported stope, a keyblock may fail by either:

- Dropping out between support units;
- Failing the support unit/s if the weight exceeds the support capacity;
- Failing a support unit by rotational leverage.

A number of analyses were carried out in which the failure modes of a keyblock with a face area of 1 m x 1 m were evaluated. In each case the support spacing was varied, and the support

77

resistance was varied to result in different support resistance safety factors ($SRSF$). The $SRSF$ is calculated as:

$$SRSF = \frac{SR_s}{SR_r} \tag{2.2.6}$$

where SR_s is the support resistance provided by the support units and SR_r is the support resistance required to hold a block in position in the hangingwall, i.e. carry the deadweight of the block. The four different block types were evaluated. The capacity of the support units was varied to result in a given $SRSF$. Table 2.2.1 shows a summary of the support spacing and capacity where the block weight was 10 kN and the $SRSF$ was 2,0. Note that the block face area was 1 m^2 in all the runs, resulting in a required support resistance of 20 kN/m^2.

The results for a block of type A, where the $SRSF$ is 2,0, are shown in Figure 2.2.13. The results show that the keyblocks fail by dropping out between supports or failing the supports by rotation. As the spacing of the supports increases, the potential for dropping out between supports increases. The potential for failure by rotation increases to a maximum of about 11 percent when the support spacing is approximately equal to the block edge dimensions. When the supports are spaced greater than the block edge dimensions, the amount of block failures between supports increases rapidly, so that failure between supports becomes the dominant failure mode, and the percentage of blocks failing by the rotational mode is reduced. This result is informative, since the $SRSF$ is 2,0 and one would not normally expect any failure of the support units.

Table 2.2.1   Example of data to ensure $SRSF$ of 2,0 for a 10 kN block.

Support spacing (m)	Support capacity (kN)
0,4 x 0,4	3,2
0,7 x 0,7	9,8
0,9 x 0,9	16,2
1,1 x 1,1	24,2
1,5 x 1,5	45,0
2 x 2	80,0
3x3	180,0

Since a large number of analyses were conducted, each producing a graph similar to the above results, a summary of only the rotational failure results are presented in Figure 2.2.14 to Figure 2.2.17. The results show that for all the block types, it is possible for rotational failure to take place, even when the $SRSF$ is greater than 2,0. If one compares the rotational failure probability of the keyblocks at a $SRSF$ value of 2,0, it is found that the probability of failure can be as high as 12 percent, 32 percent, 50 percent and 80 percent for block types A, B, C and D respectively. The peak failure probabilities occur when the support spacing is about 1,1 to 1,2 times the block edge length. At larger support spacing, the probability of rotational failure decreases because the support capacity of the individual units increases to provide the required support resistance. These results are different from the results shown in Figure 2.2.11 because the support capacity of the individual units increases with the spacing.

In a practical mining situation, the safety of a working place will depend on the number of the different block types that are present in the hangingwall of the stope. For the purpose of this

study, a number of different geotechnical areas were evaluated to establish what block types are present and how they would fail. The results are presented in the next section.
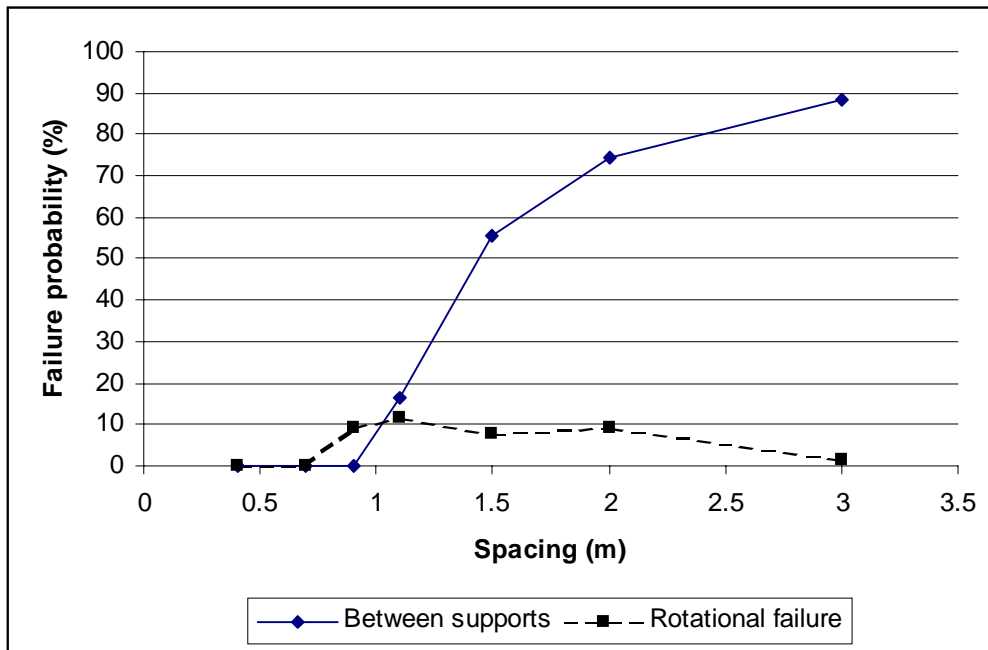
Figure 2.2.13   Failure modes for a 1 m x 1 m keyblock when the support resistance safety factor is 2,0.
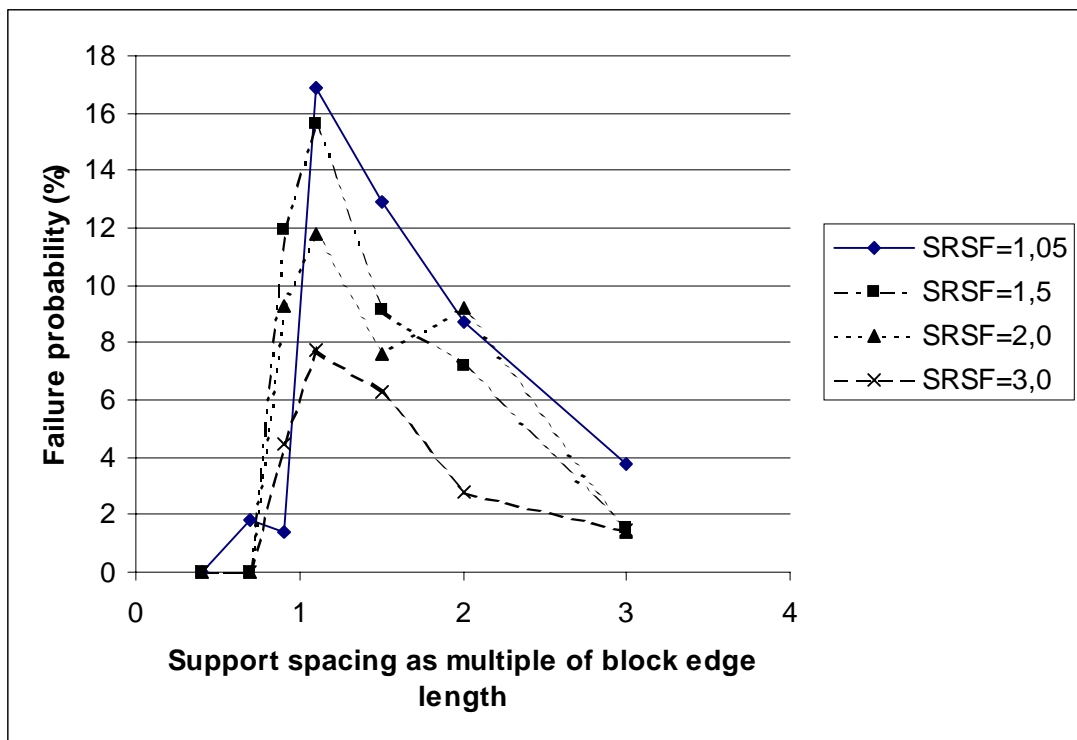
Figure 2.2.14   Effect of support spacing and support resistance on probability of rotational failure, block type A.
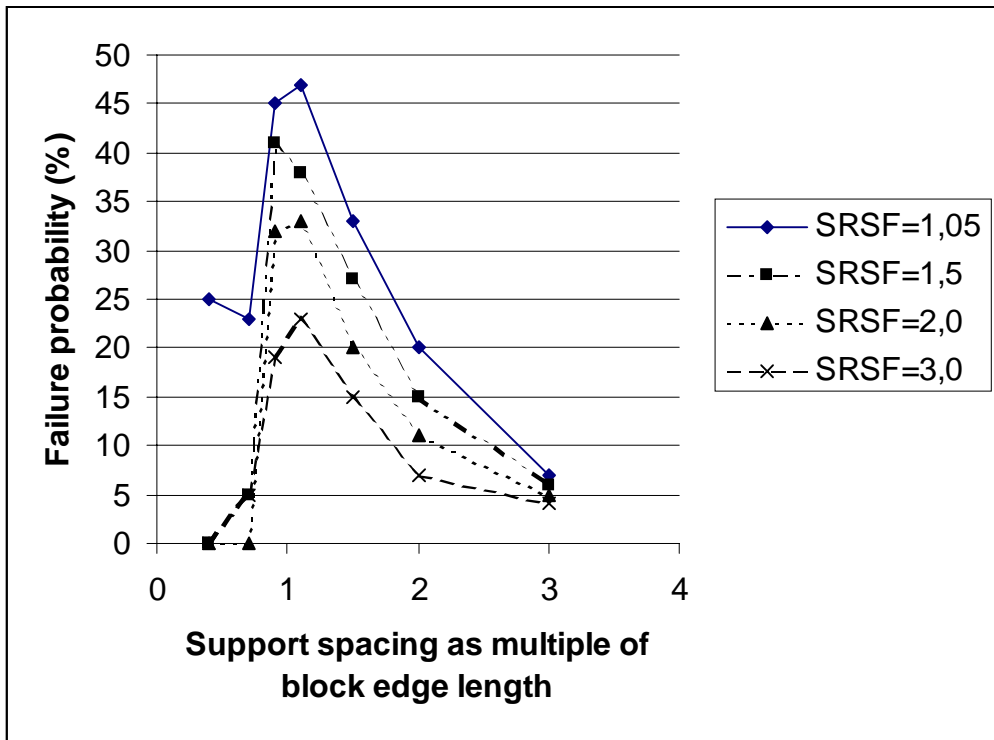
Figure 2.2.15 Effect of support spacing and support resistance on probability of rotational failure, block type B.
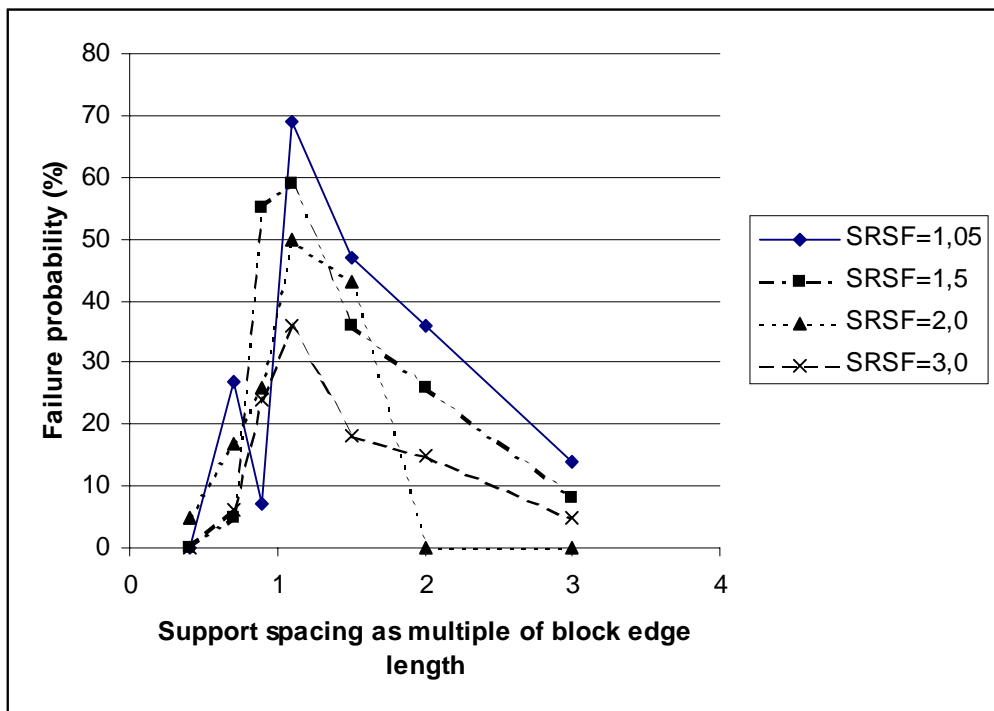
Figure 2.2.16 Effect of support spacing and support resistance on probability of rotational failure, block type C.
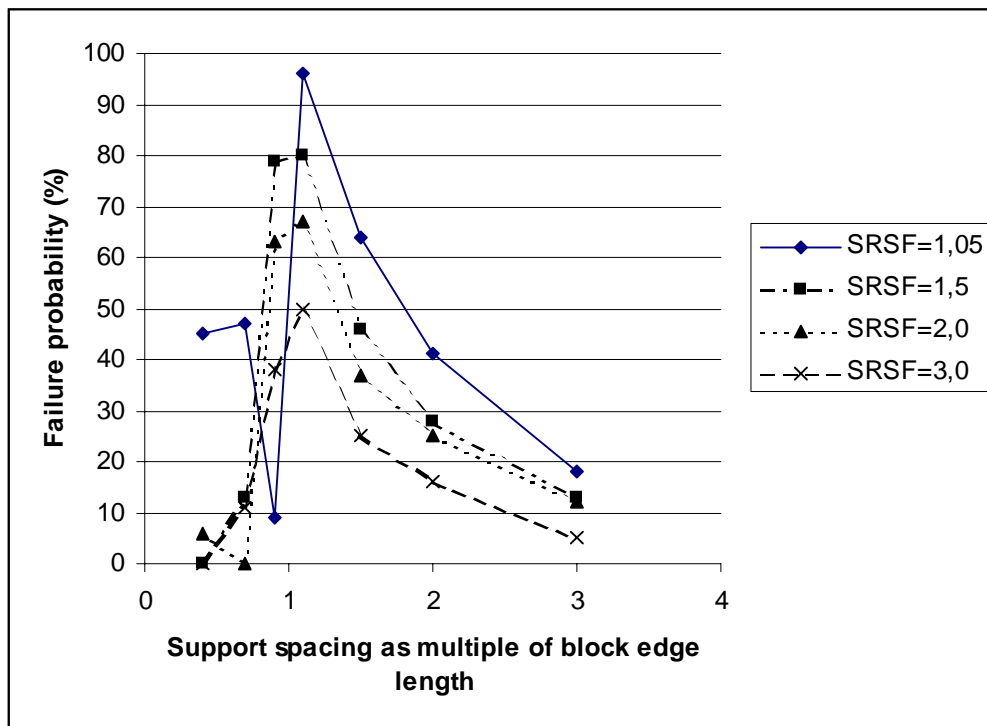
***Figure 2.2.17   Effect of support spacing and support resistance on probability of
rotational failure, block type D.***

2.2.8 Evaluation of keyblock rotation for typical Bushveld hangingwall jointing

Jointing data describing three hangingwall types in the Bushveld were obtained (Watson, 1999) and modelled using the JBlock program. The jointing data used for this analysis are summarised in Appendix 1. Note that no shallow dipping "dome" joints are included in the data.

Initial runs using the JBlock program indicated that no rotational failure was possible, because all the joint sets are steeply dipping, resulting in blocks with steep edges that are unable to rotate. Only by introducing a shallow dipping joint set, representing the "dome" structures, was rotational failure shown to be possible. The frequency and length of dome joints will therefore dictate the amount of rotational failure. For the purpose of the analysis, shallow dipping dome joints or stress induced fractures were assumed to be spaced 30 m apart along the hangingwall of the stopes and dip at 20 degrees. The dome joints formed blocks, which were typically of type A, which means that they have only one potential edge of rotation.

Initially the block sizes generated by JBlock were compared to the sizes of actual blocks in Bushveld mines. The block sizes reported by Bakker (1993) for platinum mines were used as a basis for comparison. The results for geotechnical area 3 are shown in Figure 2.2.18, which shows that the JBlock block size distribution follows a similar trend to the actual block thickness up to the 60 percent cumulative value, after which JBlock predicts larger block thicknesses.

77
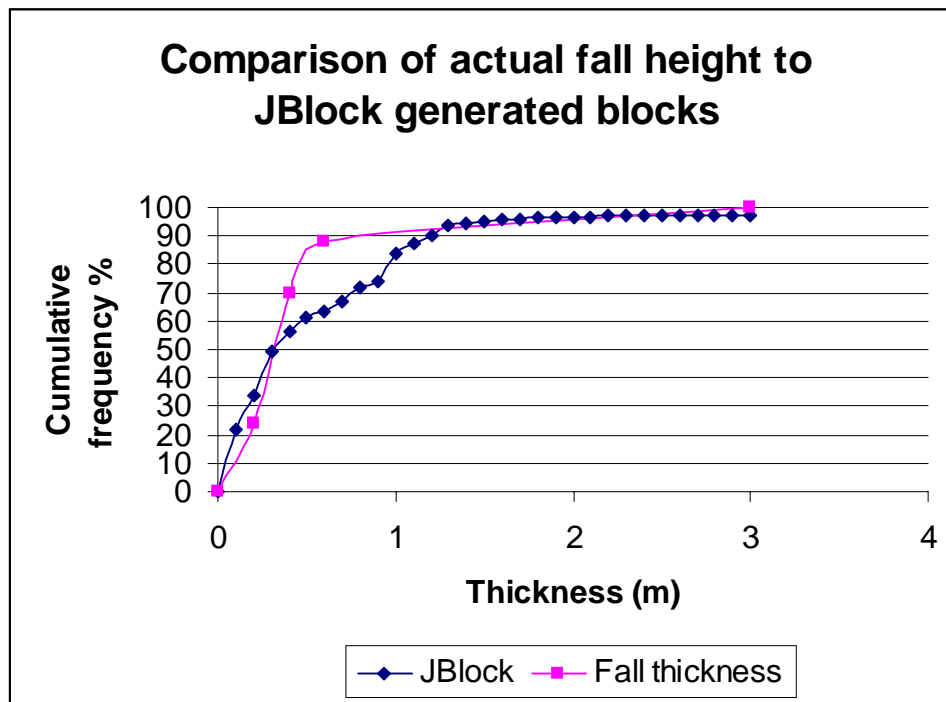
Figure 2.2.18   Comparison of JBlock generated block thickness to actual rock fall dimensions.

Only the results for geotechnical area 3 are shown here, since the block sizes are dominated by the dome joint set, which was introduced identically in all the data sets, resulting in similar size distributions for all the geotechnical areas. The distribution of keyblock sizes used in the following analyses should rather be seen as a generalisation for the Bushveld, rather than specific to a geotechnical area.

Analyses were carried out to determine what percentage of unstable keyblocks failed by rotation. A series of JBlock models were set up to simulate a stope with 200 kN capacity elongate support units. The supports were installed in a square pattern, with spacings that ranged from 1 m x 1 m, up to a spacing of 5 m x 5 m. The models were set up to simulate 5000 keyblocks in the hangingwall of a stope. For each model the number of keyblocks that failed was determined; these included falling out between supports, crushing supports and rotational failure. The number of rotational failures was expressed as a percentage of all the keyblocks that failed. The results are summarised in Figure 2.2.19, which shows that keyblock rotation forms a low percentage of all the failures. When the support spacing is about 3 m, the rotational failure reaches a maximum of 2,6 percent.

The results indicate that rotation is not a major cause of failure in a typical Bushveld stope. The reason for the low number of keyblock rotational failures may be ascribed to the fact that most of the keyblocks are of type A, which has a relatively low probability of rotation. In addition, the larger keyblocks span over a number of supports, and these factors reduce the probability of rotation further. Since the dome joint set only dips at 20 degrees, these keyblocks do not extend high up into the hangingwall, thus limiting their weight. The relationship between keyblock face area and required support resistance to hold the keyblock in place is shown in Figure 2.2.20, from which it is clear that blocks with large face areas (>20 m^2) do not necessarily require a very large support resistance to be stabilised. The largest blocks on the graph require a support resistance of 100 kN/m^2 while a support resistance of less than 40 kN/m^2 adequately supports

most of the blocks and the smaller keyblocks, which are supported by a single support unit, are unable to break the supports by rotation.
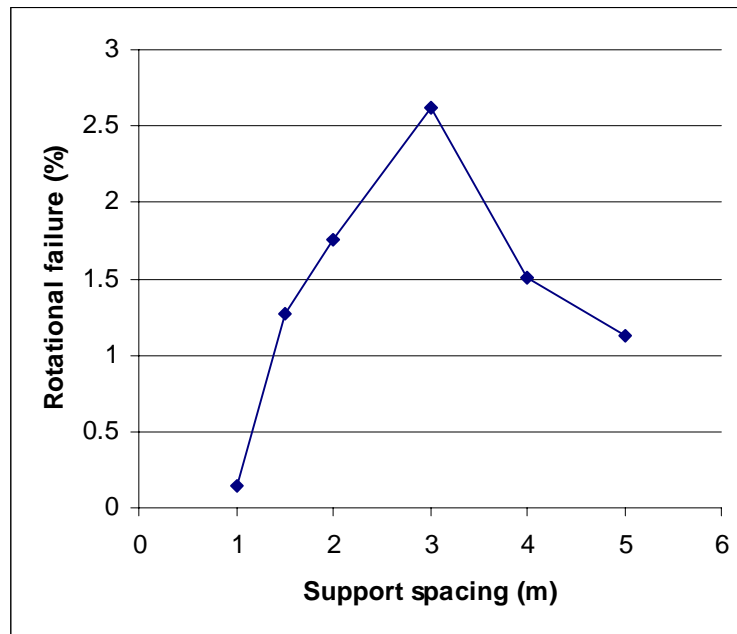
Figure 2.2.19   Effect of support spacing on percentage of keyblocks that fail by rotation using a generalised distribution of keyblock dimensions.
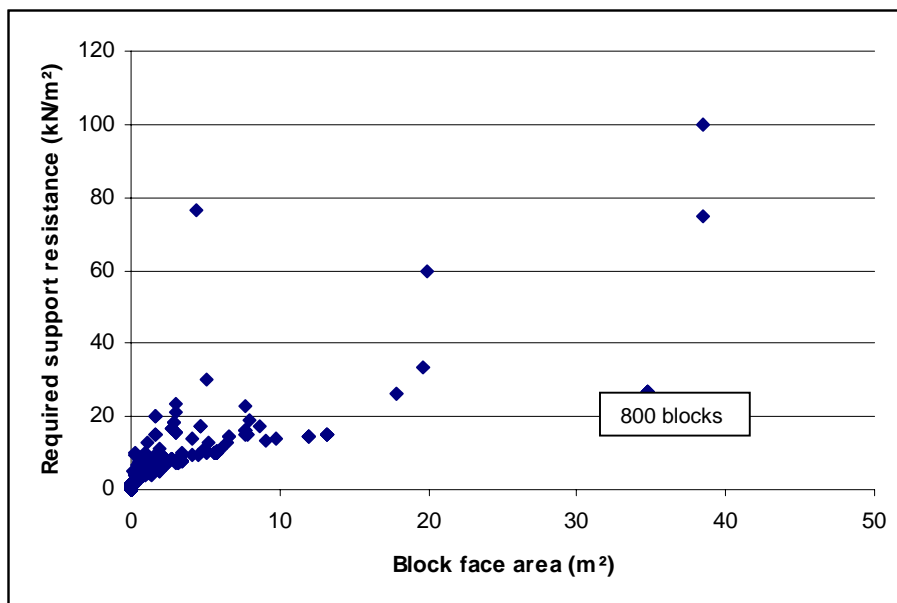
Figure 2.2.20   Relationship between JBlock generated keyblock face area and required support resistance.

2.2.9 Two-dimensional probabilistic keyblock rotation analysis

The following discussion is applicable only to cases where the keyblock geometry allows rotation (Section 2.2.3).
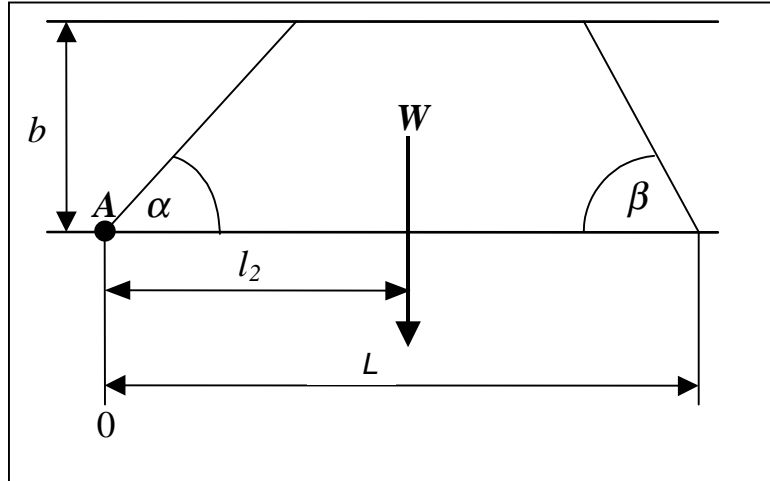
Figure 2.2.21   Keyblock with weight W.

Consider a block with weight W as shown in Figure 2.2.21, which is supported by only one support unit. Let F_{req} be the support force required to maintain equilibrium. l_1 is the distance from the point of rotation, A, to the support unit force. l_1 can lie anywhere between 0 and L, where L is the length of the keyblock. To determine a relationship between the required support unit force and the weight of the block, the moments are taken around the point of rotation. The lever-arm of W is l_2.

Equilibrium if:

$$F_{req} l_1 - W l_2 = 0 ,$$ (2.2.7)

$$\Rightarrow F_{req} = W \left(\frac{l_2}{l_1} \right).$$ (2.2.8)

W and l_2 are constants, thus F_{req} is a function of l_1, and

$$F_{req} \propto \frac{1}{l_1} .$$ (2.2.9)

The force required to maintain equilibrium is a minimum when $l_1 = L$:

$$F_{min} = W \left(\frac{l_2}{L} \right).$$ (2.2.10)

Let F_{max} be the maximum force that can be transmitted by the support unit. Thus, the minimum distance that the support unit can be placed from the point of rotation, while preventing rotation of the block, is:

$$l_{\min} = l_2 \left(\frac{W}{F_{\max}} \right), \qquad (2.2.11)$$

$$l_{\max} = L. \qquad (2.2.12)$$

Thus,

$$W \left(\frac{l_2}{L} \right) \leq F \leq W \left(\frac{l_2}{l_{\min}} \right), \qquad (2.2.13)$$

$$l_2 \left(\frac{W}{F_{\max}} \right) \leq l_1 \leq L. \qquad (2.2.14)$$

For any given support force, F, the lever-arm required to ensure equilibrium, is given by

$$l_{req} = l_2 \left(\frac{W}{F} \right), \qquad (2.2.15)$$

Thus, if $l_1 \geq l_{req}$, the block cannot rotate. If, however, $l_1 < l_{req}$, the support unit will fail.

Thus, to determine the probability that for any given support force, F, the support will not fail, it is necessary to determine the probability that F is located between l_{req} and l_{max}.

Let P be the probability that F is located between l_{req} and l_{max}. P can be calculated as follows:

$$P = \frac{l_{\max} - l_{req}}{L} = \frac{L - l_2 \left(\frac{W}{F} \right)}{L} = \frac{LF - Wl_2}{LF}, \qquad (2.2.16)$$

which can be rewritten as:

$$F = \frac{Wl_2}{L(1-P)}. \qquad (2.2.17)$$

2.2.10 Three-dimensional probabilistic keyblock rotation analysis

In Section 2.2.8 it was mentioned that rotational failure is only possible where shallow dipping discontinuities exist. The following discussion is applicable only to cases where the keyblock geometry allows for rotation (Section 2.2.3).
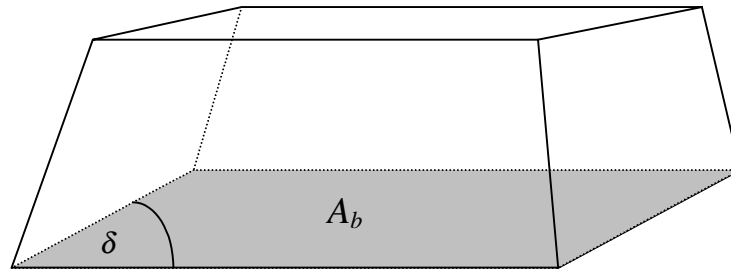
Figure 2.2.22   Three-dimensional keyblock.

Consider a block with weight W as shown in Figure 2.2.22, which is supported by only one support unit. As in the previous section, the force required to prevent the block from rotating is denoted by F_{req}. To calculate the moments of the forces about an edge, consider the base of the keyblock (the shaded area in Figure 2.2.22). Let l_1 be the lever arm of F about the edge of rotation, and l_2 the lever arm of W (Figure 2.2.23). For equilibrium,

$$F_{req}l_1 - Wl_2 = 0 \, , \qquad (2.2.18)$$

$$\Rightarrow F_{req} = W\left(\frac{l_2}{l_1}\right). \qquad (2.2.19)$$
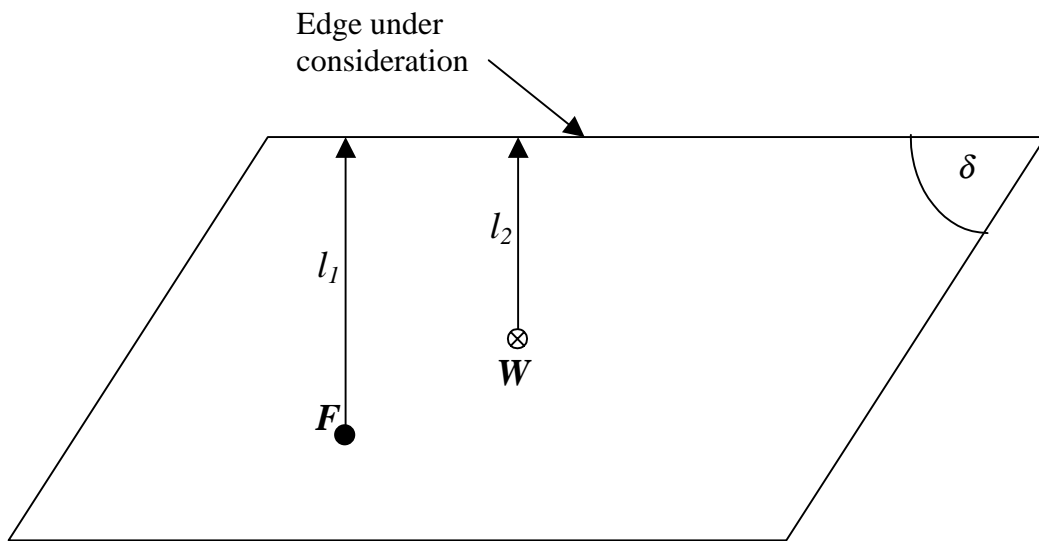
Figure 2.2.23   Moment calculation about top edge of keyblock base (plan view of keyblock).

Let f_1 be the spacing of the fractures of set 1 and f_2 the spacing between the fractures of set 2. From Figure 2.2.24,

$$L_1 = \frac{f_1}{\sin \delta} \, , \qquad (2.2.20)$$

$$L_2 = \frac{f_2}{\sin \delta} \, . \qquad (2.2.21)$$
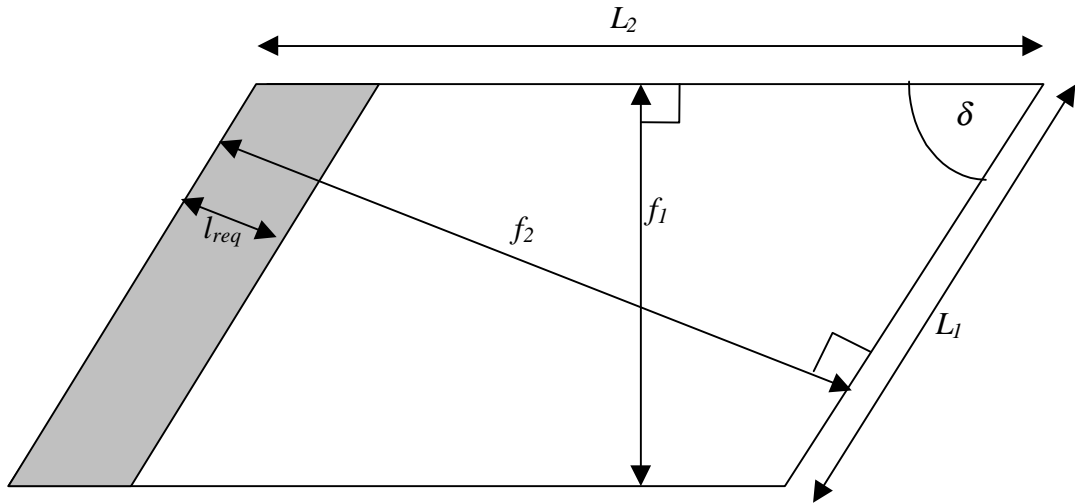
Figure 2.2.24   Keyblock formed by joint sets with spacings f_1 and f_2.

The base area of a keyblock, A_b, can be calculated as:

$$A_b = L_2 f_1.$$

<div align="right">(2.2.22)</div>

For any given support force, F, the lever-arm required to ensure equilibrium is given by

$$l_{req} = l_2 \left(\frac{W}{F} \right),$$

<div align="right">(2.2.23)</div>

where l_{req} is the required lever-arm to ensure equilibrium. Thus, if $l_1 \geq l_{req}$, the block cannot rotate. If, however, $l_1 < l_{req}$, the support unit will fail.

Thus, to determine the probability that the support won't fail for any given support force, F, it is necessary to determine the probability that F will be located between l_{req} and l_{max}, where l_{max} is the maximum perpendicular distance that F can be placed from the edge under consideration.

This calculation needs to be carried out for all the edges about which rotation is possible. The worst case is assumed for the purpose of this explanation, i.e. rotation is possible about all four edges of the keyblock. Let l_{rl} be the required lever-arm for a support force, F, to prevent the keyblock from rotating about its left edge. Similarly, l_{rr}, l_{rt} and l_{rb} are the lever-arms required to prevent keyblock rotation about the right, top and bottom edges respectively. l_{2l}, l_{2r}, l_{2t} and l_{2b} are the lever-arms of W about the left, right, top and bottom edges respectively (Figure 2.2.25).
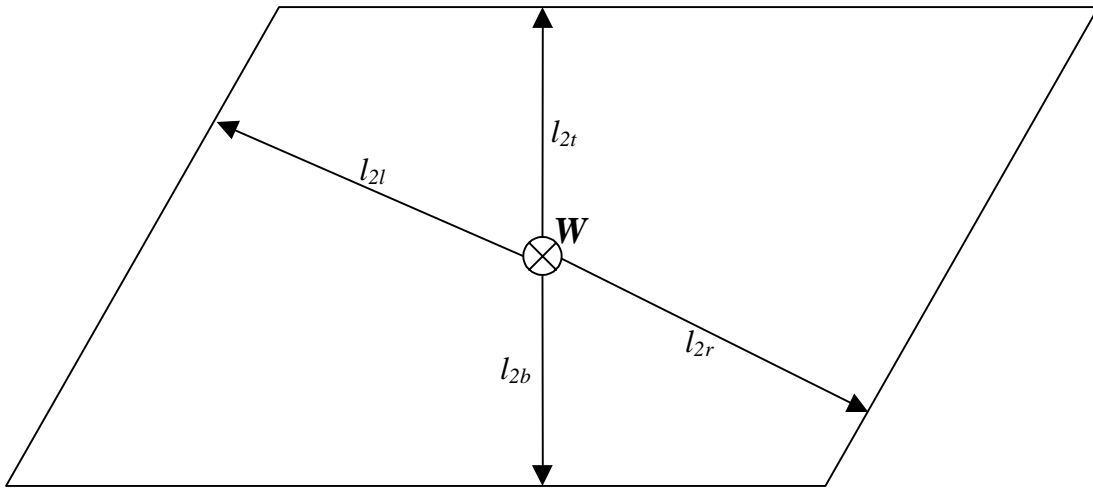
Figure 2.2.25   Schematic illustrating the lever-arms of W about the four edges of an arbitrarily shaped keyblock.

Thus,

$$l_{rl} = l_{2l}\left(\frac{W}{F}\right),$$ (2.2.24)

$$l_{rr} = l_{2r}\left(\frac{W}{F}\right),$$ (2.2.25)

$$l_{rt} = l_{2t}\left(\frac{W}{F}\right),$$ (2.2.26)

$$l_{rb} = l_{2b}\left(\frac{W}{F}\right),$$ (2.2.27)

Therefore, to determine the probability that the support will not fail, it is necessary to determine the probability that F will **not** be located in the shaded area (Figure 2.2.26).
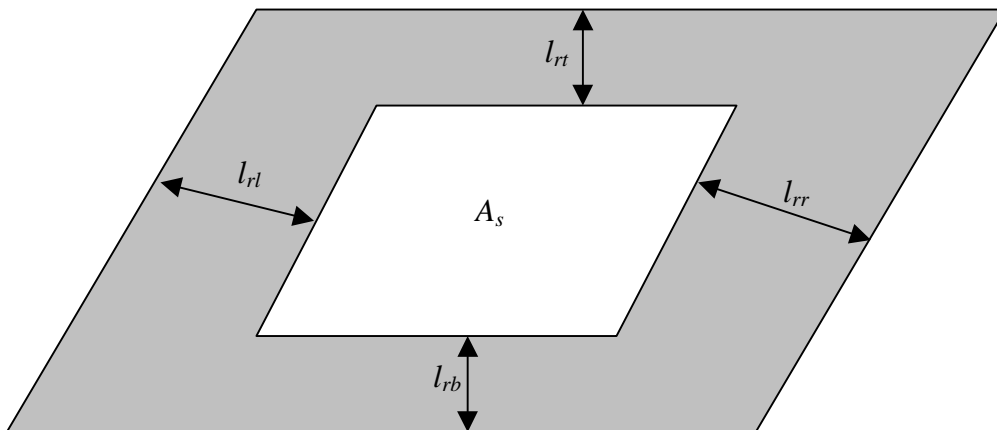
Figure 2.2.26   For a given support force, F, location of support unit within A_s will prevent keyblock rotation.

77

The probability, P, that the support unit will **not** fail, is the same as the probability that F is located in A_s, and can be calculated as follows:

$$P = \frac{A_s}{A_b} = \frac{\left(L_2 - \frac{l_{rl} + l_{rr}}{\sin \delta}\right)\left(f_1 - \left(l_{rt} + l_{rb}\right)\right)}{L_2 f_1} \ .$$

(2.2.28)

2.2.11 Rotational stability of keyblock supported by a single support unit

To simplify calculations, the base-area of the keyblocks are assumed to be square, as shown in Figure 2.2.27. Furthermore, it is desirable to consider only one case when determining the support force required to prevent rotational failure. It is therefore conservatively assumed that all blocks are able to rotate about all four edges (worst case scenario).
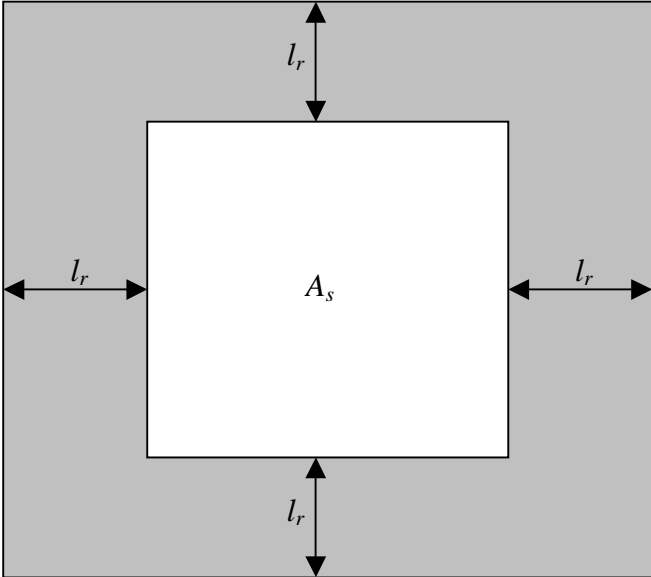
Figure 2.2.27   Square block with weight W.

The weight of the block acts at the centre. Thus, the lever-arm of the weight about each edge about which rotation is possible is the same, and this distance is denoted by l (Figure 2.2.28).
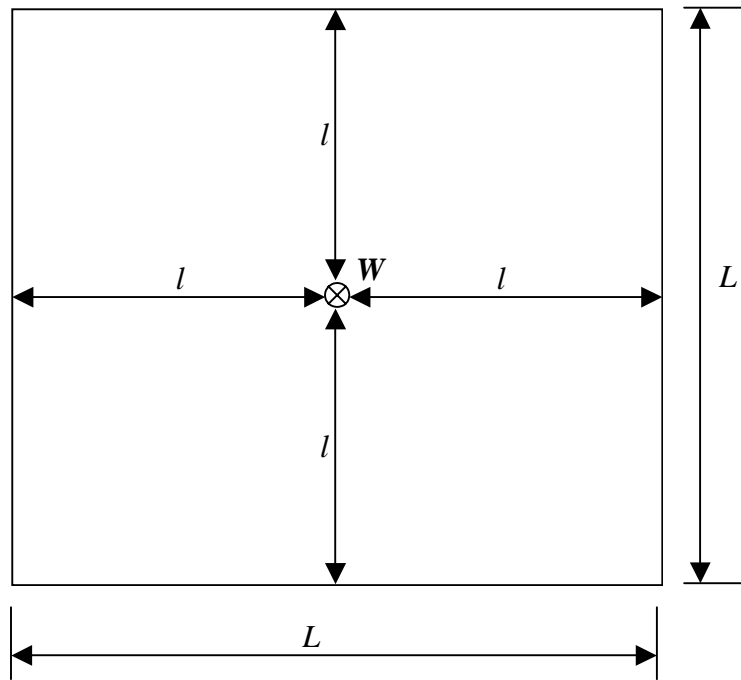
Figure 2.2.28   The weight of the block, W, acts at the centre of the block. The lever-arms about all the edges are shown.

Consider a block supported by a single support. The support force is denoted by F. The required lever-arm to prevent rotation of the block is l_r, which can be calculated as:

$$l_r = l\left(\frac{W}{F}\right), \qquad (2.2.29)$$

where l is the lever-arm of the weight about each edge of the square block. Each side of the block has a length of L. The weight acts at the centre of the block, thus

$$l = \frac{L}{2}. \qquad (2.2.30)$$

Substituting Equation (2.2.30) in (2.2.29) gives:

$$l_r = \left(\frac{L}{2}\right)\left(\frac{W}{F}\right). \qquad (2.2.31)$$

The probability, P, that the block will **not** rotate, is given by:

$$P = \frac{A_s}{A_b}, \qquad (2.2.32)$$

where,

$$A_s = \left(L - 2l_r\right)^2, \qquad (2.2.33)$$

and

$$A_b = L^2. \qquad (2.2.34)$$

77

$$P = \frac{(L - 2l_r)^2}{L^2} = \left(\frac{L - 2\left(\dfrac{LW}{2F} \right)}{L} \right)^2 = \left(\frac{F - W}{F} \right)^2, \tag{2.2.35}$$

$$\Rightarrow \sqrt{P} = \frac{F - W}{F}, \tag{2.2.36}$$

$$\Rightarrow F = \frac{W}{1 - \sqrt{P}}. \tag{2.2.37}$$

The weight of the block, W, is given by:

$$W = \rho g b L^2. \tag{2.2.38}$$

Thus,

$$F = \frac{\rho g b L^2}{1 - \sqrt{P}}. \tag{2.2.39}$$

Therefore, if a keyblock is supported by a single support unit, Equation (2.2.39) can be used to calculate the required support force (F) to prevent the block from rotating for any given probability (P).

Equation (2.2.39) can be rewritten as

$$F = kW, \tag{2.2.40}$$

where

$$k = \frac{1}{1 - \sqrt{P}}. \tag{2.2.41}$$

If the block were unable to rotate, the required support force would only be determined by the tributary area criterion and would therefore be equal to the weight of the block (W). From Equation (2.2.41) it can be seen that the ability of the block to rotate increases the force required to maintain stability by a factor, k.

Table 2.2.2   Various values of k for different probabilities

P	k
1,00	∞
0,95	40
0,90	20
0,85	13
0,25	2

From Table 2.2.2 it can be seen that the possibility of rotation causes a significant increase in the required support force if the keyblock is only supported by a single support unit. For example, if the probability that the block will **not** rotate is 95 percent, the required support force is 40 times the weight of the block (Table 2.2.2).

The above results correlate well with the findings from the JBlock analysis (Sections 2.6 and 2.8). In Section 2.6 it was found that when the support capacity exceeds the weight of the block by a factor of two, i.e. $F = 2W$ ($k = 2$), the probability of failure could be as high as 80 percent if the block was supported by one unit only. From Table 2.2.2 it can be seen that the probability that the keyblock will not rotate is 25 percent if $k = 2$, in other words, the probability of failure is 75 percent (using Equation (2.2.41)).

If a keyblock is supported by a single support unit, the unit can be located anywhere below the block, i.e. across the entire base area of the block. The greater the support force, the smaller the required minimum lever-arm, and thus the greater the probability that the keyblock will not rotate. Thus, to ensure a high probability of stability, the support force needs to be much higher than the weight of the block to ensure rotational stability (if a keyblock is supported by one support unit only).

Because each keyblock is assumed to be supported by a single support, this method does not take the spatial distribution of support units into account. Keyblocks supported by multiple support units and the effect of the spacing of support units on the location of the resultant support force are investigated in the next section.

2.2.12 Rotational stability of a keyblock supported by multiple support units

2.2.12.1 Keyblocks with square bases

In the previous section, an analysis was carried out to determine what the required support force would have to be to ensure the rotational stability of a keyblock supported by one support unit only. If, however, a keyblock is supported by multiple support units, the spatial distribution of the supports will affect the rotational stability of the keyblock.

In order to determine the effect of multiple support units on the rotational stability of the keyblock, some new terminology is introduced here.

Parameter definitions (Figure 2.2.29):

F_R resultant support force.

d perpendicular distance between the edge under consideration and the resultant support force.

δ perpendicular distance between the edge under consideration and the closest support unit to that edge.

L   length of keyblock

S   support spacing
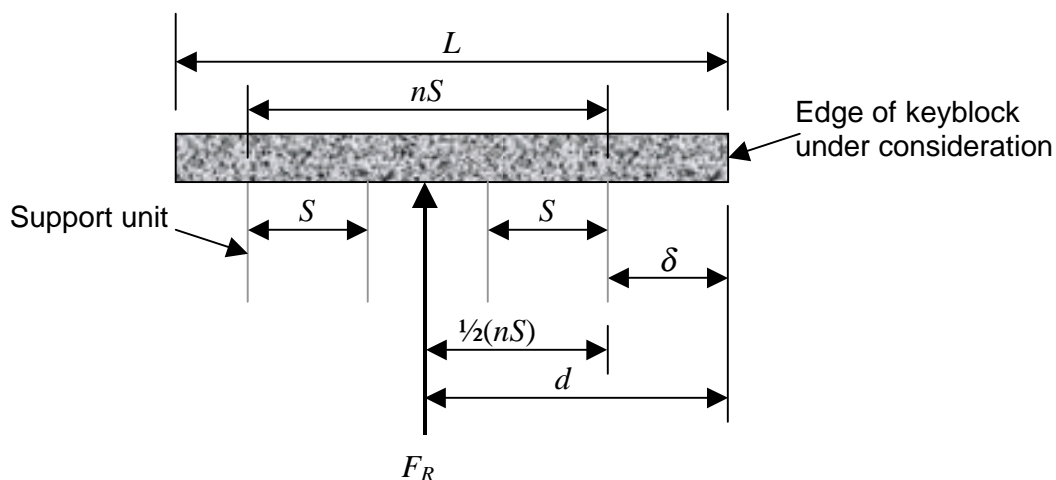
Figure 2.2.29 ***Naming conventions of parameters governing the rotational stability of a keyblock.***

The following mathematical concepts are used in the analysis:

The floor of x, $\lfloor x \rfloor$, is the greatest integer less than or equal to x, e.g. $\lfloor 4.3 \rfloor = 4$.

The ceiling of x, $\lceil x \rceil$, is the smallest integer greater than or equal to x, e.g. $\lceil 4.3 \rceil = 5$, and $\lceil 4 \rceil = \lfloor 4 \rfloor = 4$

Consider a keyblock supported by multiple support units, as shown in Figure 2.2.29.

The number of support units, N, per length, L, of the block is defined as:

$$N = \left\lfloor \frac{L}{S} \right\rfloor. \tag{2.2.42}$$

n is defined as the number of full spans between support units per length L of the block (Figure 2.2.30), and can be calculated as

$$n = N - 1. \tag{2.2.43}$$
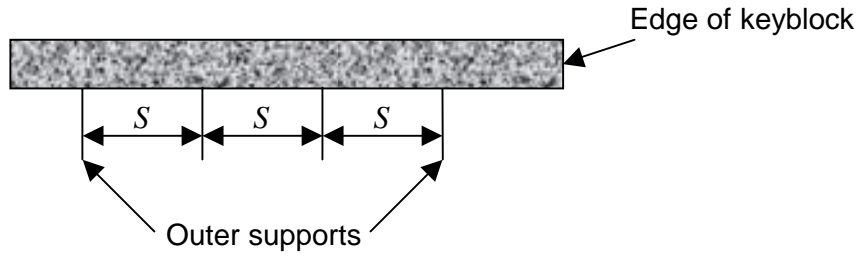
Figure 2.2.30   Schematic illustrating the concept of outer supports ($n = 3$ in this example).

Assuming all supports carry the same load and are spaced evenly, the resultant support force will always be located halfway between the two **outer supports** (the supports closest to the opposing edges of the keyblock – Figure 2.2.30). Thus, n is the number of full spans between the outer supports, and the distance between the outer supports is given by nS.

If $S \le \dfrac{L}{2}$, then $n \ge 1$, and

$$d = \delta + \frac{nS}{2},$$
(2.2.44)

but $0 \le \delta \le (L - nS)$

$$\Rightarrow d_{\min} = \frac{nS}{2}.$$
(2.2.45)

Thus, the minimum distance between the resultant support force and the edge under consideration will always be at least $d_{\min}$. In other words, $d_{\min}$ is the minimum lever-arm of the resultant support force about the edge of the keyblock. The required support force can thus be calculated as:

$$F_{req} = \frac{Wl}{d_{\min}},$$
(2.2.46)

and, from Figure 2.2.28, it can be seen that

$$l = \frac{L}{2},$$
(2.2.47)

Thus,

$$F_{req} = \frac{WL}{2d_{\min}}.$$
(2.2.48)

Hence, if $F_R \ge F_{req}$ the block will not rotate.

$$F_R = \frac{WL}{2d} = \frac{WL}{nS},$$
(2.2.49)

$$F_R = kW,$$
(2.2.50)

77

where

$$k = \frac{L}{nS}.$$ (2.2.51)

If N is the number of support units per length of block (in one dimension), then the number of support units per keyblock is given by N^2.

Thus, the force required per support unit, F, is calculated as

$$F = \frac{F_R}{N^2} = \frac{WL}{nN^2 S}.$$ (2.2.52)

The above method assumes that the block sides are parallel to the spacing pattern.
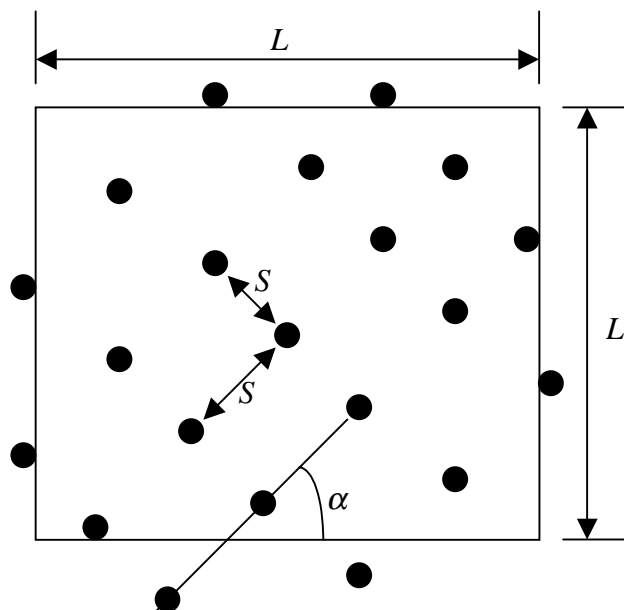
Figure 2.2.31   Supports oriented at angle α relative to the keyblock.

Consider a support system, which is oriented at an angle α relative to the keyblocks (Figure 2.2.31). The supports are arranged in a square pattern and the spacing between support units is S. To determine the number of supports per keyblock, it is assumed that there will be at least one support unit per support area, where the support area is defined as S^2. The number of support units per keyblock (M) is defined as the ratio of the keyblock area to support area:

$$M = \left\lfloor \frac{L^2}{S^2} \right\rfloor.$$ (2.2.53)

The following derivation of the minimum lever-arm of the resultant support force about any edge of the keyblock is **only applicable if** $S \le \dfrac{L}{2}$.

The requirement that S must always be less than or equal to 0,5L, ensures that each keyblock will always be supported by at least four units:

$$M \geq \left\lfloor \frac{L^2}{S^2} \right\rfloor \geq \left\lfloor \frac{L^2}{\left(\frac{L}{2} \right)^2} \right\rfloor \geq \lfloor 4 \rfloor \geq 4 .\qquad(2.2.54)$$

Now define:

$$m = \left\lfloor \sqrt{M} \right\rfloor - 1 .\qquad(2.2.55)$$

The worst case occurs when one of the four support units is on the edge of the block. Thus, the resultant support force will always have a lever-arm greater than or equal to the lever-arm in this case. The minimum lever-arm is denoted by d_{min}.
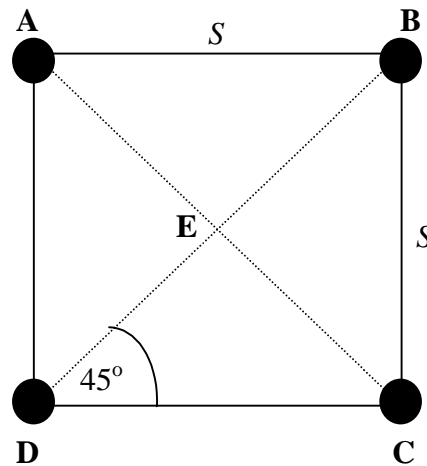
Figure 2.2.32   Support units spaced at S.

In Figure 2.2.32, $\overline{AB} = \overline{BC} = \overline{CD} = \overline{AD} = S$.

$$\overline{AC} = \overline{BD} = \sqrt{S^2 + S^2} = \sqrt{2}S .\qquad(2.2.56)$$

Thus,

$$\overline{AE} = \overline{BE} = \overline{CE} = \overline{DE} = \frac{\sqrt{2}}{2} S = \frac{S}{\sqrt{2}} .\qquad(2.2.57)$$
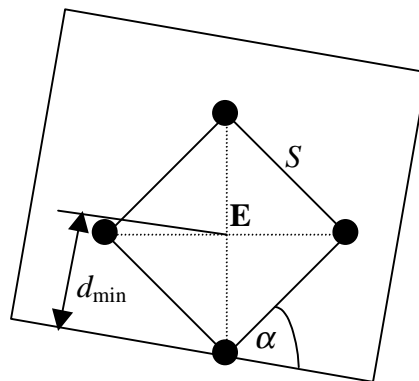
Figure 2.2.33   Determination of the minimum lever-arm, d_{min}.

77

From Figure 2.2.33 it can be seen that

$$d_{\min} = \frac{mS}{\sqrt{2}} \sin\left(\alpha + 45^{0}\right),$$ (2.2.58)

Thus, the resultant support force required to prevent rotation is given by

$$F_R = kW \,,$$ (2.2.59)

where,

$$k = \frac{L}{2d_{\min}} \,.$$ (2.2.60)

Table 2.2.3 F_R **for different values of** α**, for** $S=0,5L$**.**

α	$d_{\min}$	k	F_R
0°	0,25L	2	2W
30°	0,34L	1,5	1,5W
45°	0,35L	1,4	1,4W
60°	0,34L	1,5	1,5W
90°	0,25L	1,4	2W

From Table 2.2.3 it can be seen that the lever-arm of F_R is a minimum when $\alpha = 0°$ or $90°$. For the case where $\alpha = 0°$ and $S = 0,5L$, $d_{\min} = 0,25L$. This same result is achieved when using Equation (2.2.45), which was derived for the parallel case. Thus, although this formula presents a more general solution, Equation (2.2.62) can be used in all cases, as it is more conservative ($\alpha = 0°$), **as long as** S $0,5L$.

$$d_{\min} = \frac{mS}{\sqrt{2}} \sin\left(\frac{\pi}{4}\right) = \frac{mS}{\sqrt{2}}\left(\frac{1}{\sqrt{2}}\right) = \frac{mS}{2} \,.$$ (2.2.61)

M and N^2 both represent the total number of support units per keyblock, therefore m and n are the same and the above equation can be written as:

$$d_{\min} = \frac{mS}{2} = \frac{nS}{2} \,.$$ (2.2.62)

In Section 2.7 a JBlock analysis was carried out where each keyblock was supported by at least 15 support units. The results of this analysis showed that if the support force is more than 1,5 times the weight of the block, keyblock rotation is no longer possible.

This situation is now analysed using the formulae derived here.

If each keyblock is supported by at least 15 units:

$$M = 15$$

$$\Rightarrow m = n = \lfloor \sqrt{15} \rfloor - 1 = \lfloor 3.87 \rfloor - 1 = 3 - 1 = 2 \text{ (from Equation (2.2.55)).}$$

Furthermore, if $M = 15$, then $\dfrac{L}{4} < S \le \dfrac{L}{3}$.

Thus, using the largest support spacing for this case, namely $S = \dfrac{L}{3}$, the minimum lever-arm for each block can be calculated as (using Equation (2.2.58)):

$$d_{\min} = 0,34L \text{ (Assuming the } \alpha = 0^{\circ}, \text{ the most conservative case).}$$

Substituting the value of $d_{\min}$ in Equation (2.2.60) gives $k = 1,5$.

Thus, the resultant support force required to prevent keyblock rotation is $F_R = 1,5W$, which correlates perfectly with the findings of the JBlock analysis (Sections 2.6, 2.7 and 2.8), where it was found that if the support force exceeded the weight of the block by a factor of 1,5, rotation was no longer possible (provided that keyblocks were supported by a **large** number of support units).

2.2.12.2   Keyblocks with rectangular bases

Consider a keyblock with a rectangular base, as shown in Figure 2.2.34, where L_x is the length of the keyblock in the x-direction, L_y the keyblock length in the y-direction and S_x and S_y are the support spacings in the x- and y-directions respectively.
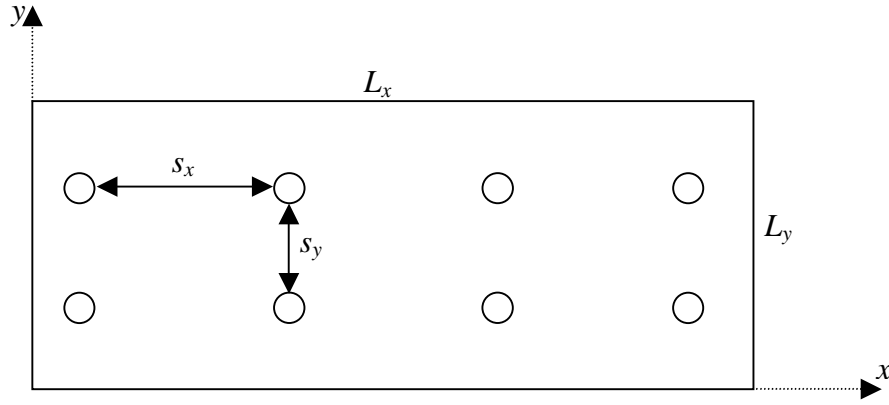
Figure 2.2.34   Keyblock with a rectangular base.

The number of support units per length of block in the x-direction is given by

$$N_x = \left\lfloor \frac{L_x}{S_x} \right\rfloor,$$ (2.2.63)

and the number of supports per length of block in the y-direction is given by

$$N_y = \left\lfloor \frac{L_y}{S_y} \right\rfloor.$$ (2.2.64)

Furthermore, n_x and n_y are defined as

$$n_x = N_x - 1,$$ (2.2.65)
$$n_y = N_y - 1.$$ (2.2.66)

The number of support units per block, M, is calculated as

$$M = N_x N_y.$$ (2.2.67)

The lever-arm of W about the x-axis is denoted by l_{wx}, where

$$l_{wx} = \frac{L_y}{2}.$$ (2.2.68)

Similarly, the lever-arm of W about the y-axis is denoted by l_{wy}, where

$$l_{wy} = \frac{L_x}{2}.$$ (2.2.69)

The following derivation of the minimum lever-arms of the resultant support force about the edges of the keyblock **only applies when** $S_x \leq \dfrac{L_x}{2}$ **and** $S_y \leq \dfrac{L_y}{2}$. This requirement ensures that each keyblock is supported by at least four support units ($M \geq 4$).

77

As in the previous sections, the worst case occurs when one of the support units is on the edge of the block under consideration.

Consider rotation about the x-axis (Figure 2.2.34):

The minimum lever-arm of the resultant support force about the edge under consideration is denoted by $d_{\min x}$, and can be calculated as

$$d_{\min x} = \frac{n_y S_y}{2} . \qquad (2.2.70)$$

Thus, the resultant support force required to prevent rotation about the x-axis (F_{Rx}) is given by

$$F_{Rx} = \frac{Wl_{wx}}{d_{\min x}} . \qquad (2.2.71)$$

Substituting Equations (2.2.68) and (2.2.70) in Equation (2.2.71), gives

$$F_{Rx} = \frac{WL_y}{n_y S_y} , \qquad (2.2.72)$$

which can be re-written as

$$F_{Rx} = k_x W , \qquad (2.2.73)$$

where,

$$k_x = \frac{L_y}{n_y S_y} . \qquad (2.2.74)$$

Consider rotation about the y-axis (Figure 2.2.34):

The minimum lever-arm of the resultant support force about the edge under consideration is denoted by $d_{\min y}$, and can be calculated as

$$d_{\min y} = \frac{n_x S_x}{2} . \qquad (2.2.75)$$

Thus, the resultant support force required to prevent rotation about the y-axis (F_{Ry}) is given by

$$F_{Ry} = \frac{Wl_{wy}}{d_{\min y}} . \qquad (2.2.76)$$

Substituting Equations (2.2.69) and (2.2.75) in Equation (2.2.76), gives

$$F_{Ry} = \frac{WL_x}{n_x S_x} , \qquad (2.2.77)$$

which can be re-written as

$$F_{Ry} = k_y W, \tag{2.2.78}$$

where,

$$k_y = \frac{L_x}{n_x S_x}. \tag{2.2.79}$$

Thus, the required resultant support force to prevent rotation about the *x*- and *y*-axes, F_R, is given by the maximum of F_{Rx} or F_{Ry}:

$$F_R = \max \begin{cases} F_{Rx}, \\ F_{Ry} \end{cases} \tag{2.2.80}$$

or,

$$F_R = kW, \tag{2.2.81}$$

where,

$$k = \max \begin{cases} k_x \\ k_y \end{cases}. \tag{2.2.82}$$

The support force required per support unit (F) is given by:

$$F = \frac{F_R}{M}. \tag{2.2.83}$$

In the JBlock analysis (Section 2.7), the blocks were 5 m x 3 m in size and the support spacing was 1 m x 1 m. This case is now analysed using the formulae derived in this section.

$L_x = 5$, $L_y = 3$, $S_x = S_y = 1$.

The number of support units in each direction can now be calculated as:

$N_x = \left\lfloor \frac{5}{1} \right\rfloor = 5$ and $N_y = \left\lfloor \frac{3}{1} \right\rfloor = 3$, and thus the number of support units per block is given by

$M = (5)(3) = 15$.

Furthermore, $n_x = 4$ and $n_y = 2$.

Rotation about the *x*-axis: $k_x = \frac{3}{(2)(1)} = 1,5$.

Rotation about the y-axis: $k_y = \dfrac{5}{(4)(1)} = 1,25$.

Thus, $k = \max \begin{cases} 1,5 \\ 1,25 \end{cases} = 1,5$

Therefore, to prevent rotation of the block, $F_R = 1,5W$ (which corresponds to the JBlock analysis results.)

A computer program has been coded to facilitate the convenient analysis of support requirements for blocks, which are prone to rotate. Details of the computer program, as well as example applications, are given in Chapter 5.

The work conducted here also offers scope for orienting the stope face at an optimum angle relative to hangingwall discontinuities. It is well known that discontinuities parallel or perpendicular to the strike direction are more prone to result in rock fall-outs, than discontinuities oriented at an angle relative to the stope face. This is supported by the findings of this project. Hence, at all times the face should be oriented obliquely to problematic discontinuity sets.

2.2.13 The effect of keyblock rotation on the performance of timber elongates

2.2.13.1 Structural analysis concepts

Some structural analysis concepts are introduced here.

Definitions: (Gere & Timoschenko, 1994).

A **beam** is a structural member, which is subjected to loads that act laterally to its longitudinal axis.

Columns are long, slender structural members, which are loaded axially in compression.

A **beam-column** is a structural member, which is subjected to both an axial compressive load and lateral bending loads

Clamped: If a beam is clamped (or fixed) at a support, it means that the edge of the beam cannot rotate or translate.

Pinned: If a beam is pinned at a support, it means that the beam is free to rotate about
             the support, but it cannot translate either vertically or horizontally.

Consider the following cases:
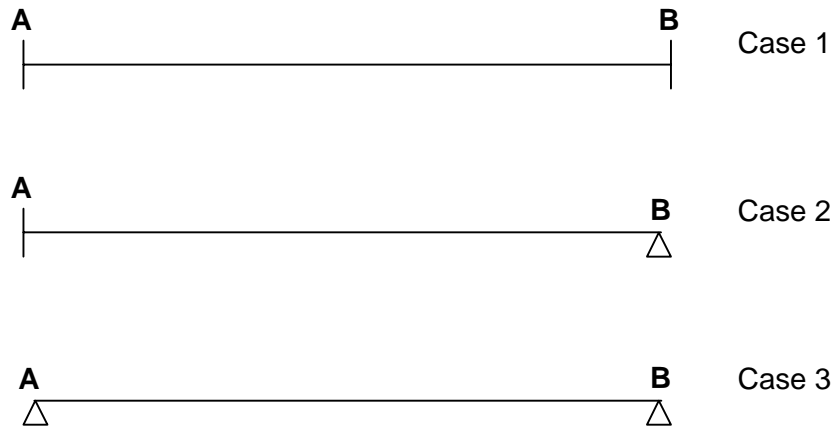
Figure 2.2.35   Beams with different end conditions.

Case 1:   Both ends of the beam are clamped.

Case 2:   One end of the beam is clamped (A) and the other is pinned (B).

Case 3:   Both ends of the beam are pinned.

If support B is now displaced through a distance, Δ, with respect to A, bending moments will be
induced in the beam. The resulting bending moment diagrams are shown in Figure 2.2.36. The
magnitudes of the bending moments generated by these loading conditions are given in Table
2.2.4.
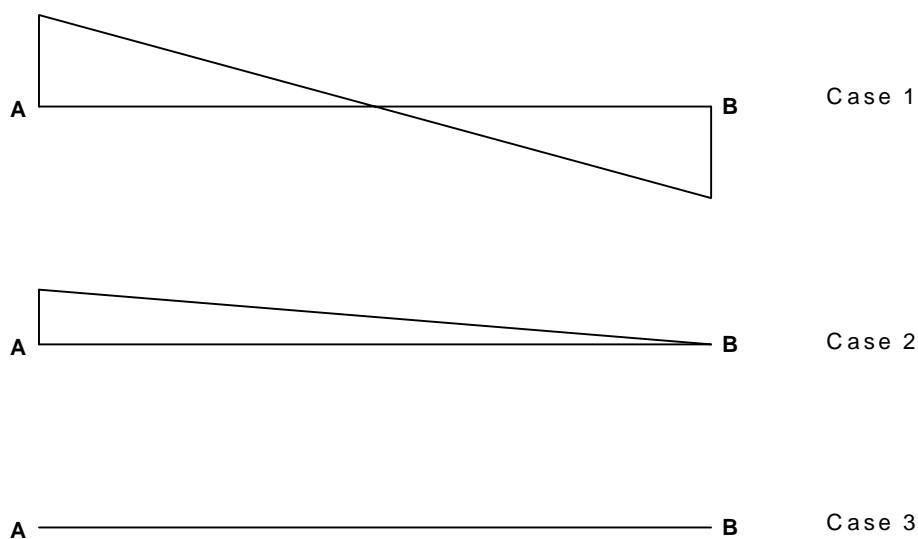
**Figure 2.2.36   Bending moment diagrams resulting from a downward
             displacement of support B with relation to support A for the three
             different cases.**

M_A denotes the bending moment at support A and M_B the moment at support B.

Table 2.2.4   ***Magnitude of bending moments at the supports resulting from a downward displacement of support B with relation to support A for the three different cases.***

Case	M_A	M_B
1	$\dfrac{6EI\Delta}{L^2}$	$\dfrac{6EI\Delta}{L^2}$
2	$\dfrac{3EI\Delta}{L^2}$	0
3	0	0

where:

E =   Elasticity modulus of timber

I = $\dfrac{\pi d^4}{64}$

d =   diameter of beam

L =   length of beam
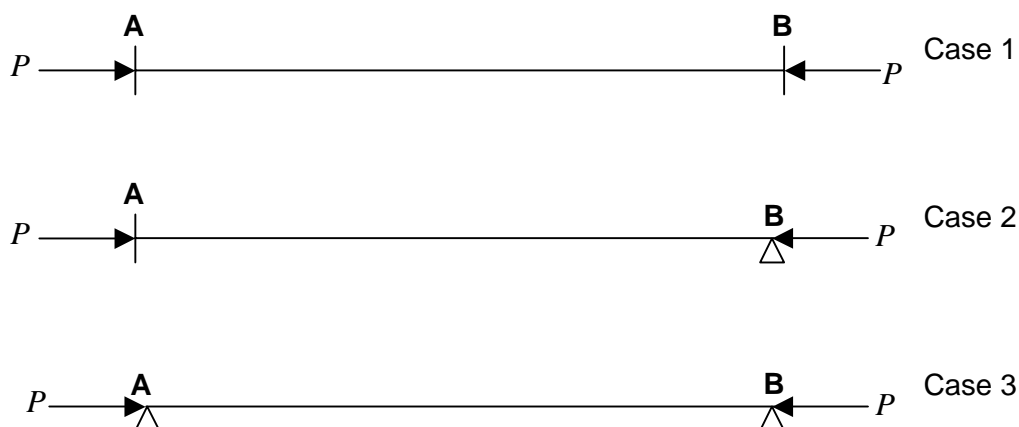
Figure 2.2.37   ***Members subjected to a compressive axial load, P.***

Now consider the beams shown in Figure 2.2.37. If support B is now displaced through a distance, Δ, with respect to A, bending moments will be induced in the beam. The resulting bending moment diagrams are shown in Figure 2.2.36 (the effects of secondary moments on beams that are pinned at both ends are ignored here), and the magnitudes of the bending moments for these loading conditions are given in Table 2.2.5.

Table 2.2.5   *Magnitude of bending moments at the supports resulting from a downward displacement of support B with relation to support A and an axial load, P, for the three different cases.*

Case	M_A	M_B
1	$\dfrac{6EI\Delta}{L^2} + P\Delta$	$\dfrac{6EI\Delta}{L^2} + P\Delta$
2	$\dfrac{3EI\Delta}{L^2} + P\Delta$	0
3	0	0

Thus, the application of a compressive axial load will increase the magnitude of the bending moments induced in the member.

2.2.13.2   Analysis of bending stresses induced in elongates

The loading conditions discussed in the latter part of the previous section can be found underground. Ride will cause a relative displacement (Δ) between the ends of the timber elongates, and the weight of the rock mass being supported by the elongate, will cause an axial load (P). Thus, timber elongates (of which one or both ends are clamped) are subject to both axial compressive loads and bending loads, and are thus referred to as beam-columns.

2.2.13.3   Timber design

The design procedure discussed here is based on the method outlined in SABS 0163-1:1994 (As amended in 1997) – The structural use of timber, Part 1: Limit-states design.

This design method is widely used in the design of structural timber members in the civil engineering industry. A simplified version of this method is presented here to illustrate some concepts.

Factors affecting strength and resistance

Certain factors cause a reduction in the strength of the timber. These factors must be taken into account during the design of timber elements.

ϕ – Resistance factor
A resistance factor is applied to a specified material property or to the resistance of a member, and takes the variability of material properties, dimensions, workmanship, type of failure and uncertainty in prediction of member resistance into account for the limit state under consideration.

γ_1 – *Partial material factor for moisture content*
Moisture content is defined as the mass of water in a sample of timber, and is expressed in terms of grams of water per kilogram of oven-dry mass of the sample. The strength of timber is determined at a moisture content of less than 180 g/kg. Timber loses strength when the moisture content increases – this is especially true for compression members.

γ_2 – *Partial material factor for pressure treatment*
If timber has been pressure treated with fire retardants, the characteristic strength is lowered.

Other factors used in the design of timber are the partial material factor for load sharing and the partial material factor for stressed volume, but these factors are not applicable here.

Design lengths

Effective lengths of compression members
When compression elements are designed, their effective length, L_e, is used in calculations.

$$L_e = KL, \tag{2.2.84}$$

where K is the effective length factor and L is the length between supports. The effective length factor, K, of a column can be determined using Table 2.2.6.

Table 2.2.6   *Effective length factors for compression members.*

Case	K
Both ends Fixed	0,5
One end fixed, one end pinned	0,7
Both ends pinned	1,0

Slenderness ratio
The slenderness ratio of a compression member is the ratio of the effective length, L_e, to the corresponding radius of gyration, r. The slenderness ratio of a compression member must not exceed 180.

Slenderness value
The slenderness, λ_d, of a compression member is defined by:

$$\lambda_d = \frac{KL}{d}. \tag{2.2.85}$$

where K = effective length factor of column
        L = length of the column between supports
        d = diameter of column

The slenderness value shall not exceed 52.

2.2.13.4   Axial Compression

Table 2.2.7 can be used to calculate the compressive resistance (capacity) of a compression member (if there are no bending moments present in the member). C_r is the maximum load that can be carried by a compression member (axial capacity).

Table 2.2.7   Compressive resistance for round sections.

λ_d	C_r
$\lambda_d \leq 9$	$C_r = \dfrac{0{,}88\phi A f_c}{\gamma_1 \gamma_2}$
$9 < \lambda_d \leq \lambda_{dcr}$	$C_r = \dfrac{\phi A f_c}{\gamma_1 \gamma_2}\left[1 - 0{,}55\left(\dfrac{\lambda_d}{\lambda_{dcr}}\right)^2\right]$
$\lambda_{dcr} < \lambda_d \leq 52$	$C_r = 0{,}3\phi\,\dfrac{AE}{\lambda_d^{1,81}}\left(\dfrac{1}{\gamma_1 \gamma_2}\right)$

where:

A =   cross-sectional area

f_c =   characteristic compressive strength

γ_1, γ_2 =   material factors described above

E =   elasticity modulus of timber

λ_{dcr} =   critical slenderness value

2.2.13.5   Axial compression and bending

If a member is subjected to both axial compression and bending (i.e. a beam-column), it must be designed so that:

$$\frac{C_u}{C_r} + U_1 \frac{M_u}{M_r} \leq 1, \qquad\qquad (2.2.86)$$

where

C_u Applied axial load

C_r Compressive resistance (axial capacity)

M_u Applied moment (bending moment generated by displacement/ride)

M_r Moment resistance (bending capacity)

U_1 (1) moment magnification factor for a beam-column

From Equation (2.2.86) it is clear that the presence of bending moments will reduce the axial capacity of the member. If no bending moments are generated in the member, the applied axial load can be equal to the axial capacity (compressive resistance). However, should for example, the generated bending moment be a quarter of the moment resistance, the axial capacity of the member is reduced by 25 percent (if $U_1 = 1$).

The design formulae presented in this section are too conservative for use in the mining context, but the principles still apply, i.e. the presence of bending moments in support units (due to ride) will reduce the axial capacity of the elongate.

2.2.14 Pre-stressing

When a pre-stressing device is used, it should be matched to the support unit. This can be done using the results obtained from load shedding tests performed on pre-stressing devices and load-deformation tests performed on support units.

Using the closure rate and the load-deformation curve of the support unit under consideration, the required initial load of the pre-stressing device can be determined, as well as the period over which the pre-stressing device is required to maintain this load.

If the support spacing is based on a support unit load of x kN, and the closure rate is δ mm/day and the support unit only reaches a force of x kN after y mm of deformation, then the pre-stressing device will be required to maintain a load of at least x kN for n days, where

$$n = \frac{y}{\delta}.$$ (2.2.87)

Using the load shedding curves obtained from tests performed on the pre-stressing devices, the suitability of the device can be determined using the above criteria.

Further details of pre-stressing devices, as well as laboratory and underground test data thereof, are given in Chapter 4.

2.3 Underground investigations into block kinematics

2.3.1 Introduction

In Section 2.2 theoretical models were developed to investigate the effects of rotating blocks on elongate performance requirements. It was shown that block rotation can impose high loads on the support system, and the simple tributary area criterion is not adequate to ensure rock mass stability. Underground observations have confirmed that elongate support systems often fail to support the thickness of hangingwall as calculated by the tributary area theory.

The aim of this section is to investigate the rock mass behaviour in the hangingwall of a panel, and to observe failure mechanisms involving timber elements.

2.3.2 Observations made at FOG sites

Seven FOG sites, at four different mines across the Bushveld Complex, were visited and elongate failure mechanisms analysed. Four of the sites involved the development of an extension fracture from the edge of the face or pillars (see Figure 2.3.1). (Since this mechanism appears to be a common cause of premature mine pole failure, it is discussed in detail in this report).
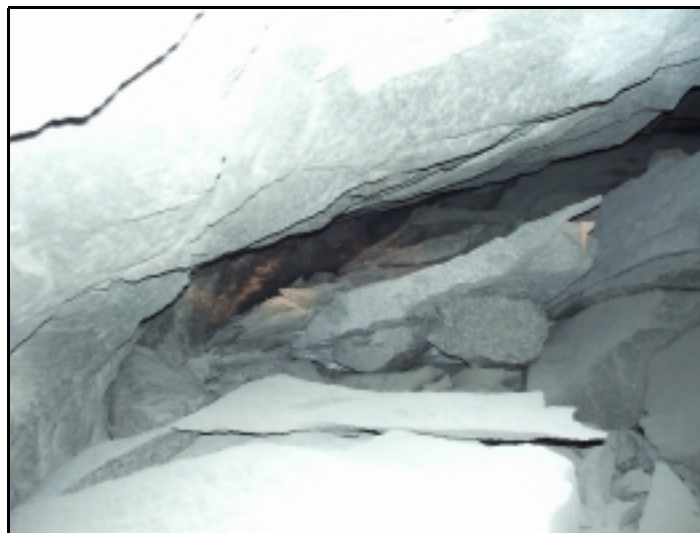
Figure 2.3.1   Photograph showing an extension fracture, which developed from the face and formed the upper boundary of a FOG.

It appears that in localised areas where the tectonic horizontal stress is high, the effect of the abutment and bending of the hangingwall is sufficient to initiate extension fracturing. Conditions at many of these sites indicate that mining proceeded in relatively competent ground without any apparent warning of an imminent FOG, when suddenly fractures developed at an abutment

and a FOG resulted. Joint analyses performed at these sites also indicated competent ground conditions, e.g. Mine B5 (Figure 2.3.2) using the classification system suggested in a previous SIMRAC report, GAP 334 (York *et al.*, 1998). Mine B5 plotted well below the critical line in Figure 2.3.2, thus indicating stable conditions. Note that the classification system given by Figure 2.3.2 does not take into account the orientation of discontinuities relative to the mining direction, i.e. an unfavourably oriented mining layout may actually result in unstable roof conditions, although, according to the critical span design chart, a stable panel span is predicted. Further work is required to modify the design chart and incorporate the influence of discontinuity orientation versus mining direction
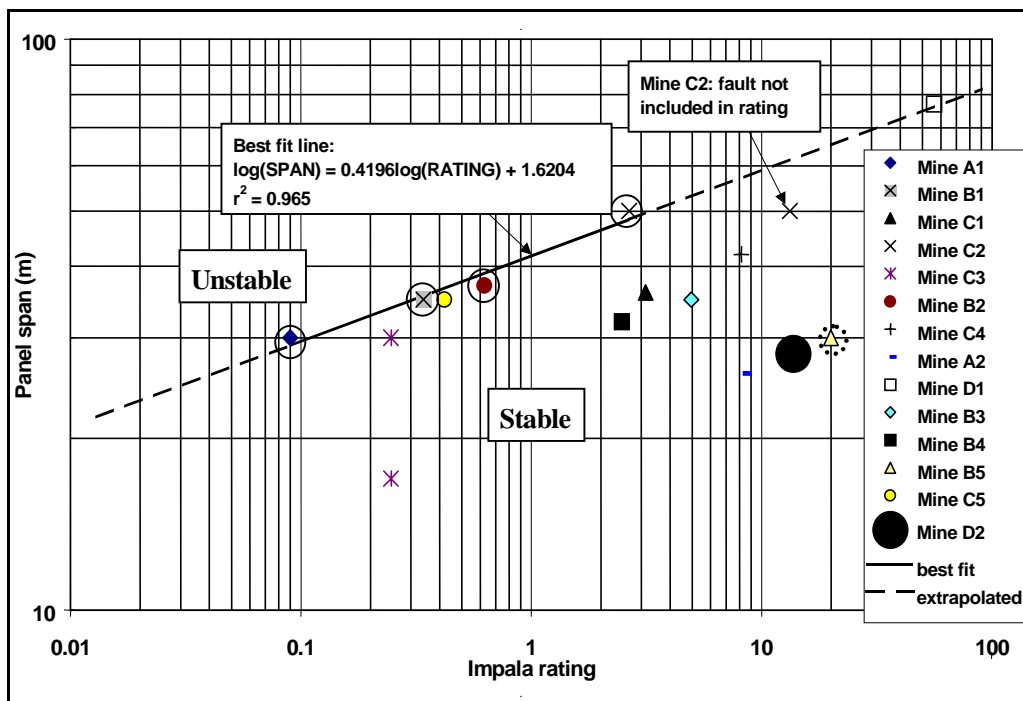
Figure 2.3.2   Critical Span Design Chart (after York et al., 1998).

It appears that either the panels approached a localised zone of high horizontal stress (see Figure 2.3.3) and the fracture developed when the stress in the hangingwall was high enough, or a localised stress condition near the pillars was increased as the span increased, thus developing extension fractures (see Figure 2.3.4). When an extension fracture develops at the face, it is usually during a blast where the unsupported zone at the face could be greater than 4 m (see Figure 2.3.4). The extension fracture creates an unsupported cantilever in this region and appears to extend under the influence of gravity, overloading the first line of support and causing the support to fail progressively, line by line away from the abutment (see Figure 2.3.5). The rotation of the cantilever often appears to have caused the mine poles to buckle in the same direction as shown in Figure 2.3.5. The effectiveness of the support in this instance is dependent on how close the elements can be placed to the face. Reducing the cantilever length not only reduces the burden on the first line of support but also reduces the rotation, which has been shown in Section 2.2 to weaken the elements. Support elements should be strong enough to contain a cantilever, should it form, from the face to the first line of support after the blast.
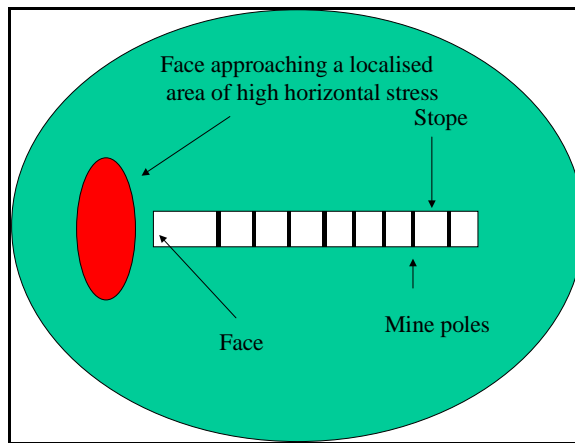
Figure 2.3.3 *Diagram showing the face approaching a local area of high horizontal stress.*
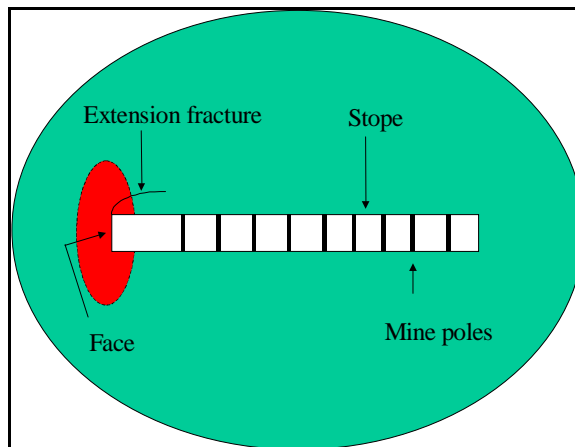
Figure 2.3.4 *Development of an extension fracture from the face.*
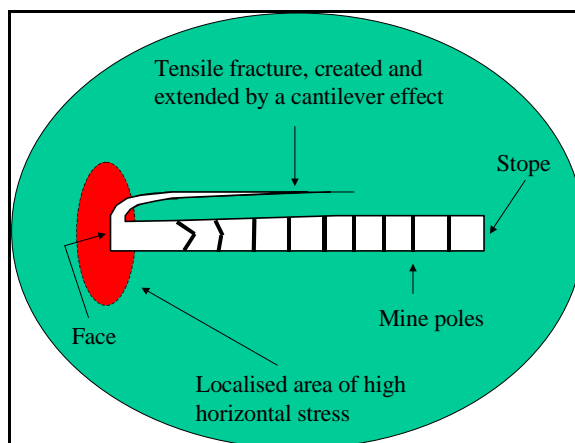
Figure 2.3.5 *Development of a tensile fracture from the extension fracture.*

Oblique loading of mine poles was often observed at FOG sites (see Figure 2.3.6) and it appears that rotation occurred during the FOG. The rotating loading conditions are considered to have reduced the strength of the elements and therefore were investigated and quantified, Section 2.2.

Figure 2.3.6   Photograph showing oblique and rotational loading of elongates.

In highly jointed areas, key blocks have been observed to fall out between support elements causing loosening of the hangingwall and resulting in other blocks falling around the sticks (see Figure 2.3.7). The surfaces of most discontinuities appear to be fairly rough and undulating, usually with amplitudes greater than 15 mm over a measured length of 1 m. Therefore, interlocking should occur on steeply dipping joints prohibiting blocks from falling out, until a key-block dislodges. This finding suggests that mine poles could be suitable for blocky ground conditions, provided that the key blocks were held in place. However, in areas where shallow dipping discontinuities exist, mine poles alone are not adequate. In these situations support systems offering high levels of areal coverage are required (e.g. mine poles with large headboards, strapping between adjacent mine poles, tendons with large base plates).

Figure 2.3.7   Photograph showing blocks fallen around a support element.

Rotational and oblique loading that occurs after a key-block has fallen out is shown in Figure 2.3.8. This appears to occur when there are persistent bedding parallel discontinuities or relatively high stresses in the immediate hangingwall.

Figure 2.3.8   Photograph showing cantilever-type block rotation.

One of the panels that were used to test the behaviour of mine poles collapsed during the programme and investigations were made to determine the mechanism. The panel face was about 50 m behind the down-dip panels and extensive mining had taken place up-dip. Several dykes intersected the panel, one of which was almost parallel to the reef strike at the top of the panel. It appears that the relatively faster daily closure rate could have been attributed to slip on this discontinuity. At the time of failure opening of discontinuities and rotation of the mine poles (see Figure 2.3.9) occurred at the centre of the panel on one of the dykes. An increased closure rate was measured 24 hours before the collapse occurred and the collapse lasted for three days. Horizontal fracturing interacted with the jointing to form a range of block sizes, most of which were less than 1 m. A breaker line of matpacks contained the FOG in the immediate region around the packs with about 0,5 m closure, i.e. in this case mine pole support was not sufficient to keep the panel open but a stiff pack support was effective in arresting the hangingwall collapse.

Figure 2.3.9   *Photograph showing the rotation of support elements during a collapse.*

After having visited numerous FOG sites, it was concluded that hangingwall behaviour is not well understood and that there was a need for instrumentation. Therefore, the site at Impala Platinum Mines, used for an investigation in GAP 334 (York et al 1998), was extended to observe the stress condition in the immediate hangingwall during mining. Some of the results appear to confirm the existence of localised pockets of high stress, which could result in the development of extension fractures as shown in Figure 2.3.3 to 2.3.5. A brief summary of the findings made before, during and after mining is given below.

2.3.3 Results of the instrumentation site at Impala Platinum

2.3.3.1 Site description

The instrumentation was installed near the face, at the centre of a proposed panel, after the panel was ledged to a span of 12 m (see Figure 2.3.10 and Figure 2.3.11). Permanent doorstoppers were installed at the same positions as the field stress instruments, to measure stress change as mining progressed to a final strike span of 48 m. Stoping on the South West side of the centre gully had taken place prior to the instrumented panel being mined while the panel immediately up-dip was mined concurrently, but ahead of the panel.
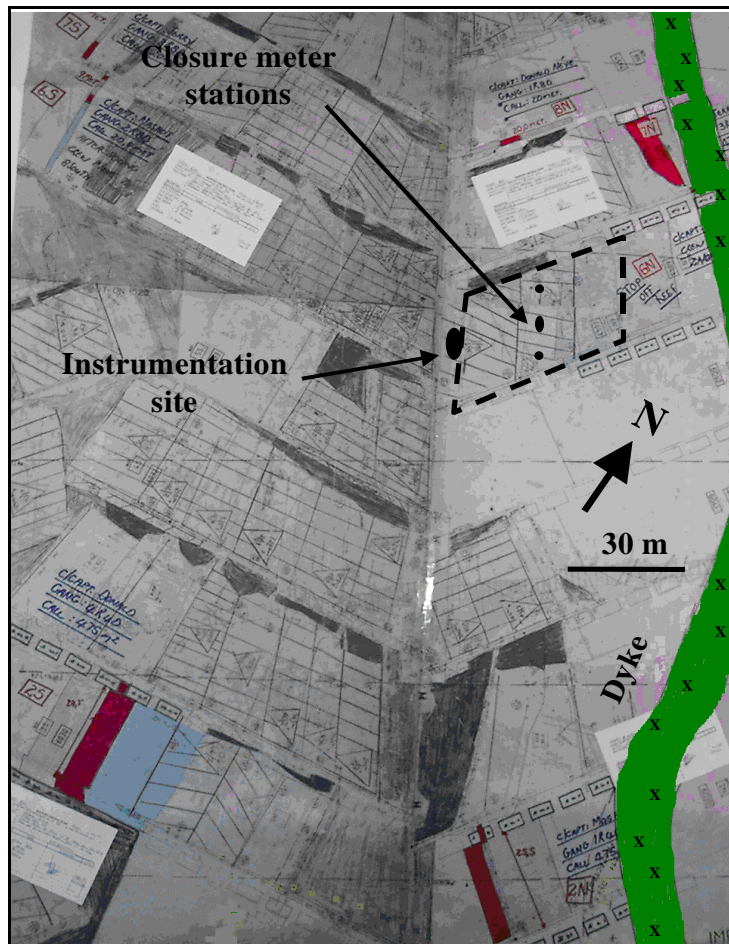
Figure 2.3.10   Stope sheet showing the instrumentation site.
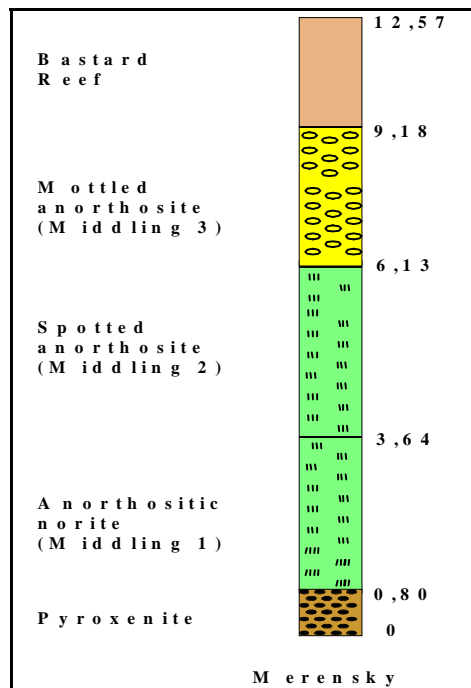
Figure 2.3.11   Stratigraphic column above Merensky Reef.

2.3.3.2 Instrumentation installations

Horizontal field stress measurements were performed using doorstoppers at several depths into the hangingwall. In addition to the stress monitoring, load measurements were made on timber props, an extensometer was installed to a depth of 20 m (which enabled monitoring of the rock mass movements within the hangingwall) and a 10 m hole was drilled for borehole camera observations (see Figure 2.3.12). (Figure 2.3.11 shows the geology in the hangingwall at the site of the borehole camera hole). Closure-ride meter stations were installed to measure closure in the panel, before and during mining. Laboratory rock tests were conducted on some of the core to determine the elastic constants, parameters used for analysing the field stress measurements.
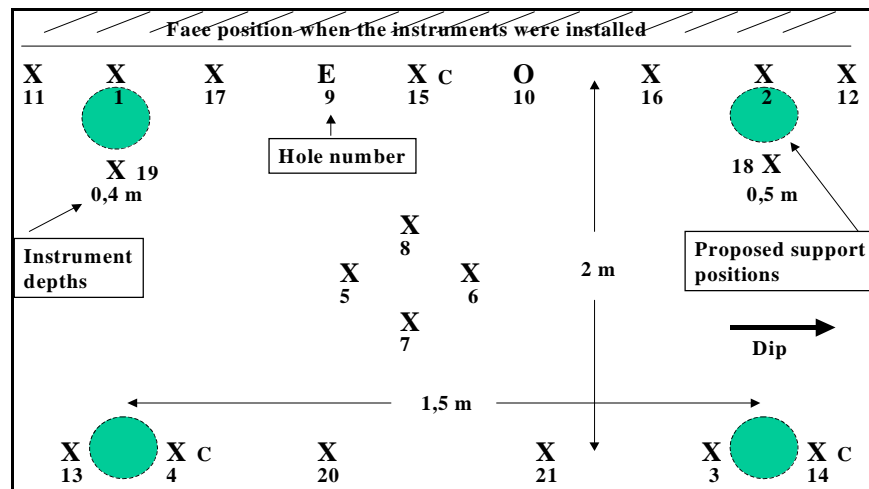
Figure 2.3.12   **Plan showing the positions and depths of the proposed stress measurements (X), closure meter stations (C) and the holes for the extensometer (E) and observation (O).**

2.3.3.3 Joint survey

A joint survey was performed to observe if there was any interaction between the joints and observed rock mass conditions during mining. Weighting of the joint data resulted in a rating of just over 10 (York *et al.*, 1998).

The plot of this data on the chart (Figure 2.3.2) was well below the critical line suggesting that the instrumentation site should have been stable. However, horizontal fracturing up to a depth of 2,57 m was observed in the hangingwall after mining had taken place. Large "inelastic" deformations were measured on the extensometer (Figure 2.3.15), which indicated that the site was unstable. A few of the vertical joints opened slightly near the centre of the panel but generally the joints appeared to remain closed.

2.3.3.4 Instrumentation results

Field stress measurements

Figure 2.3.13 shows the horizontal compressive field stress at various depths into the hangingwall, at the ledging stage of the panel development. Generally there was an increase of stress with depth but measurements in one of the holes showed the opposite trend. This reading indicated a variation in stress conditions across a discontinuity and confirmed the possibility of localised stress zones existing between some discontinuities. These conditions could be an explanation for the observed extension fracturing described in Figure 2.3.3 to Figure 2.3.5.
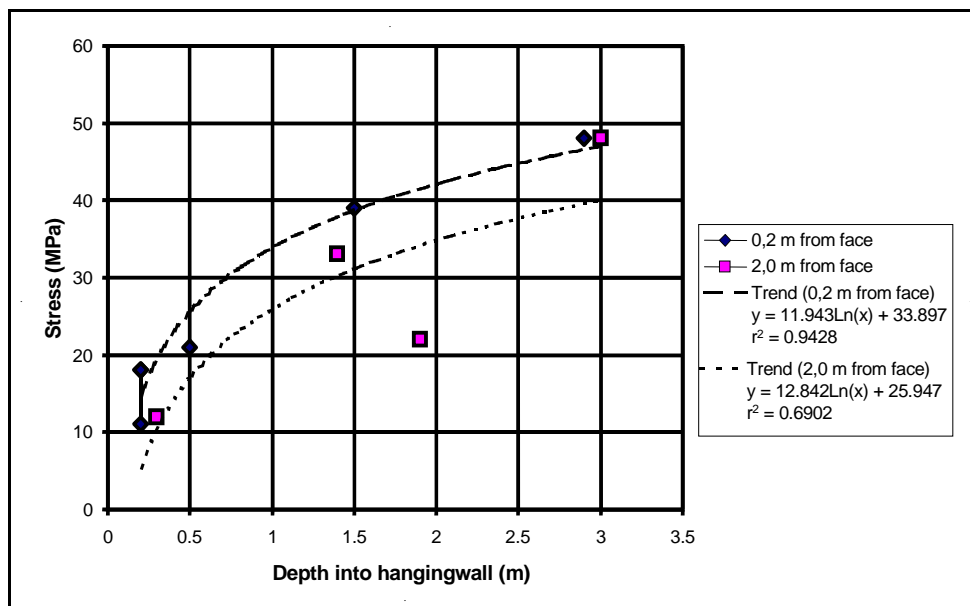
Figure 2.3.13   Horizontal compressive field stress measurements in the hangingwall of a panel, when the panel was at the ledging stage.

Stress change results

All the stresses decreased rapidly to zero during the first few metres of face advance. This phenomenon has been observed at other instrumentation sites and indicates that the sub-vertical joints in the immediate hangingwall are not clamped and therefore only held together by the roughness of the joint surfaces and cohesion of the in-fill material. Some of the stations recorded a sudden increase in compressive stress at a span of about 23 m (see Figure 2.3.14). The reason for the sudden peak is not yet understood, but is believed to be responsible for the observed horizontal stress fracturing in the hangingwall (discussed in previous section).
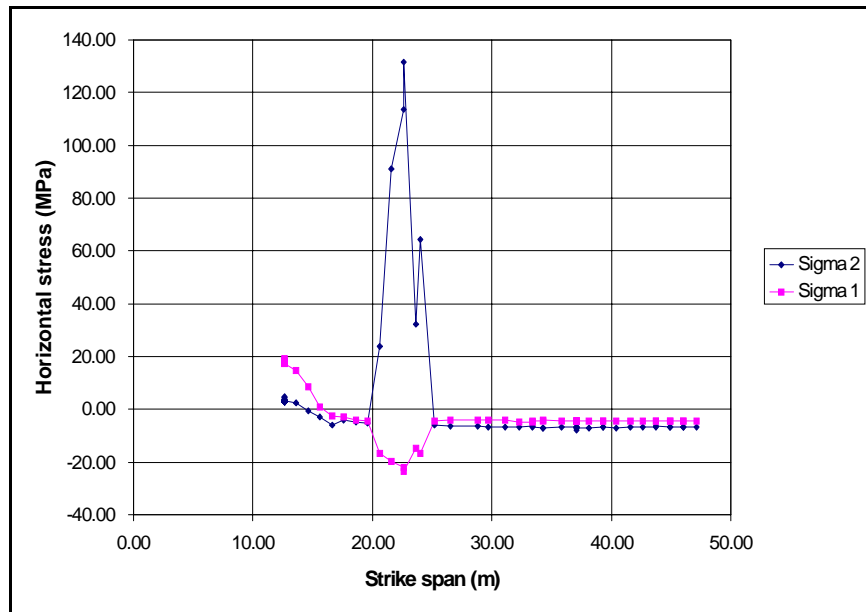
Figure 2.3.14 *Horizontal stress measurements made in hole 19 - showing the stresses which could have been responsible for the extension fracturing.*

Extensometer results

An extensometer was installed in the hangingwall amongst the first line of stress measuring instruments (see Figure 2.3.12). During the first blast, the extensometer was damaged, but in such a way that readings taken after it was repaired were not influenced (Figure 2.3.15.) Unfortunately, almost all the deformation occurred during the period that readings could not be taken.

The results indicate that parting occurred up to 10 m into the hangingwall, with the greatest vertical deformation having taken place between 2 m and 3 m.
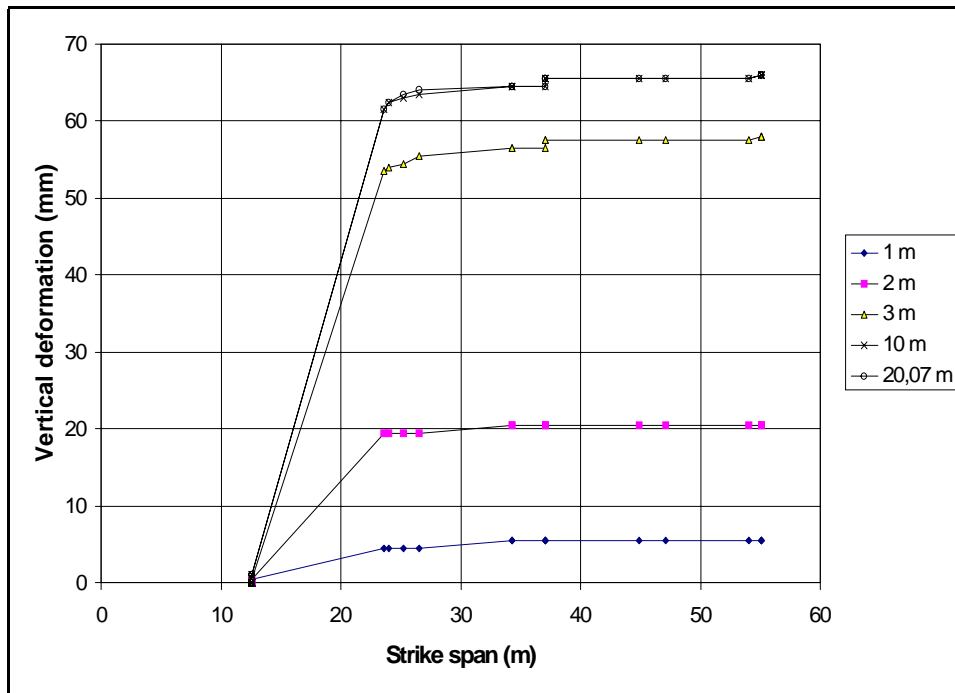
Figure 2.3.15   Extensometer results showing vertical hangingwall movement.

2.3.3.5 Visual observations made at the instrumentation site

At the ledging stage, dog-earing was observed in holes 10, 16, 2 and 12. In most of these holes, the dog-earing occurred between the depths of 0,3 m and 0,5 m, but in the observation hole it extended from 0,4 m to 1,15 m. None of the other holes were dog-eared even though some were drilled at the same distance from the face and at about the same time. This observation appears to confirm the existence of localised high stress zones within the rock mass.

At the end of the project, when the face had advanced 36,2 m, horizontal shear fractures were observed in all the hangingwall boreholes, where observations were possible, at depths of 0,62 m, 1,35 m, 1,52 m and 2,57 m. These discontinuities were not observed at the start of the project nor in the borehole core from the holes and are therefore considered to be fractures. The fracturing appears to explain the results shown in Figure 2.3.15. There appears to have been a different mechanism at this site to the cantilever effect observed at many of the FOG sites, as described above, and there was no FOG involved. The mechanism involved with the development of the high horizontal stresses shown in Figure 2.3.14 and the fracturing is not yet understood, but appears to occur only in the deeper (or relatively high stress) mining areas.

The greatest shear movement on the observed horizontal fractures was about 4 mm at 2,57 m. The vertical opening at this parting was about 6 mm. In the region of the borehole shown in Figure 2.3.16, the rock mass below the plane was relatively displaced away from the pillar on all fracture planes. The mechanism for the shearing appears to be explained by bending beams. The observed displacements at 2,57 m match the results of a simply supported beam model as shown below.
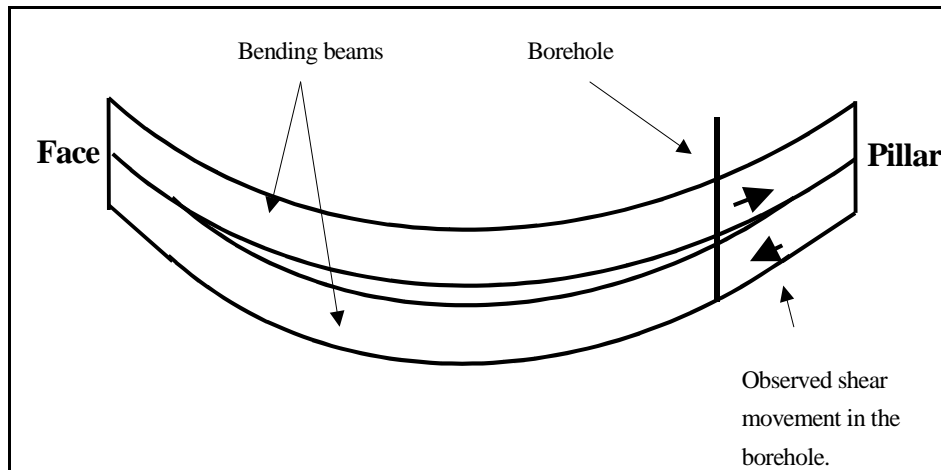
Figure 2.3.16   Bending beam model to explain observed horizontal shearing in the vertical boreholes.

2.3.4 Modelling results based on the instrumentation site

2.3.4.1 Simply supported beam model

The civil engineering formula for a simply supported beam (Equation 2.3.1; Roark & Young, 1975) was used to determine the probability of the observed parting at 2,57 m, being part of a beam extending over the dip dimension of the panel. This equation assumes that vertical cracks or joints have opened adjacent to the pillars and abutment, thus accounting for the maximum elastic deflection that could occur in the centre of the panel. The equation estimated a 7 mm deflection and a 6 mm parting was observed. The extra millimetre that was calculated can be accounted for by the elastic convergence of the rock mass above the parting, which acted in the same direction as the deflection, thus reducing the observed parting.

$$Y_{Max} = \frac{-5W_a \times l^4}{(384 \times E \times I)}$$

(2.3.1)

Where Y_{Max} = Deflection = 7 mm; W_a = Weight of material in beam per metre in the dip direction ($\rho\,g\,h$) = 77,1 kN; l = Dip span = 28 m; E = Young's Modulus = 63 GPa; $I = (^1/_{12})$ b h^3; b = Unit length in strike direction; and h = Height of the beam.

2.3.4.2 MINSIM-W

MINSIM-W modelling was conducted to simulate the results shown in Figure 2.3.13 before the ledged stope was mined and to estimate the theoretical horizontal stresses after mining the panel. The modelling result (Figure 2.3.17) correlated well with the initial field stress

measurements, but not with the stress changes after the panel was mined. The rock properties used in the MINSIM model correspond to those measured in the laboratory on a representative rock sample (Young's Modulus = 56,6 MPa and Poisons ratio = 0,11).

A comparison between the MINSIM-W results and the stress measurements showed that, initially, when the excavation was small, the rock behaved in a quasi elastic mode and creep occurred very slowly. Once significant face advance had occurred, the behaviour became more inelastic. This was confirmed by the extensometer (Figure 2.3.15) and the horizontal fracturing.
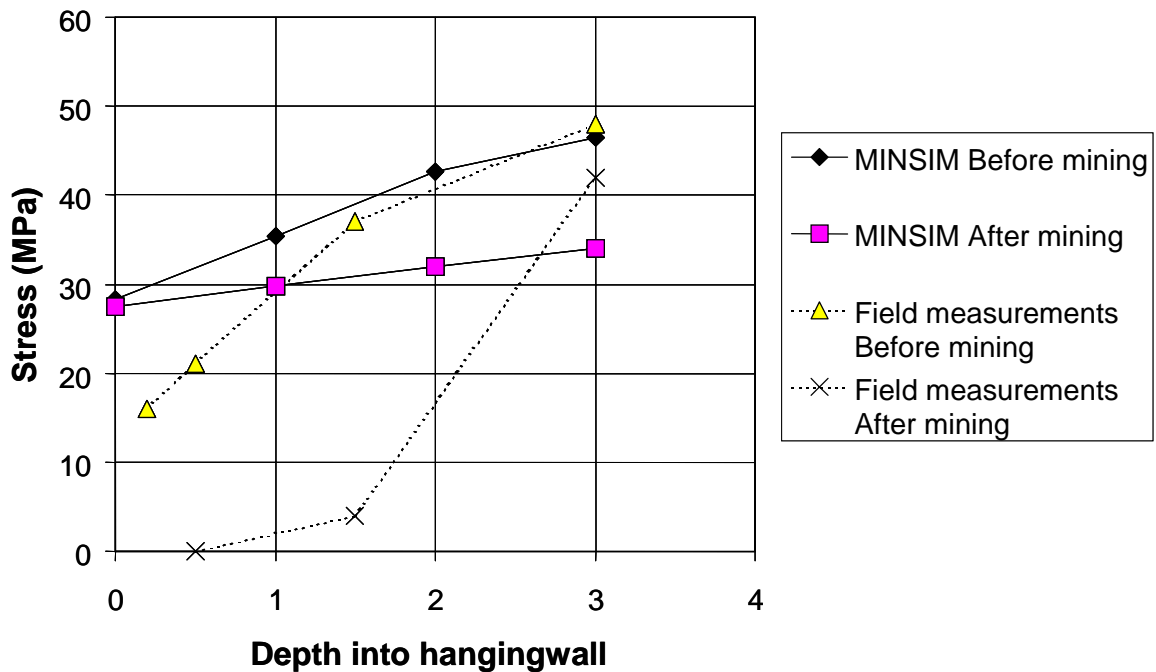
Figure 2.3.17   MINSIM-W simulation and underground measurements showing horizontal stress in the hangingwall of a panel at a depth of 1000 m at Impala 1 shaft, using a k-ratio of 1,8.

2.3.4.3 ELFEN modelling

A simple 2D, plane strain model was developed using the data from the instrumentation site to determine the possibility of horizontal extension fracturing and under what conditions such fracturing could develop. The model was constrained horizontally along the left-hand boundary, and constrained vertically along the lower boundary. Gravity acceleration was applied to the entire model. Loads were applied as initial stresses within elements, and as pressure loads along the free boundaries.

A rotating-crack non-linear material model was employed. The principal direction of softening (and subsequent cracking) for this model is normal to the major principal stress. Laboratory derived material properties for the instrumentation site were applied and a fracture-energy of 500 J/m^2 was specified. Discrete fracturing was permitted along element boundaries.

The model predicted that multiple tension fractures could have developed in the hangingwall if the panel was mined into a zone of material with a higher modulus, such as a "hard patch" (see the multiple step excavation in Figure 2.3.18). A horizontal fracture also developed without a

77

zone of higher modulus material, but an unrealistic, single step excavation had to be used in this case (see the instantaneous excavation in Figure 2.3.18).
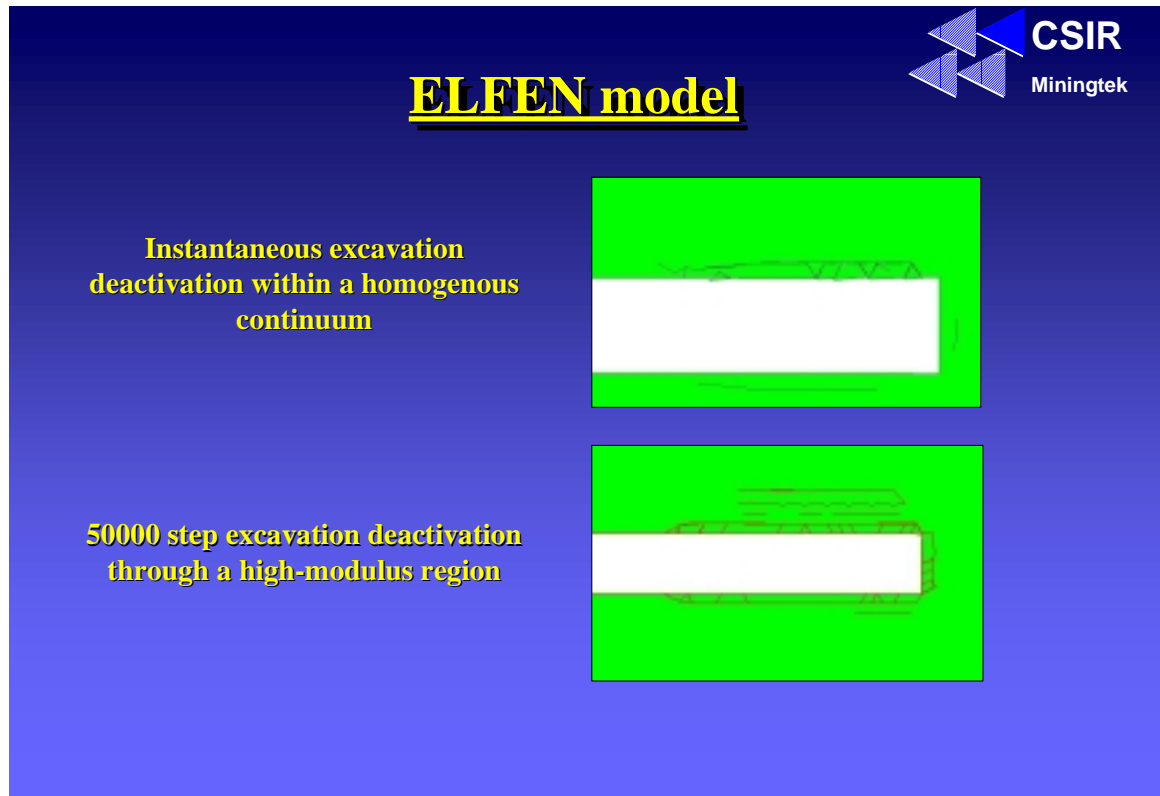
Figure 2.3.18   Results of the ELFEN model to simulate horizontal fracturing.

2.4 Conclusions

As mentioned before, the present design methodology in South Africa is based upon the tributary area concept, where a keyblock is considered to be stable if the resultant support force acting on it is equal to the weight of the block. This simple concept takes care of the equilibrium requirements in a rudimentary sense, but it does not adequately address the fact that the rock being supported is likely to be fractured and jointed and blocks may have the ability to rotate and thus apply additional loads to the support. The work done in this section has shown that, in these circumstances, the distribution of the support elements is of paramount importance.

Theoretical analyses of the kinematics of hangingwall blocks and their support requirements have indicated the following:

- In areas where rotational failure of keyblocks is possible, the resultant support force required to stabilise a keyblock is increased by a factor, k.

- The probability of blocks failing by rotating out of the hangingwall of a stope depends on the shape of the block. Blocks with shallow dipping sides rotate more readily than blocks with steeply dipping sides.

- An increase in the support capacity reduces the probability of keyblock rotation. However, even if the support capacity exceeds the weight of the block by a large factor, the probability of rotational failure is still high if a block is only supported by a single support unit.

- If a keyblock is supported by multiple support units, the probability of rotational failure is reduced, even if the combined capacity of the support units is only slightly greater than the block weight. This is because the resultant support force and the centroid of the block move closer to each other as the number of support units per block increases.

- An increase in the spacing of support units has a detrimental effect on the probability of rotational failure. When the support spacing is increased to approximately the block edge length, the probability of rotational failure increases rapidly. The probability of rotational failure reaches a maximum when the support spacing is approximately equal to the longest edge of the block. If the spacing is increased beyond this dimension, the probability remains constant, because failure (block fall-out) between supports becomes the dominant failure mode.

- If the support resistance is kept constant, and the support spacing is increased, the probability of rotational failure reaches a maximum when the support spacing is approximately equal to the block edge length.

- Relatively speaking, smaller keyblocks require a higher support resistance than large keyblocks to prevent rotational failure. Here, small implies that the length of the keyblock is in the same order as the spacing between support units, and large means that the

length of the keyblock is several times larger than the support spacing (for constant fallout thickness).

- For typical joint distributions in the Bushveld Igneous Complex, the near vertical joints do not represent a hazard in terms of block rotation. It is only when "dome" joints (ie joints that form a pyramidal shaped block) exist, or flatter dipping joints that are typical when the face approaches a pothole, that rotation becomes possible. Analyses of keyblocks representing typical block size distributions in Bushveld mines, which included dome joints, indicated that less than 3 percent of the blocks that failed did so by the rotational mode. In light of this, it is recommended that a better understanding of the statistical distribution of dome joints be obtained, so that their hazard in terms of stability may be better evaluated. In addition, modification of the JBlock software is required to accurately represent the geometry of the dome joints.

- It is prudent to apply the analytical solution for the case where the layout of the supports is parallel to the sides of the keyblocks even where the spacing pattern is oriented at an angle α with respect to the keyblocks.

- The axial loading capacity of elongates will be reduced by the presence of bending moments. These bending moments can be caused by ride or off-centre loading of elongates.

- Pre-stressing devices should be matched to elongates, by using load-deformation characteristics and load-shedding curves, to ensure active support from the time of installation of supports.

Underground observations and instrumentation resulted in an improved understanding of block rotation mechanisms and the implications for support criteria. The salient findings are reviewed below:

- Support elements should be installed as close to the face as possible, to provide for the unexpected development of horizontal extension fracturing in the hangingwall. Furthermore, the support system needs to be strong enough to cater for a cantilever that could develop between the face and the first line of support. Oblique loading of mine poles appears to occur during a FOG or where there are shallow dipping discontinuities within the hangingwall.

- One of the instrumentation sites showed an increase in closure rate before a major FOG, indicating that closure rates could be used as a warning if panels (in susceptible areas) are properly instrumented.

- Horizontal stress measurements suggest that there are no clamping stresses on the sub-vertical joints in the hangingwall (as indicated by the MINSIM model) but measurements made on the joint surfaces show that significant horizontal dilation would have to take place before blocks could fall out. The significance of maintaining the position of key-blocks is thus emphasised. Shallow dipping discontinuities and extension fractures in the immediate hangingwall significantly increase the risk of FOGs by forming

plates (beams) or wedges bounded by these features (the existence of these planes are seldom known). Conditions leading to the formation of extension fracturing have been explored using ELFEN. The model predicted that multiple tension fractures could develop in the hangingwall if the panel mined into a zone of material with a higher modulus.

It is recommended to conduct further underground measurements to quantify the characteristics of the zone with a higher modulus, and attempt to develop techniques for predicting the occurrence of a hard patch. This would facilitate the timeous modification to support systems (e.g. reduced spacing) in order to maintain hangingwall stability during the propagation of the flat-dipping extension fracture.

3 Simulation of loading conditions resulting from block rotation and oblique block movement

3.1 Introduction

The performance of timber elongates is frequently affected by oblique loading, which occurs as a result of improper installation at an unfavourable angle, or due to unpredictable movement of the rock mass. Oblique loading could affect the failure mechanism, ultimate strength, and displacement at failure.

The aim of this chapter is to quantify the effects of oblique loading, as derived from a number of possible sources. This is accomplished by conducting several different kinds of laboratory and underground tests on timber elongates, from which the effects of the oblique loading can be assessed. In order to conduct meaningful laboratory tests, it was necessary to construct a device that is able to simulate the loading mechanisms encountered underground. This chapter describes the testing equipment used and the programme followed in the tests conducted at the CSIR.

3.2 Test rig description

The press used for these tests was originally used to test small wooden packs. The press consists of a frame containing four hydraulic pistons surmounted by an 8 cm thick steel loading plate. In the original press, the loading plate was loosely fitted onto the pistons, allowing little relative displacement between pistons. The rig was modified to allow tilting of the loading plate as illustrated in Figure 3.2.1. A view from beneath the loading plate illustrates the number designations of each piston.

Pistons 1 and 4 are not in direct contact with the plate. Polyethylene skid plates are installed between the piston heads and the plate. The opposite bank of pistons (2 and 3) is bolted to the loading plate as illustrated. All the piston-tops have hinges along the axis indicated. This allows tilting between the clamped piston bank (2 and 3) and the sliding piston bank (1 and 4). Note that tilting between pistons in the same bank (i.e. between 2 and 3) must be limited to avoid the introduction of lateral forces into the platten.
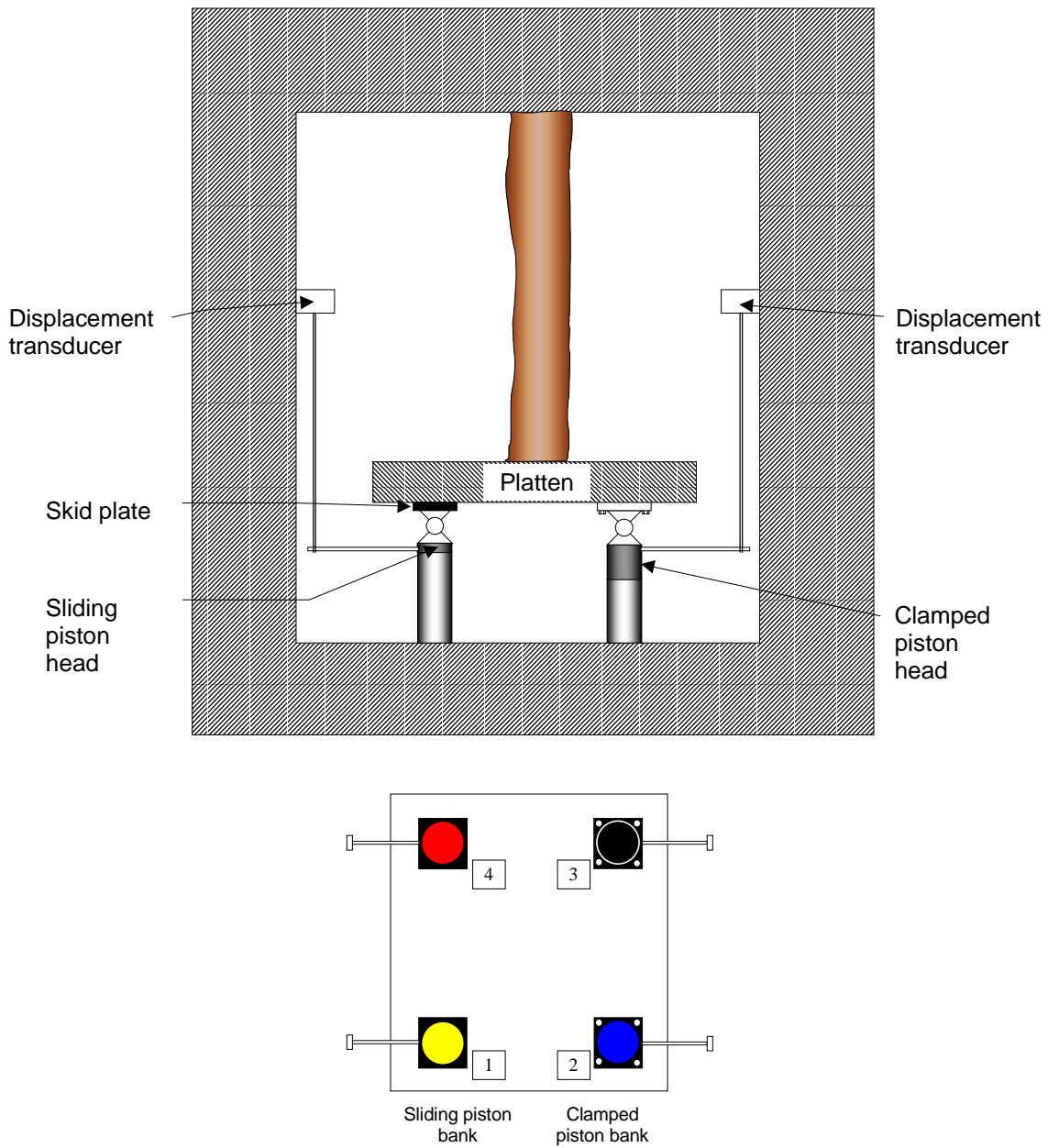
Figure 3.2.1   Rig for oblique testing

Each piston has a pressure transducer connected to its oil supply, thus indicating the load in each piston. The piston tops are connected via a cantilever and a length of wire to displacement transducers. Data from all displacement and pressure transducers are logged on ML microloggers (Digital Data Systems).

Actuation of the pistons is achieved by a pneumatic pulsing system. Air is used to pump oil into the pistons. The relationship between pulse length and achieved displacement is non-linear and dependent on the amount of resistance acting on each piston. This relationship is also different for

each piston. A control programme is therefore necessary to ensure uniform motion of the loading plate.

The control program operates as shown in Figure 3.2.2.
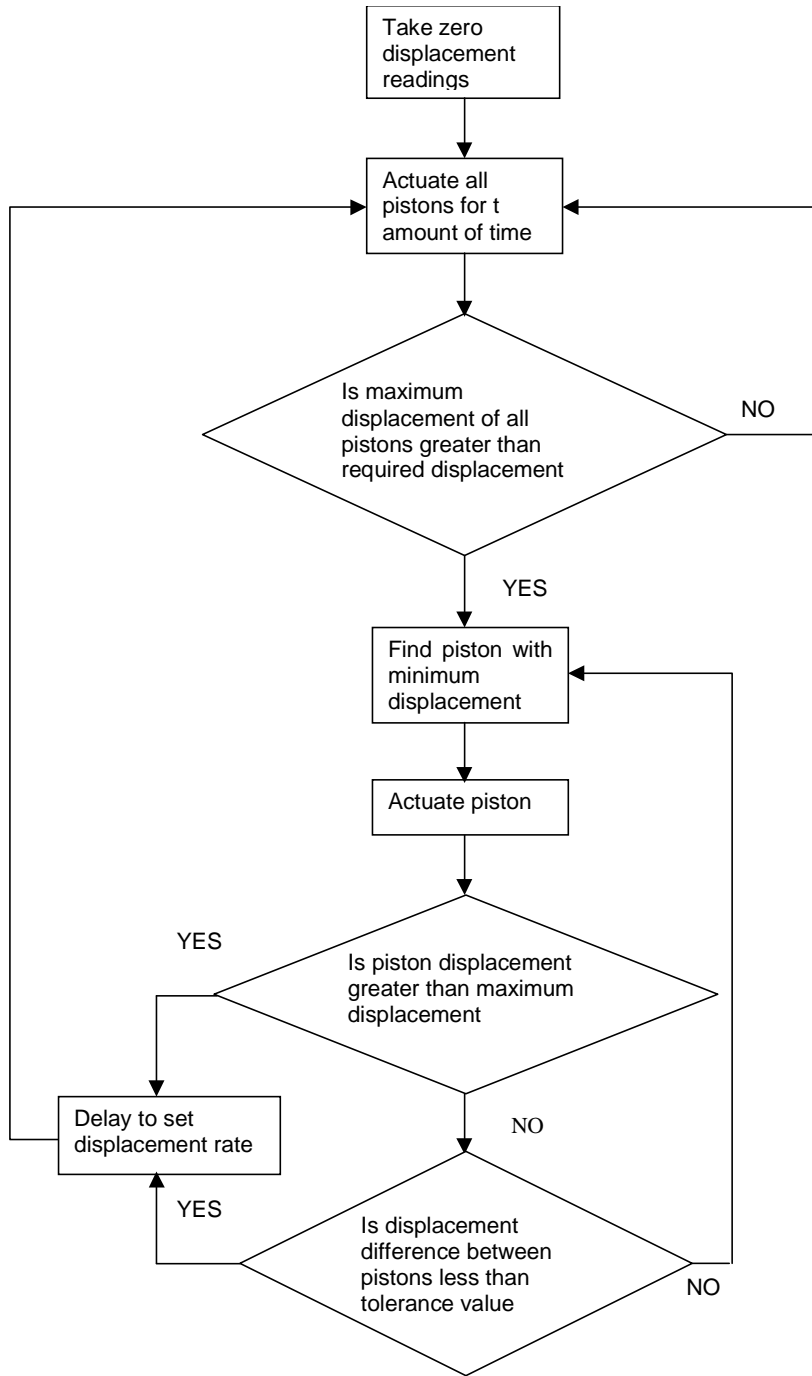
Figure 3.2.2   Operation of control program.

Note that where 'all pistons' are referred to, this may also refer to one bank of pistons. The rotating loading plate tests are performed by moving only one bank while maintaining the position of the other.

The maximum available stroke of the pistons is 450 mm and the maximum length of the test sample is 1,2 m (reduced to 350 mm and 1 m respectively with the hinged piston heads in place.). The distance between piston centres is 320 mm.

3.3 Test programme

The aim of the compression tests was to demonstrate the effect of the oblique installation or loading of timber sticks. The tests must be representative of conditions encountered underground. The following types of tests were conducted:

STRAIGHT/
VERTICAL
TESTS

INCLINED
STICK
TESTS

INCLINED
PLATTEN
TESTS

ROTATING
PLATTEN
TESTS
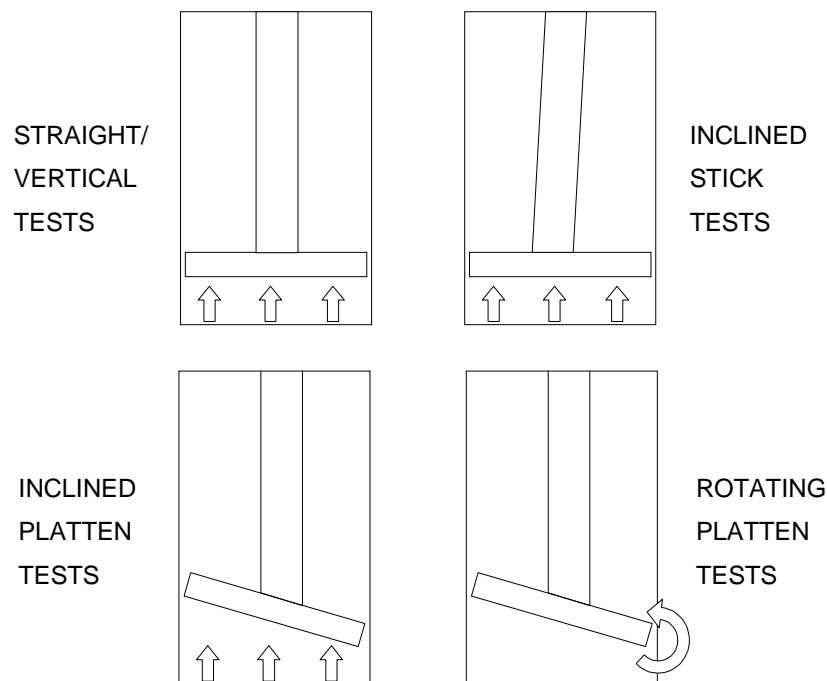
Figure 3.3.1   Illustrations of test types.

These tests were all performed at a relatively rapid load rate of between 1 mm/min and 3 mm/min.

The oblique stick tests represent sticks installed at an angle less or greater than 90^0 to the reef dip. This occurs when the elements are installed vertically into a dipping stope (typically between 10^0 and 20^0 on the Platinum mines). Oblique installation also occurs where elements are installed under local undulations or discontinuities in the hangingwall. The ends of such sticks are usually roughly cut and wedged in place. Installing wedges for the current test programme would significantly increase uncertainties in the system and reduce consistency between results. The ends of the sticks were therefore cut to match the angle of installation.

Oblique loading plate tests and rotating loading plate tests represent the situation where a support unit is installed into a stope where the hangingwall and footwall are not parallel, usually under a localised dipping feature of the hangingwall. In the one case, the feature is assumed to be fixed in the hangingwall and compresses the stick uniformly. In the other case, the feature is assumed to pivot about one edge, simulating a rotating block and represented by rotation of the loading plate. The loading plate is rotated by actuating the 'lower' pistons while the other piston bank remains stationary.

To reduce the scatter of results obtained at the various angles, the ultimate loads obtained may be normalised with respect to the same stick under uniform straight loading. This may be achieved by cutting long poles in two and performing a straight test on the one half, and an angled test on the other half. The result for the angled stick may then be expressed as a fraction of the strength of the straight stick. Normalised results are statistically evaluated along with the raw data.

4   Evaluation of timber elongate performance under rotational and oblique loading conditions

4.1 Introduction

The performance of elongate support is crucial for the maintenance of stable tabular excavations. In particular, timber props or mine poles are both economical and capable of withstanding high loads. The performance of these units is frequently altered or even compromised by oblique loading. This type of loading may arise as a result of improper installation at an unfavourable angle, or due to unpredictable movement of the rock mass. Oblique loading may have the effect of altering the failure mechanism, the ultimate strength, and the displacement at failure.

Rock engineers generally base the design of elongate support layouts on timber strengths derived by downgrading laboratory test results to cater for the difference in loading rates underground and in the laboratory. Many underground observations have, however, indicated that the actual strength of the support units is less than the strengths derived in this way. This has been attributed to the effects of installation angle and rotation during loading. The effects of the angle of installation and oblique loading are investigated underground and in the laboratory and the results are presented here. During the course of the testing programme it became apparent that other factors affect timber performance more significantly than the angle of installation, and this is highlighted in the text.
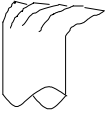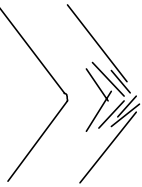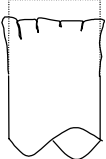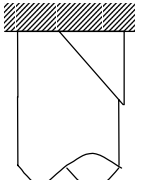
The aim of this chapter is to quantify the effects of oblique loading, as derived from a number of possible sources. Various types of loading are considered and a number of tests performed using a modified pack-testing frame (described in Chapter 3). Laboratory and underground tests are conducted to evaluate various elongates loaded by rotating blocks and oblique block movement. The results from these tests are analysed using statistical techniques and conclusions are drawn from the normalised results.

4.2 Literature review

4.2.1 Sensitivities and failure mechanisms

Roberts *et al.* (1987) conducted an evaluation of the underground and laboratory performance of various elongates. Sensitivities to various parameters were identified and quantified. Various failure mechanisms were described and illustrated. These mechanisms are as follows:

Table 4.2.1   Typical failure mechanisms of timber mine poles.

Failure mode	Description	Illustration
Folding/ Brushing	Bending of wood fibres localised around the point of contact with the platen/rock surface	
Buckling	Column instability failure. Characterised by bowing of the prop and failure of fibres on the tension side. Influenced by length to diameter ratio and the presence of stress concentrations. Buckling may lead to longitudinal splitting of the prop, depending on confinement at the end of the prop.	
Compaction	Crushing due to compression of wood fibres. Props displaying only this failure mechanism have a very high strength.	
Shear	Failure of fibres in a plane between 45° and 90° to the elongate axis. Mechanism is associated with buckling.	

The following factors were found to significantly affect the performance of elongates:

1.   Loading rate

- It was recognised that timber props withstand higher loads at higher loading rates, due to the time-dependent weakening effects of wood creep.

- An empirical table was presented for the downgrading of results obtained at high loading rates to those loading rates, which would be expected underground. For example, forces

from a laboratory test conducted at 30 mm/min are downgraded by a factor of 0,67 to obtain the expected performance of the same prop at an underground convergence rate of 10 mm/day (Roberts *et al.*, 1987).

- The mode of failure of the prop may be affected by the loading rate. It was found that in some cases, the strength of the elongate at low loading rates was higher than that at higher loading rates. Examination of the poles revealed that buckling was more prevalent at the higher loading rate, and that localised folding at the ends of the elongate was evident at the slow loading rate. However, it was also found that in props with notable stress concentrations (e.g. knotholes, large diameter changes) the incidence of buckling was increased at low loading rates.

2. Temperature and humidity

a. The effect of temperature changes on wood strength is described by Banks *et al.* (1976) as follows. '*In general, when the temperature of wood is raised it becomes weaker in most strength properties, and when the temperature is lowered it becomes stronger. This effect is immediate, and its magnitude depends upon the moisture content of the wood during the period of exposure and upon the time of exposure.*'

b. Gerhards (1982) shows that for low moisture content timber the compressive strength parallel to the grain decreases by 10 % if the temperature increases from 20 ^{o}C to 50 ^{o}C, i.e. a 3,3 % decrease in strength in the temperature range of 20 ^{o}C in the laboratory test and 30 ^{o}C, the temperature that can be expected in some stopes (assuming a linear strength versus temperature relationship). The type of support units that would be loaded parallel to the grain would be yielding timber elongates.

c. More substantial is the 20 % reduction of the compressive strength perpendicular to the grain, if the temperature increases from 20 ^{o}C to 50 ^{o}C which is a 6,6 % decrease in strength in the temperature range of 20 ^{o}C in the laboratory test and 30 ^{o}C in a stope. The type of support units that would be loaded perpendicular to the grain is timber packs.

3. Contact

- Tests were conducted on props with an inclined platen, with a stepped platen and with an inclined prop. Note that these tests are not the same as those discussed in this report. The ends of the props were not cut at angles or wedged in place to ensure good contact. The aim with the tests in the literature was to assess the effect of variable contact surfaces, not the effect of inclining the prop or platen.

- Inclined platen (5°): No consistent effect.

- Stepped platen: 23 % reduction in strength for 20 mm step, 59 % reduction for 50 mm step.

- Inclined prop (5°): 40 % reduction in initial stiffness. No consistent strength reduction.

- The surface roughness of the platen was varied, and no consistent effect was observed.

4.   Environment

- The moisture content of props was found to be significant only when the timber was dry (less than 15 % moisture), at which point the props failed by splitting and buckling.

- The presence of high humidity in some stopes in the deeper portions of the South African gold has the potential to increase the moisture content of timber support units, thereby reducing the force-deformation behaviour. However, Turner (1998) is of the opinion that over the length of time that these support units are required in the stope face working area, this effect is not significant and can be disregarded.

- Laboratory testing at various humidities had no effect on the prop, except in terms of increasing the moisture content.

- Fungal invasion had a significant effect on the performance of props, but over such long time periods as to be irrelevant to this laboratory investigation.

The aim of the Roberts *et al.* (1987) investigation was to correlate the load-deformation characteristics obtained underground with those obtained in the laboratory. Laboratory tests were conducted at a relatively high loading rate of 30 mm/min, allowing for comparatively little wood creep. The results from the laboratory tests were hence corrected for temperature and rate effects. It was found that the corrected laboratory results corresponded with those obtained underground, in terms of average performance, and within 95 % confidence limits (described below).

Roberts (1995) reiterated the loading rate dependence of timber props. An expression was presented for the correction of forces obtained from laboratory tests at relatively high loading rates. This equation is as follows:

$$F_{u/g} = F_{lab}\left[m \log\left(\frac{v_{u/g}}{v_{lab}} \right) + 1 \right],$$

(4.2.1)

Where: $F_{u/g}$ is the force corrected for underground loading rates,

       F_{lab} is the force obtained (e.g. from a laboratory test),

$v_{u/g}$ is the underground closure velocity,

v_{lab} is the laboratory test velocity, and

m is an empirical factor ($m = 0,123$ for rockbursts and $m = 0,084$ for rockfalls).

4.2.2 Results processing and interpretation

Results from strength tests on wood with variable properties can contain a large amount of scatter. This scatter must be interpreted and the final result expressed in terms of an average constrained between confidence limits. A statistical method is hence employed to assess the performance of props for different tests. As stated by Daehnke *et al.* (1998), this scatter may be rationalised by obtaining a mean value (μ), a standard deviation (σ) and a probability distribution. A probability distribution is ideally chosen by generating a histogram and then assessing the applicability of a number of possible distributions. For most experimental programmes, as is the case with the current research, a normal probability distribution is selected.

The mean and standard deviation must be calculated at discrete displacement intervals for all the tests being analysed. All of the raw load-displacement data is therefore interpolated such that loads are reported at 0,5 mm intervals. The recorded loads corresponding to these displacement intervals are averaged and the standard deviation calculated.

The 'confidence curves' can hence be calculated as follows:

$$y_i = \mu_i - k\sigma_i ,$$
(4.2.2)

where: y is the load value at displacement interval i and at the confidence level determined by k,

is the mean for displacement interval i,

is the standard deviation for displacement interval i, and

k is a parameter which determines the level of confidence.

A practical interpretation of the confidence curve is that x percentage of samples will perform *at least* as well as the curve predicts. The value of x is determined by the parameter k. For example, if $k = 1$, then the level of confidence for a single support unit is 84 %. This is the case where only one support unit is relied upon to perform according to the curve. Where a number of units make up the support resistance, more units can be relied on and k becomes a function of n – the number of support units. Table 4.2.2 illustrates the relationship between k and n.

Table 4.2.2   ***Values of k for various probabilities and numbers of support units.***

	90 %	95 %	99 %
$n = 1$	1.282	1.645	2.326
$n = 3$	0.74	0.95	1.343
$n = 10$	0.405	0.52	0.736
$n = 30$	0.234	0.3	0.425

4.3 Laboratory test results and evaluation of Minepoles

4.3.1 Sample data

The mine poles tested were obtained from Impala Platinum Mine and had a nominal diameter of 160 mm. The actual diameters of the poles were found to lie between 140 mm and 180 mm, with some significant variations in diameter along the length of some of the poles. Measurements were taken at either end and in the middle of the prop to obtain an average diameter. The mean of all the props tested was found to be 158 mm.

Moisture content tests were performed on a number of samples, yielding a moisture content of between 10 % and 15 %.

The profiles of the props varied considerably. Many of the props had a visible "dog-leg" appearance; some tapered markedly and contained knots and splits. The original condition of all the props was recorded and is presented in Appendix 1. The density of the props was also found to be variable.

The testing program was as follows:

Vertical tests (axial loading):   25 tests

Inclined props: 5 tests at 5^0

                                    5 tests at 10^0

Inclined plate: 5 tests at 10^0

                                    5 tests at 20^0

                                    5 tests at 30^0

Rotating plate: 1 test at 3°

                                    2 tests at 5°

                                    2 tests at 10°

Creep tests: 2 tests monitored for 7 days

4.3.2 Normalisation of results

As stated above, the diameters and profiles of the mine poles vary significantly. To express the results in terms of load rather than stress, the loads are normalised with respect to the average area of all the props (158 mm). This was achieved by converting the loads to stresses (using the measured diameter of each prop) and normalising with respect to the mean area to convert back to loads.

It was found that the control programme could not maintain a consistent load rate for each test, due to the variable amount of time required for the correction phase. The tests were conducted with effective load rates of between 1 mm/min and 3 mm/min. The data is therefore normalised to a load rate of 1 mm/min, using Equation (4.2.1).

4.3.3 Test results at rapid loading rate

4.3.3.1 Results for vertical tests (axial loading)

Twenty five vertical (straight) tests were conducted, two of which were discarded due to erroneous readings. The normalised load-displacement curves for all tests and the resultant mean and 84 % confidence line are presented in Figure 4.3.1.
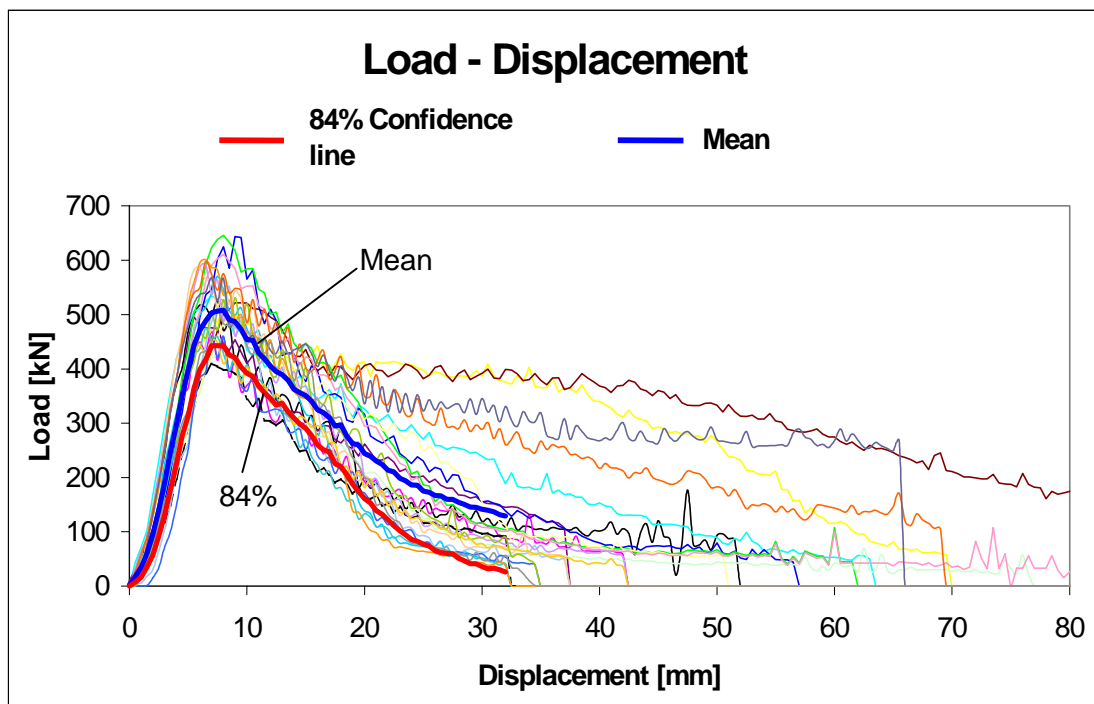
Load - Displacement

Figure 4.3.1   ***Normalised load-displacement curves for vertical tests on 160 mm mine poles.***

It is evident even from the load-displacement curves that different failure mechanisms are involved for different samples. The mean indicates typical behaviour, where peak strength is realised in less than 10 mm deformation and the residual strength is relatively low (< 10 % of peak). This type of behaviour is associated with buckling. In some cases, the mine pole shows post-peak yielding behaviour, where up to 50 % of the peak load can be sustained at over 70 mm displacement. This is indicative of a brushing or splitting failure. Roberts *et al.* (1987) found that in the majority of underground cases, brushing and splitting is promoted by the uneven hangingwall and footwall. The statistical incidence of each of these failure mechanisms is important in terms of predicting prop performance.

Table 4.3.1 presents the failure mechanisms observed in each vertical test.

Table 4.3.1 **Failure mechanisms observed for straight/vertical tests.**

Test number	Failure mechanism	Peak Load	Displacement at 200 kN
10	Buckling	535	32
11	Buckling	496	25
20	Buckling	646	25
21	Buckling	432	21.5
1	Buckling	470	20
13	Buckling	552	24.5
22	Buckling	498	28.5
38	Buckling	586	19.5
36	Buckling	591	20.5
6	Buckling	460	19
31	Buckling	531	22
37	Buckling	505	20.5
35	Buckling	601	18.5
39	Buckling *	598	45
Mean		*536*	*24.4*
7	Buckling with splitting	610	24.5

41	Buckling with splitting	475	18
32	Buckling with splitting	453	19
15	Buckling with splitting	410	17.5
17	Buckling with splitting	570	18.5
Mean		*504*	*19.5*
12	Splitting followed by buckling +	-	-
14	Brushing followed by splitting	522	72
40	Splitting followed by brushing	567	>66
16	Splitting followed by brushing	643	29
8	Shearing and splitting	526	20
3	Shearing and splitting	504	55.5
2	Brushing +	-	-
33	Brushing +	-	-

*   It was found that the fibres had 'bunched' (as opposed to split or torn) at the point of failure, effectively initiating a localised folding-type failure at the centre of the prop.

+   The test results for props 2, 33 and 12 were discarded due to a logger problem.

It can be seen that the greatest displacements are found where brushing and splitting failures were observed. It is also significant that initial splitting leads to a brushing-type failure, whereas splitting associated with buckling is clearly a secondary mechanism that does not significantly affect the response of the unit.

Table 4.3.1 also indicates that there is no obvious correlation between peak loads and failure mechanism. The displacement values therefore identify which mechanism led to the failure of the prop. The displacement values corresponding to post-peak loads of 100 kN, 200 kN and 300 kN were extracted for each test. A cumulative percentage graph is generated, indicating at each point the maximum percentage of props reaching the corresponding displacement at that reaction load. This graph is presented in Figure 4.3.2. Reading from Table 4.3.1, five out of the twenty four recorded tests showed splitting and/or brushing failure. This equates to 21 %, which is indicated on the graph. Note that the 21 % line crosses the load lines at a point where all of them start to show clear non-linearity. This illustrates a clear statistical relationship between failure mechanism and the capability of the unit to sustain load at high displacements.

The initial stiffness of the response of all the props is relatively consistent. An average value of 79 MN/m is calculated with a standard deviation of 16,7 MN/m.

Cumulative Percentage of Displacements Corresponding to Post-Peak Loads
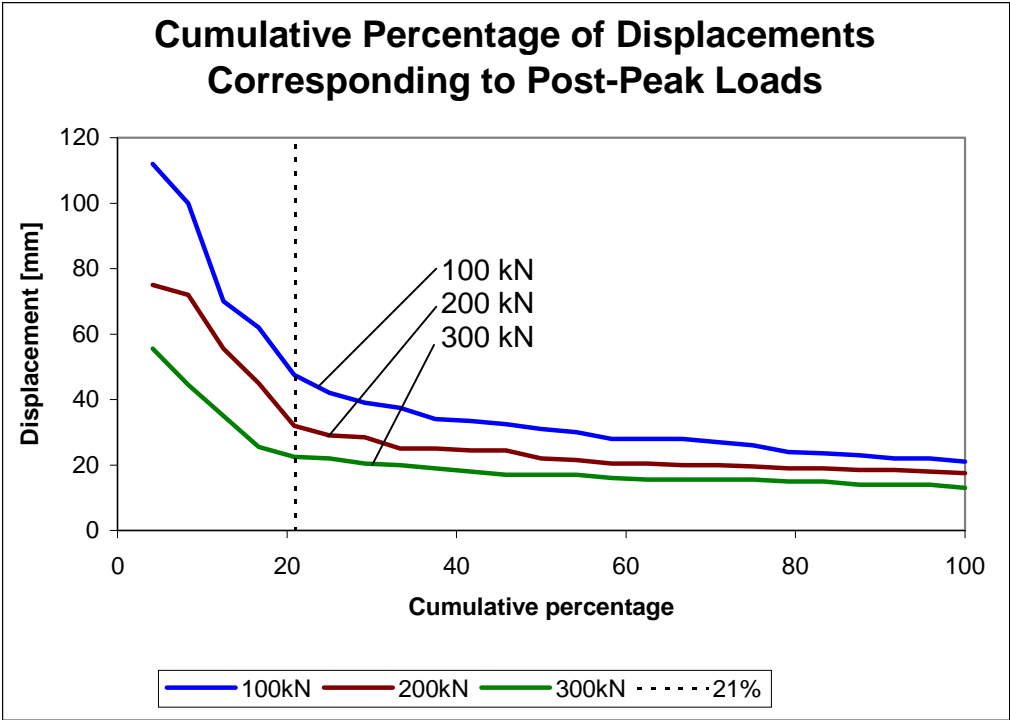
Figure 4.3.2   Cumulative percentages of displacements at various post-peak load levels.

4.3.3.2 Results for inclined prop tests

Four tests were performed with a 5° inclined prop, and four were performed on a 10° inclined prop. The normalised load-displacement curves, with the mean and 84 % confidence curve, are presented in Figure 4.3.3 (5°) and Figure 4.3.4 (10°). Note the different displacement scales.
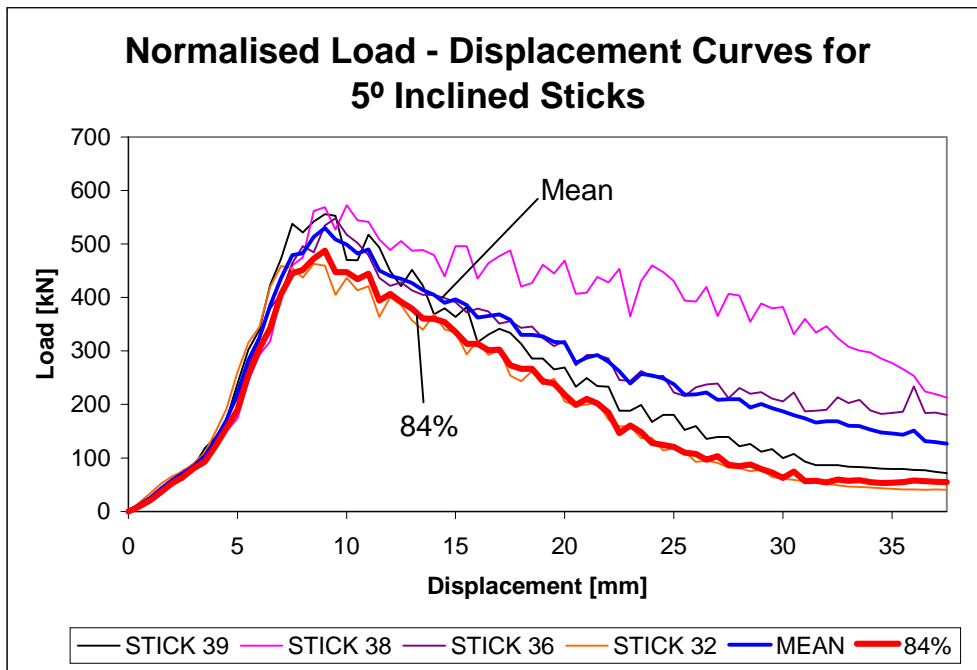
Figure 4.3.3   Normalised load-displacement curves for 5° inclined props.
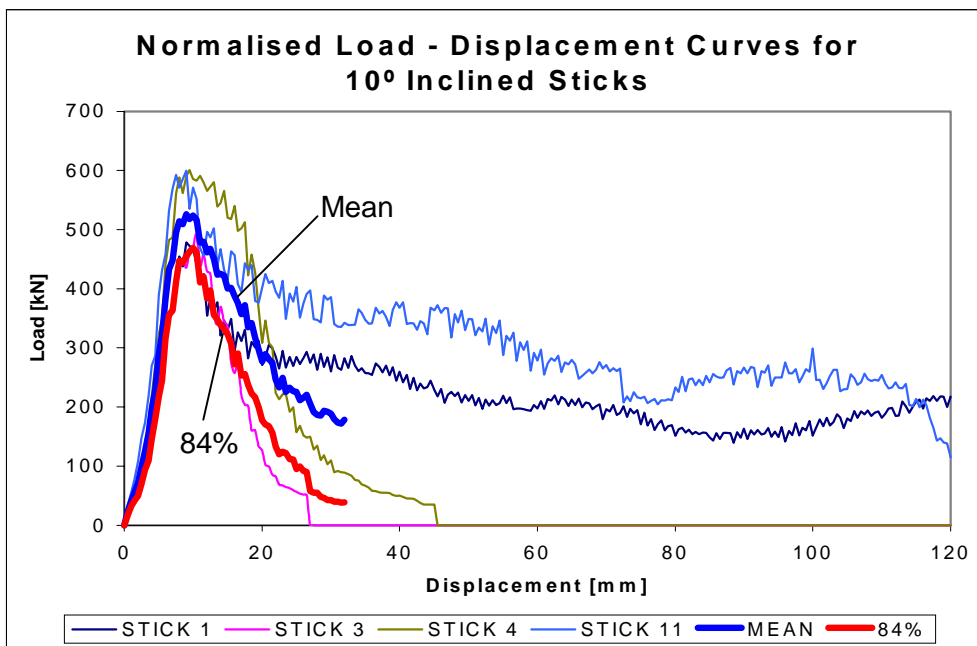
Figure 4.3.4   Normalised load-displacement curves for 10° inclined props.

The failure mechanisms observed are presented in Table 4.3.2.

Table 4.3.2   ***Failure mechanisms observed for inclined prop tests.***

Test number	Angle	Failure mechanism
40	10	Buckling
3	10	Brushing and splitting
1	10	Brushing
11	10	Brushing
32	5	Shearing followed by buckling
39	5	Brushing
36	5	Shearing followed by splitting
38	5	Shearing followed by brushing

There are only two clear incidences of buckling for the inclined props. All the other props failed through a combination of shearing, splitting and brushing. It should be noted that, where splitting resulted in a yielding-type response for vertical tests, shearing is more commonly the cause of a yielding response for the inclined props.

4.3.3.3 Results for inclined platen tests

Five tests were performed with a 10° and 20° inclined platen. The normalised load displacement curves for the 10° and 20° tests are presented in Figure 4.3.5 and Figure 4.3.6 respectively. In addition, three tests were performed with a 28° inclined platen, presented in Figure 4.3.7. All of the props at 10° and 20° failed by buckling. The props at 28° slipped at the platen. It was observed that slipping was accompanied by very loud cracking, indicating a significant release of energy with each slip. The load-displacement curves reflect this behaviour up to 30 mm displacement, at which point all of the props slipped at a constant load.
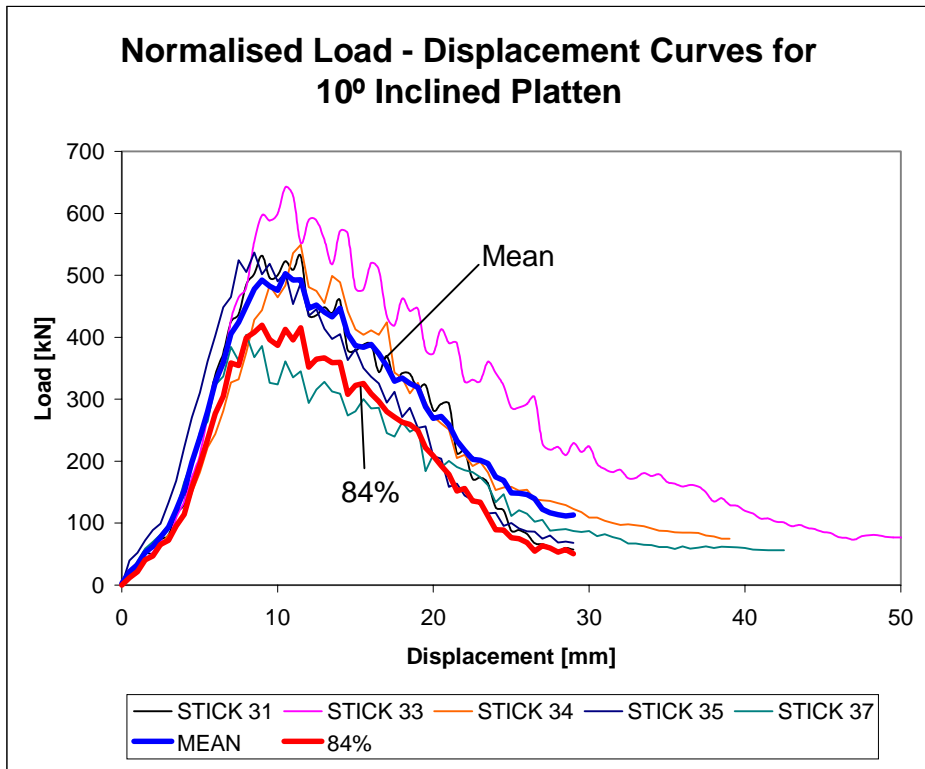
Figure 4.3.5   Normalised load-displacement curves for 10° inclined platen.
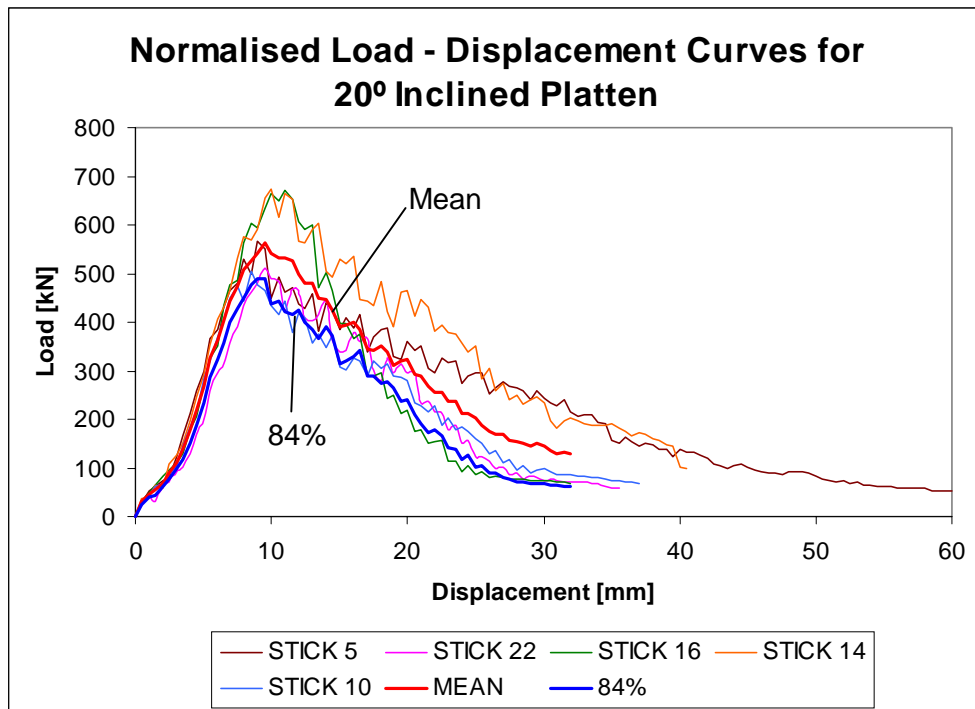
Figure 4.3.6   Normalised load-displacement curves for 20° inclined platen.

154
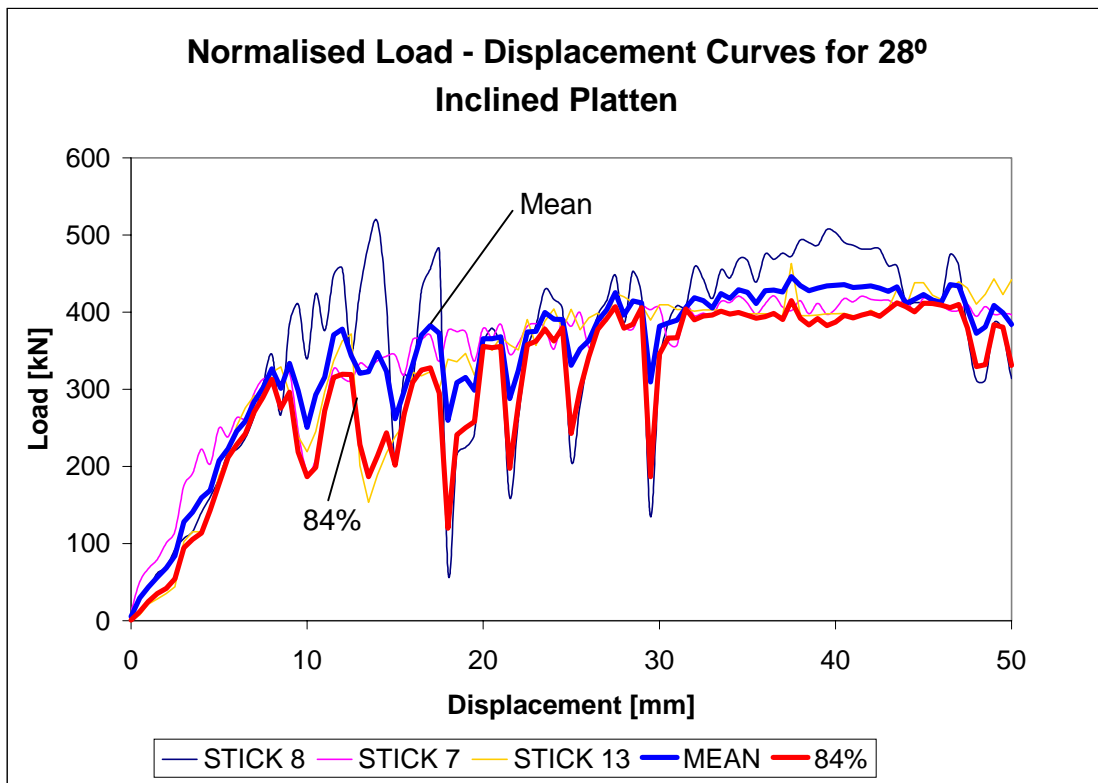
Figure 4.3.7   ***Normalised load-displacement curves for 28° inclined platen.***

The contact between the mine pole and the loading platen may be described by a Coulomb friction relationship.

4.3.4 Results of the tests performed at a slow loading rate

4.3.4.1 Introduction

Axial and inclined platen tests were performed on mine poles with pre-stressing units (pots), to simulate the underground tests performed at Impala Platinum. A deformation rate of 20 mm per day was used in the investigation. The mine poles and the pots were received from the shaft where the underground investigation was made.

4.3.4.2 Test results

Three axial and four inclined platen tests were performed. In each case both ends of the mine pole were cut carefully to ensure contact across the whole surface area and the pot was installed on the top (see Figure 4.3.8).

Figure 4.3.8 **Photograph showing the test set-up for the slow deformation rate tests.**

No quantifiable effect is observed by inclining the platen (as illustrated in Figure 4.3.8) until the onset of slip, which occurs at 23^0. All the tests, where no slip occurred (Table 4.3.3), are therefore included in the analysis and the effect of inclination is discarded.

Table 4.3.3   Results of the slow deformation rate tests.

Test no.	Failure mechanism	Peak Load (kN)	Normalised Peak Load (kN)	Displacement at 200 kN (mm)
Bs0_2	Brushing	584	570	64,5
Bs10_2	Brushing	695	608	63,0
Bs0_3	Buckling	641	554	58,5
Bs0_1	Buckling	453	546	48,5
Bs10_1	Buckling	418	573	27,5

Figure 4.3.9 shows a fairly large scatter in failure loads. However, once these results are normalised with respect to a nominal 158 mm diameter (see Table 4.3.3), this scatter is reduced significantly (see Figure 4.3.10). The failure mechanism has little effect on the peak load but definitely influences the yielding capability.
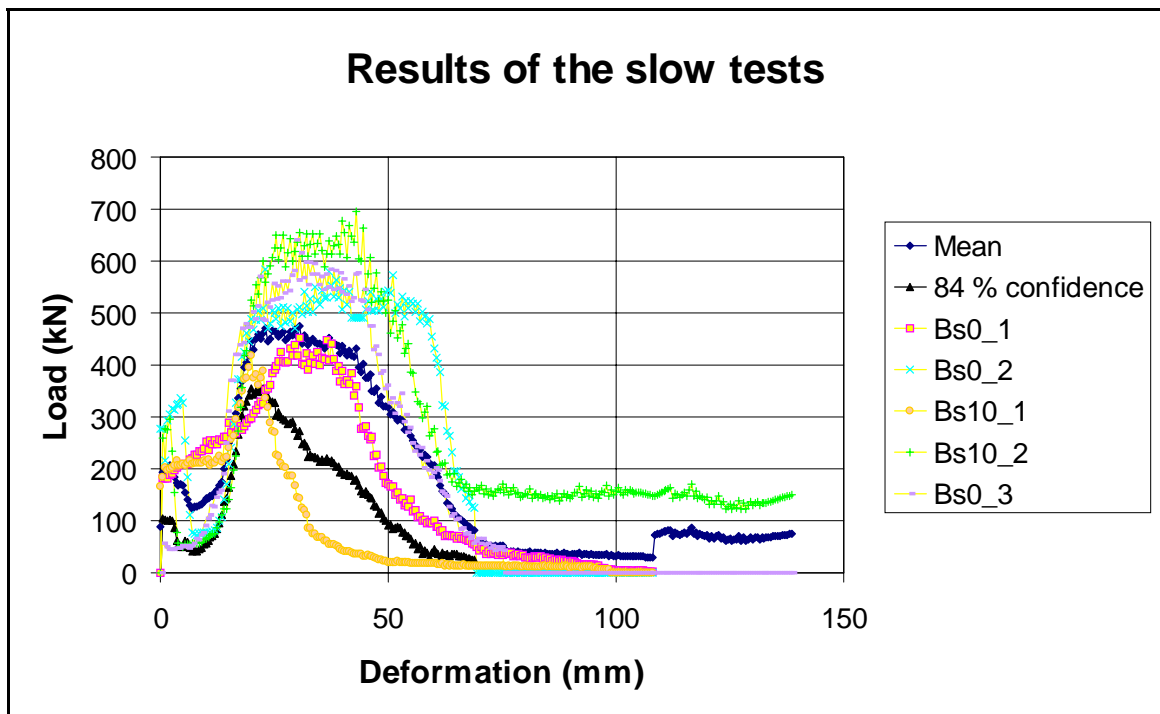
Figure 4.3.9   Load-deformation curves for the slow deformation rate tests.
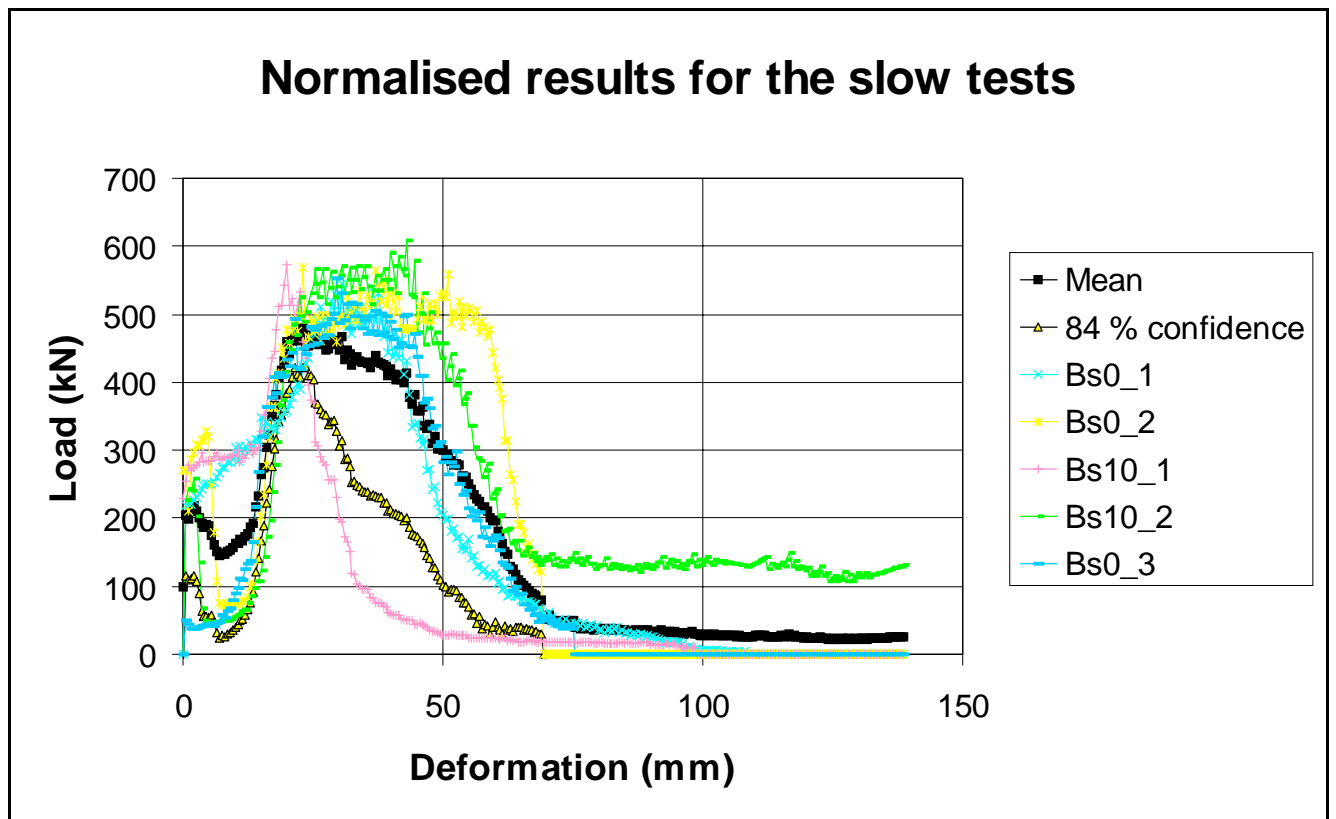
Figure 4.3.10   Normalised load-deformation curves for the slow deformation rate tests.

Two tests were performed with the loading platen inclined at 23^0. Both samples slipped during loading, thus influencing the deformation, but the failure loads were unaffected. The results are shown in Table 4.3.4 and Figure 4.3.11.

Table 4.3.4   Results of the samples tested with the loading platen inclined at 23^0.

Test no.	Failure mechanism	Peak Load (kN)	Normalised Peak Load (kN)	Displacement at 200 kN (mm)
Bs20_4	Buckling	580	566	58.5
Bs20_3	Brushing	651	531	>42.5
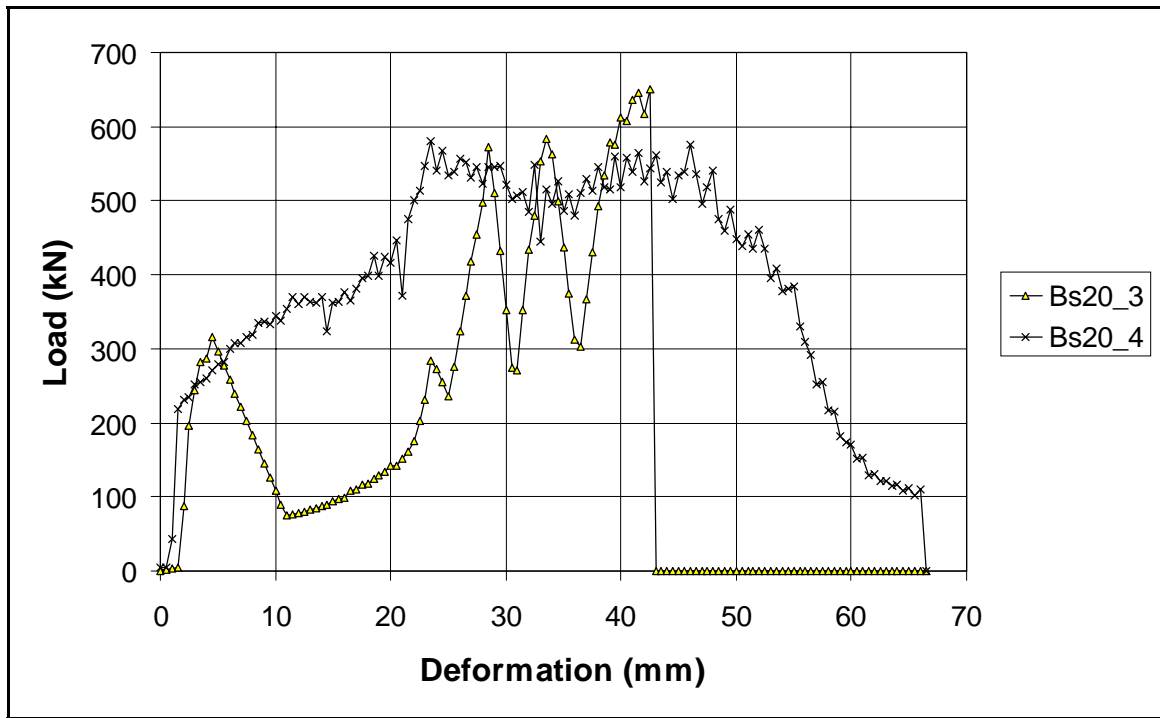
Figure 4.3.11   Results of the slow tests with the loading platen inclined at 23°.

4.3.5 Analysis of the slow test results

The load-displacement curves, mean curve and confidence curves for the slow laboratory tests are presented in Figure 4.3.12. The method by which these curves are obtained is described in Section 4.2.2 and Chapter 3. The dip in load, which occurs soon after installation, is attributed to pot failure that was observed in some of the tests. This phenomenon was observed in three of the five tests presented, hence are included in the mean curve. It should be noted that this only occurs when pot failure is evident – the results for samples BS10_1 and BS0_1 show typical results where the pot has not failed.

Although the drop in load is probably significant enough to allow loosening of some large blocks in an underground situation, complete loss of load was never observed in the test laboratory or underground. The pressure at which the pots burst underground was much lower than in the test laboratory, and the pot deformations resulting from pressure within the pot were greater underground than in the laboratory, indicating the loading condition underground to be much softer. This is most likely due to the fragmented footwall.

In blocky hangingwall conditions, the curve for $n = 1$ (Figure 4.3.12) is appropriate. The peak load for the $n = 1$ result is 69 per cent of the mean and 88 per cent of the normalised mean.
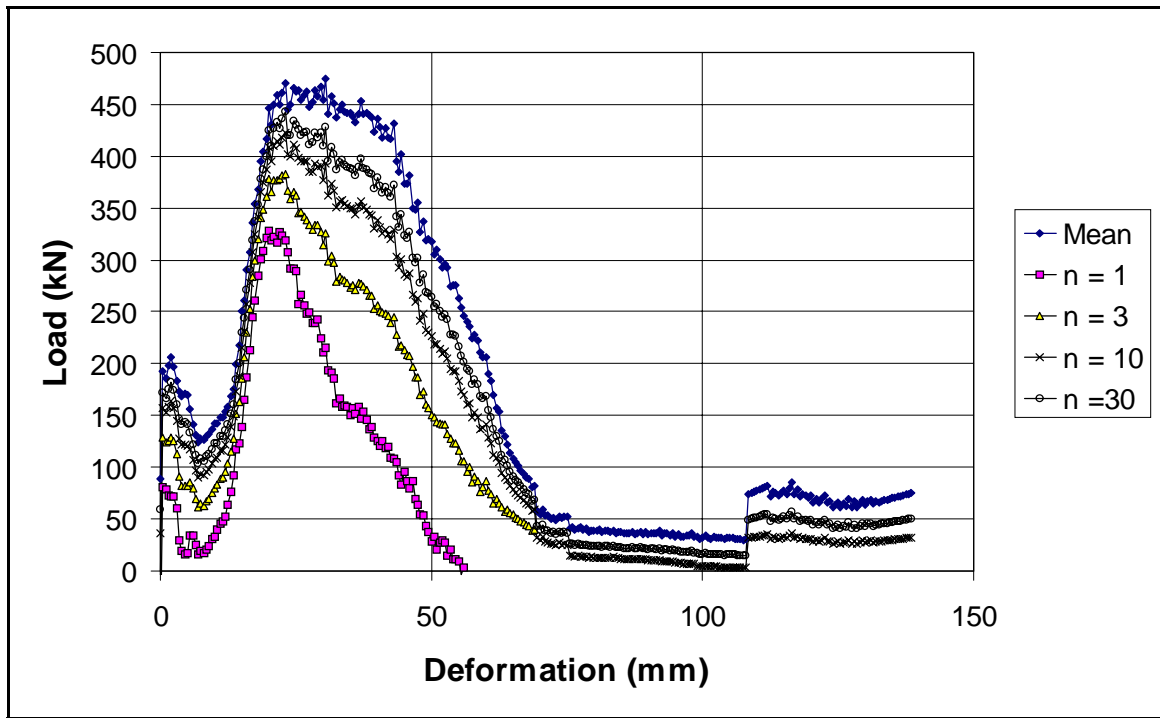
***Figure 4.3.12   Statistical analysis showing the results of a 90 per cent confidence
rating performed on the raw data of the slow tests (excluding the
samples that slipped).***

The slow loading rate increases the deformation at failure, but has little, if any, effect on the load
bearing capacity of the timber. Equation (4.2.1) was derived empirically by Roberts 1995, based
on the assumption that timber creep was mainly responsible for the difference between
laboratory and underground load performance. The equation is used in Figure 4.3.13 to relate
the laboratory tests performed at 20 mm per day to the underground results presented in
Chapter 3. The corrected loads are clearly over-estimated in relation to the results obtained
underground.

Normalised mean results

Load (kN) vs Deformation (mm)

Legend:
- 20 mm per day (lab results)
- 3,7 mm per day
- 0,7 mm per day
- Corrected 20 mm per day to 0,7 mm per day

Underground results
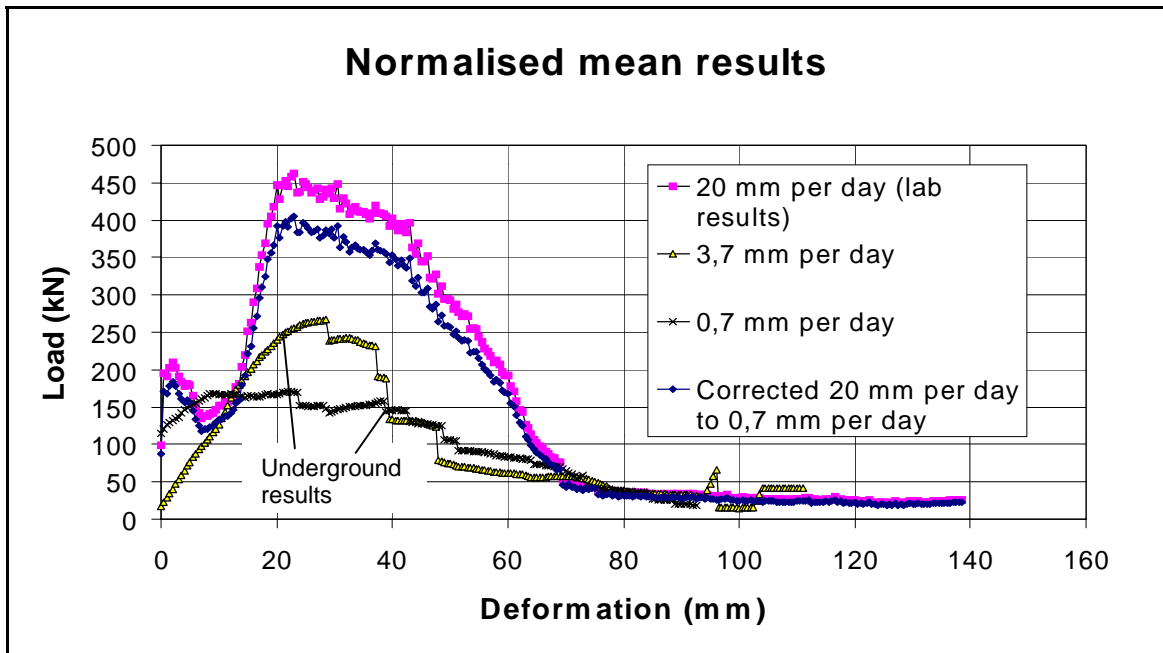
Figure 4.3.13   Comparison between the slow tests and the underground results.

Although the deformations in the slow tests are similar to the underground tests, the peak loads are much higher.

An evaluation of Equation (4.2.1), relating loads at different velocities, is performed by using the equation to compare rapid laboratory tests, slow laborartory tests and underground results. Equation (4.2.1) can be rewritten as

$$\frac{F_{u/g}}{F_{lab}} = m \log\left(\frac{v_{u/g}}{v_{lab}}\right) + 1. \tag{4.3.1}$$

Plotting $F_{u/g}/F_{lab}$ against $\log(v_{u/g}/v_{lab})$ yields a straight line of slope m. The slope of the best fit to the available data will therefore indicate the accuracy of Equation (4.2.1), where a value of 0,084 is specified for m for rockfall conditions (Roberts *et al.*, 1987). The work conducted as part of this project results in a more representative value of m, which is specifically applicable to mine poles. The data and the best-fit line (using Equation 4.3.1 with $m = 0,145$) are presented in Figure 4.3.14.
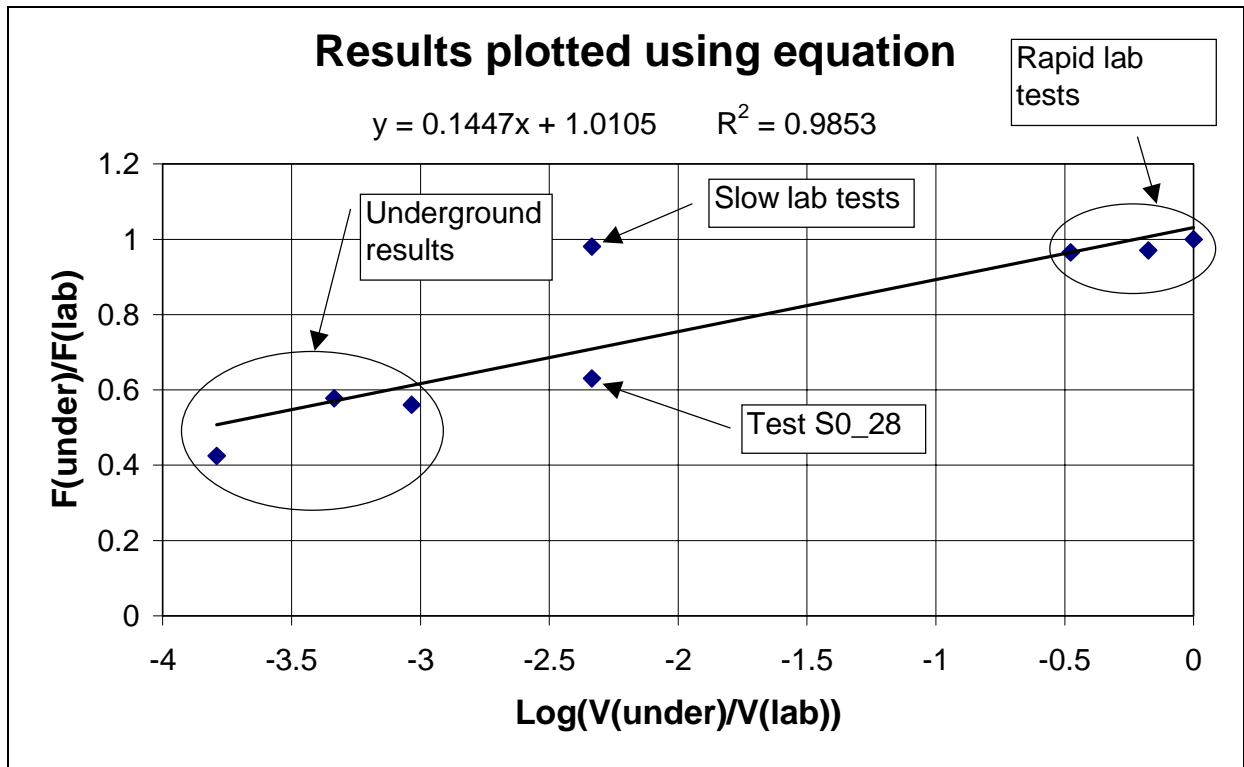
Figure 4.3.14   Comparison between mine pole failure loads at various deformation rates.

The improved relationship correlating the laboratory test results with underground data is given below in Equation (4.3.2).

$$F_{u/g} = F_{lab}\left[m\log\left(\frac{v_{u/g}}{v_{lab}}\right) + 1 \right],$$ (4.3.2)

where: $F_{u/g}$ is the force corrected for underground values,

F_{lab} is the force obtained from a standard laboratory test,

$v_{u/g}$ is the underground closure velocity,

v_{lab} is the laboratory test velocity, and

m is an empirical factor (m = 0,145 for mine poles used in rockfall conditions).

For example, consider a laboratory compression rate of 30 mm/min and an underground convergence rate of 3 mm/day. Since $\log(v_{u/g} / v_{lab})$ is –4,16, the load correction is $F_{u/g} / F_{lab} = 0{,}40$ (for $m = 0{,}145$). This compares to $F_{u/g} / F_{lab} = 0{,}65$ for $m = 0{,}084$. The new data, which is specifically applicable to mine poles, thus further downgrades the laboratory data. The importance of using appropriately downgraded laboratory curves to approximate the *in situ* performance of mine poles is emphasised.

The capacity of the prop highlighted in Figure 4.3.15 (S0_28) is lower than other specimens tested at similar loading rates. In this case the mine pole was tested under more erratic deformation conditions, which was achieved by repeating cycles of relatively rapid loading for a total compression of ≈ 4 mm (simulating blasting, underground), followed by long periods of static conditions. Timber creep caused a reduction in load between the loading intervals. The mine pole for this test was roughly cut, so that the full loading surface of the element was not in contact with the press at the start of the test (see Figure 4.3.16). The result of this experiment (S0_28) nevertheless plots close to the linear regression line shown in Figure 4.3.14.
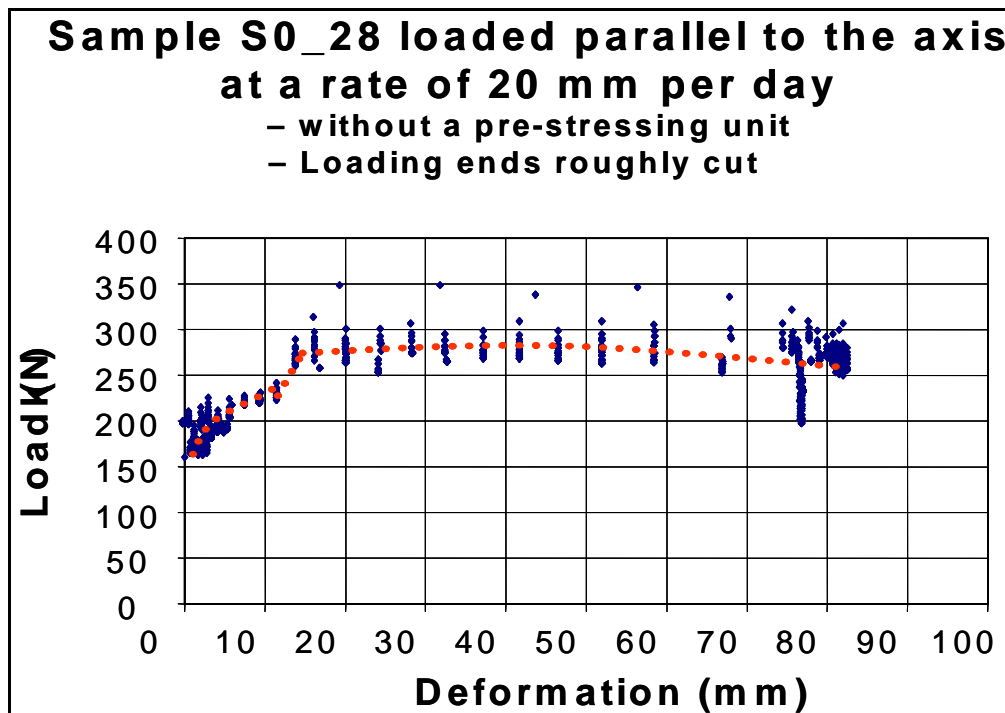
Figure 4.3.15   Results of a roughly cut mine pole, loaded erratically.

Figure 4.3.16   Photograph of the roughly cut mine pole.

The diamond shaped points in Figure 4.3.15 indicate the load and deformation recorded at 10 minute intervals. As the load approaches the failure condition of the element, the creep behaviour also increases, thus promoting a large discrepancy between the loads just after a deformation change to just before the following period of compression. The dotted line plots an average load between the closure events, which could correspond to a reading taken underground during a shift, between blasts. This effect explains some of the difference between the measured loads underground and the test laboratory. Similar loading rate dependence was measured underground by continuous force-deformation monitoring equipment (see Section 4.5.5.2).

Figure 4.3.17 shows the mean results for the 2 mm per minute laboratory tests compared to the 3,7 mm per day underground tests. Also shown is the laboratory curve adjusted to approximate the underground performance (using Equation 4.3.2). The results indicate the need to adjust the pre-failure modulus of the laboratory tests to adequately predict the underground behaviour. Due to the uneven underground hangingwall / footwall conditions, the pre-failure modulus is reduced. Hence Equation (4.3.3) is proposed. The laboratory results are correlated to the Union site tests to eliminate the effects of pre-stressing pots. It should be noted that no moisture content tests were performed on the underground test specimens and the laboratory test specimens had a low moisture level, indicating that the value of *m* could change slightly if tests of the same moisture content were compared.
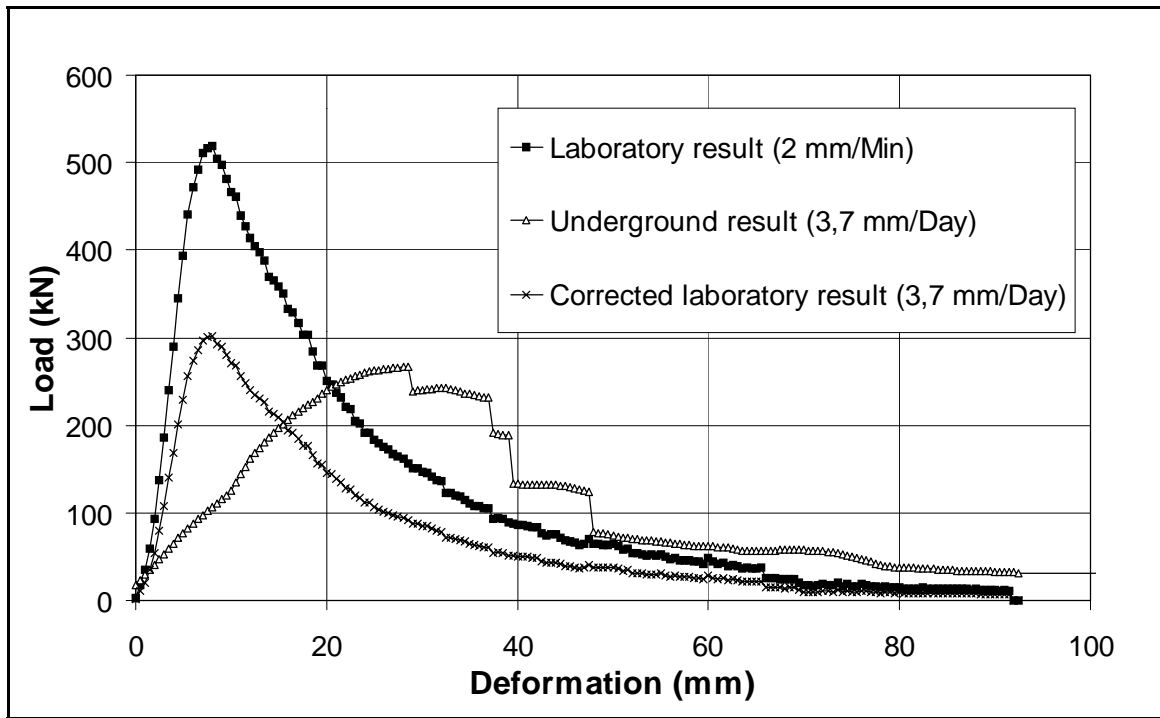
Figure 4.3.17   Comparison between laboratory and underground results.

$$d_{u/g} = d_{lab}\left[m\log\left(\frac{V_{lab}}{V_{u/g}}\right) + 0{,}8512 \right]\left(\frac{l_{u/g}}{l_{lab}}\right),$$
(4.3.3)

where: $d_{u/g}$ is the deformation corrected for underground results (prior to failure),

d_{lab} is the deformation obtained from a standard laboratory test,

$v_{u/g}$ is the underground closure velocity,

v_{lab} is the laboratory test velocity,

m is an empirical factor (m = 0,939 for rockfall conditions),

$l_{u/g}$ is the length of the unit underground, and

l_{lab} is the length of the unit in the test lab.

154

The effect of applying Equation (4.3.3) to the laboratory test results as described above is shown in Figure 4.3.18. The mean of the normalised laboratory tests is correlated to the mean of the normalised underground results from the Union site. Note that the deformation adjustment proposed by Equation (4.3.3) should only be applied to the section of the curve before failure, i.e. the approximately linear part of the curve before the peak load has been attained.
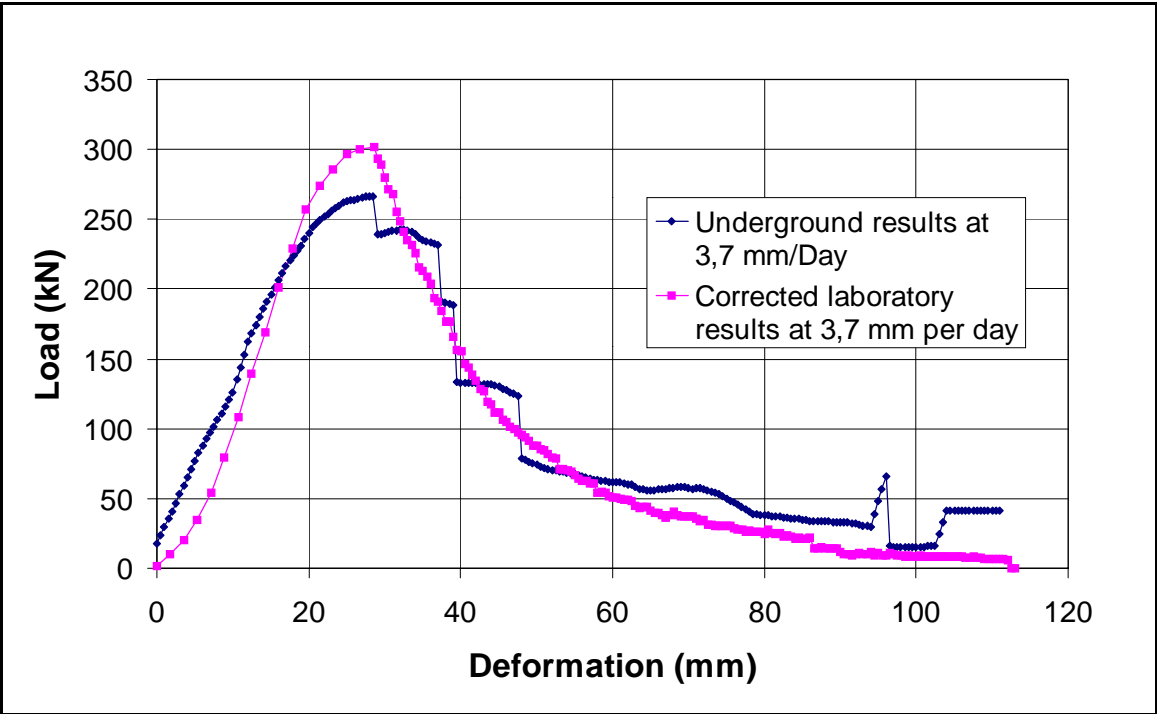
Figure 4.3.18   Comparison between underground and laboratory results after applying the deformation correction formula.

4.3.6 Results of the rotating platen tests

4.3.6.1 Introduction

Tests were performed to simulate blocks rotating during loading. This represents loading situations in blocky ground conditions, where a prop is located off-centre on a block, which can subsequently rotate, thus subjecting the mine pole to rotational and compression forces.

4.3.6.2 Test method

Long mine poles are cut in half and the loading surfaces cut perpendicular to the long axis of the pole. A special saw rig was constructed to ensure a high degree of accuracy in flatness and angle. One half of the mine pole is tested normally at approximately 2 mm per minute. The load-bearing capacity of the second half is tested by installing the mine pole in the press and rotating one loading platen. Various rotation angles are applied, after which normal loading continues until the element can no longer sustain a reasonable load. During rotation the elements are also compressed as shown in Figure 4.3.19.
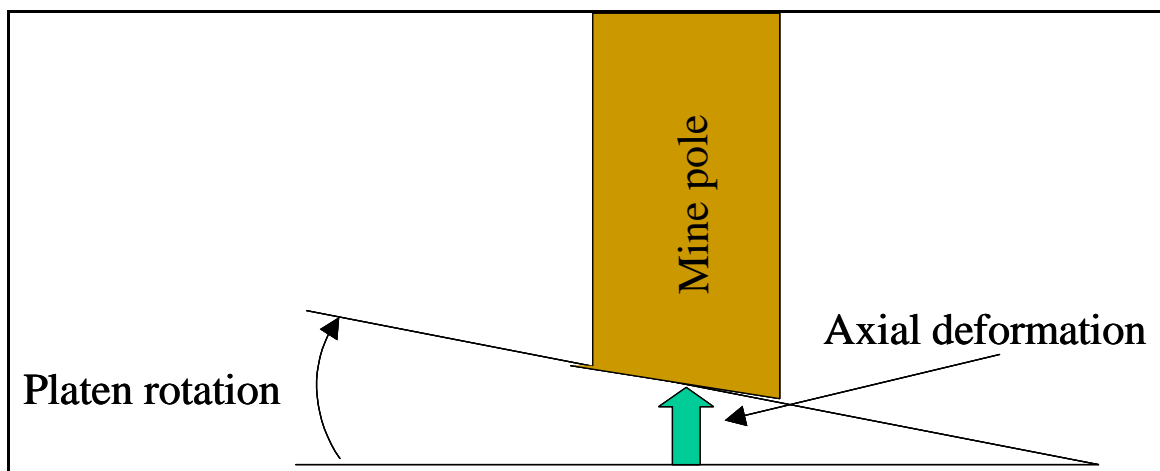
Figure 4.3.19   Schematic showing the test set-up for the rotation tests.

4.3.6.3 Test results

The results shown in Figure 4.3.20, Figure 4.3.21, Figure 4.3.22 and Table 4.3.5 are normalised with respect to a nominal mine pole diameter of 158 mm. Each of the three figures compares the effects of rotation against a twin element tested normally. The deformations that occur during rotation are averaged to give the deformation at the centre of the support element end. Curves of the individual tests are included in the appendix and the component of deformation during rotation is clearly shown.
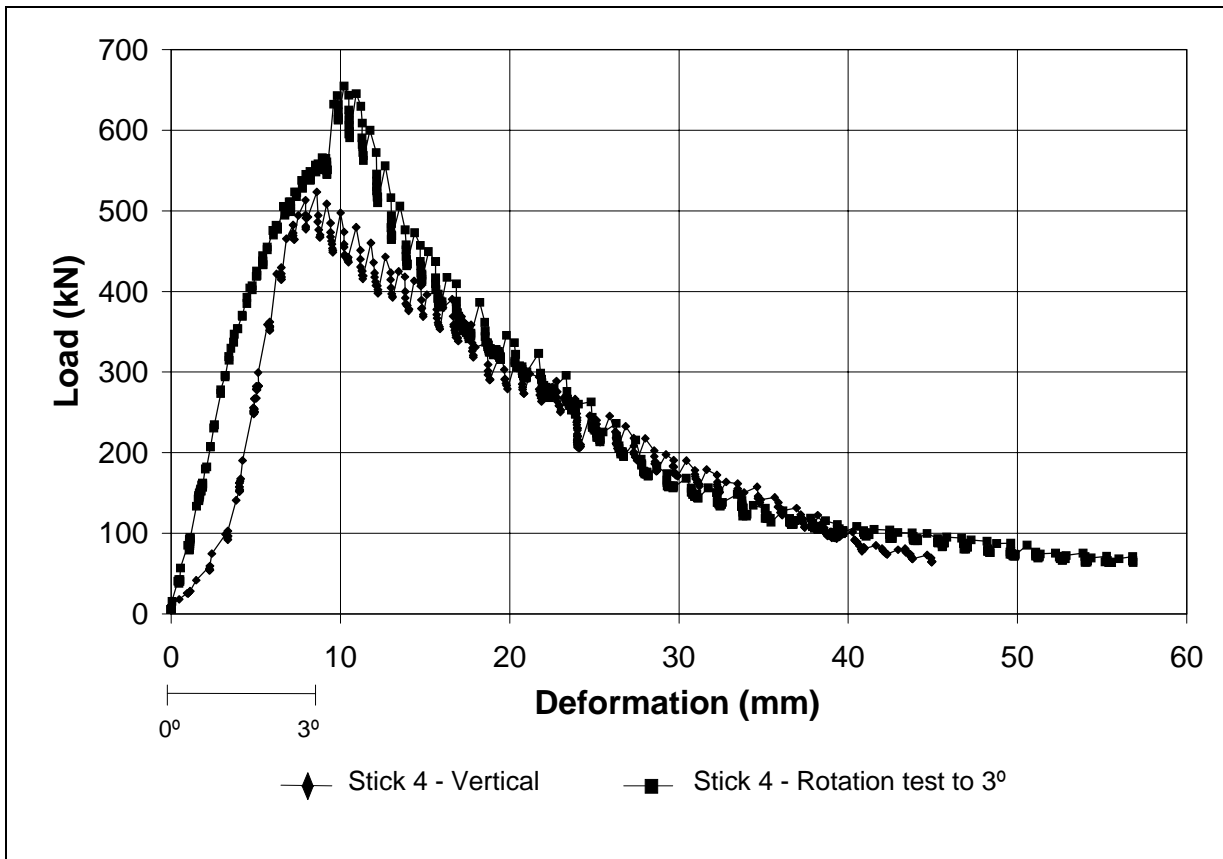
Figure 4.3.20   Comparison between the results of an axial and rotational test (to three degrees) on twin elements.
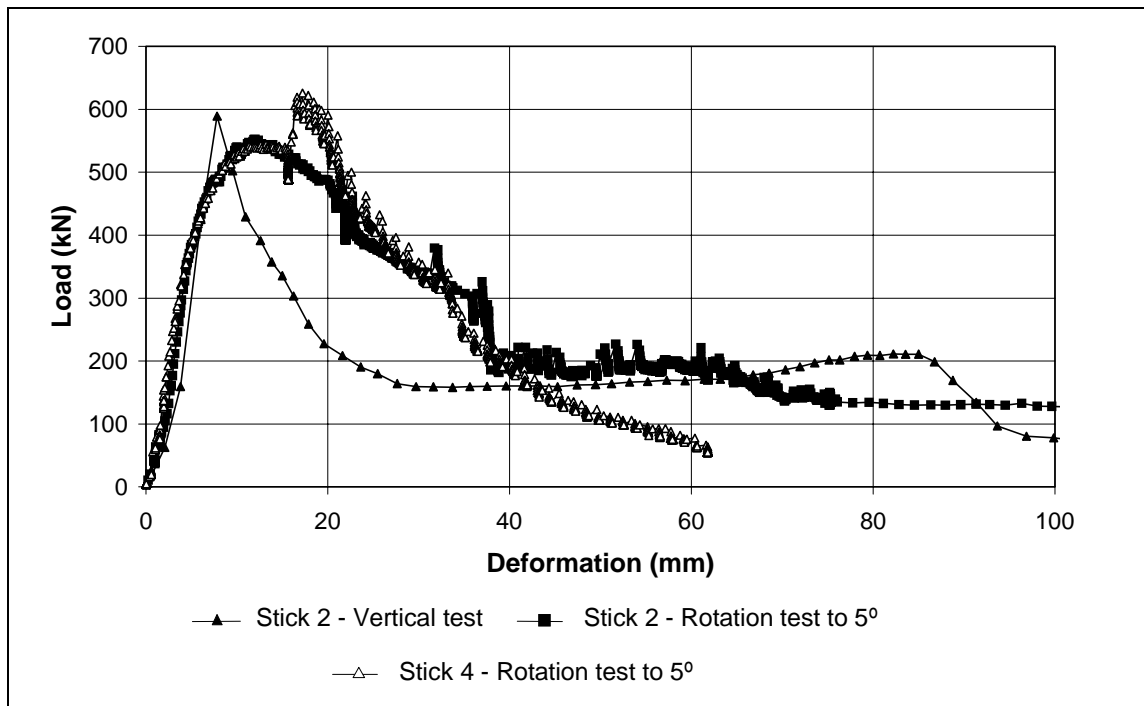
Figure 4.3.21   Comparison between the results of an axial and rotational tests (to five degrees) on twin elements.
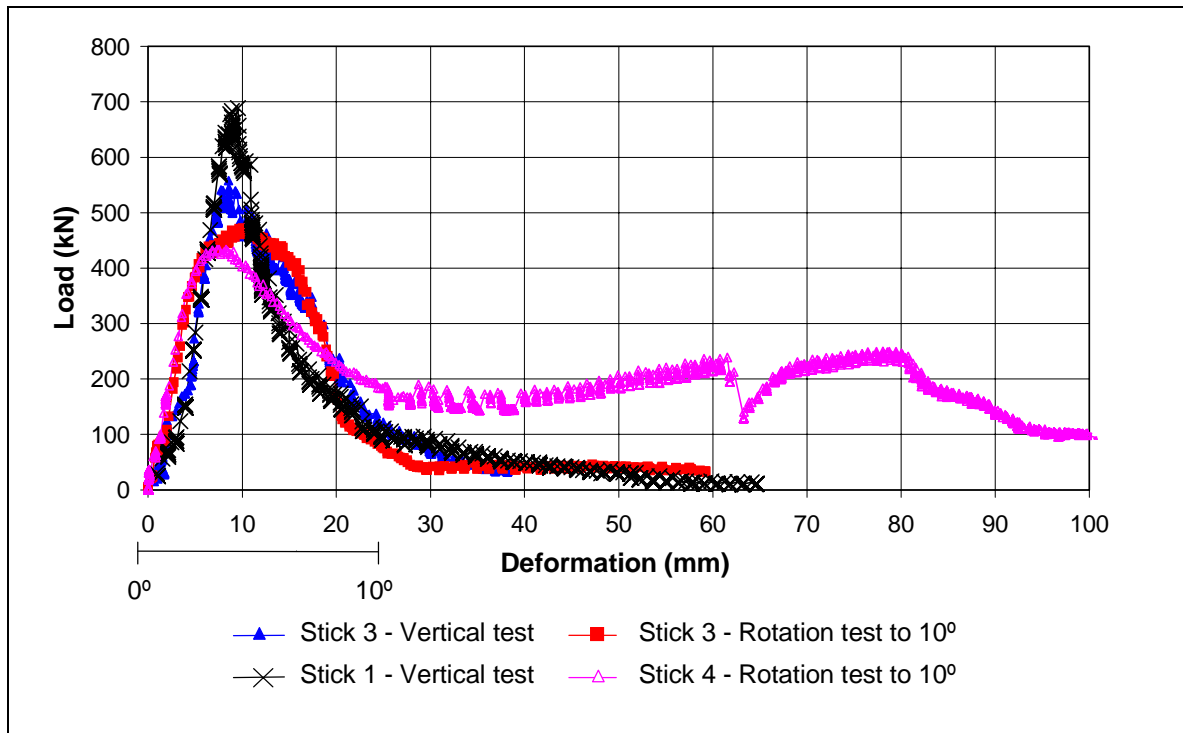
Figure 4.3.22   Comparison between the results of axial and rotational tests (to ten degrees) on twin elements.

Table 4.3.5   Results of the rotation tests.

Test no.	Failure mechanism	Rotation (Degrees)	Peak load (kN)	Normalised peak load (kN)
R0_4b	Buckling	0	564	523
R3_4a	Splitting and buckling	3	706	655
R0_2b	Brushing and splitting	0	748	589
R5_2a	Brushing	5	647	552

R5_5a	Splitting and buckling	5	683	626
R0_1b	Splitting and buckling	0	706	688
R10_1a	Brushing	10	445	434
R0_3b	Buckling	0	708	558
R10_3a	Buckling	10	606	472

4.3.7 Analysis of the rotation tests

The results shown in Figure 4.3.21, Figure 4.3.22 and Table 4.3.5 indicate that rotation does have a weakening effect on the timber and a trend of progressive weakening with angle. Figure 4.3.20 indicates the opposite trend, but this is because the shape of the timber used for the axial test was "bowed", thus promoting buckling and a weaker failure load. However, since the rotation test in Figure 4.3.20 has a similar strength to the axial test (R0_1b shown in Figure 4.3.22 and Table 4.3.5), it is assumed that a small rotation of this magnitude probably has little or no effect on timber strength. Both mine poles that were rotated to 10^0 failed during the rotation process and therefore higher angles were not necessary.

If the component of axial deformation is reduced, by moving the element closer to the fulcrum, however, a higher rotation does further reduce the timber strength. The result for prop 4 in Figure 4.3.21 indicates that, if the element had not failed during rotation, the final strength could be similar to an axially loaded element. Therefore, the effect of rotation depends on the component of axial deformation incurred during rotation, thus making a direct quantification of rotational effects difficult.

4.3.8 Results of the creep tests

4.3.8.1 Introduction

Creep tests were performed on mine poles and pre-stressing pots to establish their respective creep properties.

4.3.8.2 Test method

Two tests were performed. One of the tests monitored the creep effects of the pot only. For this test a steel cylinder of the same diameter as the average mine pole was pressurized by the pot in a frame. An in-line load cell measured the load change. The second test included a mine pole from the same batch of timber used to perform the slow tests. This system was monitored for seven days.

4.3.8.3 Test results

Figure 4.3.23 shows the results of the test performed with a metal cylinder. There is a nine per cent drop in load due to deformation of the pot itself, which occurred over a three-day period. The subsequent increase in load is the result of rising temperatures in the test laboratory, and the smaller oscillations are the result of day and night temperature changes.
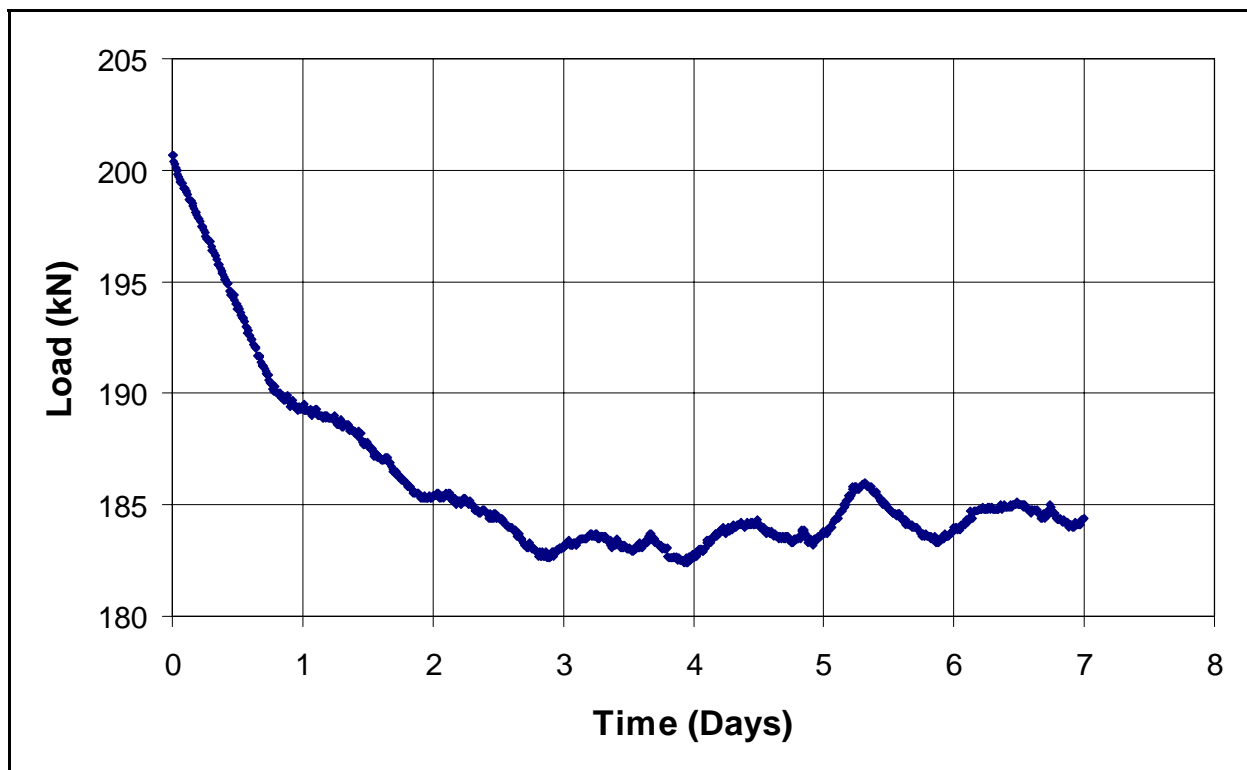
Figure 4.3.23   Creep effects of a pot only.

The results shown in Figure 4.3.24 and Figure 4.3.25 provide information on the effect of pre-stressing a mine pole in a static situation. A stiff load frame was used for the experiment. Figure 4.3.24 indicates that most of the creep effects occur immediately after installation, and drop off exponentially with time. Approximately six per cent of the installation load is lost in the first five minutes.
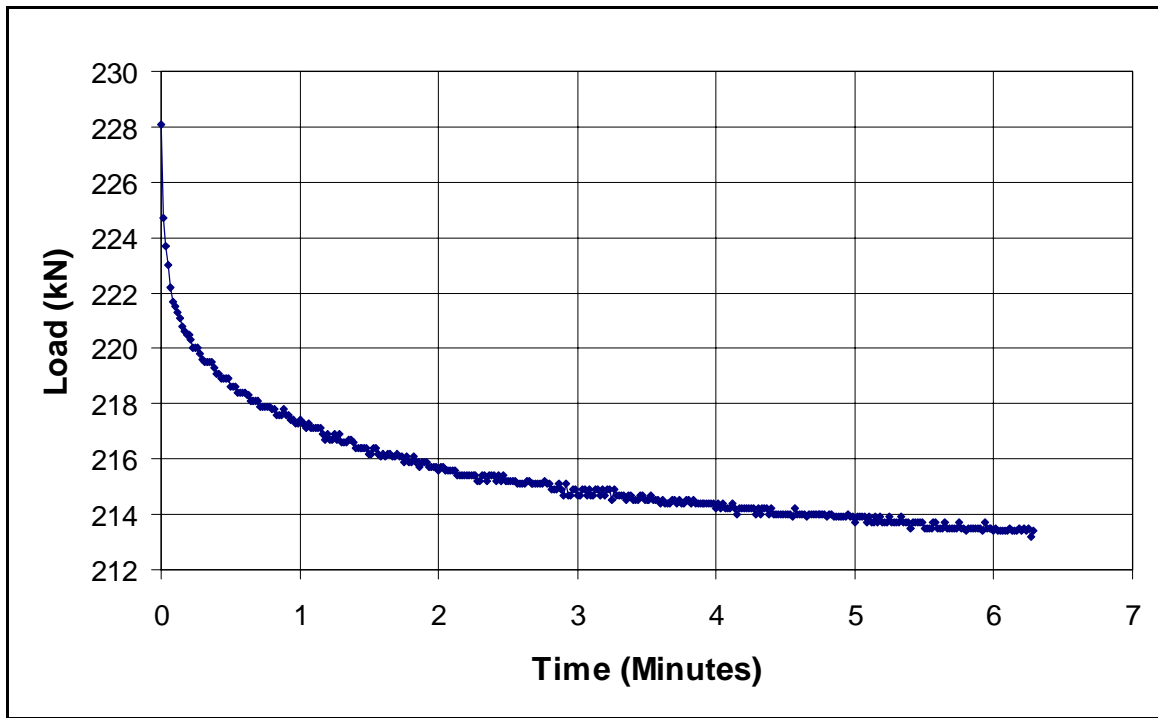
Figure 4.3.24   Creep effects of a pot and a mine pole, of 1 m length, within 7 minutes of loading.

Figure 4.3.25 shows the results of the same test as in Figure 4.3.24, but left under static for a longer period. The system stabilised after about six days, with a total load drop of about 15 per cent.
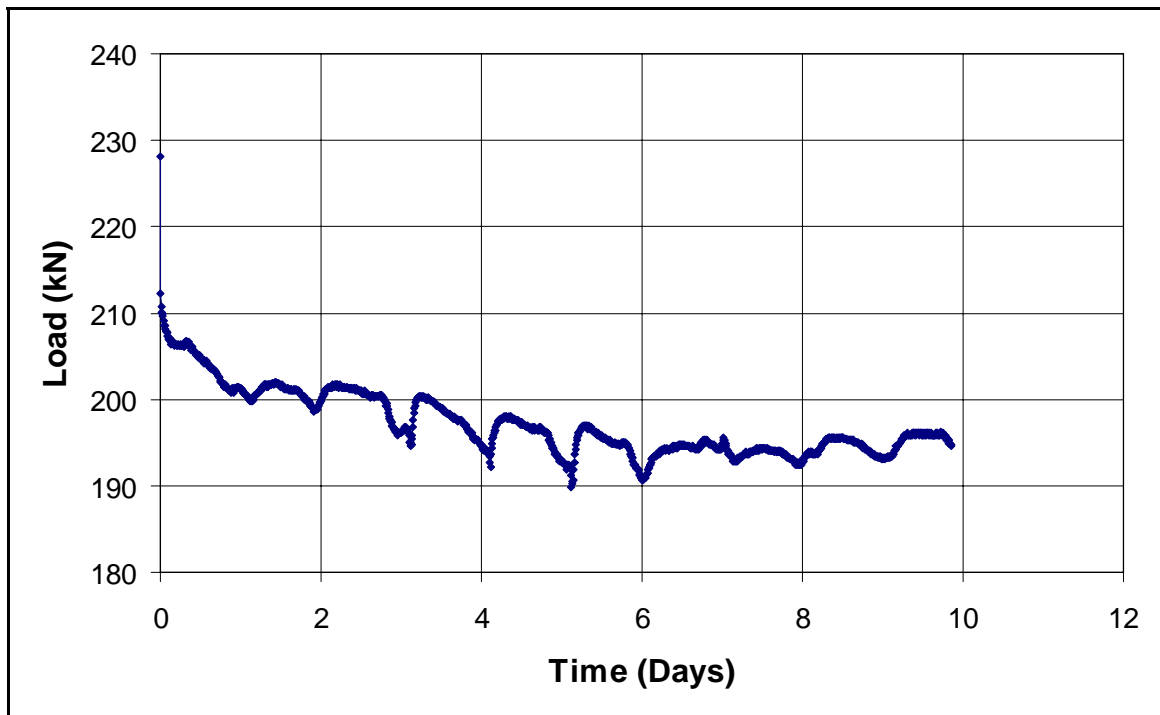
Figure 4.3.25   Creep effects of a pot and a mine pole, of 1 m length, over 10 days.

4.3.9 Analysis of the creep test results

The creep effects of the pot itself, shown in Figure 4.3.23, indicate that in situations where the load (hence the pressure within the pot) was increasing as a result of closure in an underground situation, this plastic deformation could perpetuate and enhance the deformability of the support system. The underground tests indicated that at some point, plastic deformation resulted in pot failure but never resulted in complete load loss.

At this stage the reasons for load increases (e.g. between day 5 and 6, Figure 4.3.23) have not been investigated in detail. A possible reason might be an increase in the ambient temperature. Further research is required to substantiate this.

4.3.10 Conclusions

In this subsection the salient findings of the laboratory testing programme on mine poles are reviewed. The findings are reviewed according to their broadly defined testing category, i.e. rapid testing, slow testing, rotating loading plate testing, and creep testing.

4.3.10.1   Rapid test results

The effect of oblique loading on Minepoles may be quantified by comparing the mean and confidence curves of vertical and angled tests. Figure 4.3.26 shows the load-displacement curves for all types of tests at an 84 % confidence level.
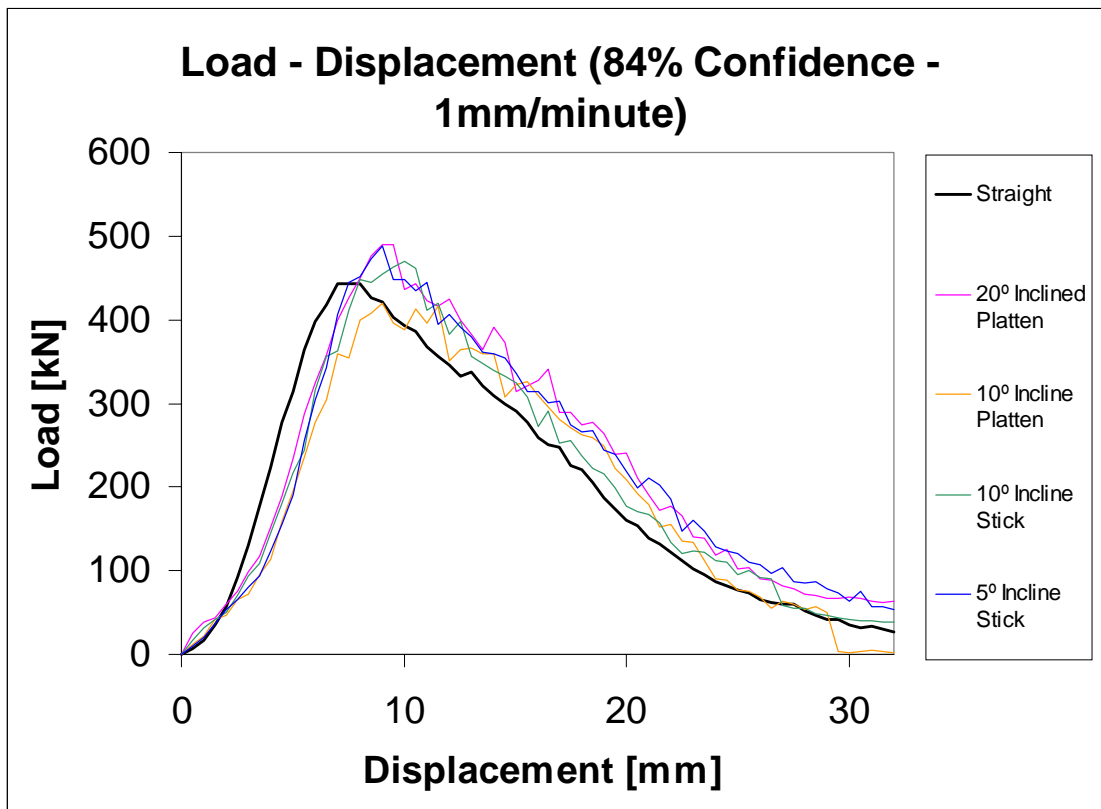
Figure 4.3.26   84 % Confidence curves for all vertical and angled tests.

These curves clearly indicate that there is little difference between the response for vertical and oblique loading, either in terms of displacement or load. The initial portion of the response for oblique tests is less stiff than that of the vertical tests. The reason for this is that the ends of the obliquely cut props 'bite' into the loading platen before the load path is fully established. Following this stage, the initial linear stiffness of the response of all tests is comparable.

The contact between the loading platen and the props can be described by a Coulomb friction and cohesion law.

It was found that there is no significant correlation between the same half-prop tested vertically and inclined. Figure 4.3.27 shows that there is no consistent increase or decrease in strength between vertical and inclined props.
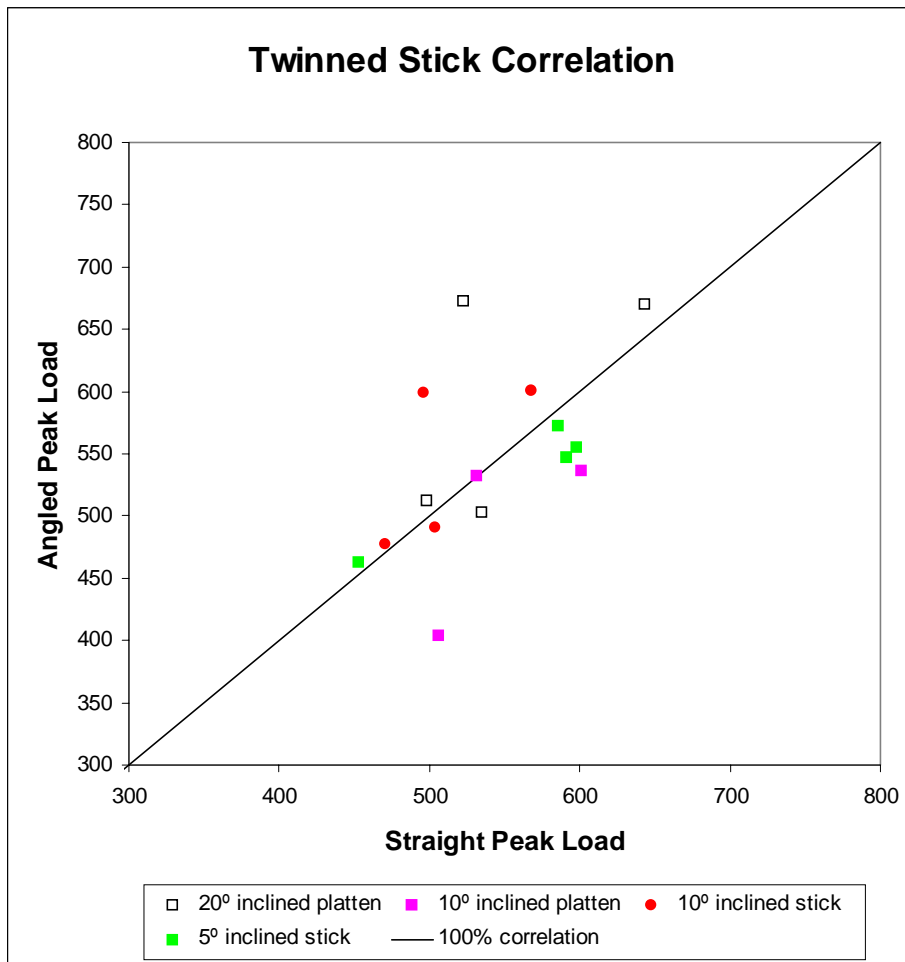
Figure 4.3.27   Correlations between inclined and vertical tests for twinned samples.

The failure mechanisms of the props are influenced by oblique installation of the prop. The inclined props failed predominantly by splitting and brushing, while the inclined platen tests all showed buckling failure. The vertical tests showed that 21 % of props failed by a splitting/brushing mechanism. The relationship between failure mechanism and load response may be described as follows.

Figure 4.3.28 shows a typical load-displacement curve for a mine pole that has failed by buckling. The response is divided into stages. The first portion of the response is a non-linear load-uptake stage, where the end of the prop is compressed into the loading surface. Once the load path is established, a linear portion follows, where the unit shows a linear increase in load with displacement.

The unit then begins to fail and the response becomes a non-linear, decreasing modulus until the peak load is reached, whereupon a softening stage is initiated. The softening stage is terminated when the prop has failed to the degree that only a residual amount of load response is possible. At this stage the unit has buckled to the extent that the ends have pivoted, reducing the contact area significantly.

154

The response for a brushing/splitting failure (Figure 4.3.29) is similar up to the point of peak load. The response beyond this point shows a much more gradual softening than observed with the buckling failure modes. The contact area for this failure mechanism may increase as brushed fibres on the side of the prop make contact with the loading surface (see Figure 4.3.30).
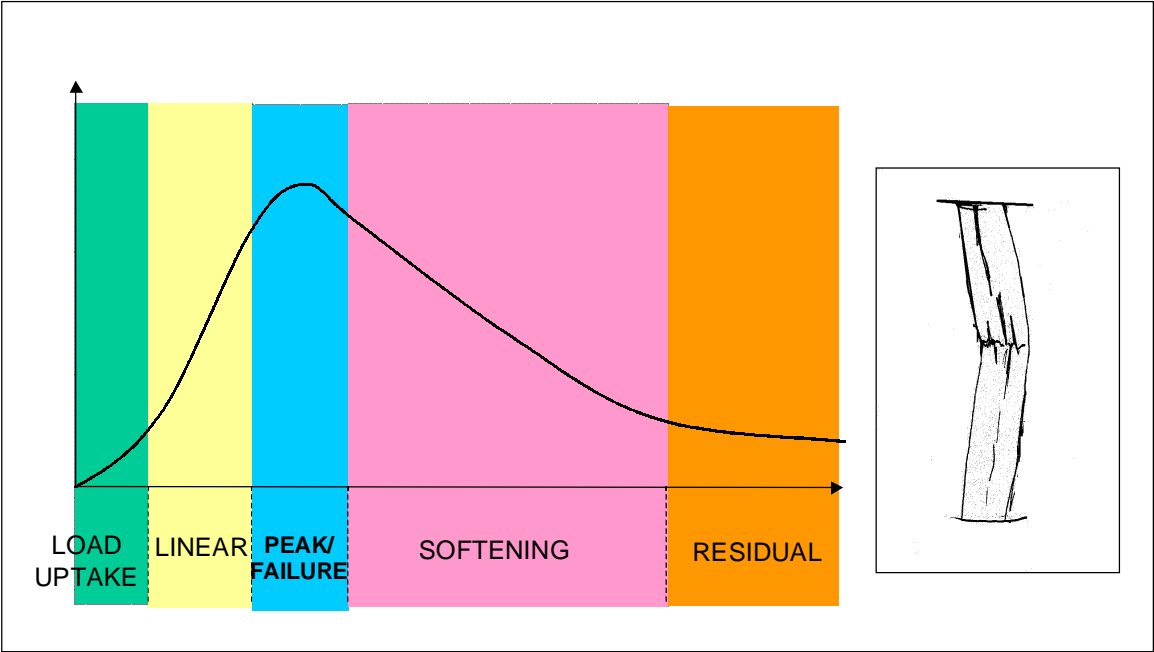
Figure 4.3.28   Typical response for a buckling failure.
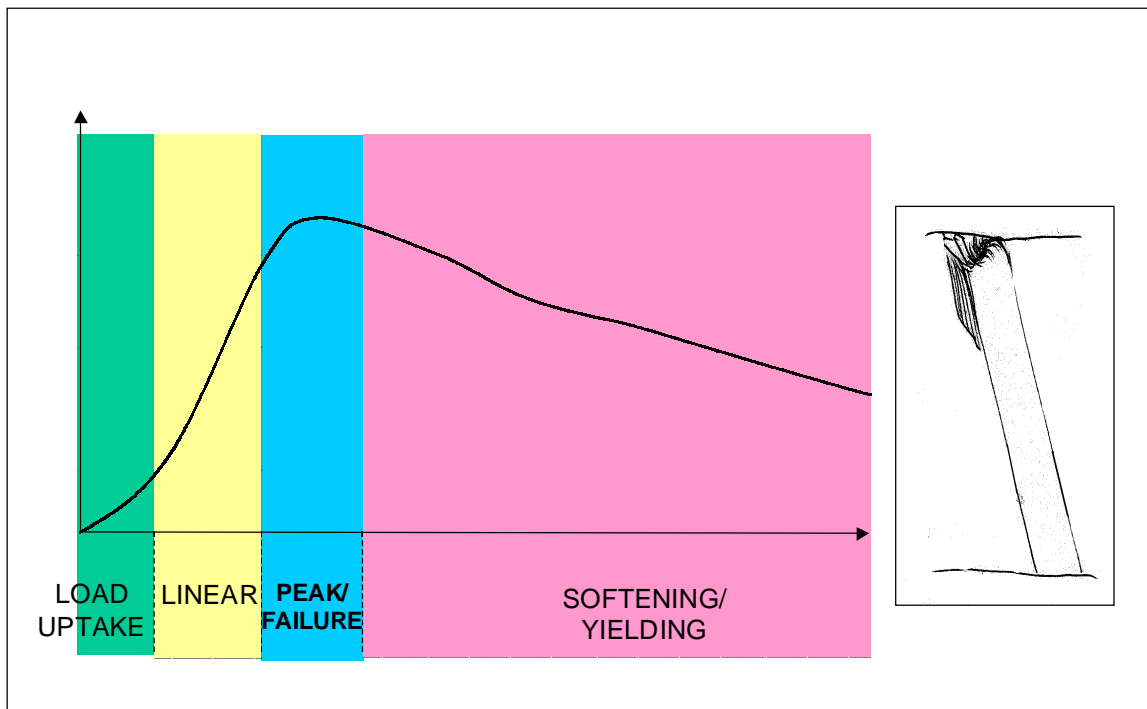
Figure 4.3.29   Typical response for a brushing failure.
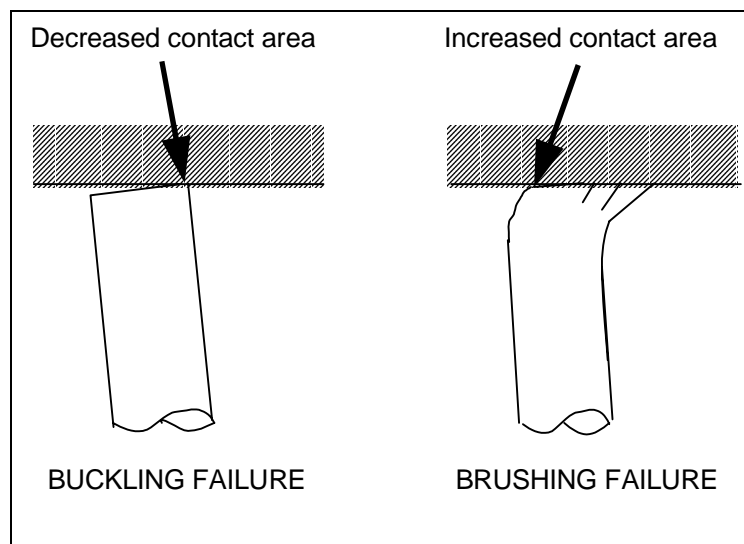
Figure 4.3.30   Contact conditions for brushing and buckling failures.

From these observations, it is evident that it is advantageous for a wooden elongate to fail by brushing and/or splitting rather than by buckling. The increased load-carrying capacity at large deformations is clearly an advantage in a displacement-driven environment. Results from tests

154

on profile props demonstrate how the failure mechanism may be engineered into the design of the support unit.

4.3.10.2 Slow test results

Loading with a tilted platen has little effect on the results, until the friction angle of the contact between the timber and platen is exceeded. This finding is the same for the rapid laboratory and underground results. Therefore, all the tests are included in the analysis, excluding those that slipped.

The results show similar failure loads to the rapid tests (Figure 4.3.14), violating the time-dependent weakening theory behind Equation (4.2.1). One of the laboratory tests (Figure 4.3.15) indicates that the frequency of measurement plays a more important role in the difference between laboratory and underground results than loading rate. Other factors that influence the load are the loading surface and timber shape.

The difference between the rapid laboratory results and the underground tests is greater than predicted by Equation (4.2.1) (see Figure 4.3.14), and therefore a modified value of *m* is proposed in Equation (4.3.2). There is also a difference, between the laboratory and underground results, in the pre-failure stiffness modulus of the timber. Chapter 3 shows the importance of deformation in the analysis of timber behaviour and therefore Equation (4.3.3) was developed to predict underground deformations from laboratory results. It should be noted that the moisture content of the underground tests were not tested and this could influence the equation.

Statistical analyses using a confidence level of 90 per cent are performed on the tests, and the results show that for blocky ground conditions only 69 per cent of the average load at failure should be used in an evaluation.

4.3.10.3 Rotating loading plate test results

The results of these tests indicate that rotation of a loading surface can weaken the timber strength. Very little damage is caused up to about 3°, and that damage is proportional to the angle of rotation. Failure occurs at a rotation of less than 10° with the test configuration shown in Figure 4.3.19.

4.3.10.4   Creep test results

Approximately nine per cent of the pre-stressing load is "lost" as a result of creep in the pot only, and a further six per cent due to timber creep. The total creep results in a 15 per cent drop in the load over a period of six days.

4.4 Laboratory test results and evaluation of profile props

The profile props (unturned) tested were obtained from Mondi Mining Timber and comprise a 200 mm diameter prop barrel capped by the frustum of a cone. The diameter of the frustum varied from 130 mm at the top to 180 mm at the base (1 m length tested). The test set-ups for the various programmes are as described in the previous sections.

The testing program was as follows:

Vertical tests: 5 tests

Inclined props: 4 tests at 5⁰

                         5 tests at 10

                         3 tests at 15⁰

Inclined platen: 3 tests at 2.5⁰

                         4 tests at 5⁰

                         5 tests at 10⁰

The angles of the props were slightly variable with up to 2,5º deviation from the above.

The normalisation procedure as discussed in Section 4.2.2 was followed in the processing of the results.

4.4.1 Results for vertical tests

The normalised load-displacement curves for all five vertical tests and the resultant mean and confidence lines are presented in Figure 4.4.1. Brushing type-failure was typical of the vertical tests and accounts for the comparatively high post-peak yielding behaviour of the profile props.

Table 4.4.1 presents a summary of the failure mechanisms observed in each vertical test. It can be seen from Table 4.4.1 that there exist a correlation between peak loads and failure mechanism. High peak loads are associated with brushing-type failure, however these are reduced when other failure mechanisms, such as splitting or shearing, are encountered.
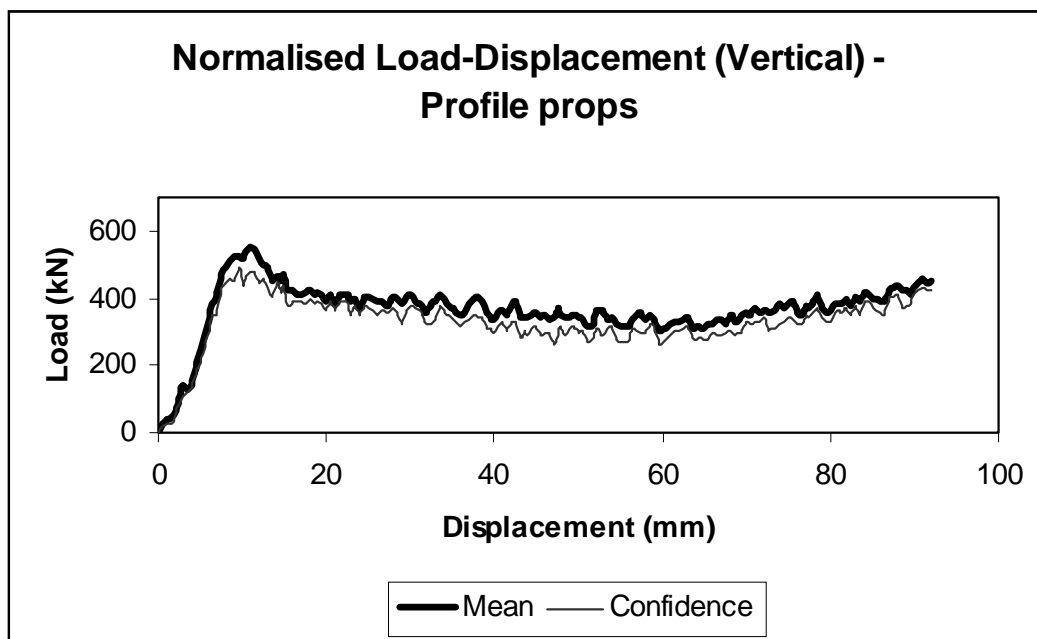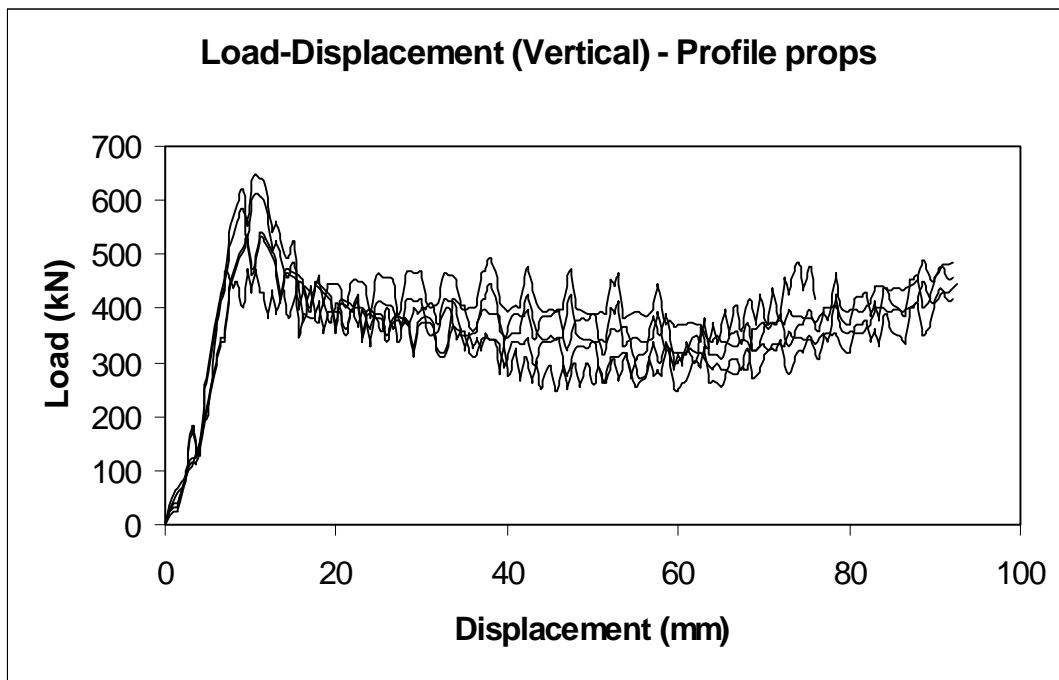
Figure 4.4.1 *Load-Displacement curves for vertical tests and the resultant mean and 84 % confidence curves.*

Table 4.4.1   Failure mechanisms observed for straight/vertical tests.

Test number	Failure mechanism	Peak Load (kN)
1	Brushing with spitting	486
2	Brushing with shearing	541
3	Brushing	613
4	Brushing	648
5	Brushing with shearing	532

4.4.2 Results for inclined profile prop tests

Four tests were performed with 5° inclined props, five with 10° inclined props, and three were performed with 15° inclined props. The normalised load-displacement curves, with the mean and 84 % confidence curve for the 5°, 10° and 15° inclined props are presented in Figure 4.4.1, Figure 4.4.2 and Figure 4.4.3, respectively.
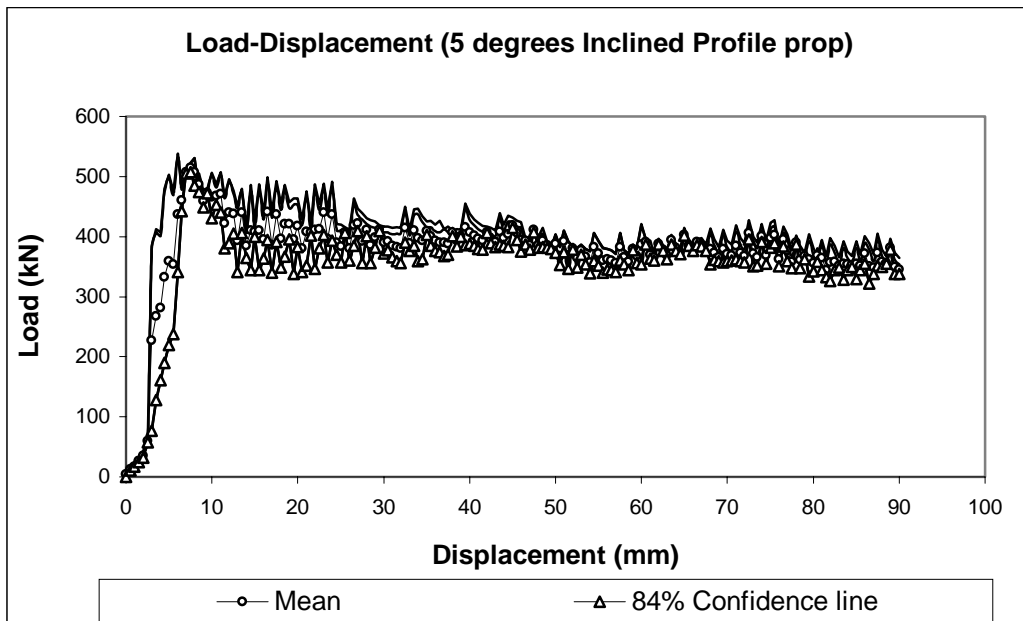
Figure 4.4.1   Mean and 84 % confidence curves for all 5° inclined prop tests.
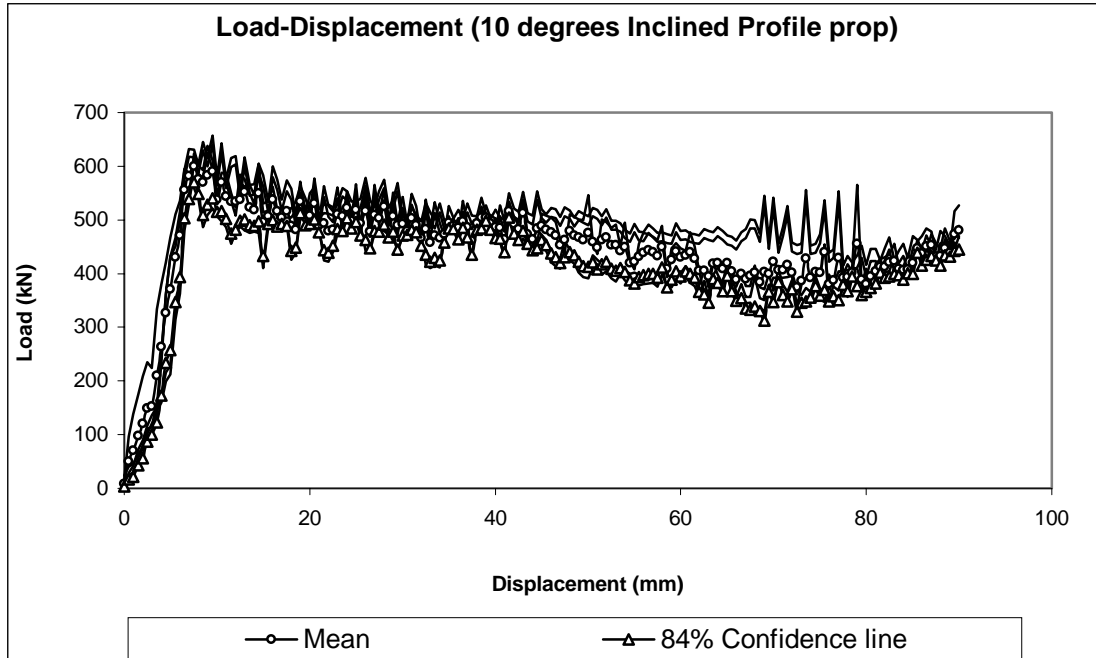
Figure 4.4.2   Mean and 84 % confidence curves for all 10° inclined prop tests.
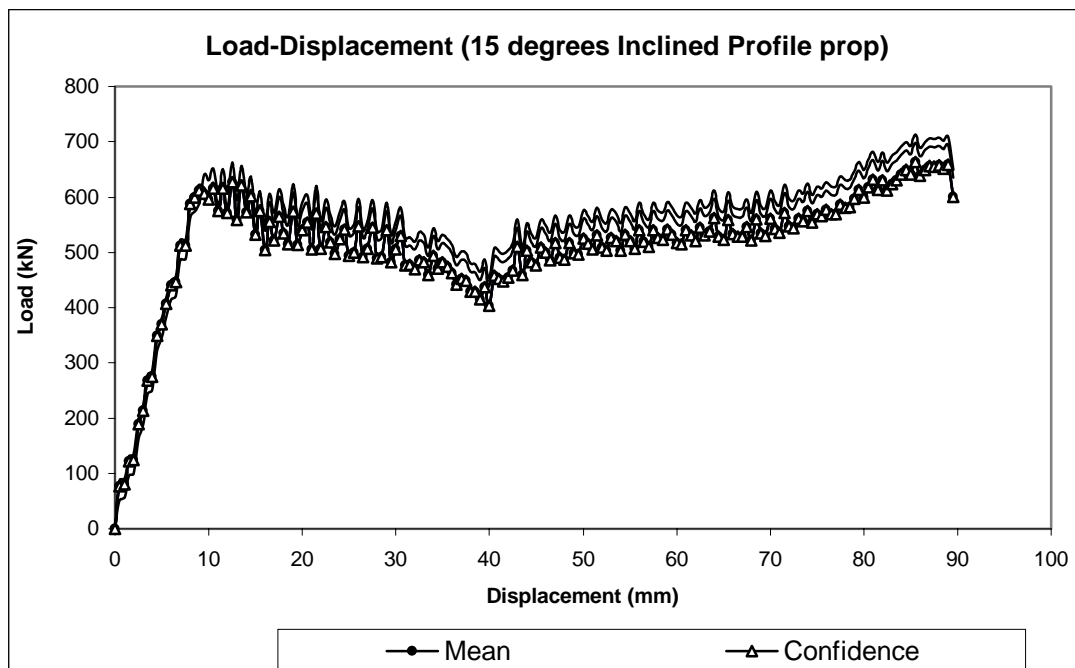
Figure 4.4.3   Mean and 84 % confidence curves for all 15° inclined prop tests.

The failure mechanisms observed are presented in Table 4.4.2.

Table 4.4.2   Failure mechanisms observed for inclined profile prop tests.

Test number	Angle (°)	Failure mechanism	Peak load (kN)
6	5	Brushing followed by splitting	517
7	5	Brushing with shearing	525
8	5	Brushing	530
9	5	Brushing with shearing, splitting	513
10	10	Brushing with splitting	615

11	10	Brushing	640
12	10	Brushing with shearing	622
13	10	Brushing followed by splitting	624
14	10	Brushing with shearing, splitting	548
15	15	Brushing with shearing	630
16	15	Brushing with shearing	623
17	15	Brushing with shearing, splitting	570

The predominant mode of failure is brushing and/or in combination with shearing or splitting. The brushing and shearing resulted in a yielding-type response for the inclined prop tests.

4.4.3 Results for inclined platen tests

Three tests were performed with a 2.5° inclined platen, four with a 5° inclined platen, and five were performed with a 10° inclined platen. The normalised load-displacement curves, and the mean and 84 % confidence curves, for the 2.5°, 5° and 10° are presented in Figure 4.4.4, Figure 4.4.5 and Figure 4.4.6, respectively. None of the profile props slipped during the 2.5°, 5° or 10° tests. The results for the inclined platen tests are summarised in Table 4.4.3. As can be seen from table 4.4.3 there was no consistency in the failure mechanism, i.e. various failure mechanisms occurred and the peak load could not be correlated to the type of failure mechanism.
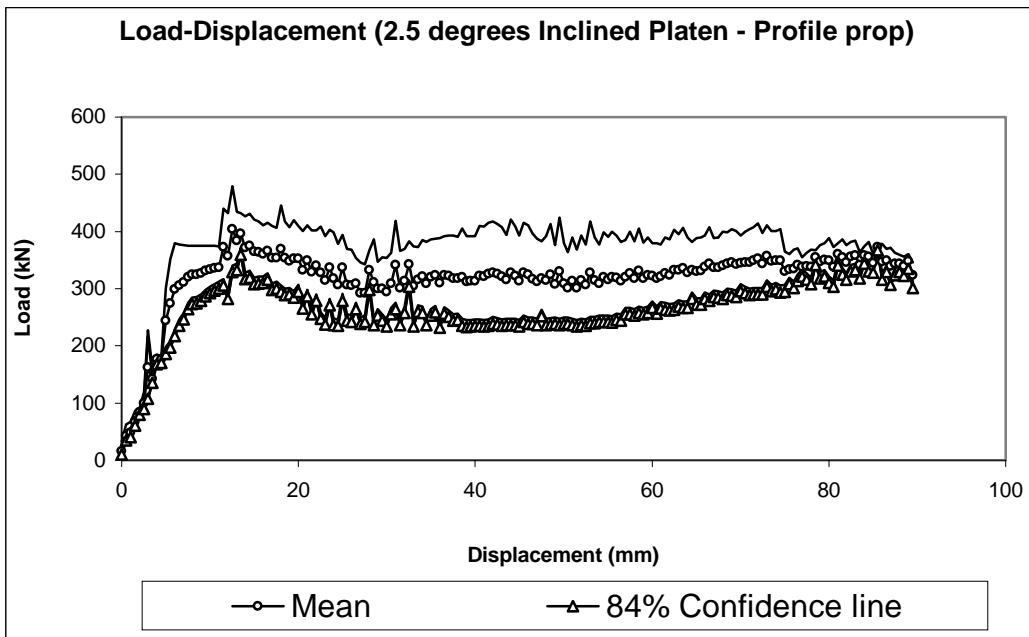
Figure 4.4.4 *Mean and 84 % confidence curves for all 2.5° inclined platen tests.*
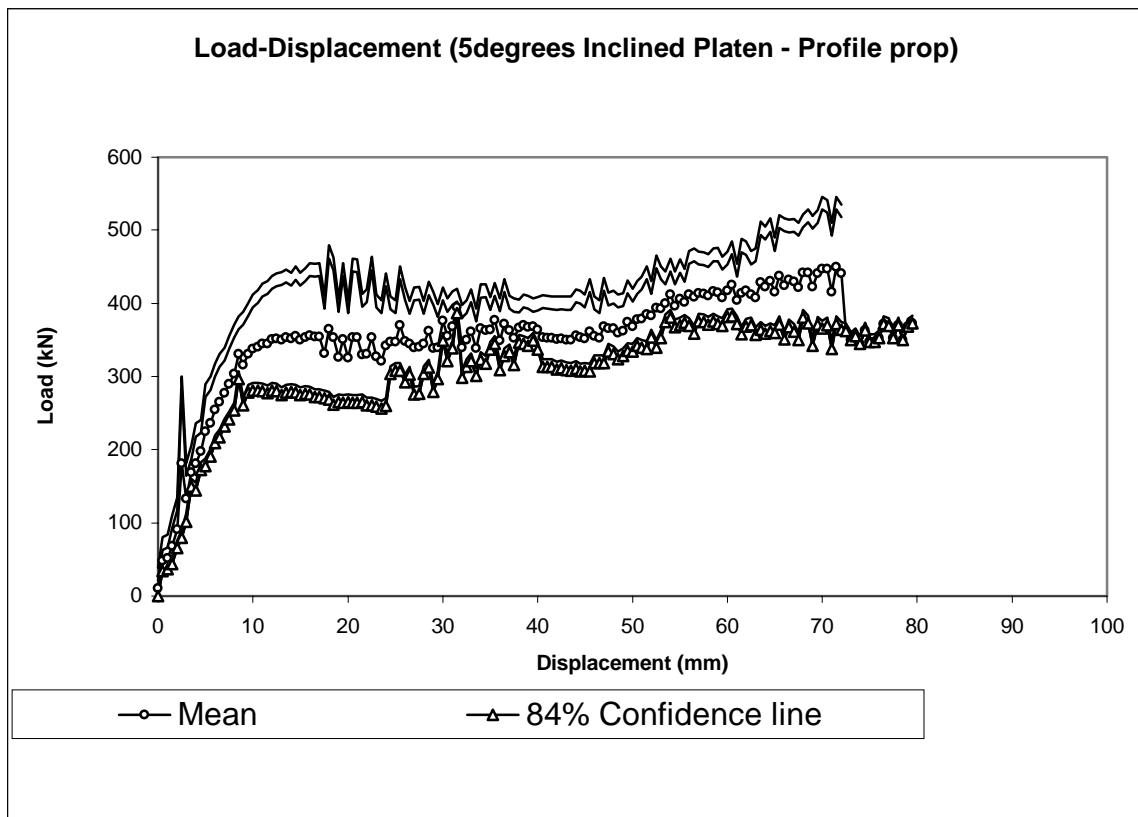
Figure 4.4.5 *Mean and 84 % confidence curves for all 5° inclined platen tests.*
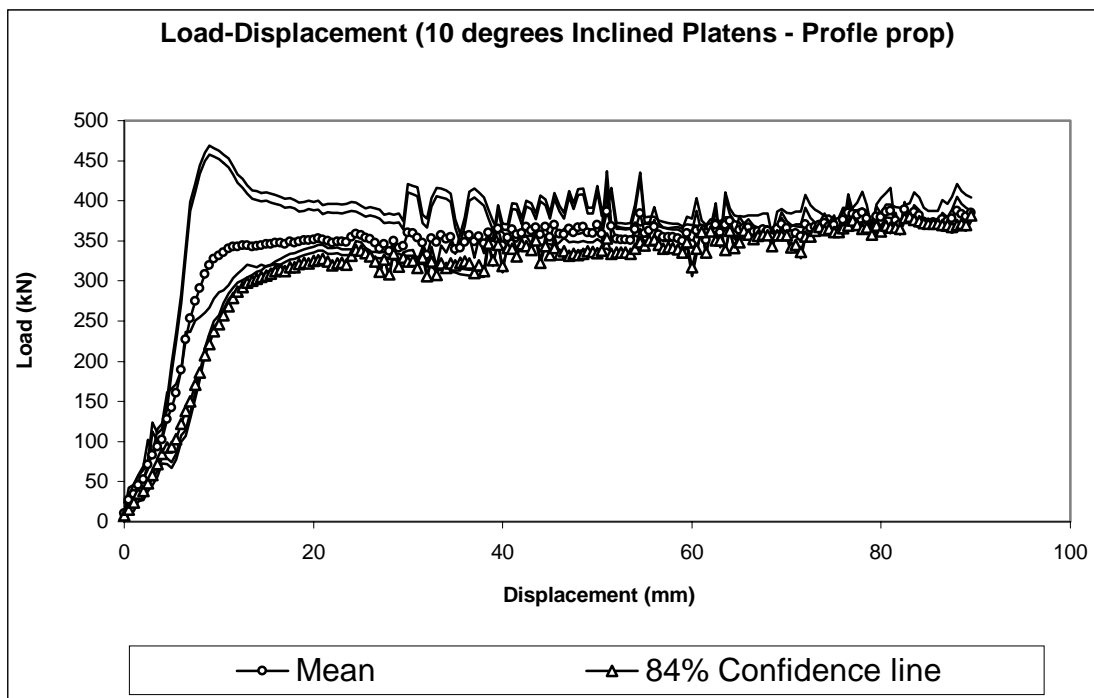
Figure 4.4.6 **Mean and 84 % confidence curves for all 10° inclined platen tests.**

Table 4.4.3 **Failure mechanisms observed for inclined platen tests.**

Test number	Angle (°)	Failure mechanism	Peak load (kN)
18	2,5	Shearing	480
19	2,5	Shearing with splitting	389
20	2,5	Shearing	402
21	5	Shearing with brushing	475
22	5	Brushing	485
23	5	Shearing with brushing	410
24	5	Shearing with brushing	420

25	10	Splitting with brushing	375
26	10	Splitting with brushing	367
27	10	Splitting with brushing	380
28	10	Brushing	473
29	10	Shearing with brushing	470

4.4.4 Discussion of results for profile prop tests

In the compression tests conducted here buckling failure was absent due to the design of the yielding mechanism of the prop, which ensures that the conical frustum and the barrel of the prop are aligned. Thus the prop is symmetric and any asymmetry, which could lead to prop buckling, is eliminated. With increasing length, however, the buckling potential increases and prop buckling is possible.

The mean results for the inclined props, inclined platen and vertical props are summarised in

. As can be seen from the graph, the inclined props are initially stiffer, and the degree of stiffness increases with increasing prop angle (67,5 MN/m for 5° incline prop compared to 75 MN/m for 15° incline prop). At this stage the cause of this trend is not evident and further work is required to identify the mechanisms leading to the increased stiffness. The profile props offering the lowest stiffness were obtained from tests performed with the loading platens inclined (20 MN/m and 32 MN/m for 2,5° and 10° inclined platens, respectively).

Significantly higher peak loads are associated with inclined props (517-640 kN), as compared to inclined platen tests (280-350 kN). In general it appears that, for the 200 mm unturned profile props tested here, the peak load is directly related to the degree of stiffness.

The behaviour of the profile props tested vertically fell between that of inclined props and inclined platen tests.

The post-peak behaviour of all the profiles appears to be similar. In general, there seems to be little difference between the response for vertical and oblique loading, either in terms of displacement or peak load.
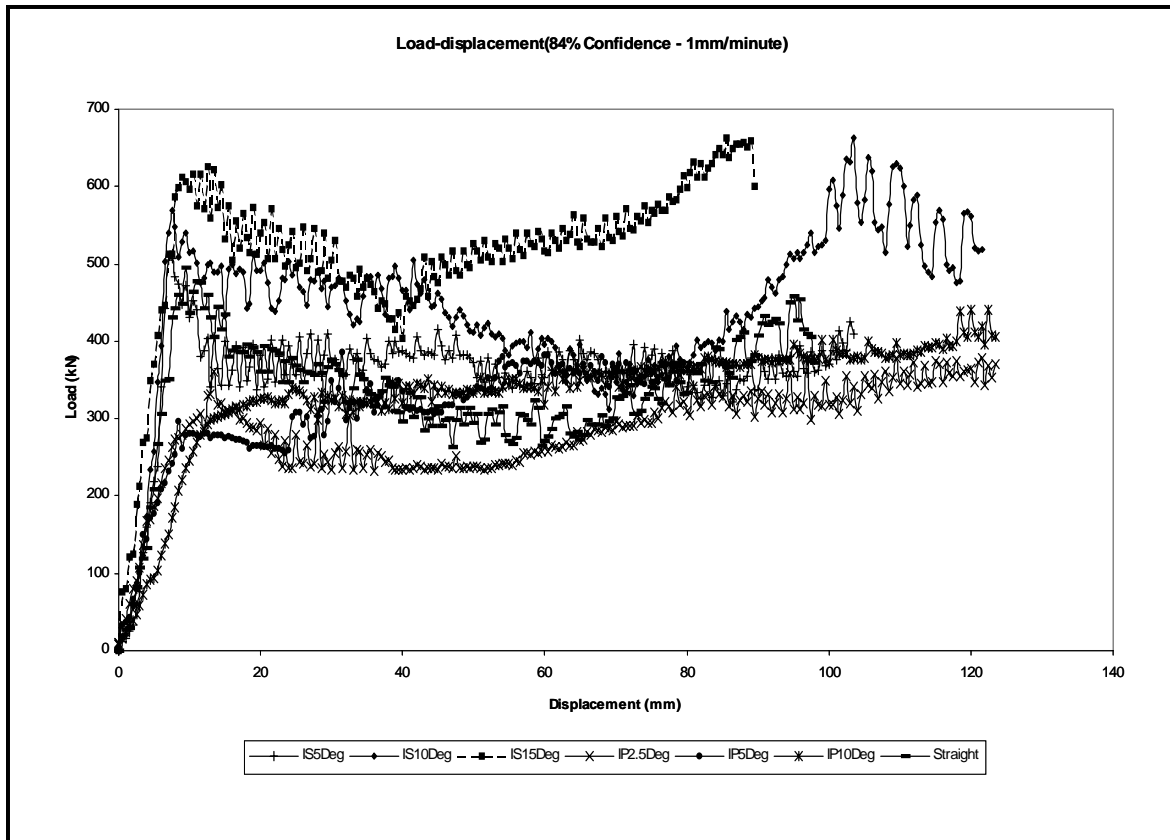
Figure 4.4.8 *Normalised mean load-displacement curves for 5° inclined props (IS5Deg), 10°inclined props (IS10Deg), 15° inclined props (IS15Deg), 2.5° inclined platen (IP2.5Deg), 5° incline platen (IP5Deg), 10° incline platen (IP10Deg) and vertical tests (straight).*

4.5 Underground test results and evaluation

4.5.1 Introduction

Many underground observations have indicated that the actual strength of the support units is less than the strengths derived from laboratory tests. The effects of the angle of installation and oblique loading were investigated underground. The methodology, test data and main findings of the underground testing programme are reviewed below.

4.5.2 Test sites

Four locations, covering a variety of loading conditions, were chosen on two mines. Eighteen 140 mm diameter mine poles were instrumented in three panels at Impala 12 shaft, where the dip of the reef is 10°. Pre-stressing units are used as a standard item on the mine and were included in the test programme. Six 170 mm diameter mine poles were evaluated without pre-stressing units at Union Section, where the reef dip is approximately 18°. Loading angles between 0° and 40° were employed at the Impala site and 0° to 30° at the Union site.

4.5.3 Presentation of results

Figure 4.5.1 shows the effect of installation angle on the peak load recorded for each instrumented unit. The results indicate that installation/loading angle has very little effect on mine pole performance until the onset of slip, which appears to initiate at an installation angle of between 25° and 30°. Hence, the friction angle between timber and rock is between 25° and 30°. The laboratory press was modified, by using a roughened plate as the loading surface, to simulate the underground friction angle of 25° to 30°.

Two major failure modes are observed and several timber conditions promoted either one or the other mode. The modes are:

- Buckling (Figure 4.5.2), where the timber snaps near its centre and loses load comparatively rapidly.

- Brushing over near the top or bottom (Figure 4.5.3), with little load loss and the ability to sustain fairly large deformations.

Buckling is the more common failure mode. Further details of the occurrence of the various failure modes are given in Section 4.5.4.
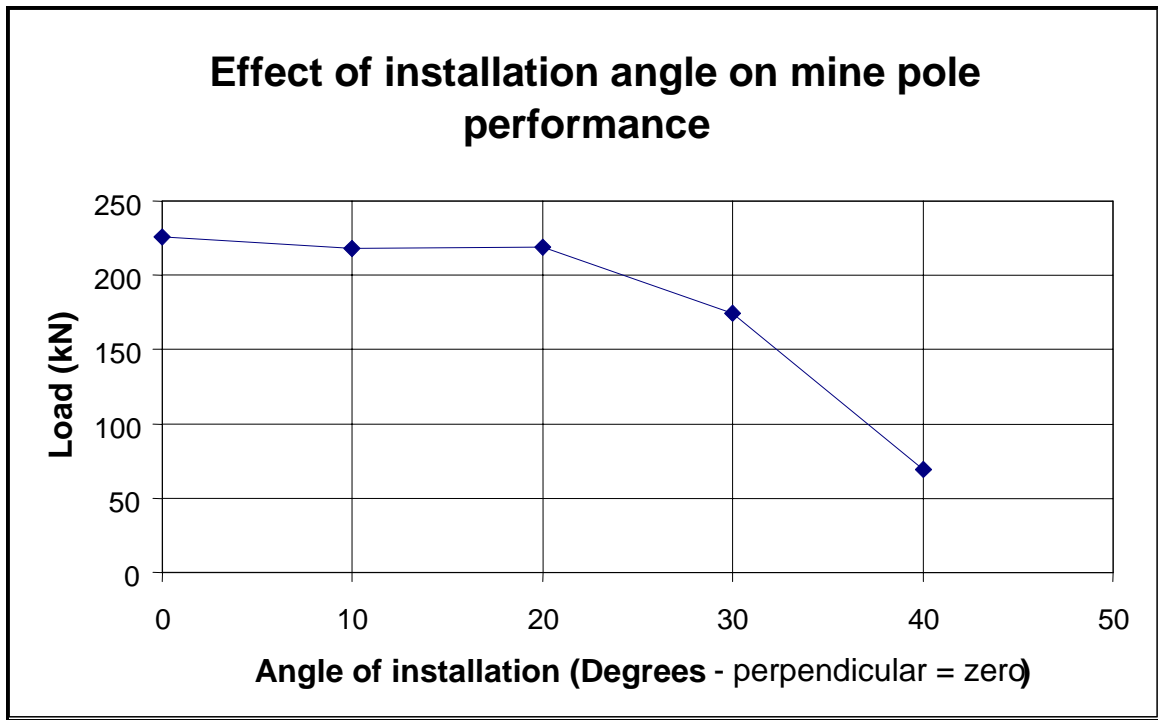
Figure 4.5.1   Average underground test results for oblique loading of Minepoles.

Figure 4.5.2   Photograph showing the buckling failure mode.

Figure 4.5.3   Photograph showing the brushing failure mode.

4.5.4 Discussion of results

Failure modes have a greater influence on prop performance than the installation angle. Figure 4.5.4 shows the average peak load for each of the identified failure mechanisms, and Figure 4.5.5 illustrates the average maximum deformation for each mode. The major modes are brushing, buckling and slip. Splitting of timber was observed underground but did not occur in any of the tests. Blast damage usually causes buckling, but it is compared to the failure modes shown in Figure 4.5.4 and Figure 4.5.5 because of the weakening effect it has on the timber.

Occasionally the timber bulges at the loading surface, apparently because of the confining effect of the loading surface. Timber that bulges is able to sustain large deformations and high loads. There are also indications of the development of a brushing type failure. The results of the bulging mine poles are therefore included with the brushing mode.
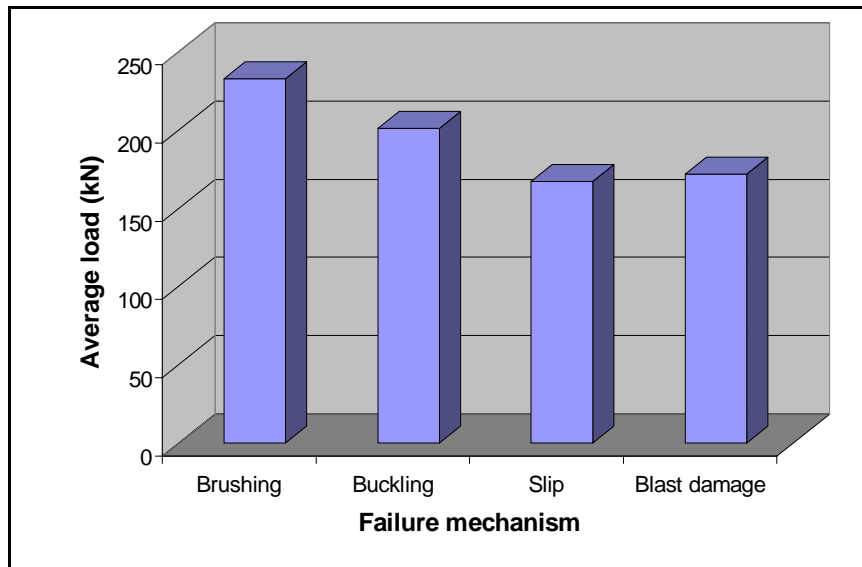
Figure 4.5.4 Effect of failure mechanism on load.
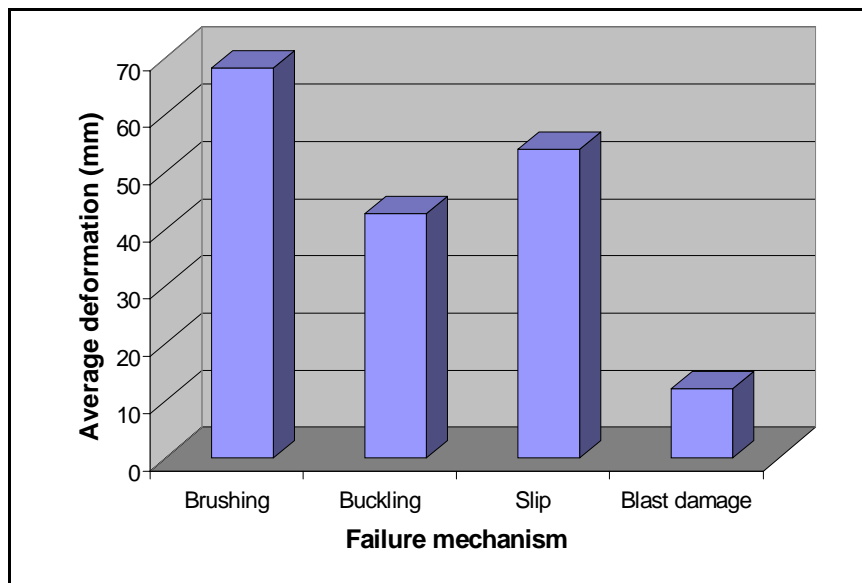
Figure 4.5.5 Effect of failure mechanism on deformation.

The results shown in Figure 4.5.4 and Figure 4.5.5 indicate that the mode of failure with the least deleterious influence on performance is brushing, since this mechanism allows a slightly higher load capacity and much larger deformation than the buckling mode.

Several factors influence the failure mode, some of which are listed below:

- Initial timber shape (Figure 4.5.6), i.e. bowed timber will fail by buckling.

- Condition of the timber, i.e. cracks in the timber (Figure 4.5.7 - the effect of cracks appears to be greater at very slow loading rates). This effect causes buckling.

- Loading surface profiles (Figure 4.5.8). This often causes splitting and subsequent buckling.

- Severe blast and scraper rope damage causes buckling.

The curve and photograph to the left of Figure 4.5.6 are compared to a similar mine pole, tested under similar loading conditions, which was not bent (bowed) before installation.
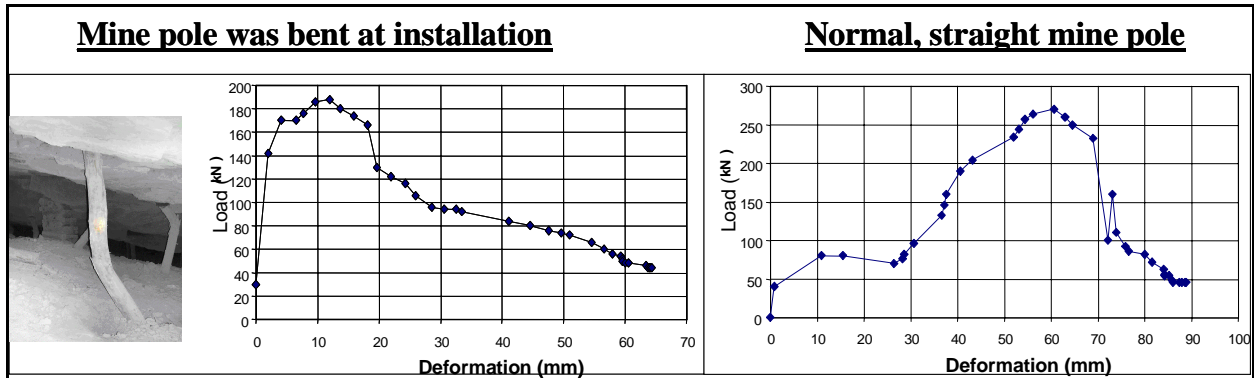
Figure 4.5.6 Effect of initial timber shape on performance.

Figure 4.5.7 shows a comparison between a mine pole with severe cracking under very slow loading conditions, on the left, to an element with only minor cracks under the same loading conditions, to the right of the Figure.
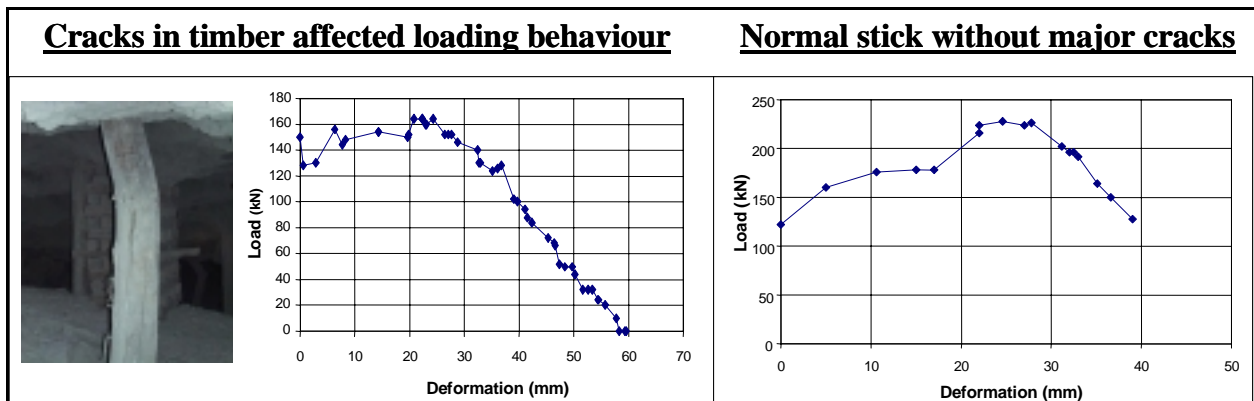
Figure 4.5.7 The effects of cracks in the timber are more apparent at very low loading rates.

The photograph and curve to the left of Figure 4.5.8 are compared to the results of a mine pole that was loaded on relatively flat loading surfaces. All other conditions were similar.

154

Effects of an uneven hangingwall	Normal, relatively smooth hangingwall conditions
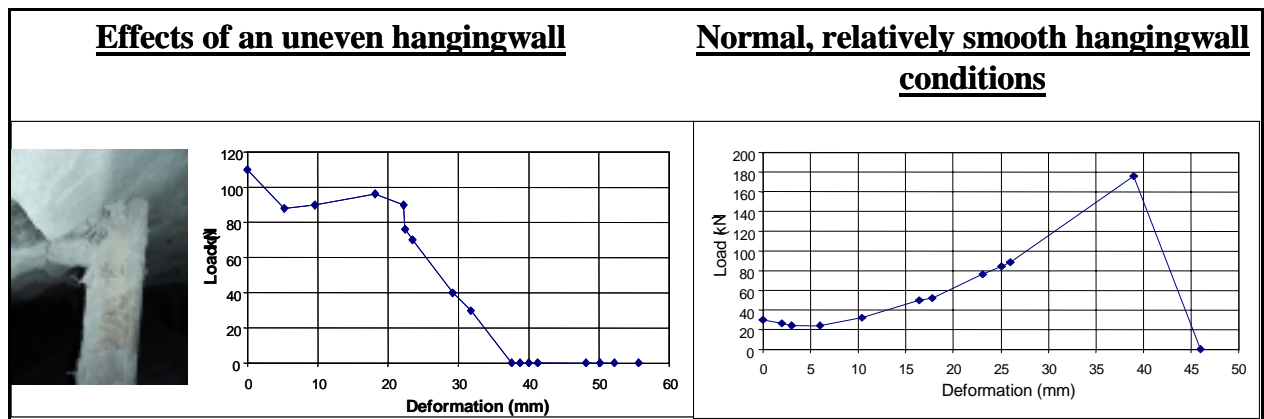
Figure 4.5.8 Effects of uneven hangingwall or footwall.

4.5.5 Observations

Uneven hangingwall or footwall, scraper rope and blast damage (Figure 4.5.9) have a greater influence on timber strength than installation angle or loading angle. Uneven loading conditions lead to progressive and premature failure. Scraper ropes often tend to cut into the timber, thus providing a weakness where buckling can initiate. Blast damage affects the outer layers of the pole. The outer layers of the pole (where failure is typically initiated) provide a significant proportion of the load bearing capacity of timber. It is therefore important to protect the timber from this type of damage.

Mine pole damaged by blast	Mine pole under similar loading conditions but no blast damage
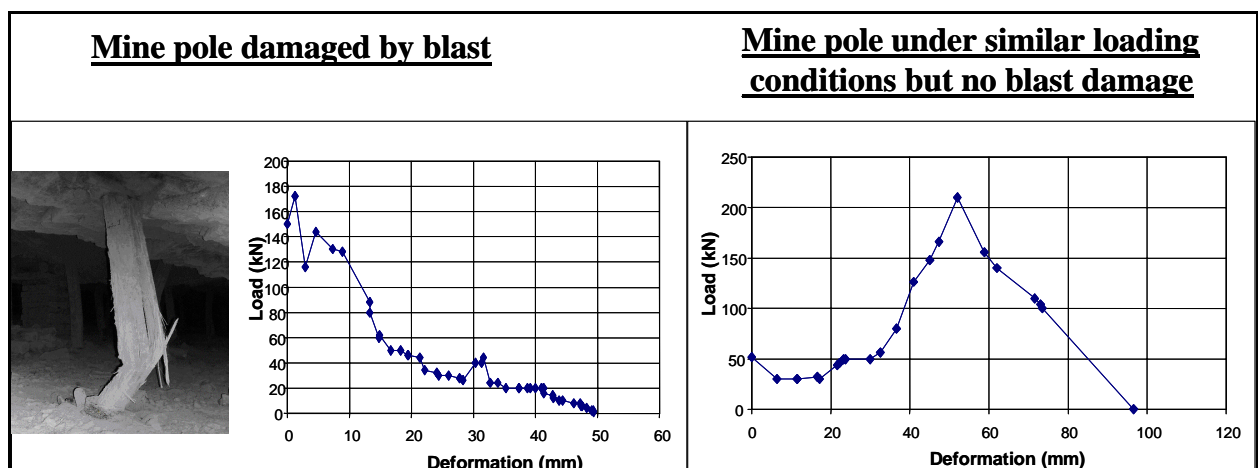
Figure 4.5.9 Effects of blast damage on support elements.

154

4.5.5.1 Effect of pre-stressing

The pre-stressing units (pots) used for the tests had limited, if any, effect on reducing the yield capacity of the mine poles. In some cases, where the props were cut shorter than recommended, the yield appears to have increased. The reason is that the steel on the inside of the pot yields at approximately 150 kN (depending on the diameter of the prop in contact with the unit). Thus, the volume of water above the prop is transferred to the side of the prop until the gap between the timber and loading surface is reduced to zero or the pot fails. In the laboratory, much higher loads are achieved for the same timber and pots. This discrepancy has been attributed to a softer loading environment underground, in particular the damaged footwall, which allows more deformation to take place on the pots. This inelastic deformation weakens the pots. Many pots were discarded because of failure during installation, but these were generally the result of faulty valves. After successful installations, pot failures often occurred at some distance from the face (Figure 4.5.10), but none of the instrumented props lost load completely. Figure 4.5.10 shows that the pot fails at 10 m behind the face and the load drop is 120 kN. The pot failure causes premature mine pole failure, but the load bearing capacity of the element at this point is still greater than 200 kN.
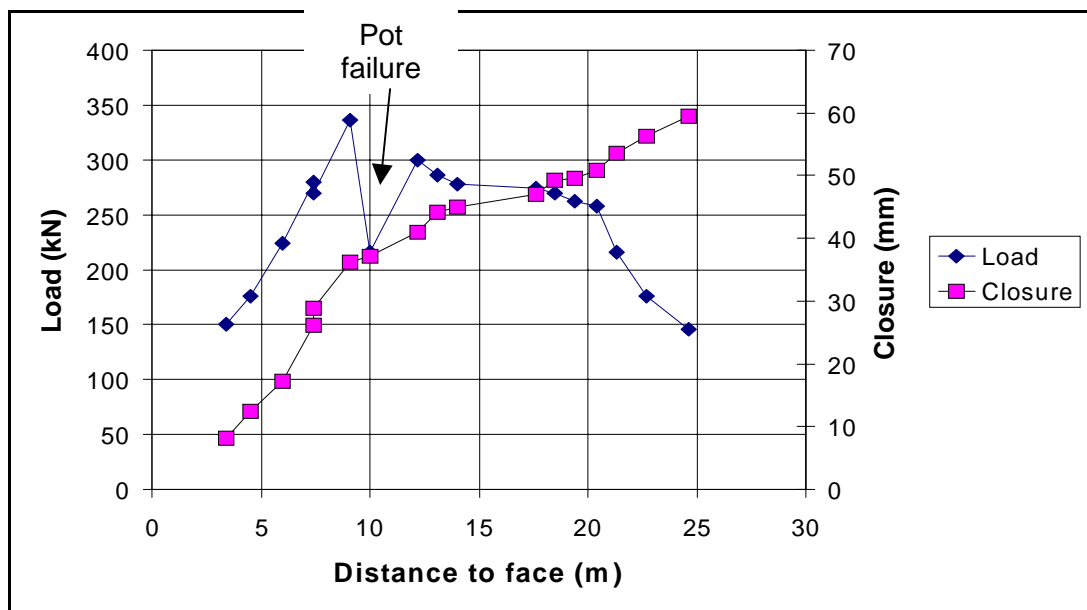
Figure 4.5.10   Effect of a pot failure on prop behaviour.

4.5.5.2 Effect of the blast on timber performance

Loading rates on support elements underground are not constant. Figure 4.5.11 is a time history of stope closure and mine pole load, indicating that relatively high rates of closure occur immediately after the blast, especially near the face.
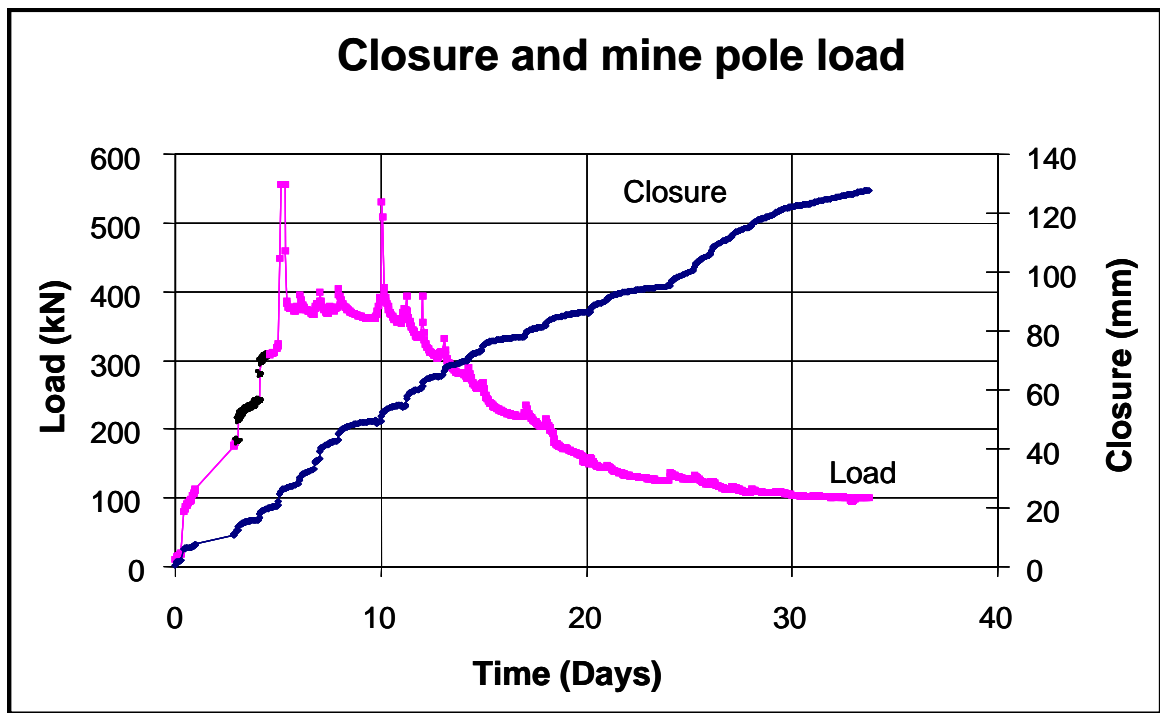
Figure 4.5.11   *Effect of blasting on loading rate.*

At the Impala site the closure rates are generally low and the support elements were not highly stressed near the face. Therefore, the loading effects of the blast were small. At the Union Section site, however, the closure rates are relatively high and the blast caused premature failure of the timber, by initiating high loads during rapid closure rates (see Figure 4.5.11.) A daily instrumentation reading rate at this site would have missed the peak load on the prop and the true, erratic loading conditions.

Figure 4.5.12 is a snapshot of the mine pole behaviour during a blast, after failure of the element has taken place. Readings are taken at two-minute intervals and show a rapid increase in load over a 12-minute period and a slower reduction load after the peak. The whole event is completed in approximately one hour.
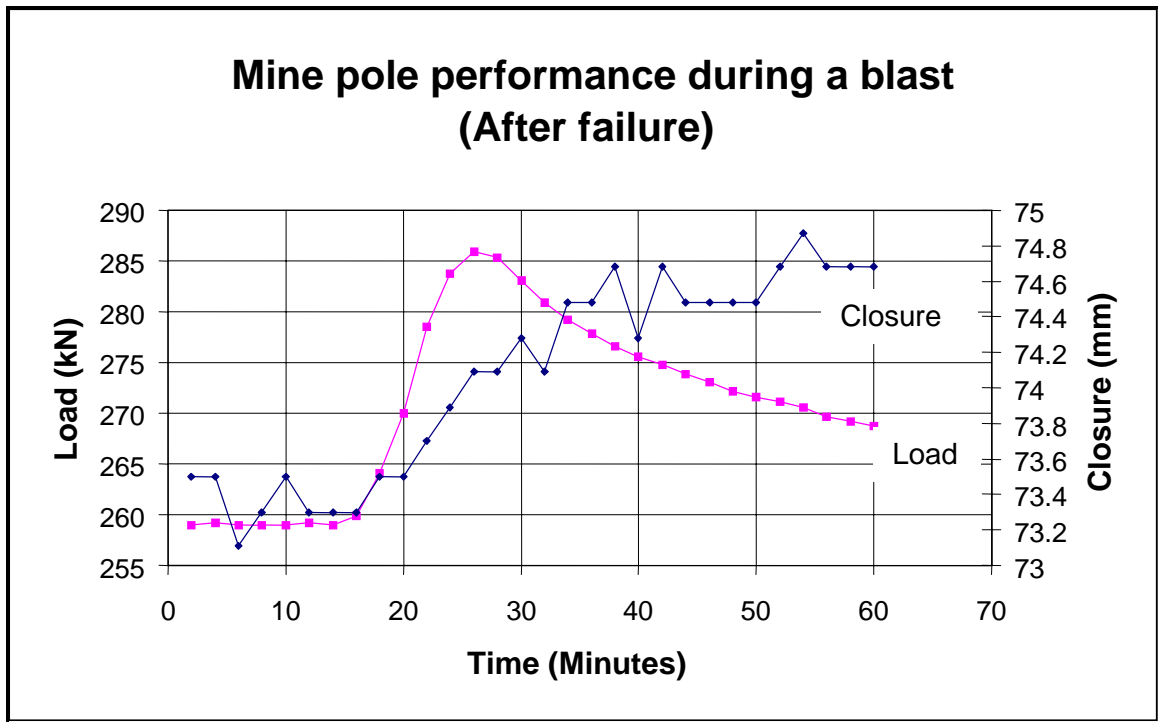
Figure 4.5.12   Effect of the blast on a mine pole after failure.

Geophones (their recordings are shown in Figure 4.5.13) were installed at the Union site, on mine pole number 1N_1 and on the hangingwall and footwall near the element. The experiment did not provide much information because the geophones were too sensitive and the unit attached to the mine pole was malfunctioning. However, the equipment indicated that vibrations in the hangingwall were more severe than in the footwall despite the fact that the footwall appeared crushed.

It is recommended that further geophone tests be conducted to evaluate the dynamic performance of elongates, and specifically investigate the dynamic interaction of the support unit with the hanging- and footwall during seismic events. These tests are of particular relevance in a deep-level mining environment, where effective rockburst resistant support systems are required to maintain stability of the rock mass during seismic events.
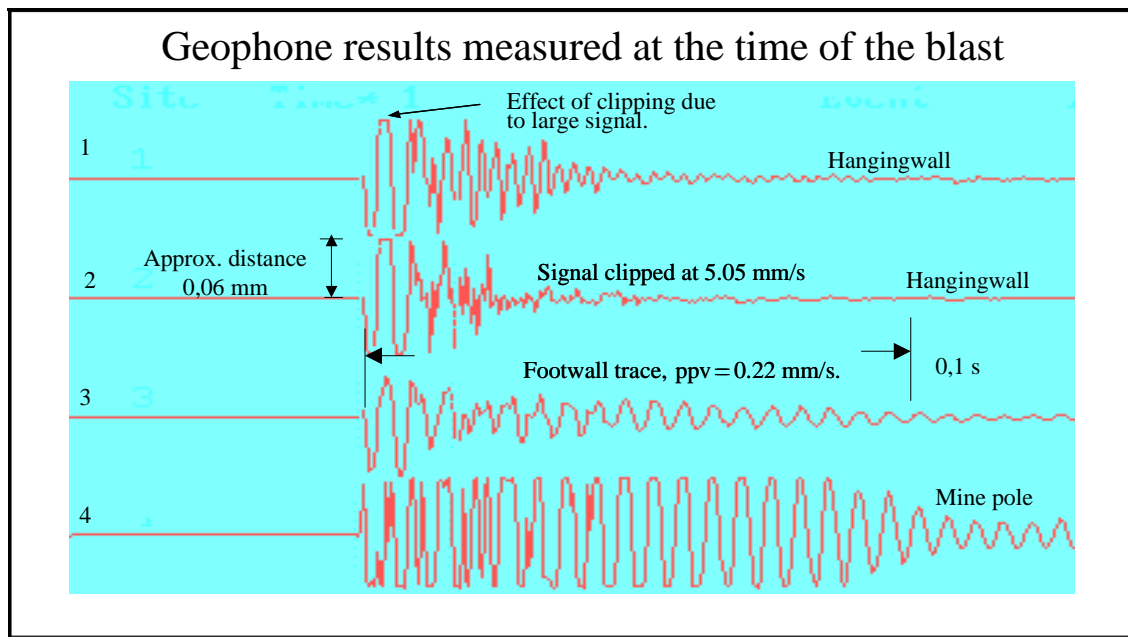
Figure 4.5.13   Seismogram results for the hangingwall, footwall and mine pole.

4.5.6 Analysis of results

4.5.6.1 Evaluation of individual mine pole performance

140 mm diameter mine poles with pre-stressing units

Figure 4.5.14 shows the results of individual tests, and indicates that the weakest element has a load capacity of approximately 135 kN. It should be noted that this result is stronger than the statistical evaluation of the same data, shown in Figure 4.5.18 or Figure 4.5.19, because the tests are evaluated individually and not affected by other failed or partially loaded elements in the neighbourhood. This analysis allows design considerations, based purely on timber strength, where a percentage of intact mine poles can be used in an evaluation (i.e. if 90 per cent is considered acceptable then a load capacity of 150 kN can be assumed from the curve in Figure 4.5.14). This strength can be downgraded to account for the failed elements.

Maximum load capacity of 140 mm diameter mine pole
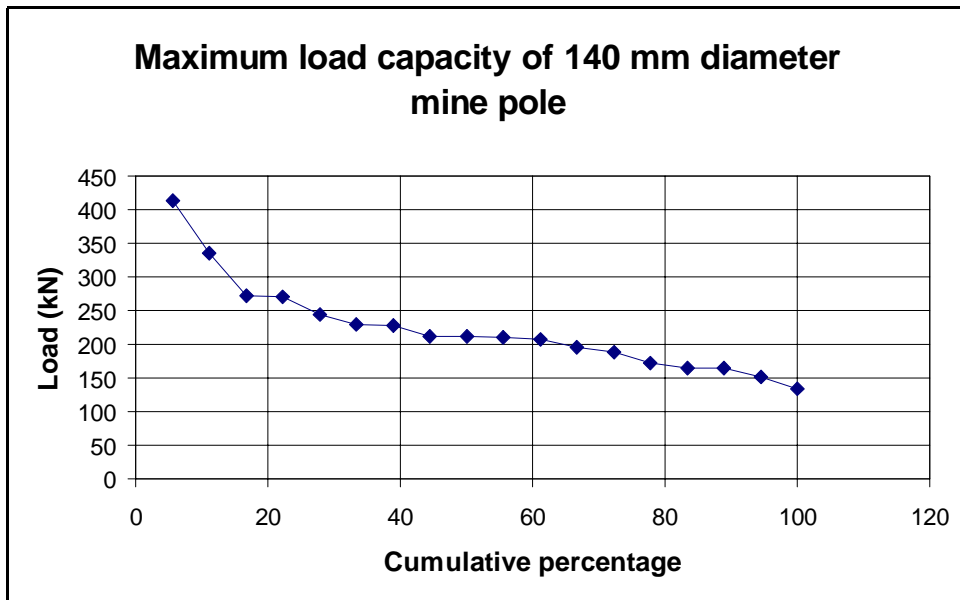
Figure 4.5.14   Cumulative evaluation of load capacity in terms of percentage of all tests installed up to an angle of 20^0.

The set of tests shown in Figure 4.5.14 are also analysed in terms of deformation and presented in Figure 4.5.15. In this analysis the deformation is recorded at the point where the load had dropped to 100 kN. Figure 4.5.15 can be used to determine the distance from the face at which some or all elements will be able to carry 100 kN. The face advance scale on the right of Figure 4.5.15 is calculated using the data shown in Figure 4.5.20 and can be applied to panels with a closure rate of approximately 0,7 mm per metre face advance. In this situation Figure 4.5.15 indicates that up to a distance of seven metres behind the face, the support resistance is greater than 25 kN/m^2 assuming a spacing of 2 m x 2 m (based on a 100 kN load capacity, see Figure 4.5.14 and Figure 4.5.19). This is sufficient to support a 0,83 m thickness of hangingwall strata (assuming ρ_{Rock} = 3000 kg/m^3).

Deformation at 100 kN load on 140 mm diameter mine poles
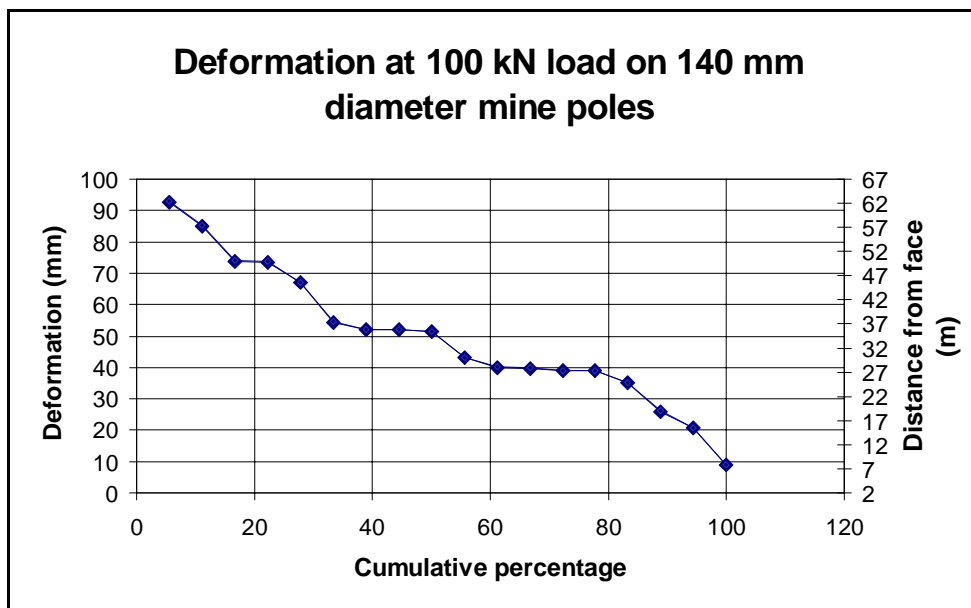
Figure 4.5.15   Cumulative evaluation of deformation at 100 kN in terms of percentage of all tests installed up to an angle of 20^0.

170 mm diameter mine poles

The results in Figure 4.5.16 show individual performances of 170 mm diameter mine poles. The analysis indicates that all elements are able to support a load of 200 kN.
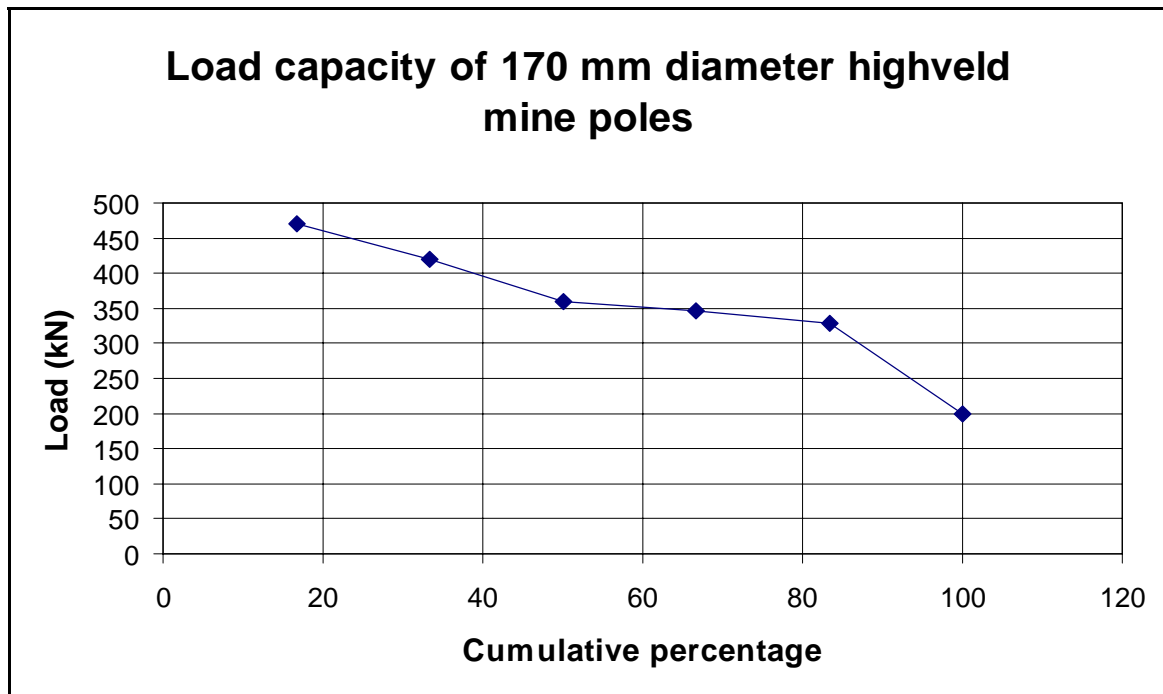
Figure 4.5.16 *Cumulative evaluation of load capacity in terms of percentage of all 170 mm diameter mine poles.*

The analysis shown in Figure 4.5.17 is similar to the analysis described for Figure 4.5.15, except that a load of 200 kN is used to determine the deformation.
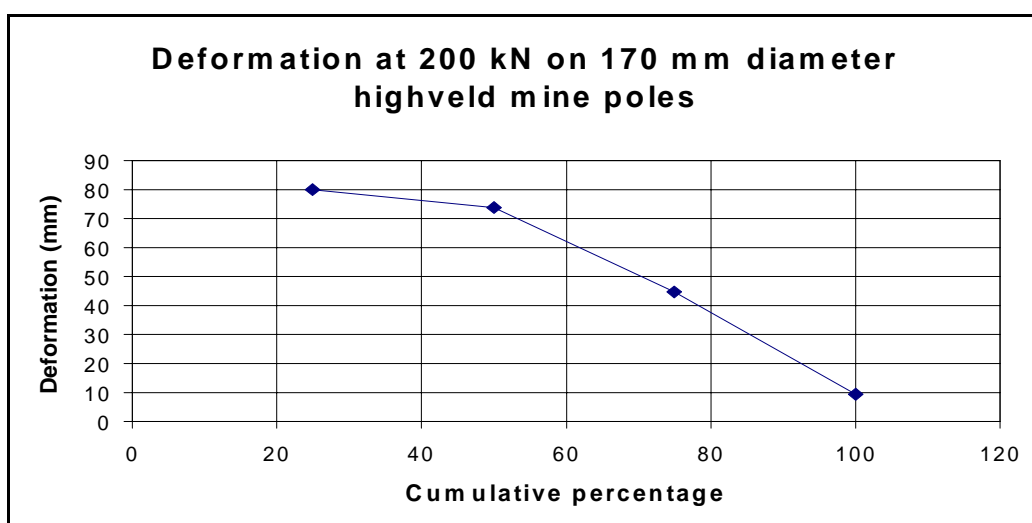
Figure 4.5.17 *Cumulative evaluation of deformation at 200 kN in terms of percentage of all the tests performed on 170 mm diameter mine poles.*

4.5.6.2 Evaluation of the data from multiple mine pole tests using statistical methods

140 mm diameter mine poles with pre-stressing units

Since the loading angle has very little effect on mine pole capacity (Figure 4.5.1), all tests performed at installation angles of 20^0 and less are included in the analysis shown in Figure 4.5.18.

Mean and standard deviations for 140 mm diameter mine poles

(Installation angles up to 20 degrees)
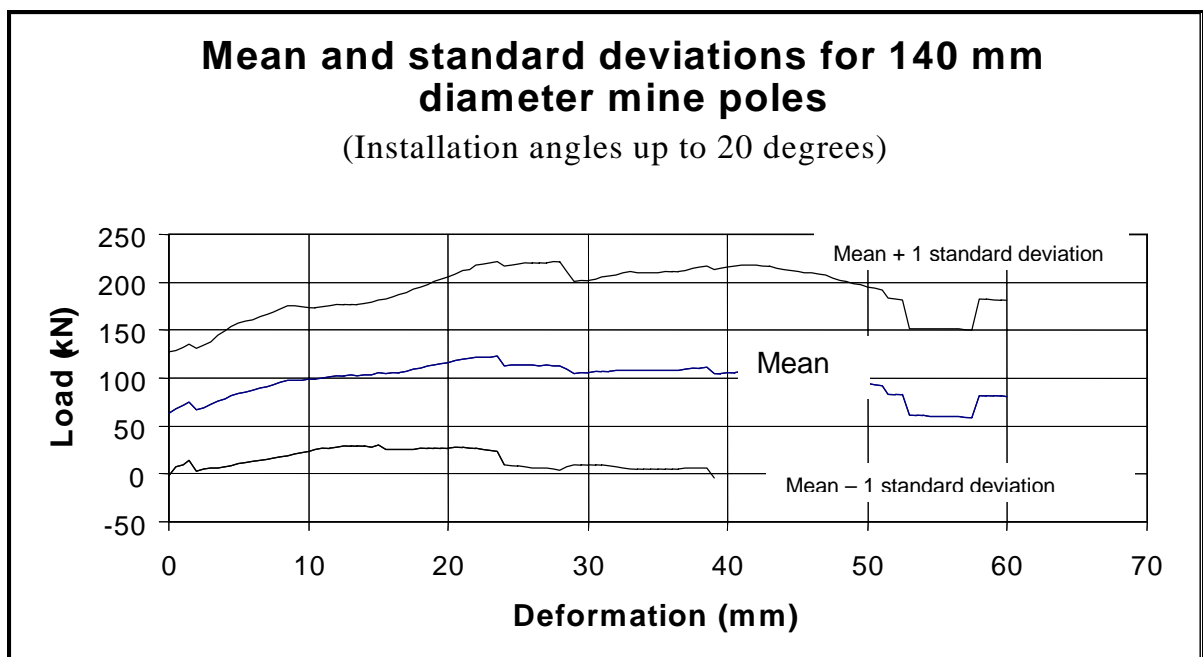
Figure 4.5.18   Analysis of all 140 mm diameter mine pole tests, up to an installation angle of 20^0, performed at the Impala site.

It should be noted that, although the load-bearing capacity of individual support units is highly variable, the mean of the load-deformation curves is comparatively smooth with a peak load between 100 kN and 150 kN. In Figure A1.1 it can be seen that samples 2 and 7 show a softer response with peak loads recorded between 50 mm and 80 mm displacement. Samples 10 and 11 show a stiffer response with peak loads occurring at between 5 mm and 15 mm. This variability results in the mean curve being flatter and the mean loads being lower than the peak loads of individual support units. This is confirmed by the fact that the average peak load for the samples used in the statistical analysis is approximately 220 kN, while the peak load indicated for the mean curve is less than 130 kN.

Hence the statistical analysis of the underground results shows approximately half the expected load capacity of 200 kN and a larger than expected deformation capability.

To ensure a high probability of the support system to at least meet the load capacity requirements, a statistical interpretation of the load-deformation curves is required. Daehnke *et al.* (1998) present a system for calculating the confidence curves for any number of active support units. The equations relating mean, standard deviation and confidence level are presented in Table 4.5.1. These equations are applied to the results shown in Figure 4.5.18 and 90 % confidence performance curves are given in Figure 4.5.19. The performance curves are given for various values of *n*, where *n* is the number of support units governing the local rock mass stability. In a highly discontinuous hangingwall (i.e. each keyblock is supported by a single support unit), a value of *n* = 1 is applicable. For a more continuous hangingwall with comparatively large keyblocks, the stability depends on multiple support units, and *n* = 10 to 30 is be applicable.

From Figure 4.5.19 it is apparent that it is not feasible to use 140 mm diameter mine poles if the local rock mass stability is dependent on single support units (i.e. *n* = 1). In areas where larger FOGs are expected (where 30 or more mine poles are involved) the design capacity that should be used is approximately 80 kN per unit over a deformation of approximately 40 mm.

Figure 4.5.20 relates face advance to closure (measured 2 – 3 m from the stope face), indicating that under typical mining conditions at 1000 m below surface, 40 mm convergence equates to approximately 25 m face advance.

Table 4.5.1   Relating design capacity ($\bar{x}$), mean capacity ( ) and standard deviation ( ) of support elements, for probability levels of 90 per cent, 95 per cent and 99 per cent (after Daehnke et al., 1998).

Number of props	Degree of confidence		
	90 %	**95 %**	**99 %**
$n = 1$	$\bar{x} = \mu - 1{,}282\sigma$	$\bar{x} = \mu - 1{,}645\sigma$	$\bar{x} = \mu - 2{,}326\sigma$
$n = 3$	$\bar{x} = \mu - 0{,}740\sigma$	$\bar{x} = \mu - 0{,}950\sigma$	$\bar{x} = \mu - 1{,}343\sigma$
$n = 10$	$\bar{x} = \mu - 0{,}405\sigma$	$\bar{x} = \mu - 0{,}520\sigma$	$\bar{x} = \mu - 0{,}736\sigma$
$n = 30$	$\bar{x} = \mu - 0{,}234\sigma$	$\bar{x} = \mu - 0{,}300\sigma$	$\bar{x} = \mu - 0{,}425\sigma$
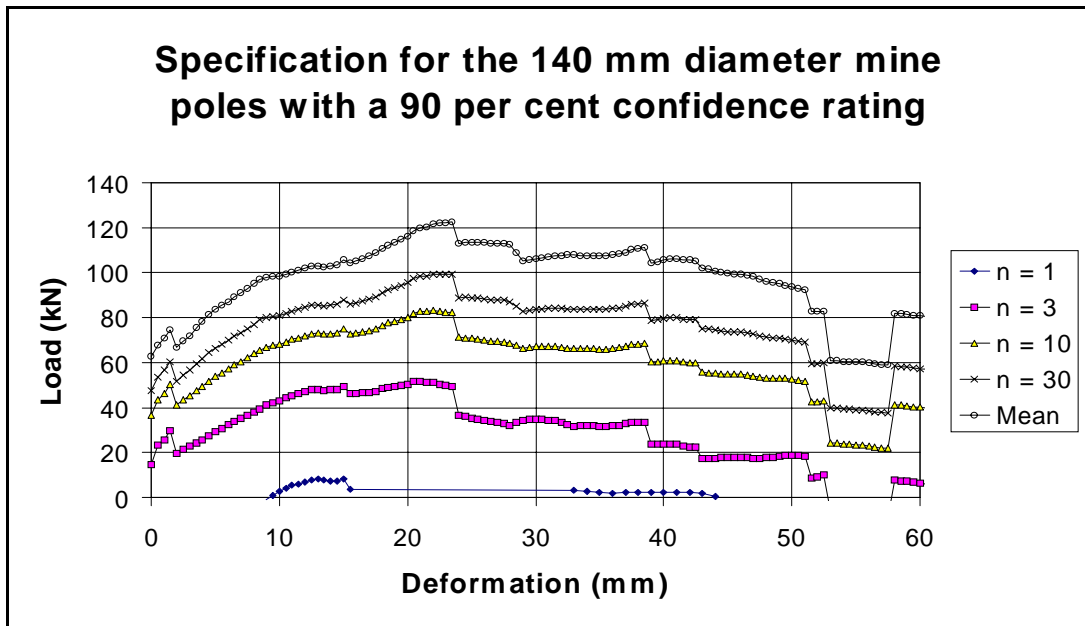
Figure 4.5.19 *Statistical results of the underground tests performed on 140 mm diameter mine poles, using the equations given in Table 4.5.1.*
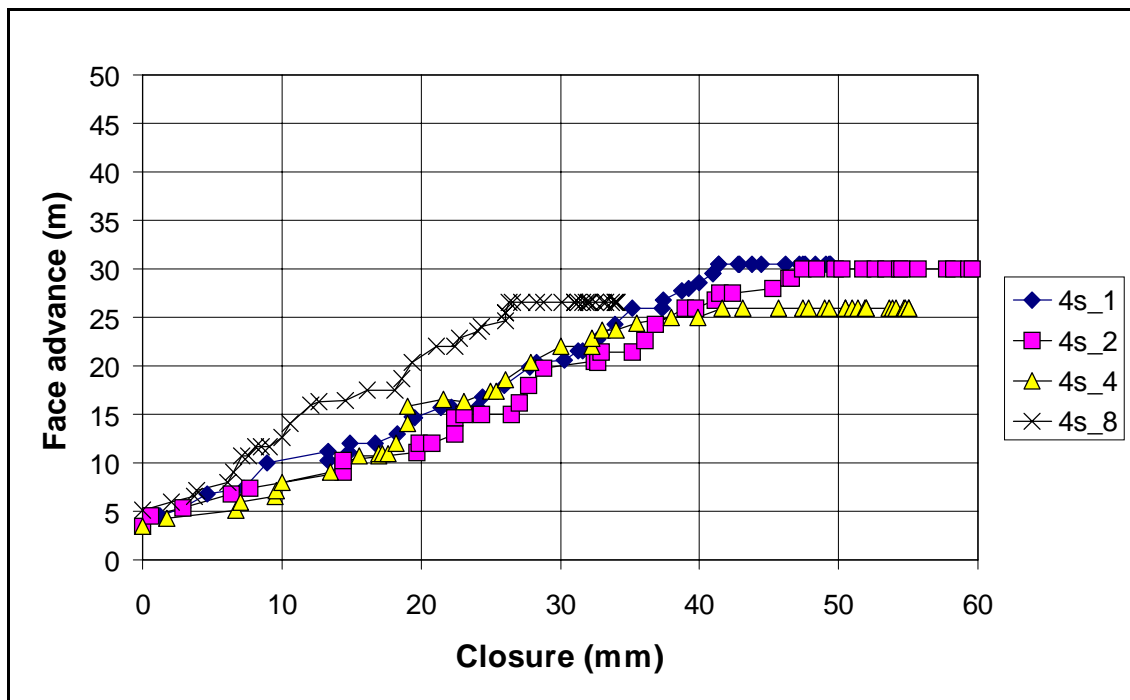
Figure 4.5.20 *Closure in a panel at approximately 1000 m below surface.*

170 mm diameter Highveld mine poles with no pre-stressing units

The tests were performed at Union Section where the closure rate is approximately 3,7mm per day. Several conditions were different at this site compared to the Impala site:

- The dip of the reef is steeper (approximately 18^0 compared to 10^0).

- There was considerable ride as shown in Figure 4.5.21 (the ride measured at Impala was negligible).

- The hangingwall conditions are more blocky.

- Grout packs are used in addition to mine poles.

- The stoping width is slightly narrower (1,0 m instead of 1,2 m).

- The footwall is softer and less competent.

- Face advance is 0,5 m per blast whereas, at the Impala site, 1,0 m advances are achieved.
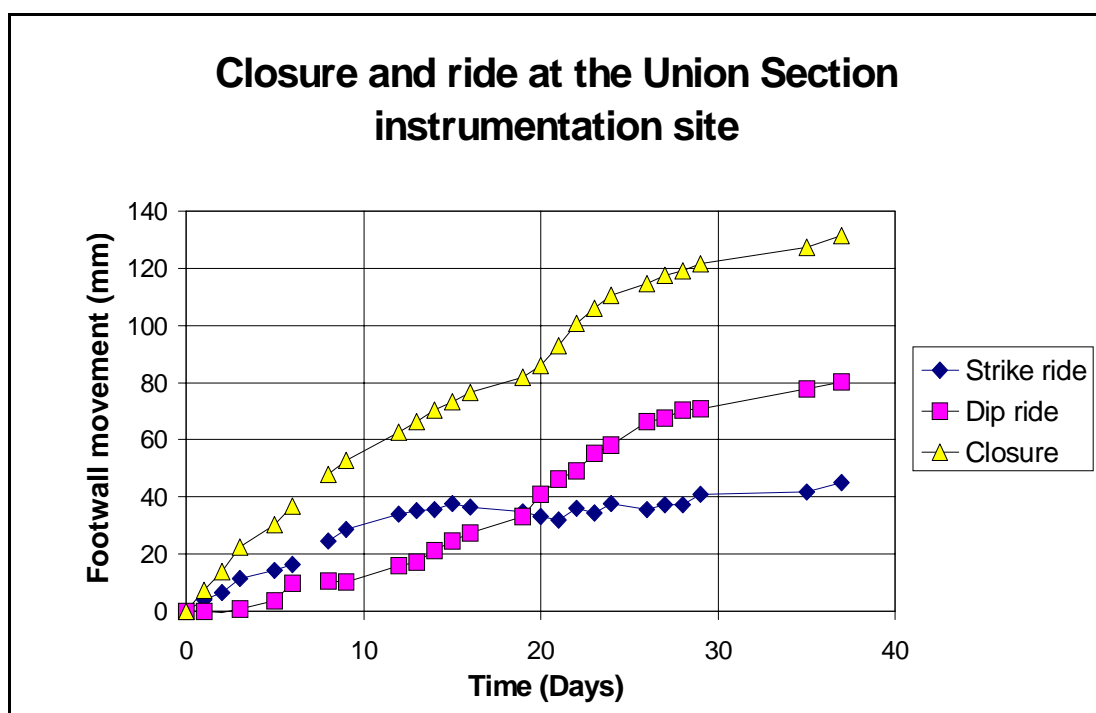
Figure 4.5.21   Closure and ride measured at the Union Section instrumentation site (measurements stations initially installed 2 – 3 m from the stope face).

The ride rotated the props slightly during loading, but was less than 1° when the element had reached peak load and a maximum of approximately 4° during the working lifetime of the prop.

Work performed in the test laboratory indicted that 1° – 4° does not significantly affect the performance, and hence the effect of dip ride at the Union Section site could be neglected.

The mean and 84 % confidence lines (plus and minus one standard deviation) for the 170 mm diameter mine poles tested at Union Section are presented in Figure 4.5.22. The individual results for these mine poles are presented in Figure A1.3. The performance variability of the 170 mm diameter mine poles is not as high as the performance variability of the 140 mm mine poles. This, coupled with the fact that the 170 mm diameter mine poles offer a higher load bearing capacity, result in higher 90 % confidence performance curves.

The results indicate that the 170 mm mine poles are more suited to blocky hangingwall conditions than the 140 mm diameter elements tested at Impala, because the statistical analysis shown in Figure 4.5.23 indicates a high probability that a single element will be able to sustain a significant load capacity (peak load exceeding 200 kN).

Figure 4.5.23 shows that in blocky ground conditions, where each element supports the tributary area around it, 90 per cent of the elements will remain intact provided the closure is less than 29 mm and the load imposed by the dead weight of loose material is less than 200 kN. In this case, the thickness of hangingwall that the system is able to carry can be calculated by using the curve with $n = 1$ (Figure 4.5.23). For example, a support spacing of 1,6 m on dip and 2 m on strike can carry a slab approximately 2 m thick. Approximately half this thickness can be supported for 40 mm closure.
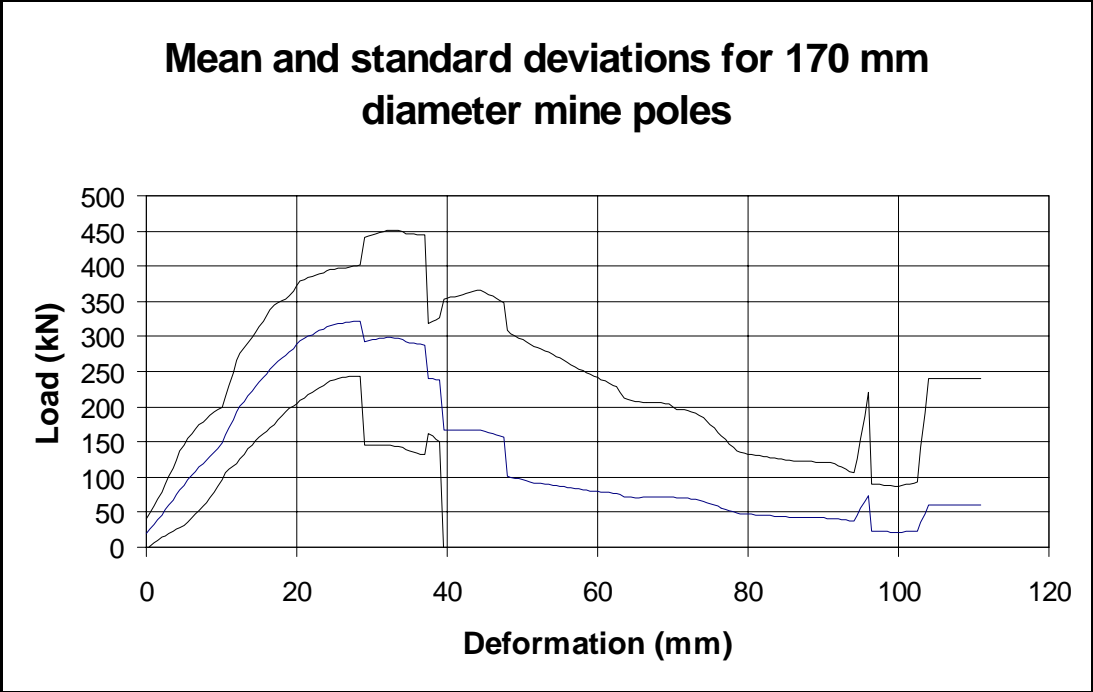
Figure 4.5.22   Analysis of the 170 mm diameter mine poles, performed at Union Section.

154

Specification for the 170 mm diameter highveld mine poles with a 90 per cent confidence rating
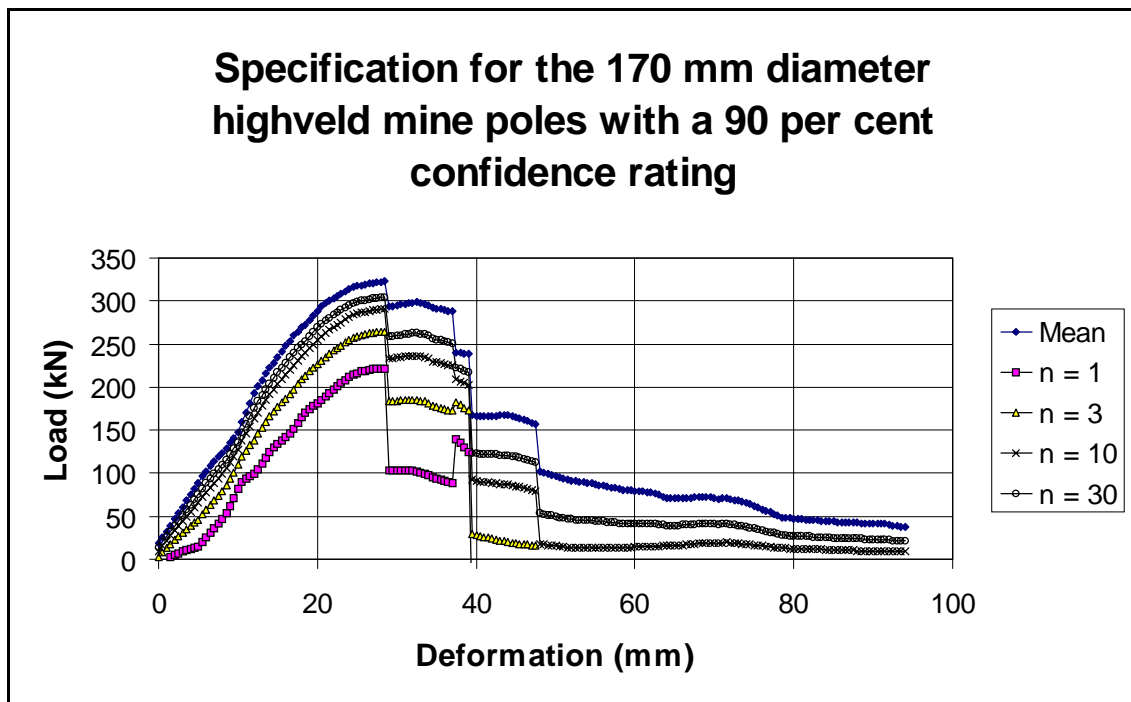
Figure 4.5.23   Downgraded results of the underground tests performed on 170 mm diameter, mine poles, using the equations given in Table 4.5.1.

Figure 4.5.24 shows the absolute closure at the two positions where the investigation was conducted. Three tests were initiated at 1,9 m, and three at 15 m from the face. Using the analysis discussed above, elements installed approximately 1,5 m from the face are expected to maintain their load-bearing capacity (at least 200 kN) for approximately 3,0 m face advance.
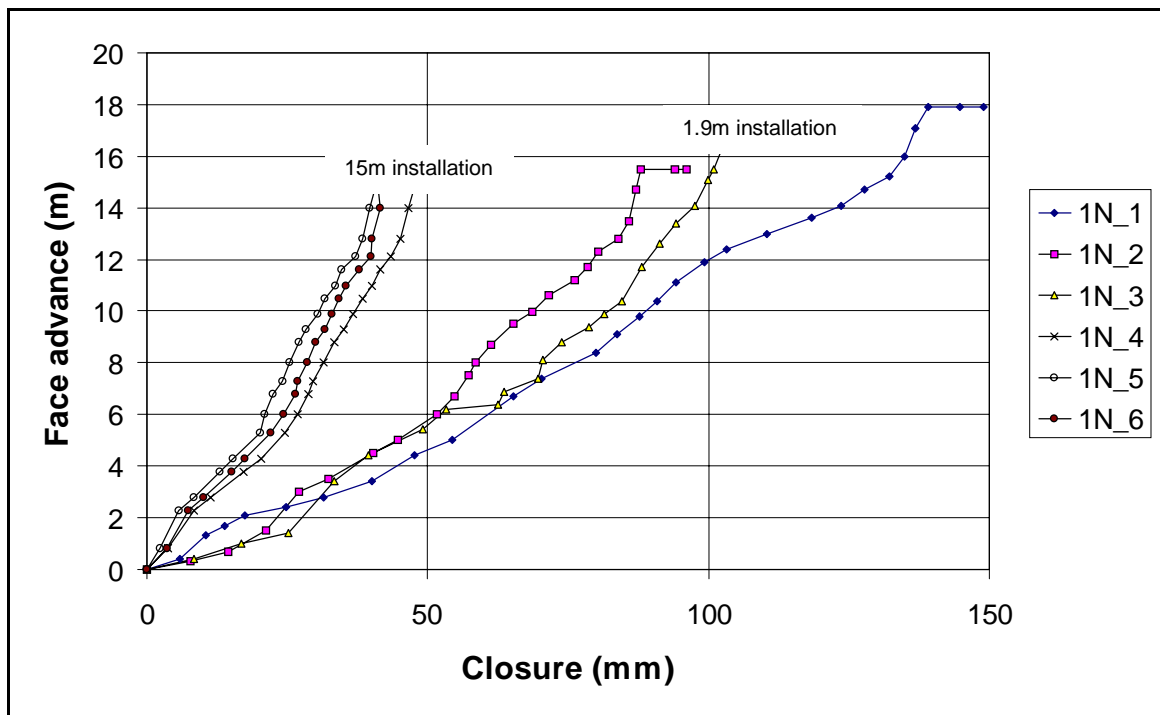
Figure 4.5.24   Closure rates at two distances from the face at the Union Section instrumentation site.

4.5.7 Conclusions

Up to the point of slip, there is no measurable effect of installation angle or loading angle on the performance of the mine poles that were tested. At angles of 30^0 and above, slip occurs, reducing the load-bearing capacity of the unit. Other factors such as blast and scraper rope damage, uneven loading conditions, severe cracking and pot interaction have a more significant effect on timber performance. Two major failure modes are observed in the tests, namely buckling and brushing. Splitting is also observed underground, but did not occur in any of the tests. The most common mode is buckling. Buckling usually results in failure at relatively small deformations and slightly lower loads than when the timber brushes.

The variation in failure loads for a given closure results in the timber failing at various stages of face advance, thus lowering the average load bearing capacity of the support system. In areas where the hangingwall conditions are blocky, each support element can only support the zone directly above. The number of units relied upon to support a given weight is therefore reduced as hangingwall conditions become more blocky. Under such conditions, 140 mm mine poles (with an average strength of 130 kN) are unsuitable. The performance of the 170 mm mine poles is less variable and therefore more suitable to blocky conditions.

The variable performance of the 140 mm mine poles is due to the variation in the initial stiffness of the response. A soft initial response results in the ultimate load being realised at higher displacements. Laboratory tests reveal that the response should be stiffer than those observed for samples 6s_2 and 6s_7 in Figure A1.1.

In the underground situation, there are additional factors, which contribute towards the load response, reducing the initial stiffness. These factors include the contribution of the pre-stressing unit, the deformation of the fractured footwall and effects introduced by uneven contact between the support unit and the hangingwall.

Consider the conceptual model presented in Figure 4.5.25. The potential causes of the 'softness' of the response are illustrated. The contributions of the various relevant components may be expressed as non-linear springs in series.
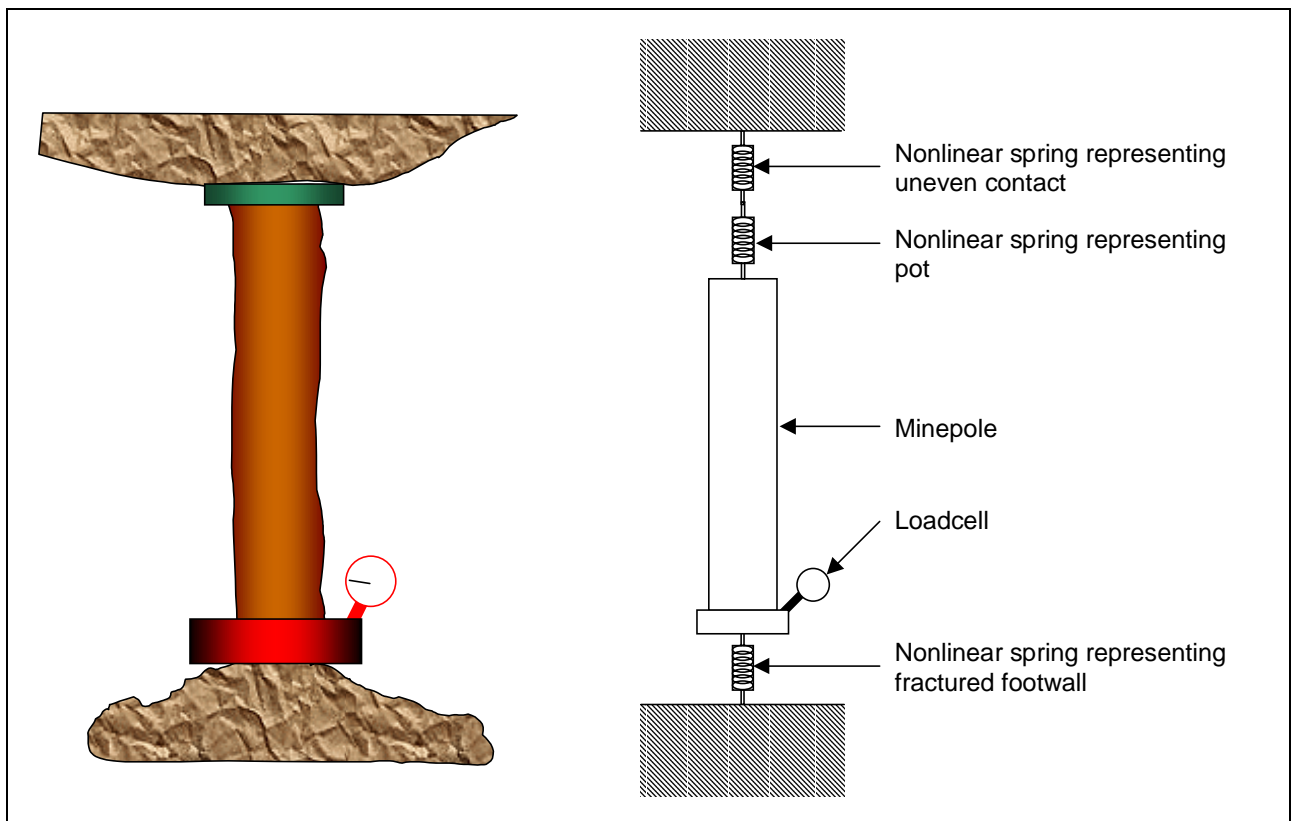
Figure 4.5.25 Conceptual illustration of the components of the support unit response.

The contribution of each component is very difficult to quantify from the test data. While the individual contribution of the pre-stressing unit may be evaluated through laboratory tests, the unevenness of the hangingwall is difficult to simulate, and the compression of the fractured footwall varies from site to site.

The overall contribution of these factors may be expressed in terms of an equivalent stiffness. The three springs illustrated in Figure 4.5.25 may each be described by a non-linear relationship between load and displacement. The contribution of each component may be expressed (in the linear portion of the response) as:

154

$$K_{su} = \frac{K_m + K_p + K_c + K_f}{K_m K_p K_c K_f} \qquad (4.5.1)$$

Where K_{su} is the overall stiffness of the support unit

K_m is the stiffness of the mine pole

K_p is the stiffness of the pre-stressing unit

K_c is the equivalent stiffness of the uneven hangingwall contact

K_f is the stiffness of the footwall

The contribution of the pot, uneven hangingwall, and uneven and crushed footwall may also be expressed as a single spring in series with the mine pole. In an attempt to quantify the initial stiffness of the specimens, which indicate a "soft" response, it becomes evident that the initial (pre-peak) stiffness of the mine pole is non-linear. This implies that the contributions of the above-mentioned factors are realised at different displacements and that the analysis is therefore too complicated to undertake with the limited information available.

To fully describe the response of a mine pole, it is necessary to quantify the load-deformation characteristics of all of these components individually. The response of pre-stressing units *in situ* has not been rigorously quantified, though it is known that many pots fail on installation. Further tests need to be conducted in order to quantify this component.

The response of the crushed footwall may be obtained by repeating the underground experiment with a steel tube in place of the mine pole. The linear response of the steel can easily be subtracted from the overall response. As stated above, the response may vary considerably in different locations, therefore it might be necessary to apply a statistical method.

Note that the "uneven-hangingwall" component of the response may also refer to a mine pole, which is installed in blocky ground. The end-profile of the prop may be smooth, however, the profile of the hangingwall plays an equally important role in determining the response. In the case of a blocky hangingwall, the hangingwall itself becomes a non-linear spring.

Where such conditions are observed (i.e. where additional components affect the response of the unit under investigation), it may be said that the unit is subjected to "soft" loading conditions.

5 Assessment of the suitability of elongate support systems for use in Bushveld mines

5.1 Introduction

The primary outputs of this project are (i) a confirmation as to whether or not it is kinematically possible for jointed blocks to rotate or move obliquely downwards, and (ii) an assessment of the capabilities to support such unstable blocks and the suitability of elongate support for use in most shallow gold and Bushveld mines. This chapter interprets the main findings of the previous chapters and summarises the effectiveness of elongates in supporting a jointed hangingwall. In essence, this chapter correlates the findings of Chapters 2, 3 and 4, and makes appropriate recommendations regarding the suitability of elongate support systems for use in the Bushveld mines.

5.2 Block kinematics in Bushveld mines (main findings of Chapter 2)

It is kinematically possible for jointed blocks to rotate and/or move obliquely downwards (see Figure 2.2.1, Section 2.2.1). However, block rotation is only possible if the block is delineated by comparatively shallow dipping discontinuities. Figure 5.2.1 gives the maximum non-rotating span as a function of discontinuity angle (relative to the horizontal) and bedding thickness (height of instability). For example, consider a hangingwall discretised by joints dipping at 70 degrees with a prominent parting 1 m from the hangingwall skin. Using Figure 5.2.1 it is evident that as long as the unsupported span is less than 3 m, keyblock rotation is kinematically impossible.

Note that, when investigating the possibility of block rotation, all sides and associated discontinuity angles delineating the potentially unstable block should be checked for possible rotation (making use of Figure 5.2.1 for each side).
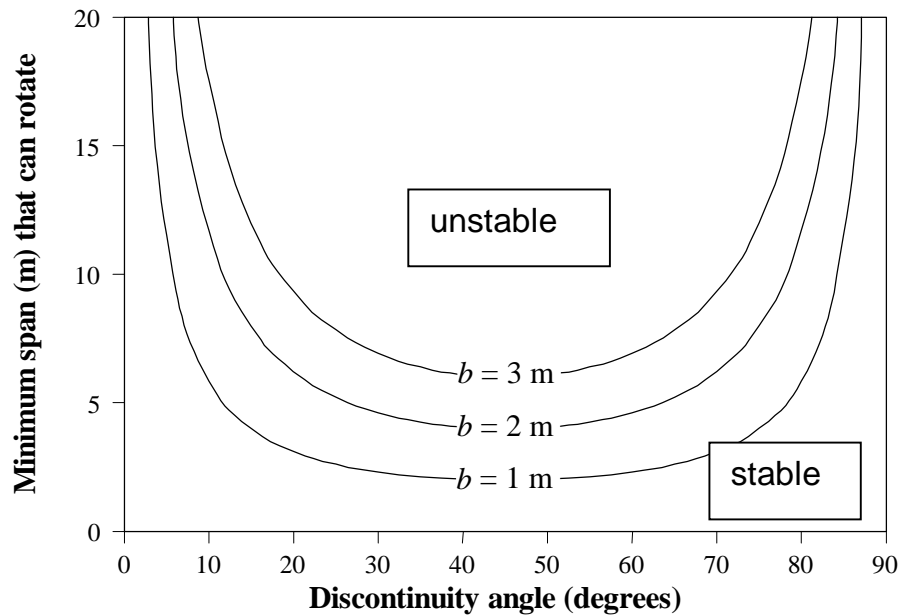
Figure 5.2.1   ***Minimum span that can rotate as a function of discontinuity angle and bedding thickness.***

It is recommended that the rock engineer conduct an in-depth geotechnical area specific investigation to determine if block rotation is a hazard and compromises the hangingwall stability. In the worst case, ubiquitous shallow dipping joints (i.e. dipping at 30° to 60°) will compromise the complete hangingwall stability. However, typical joint distributions in the Bushveld Igneous Complex tend to be oriented near vertical (> 80 degrees) and in most cases block rotation will occur locally (e.g. domes). Joints become flatter, however, when the stope face is mining towards a pothole. It is well known that bad ground conditions occur when this is the case. This study has also shown that shallow dipping extension fractures at the stope face (propagated by high horizontal stresses; see Section 1.3.2) can result in hangingwall slab rotation.

If it has been established that there is no possibility of block rotation, the tributary area method of support system design can be applied, i.e.

$$F = W_{T.A.} = \rho \, g \, b \, A \, , \tag{5.2.1}$$

where: F =   load carried by a single support unit (N),

             $W_{T.A.}$ =   weight of hangingwall associated with the tributary area supported by a single support unit (N),

             ρ =   rock density (kg/m^3),

             g =   acceleration due to gravity (≈ 10 m/s^2),

             b =   height of instability (m), and

             A =   tributary area (m^2),

If, however, it has been established that block rotation is possible, the support criteria need to be modified to account for the increased support loading induced by block rotation. A relationship describing the increased support loading is derived in Section 2.2.12.

In Chapter 2, the emphasis was placed on determining the required resultant support force to maintain the stability of a keyblock for a given support spacing, in areas where keyblock rotation is possible. In the design of support systems, however, the rock engineer will know what kind of support units are going to be installed, and what force those units are capable of generating. It is thus necessary to determine the spacing of the support units.

The formulas derived in Section 2.1.12.2 are the most general and should be used to determine the spacing, as it caters for both rectangular and square blocks, with rectangular and square support spacing patterns. **Note that these equations are only valid if** S **0,5L** (where S is the support spacing and L is the length of the keyblock). (Refer to Section 2.1.12.2. for a more detailed explanation.)

The relationships quantifying the support requirements for rotating keyblocks are based on rectangular keyblocks supported by props spaced in a rectangular pattern, where the axes of the keyblock and spacing pattern are aligned (see Figure 5.2.2). In practice, however, the keyblock is not necessarily aligned with the support spacing pattern (see Figure 5.2.3). The work conducted here has shown that keyblocks aligned with the support pattern (i.e. Figure 5.2.2) are always more likely to rotate and impose increased load on the support elements, than unaligned keyblocks (i.e. Figure 5.2.3). Thus, by designing support systems based on keyblocks aligned with the support system, the worst-case situation is analysed, i.e. a conservative approach to support design is followed.

It is hence recommended that the relationships quantifying the support requirements for rotating keyblocks be applied to all keyblock shapes and orientations (with respect to the support layout).
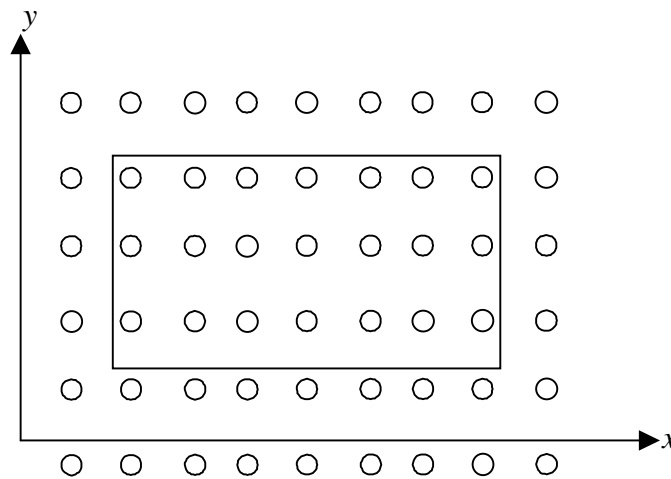
Figure 5.2.2   The axes of the support spacing pattern aligned with Keyblock.

164
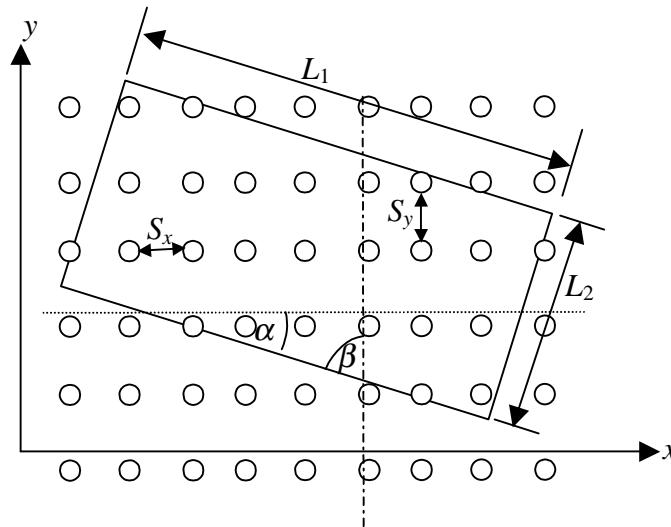
Figure 5.2.3   Keyblock oriented at an angle to the support layout.

For keyblocks which are not aligned with the support system, it is recommended that, when calculating S_x and S_y:

If $\alpha > \beta$, $L_x = L_2$ and $L_y = L_1$.

If $\alpha \leq \beta$, $L_x = L_1$ and $L_y = L_2$.

A brief review of the relationships quantifying support requirements for rotating keyblocks follows:

The number of support units per block, M, is calculated as

$$M = N_x N_y,$$ (5.2.2)

where the number of support units per length of block in the x-direction is given by

$$N_x = \left\lfloor \frac{L_x}{S_x} \right\rfloor,$$ (5.2.3)

and the number of supports per length of block in the y-direction is given by

$$N_y = \left\lfloor \frac{L_y}{S_y} \right\rfloor.$$ (5.2.4)

164

Thus, the required resultant support force to prevent rotation about the x- and y-axes, F_R, is given by:

$$F_R = kW ,$$ (5.2.5)

where,

$$k = \max \begin{cases} k_x \\ k_y \end{cases} .$$ (5.2.6)

The support force required per support unit (F) is given by:

$$F = \frac{F_R}{M} = \frac{kW}{M} .$$ (5.2.7)

Note that, when meeting the tributary area criterion (i.e. no block rotation is possible), $k = 1$. The function k is graphically illustrated in Figure 5.2.4. It is evident that the value of k depends on the keyblock size and the number of support units directly in contact with the keyblock. As the ratio of block size to support spacing increases, the value of k tends to unity.

As an example, consider a stope with 7 m x 7 m keyblocks prone to rotational movement. The support spacing is 2 m x 2 m. From Figure 5.2.4 it is apparent that, as $\frac{L}{S} = 3.5$, k = 1,75. Thus, to prevent any rotational movement, the load capacity of a single support unit should exceed 1,75 times the weight of the hangingwall associated with the tributary area supported by a single support unit.
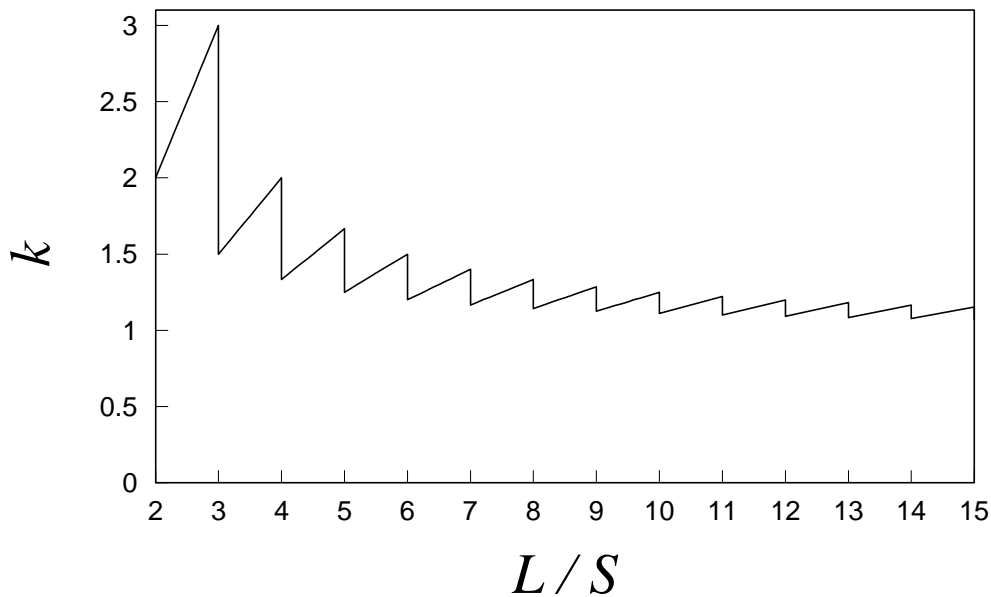
Figure 5.2.4   **The value of k as a function of L / S.**

164

Equation (5.2.7) cannot be re-written to give an explicit expression for S. An iterative process is thus required. This is done by assuming a value for S_y and calculating S_x based on this value, such that F_{Ry} F (where F is the force that can be generated by a support unit). This value of S_x is then used to recalculate S_y, so that F_{Rx} F. The new value of S_y is now used to recalculate S_x. This process is repeated until convergence.

To facilitate the rapid and convenient evaluation of support system requirements for rotating keyblocks, software has been developed to calculate the support spacing, using the above methods. Example applications of the software are given below.

**Figure 5.2.5   Support design example based on 150 kN props and a
10 m x 7 m x 1 m keyblock.**

Based on the keyblock dimensions given in Figure 5.2.5, the recommended support spacing is 2 m and 1,7 m in the x- and y-direction, respectively. Note that if the keyblock cannot rotate, the maximum tributary area per support unit is 5,1 m^2. This exceeds the maximum tributary area for a rotating keyblock, i.e. 2 m x 1,7 m = 3,4 m^2 < 5,1 m^2.
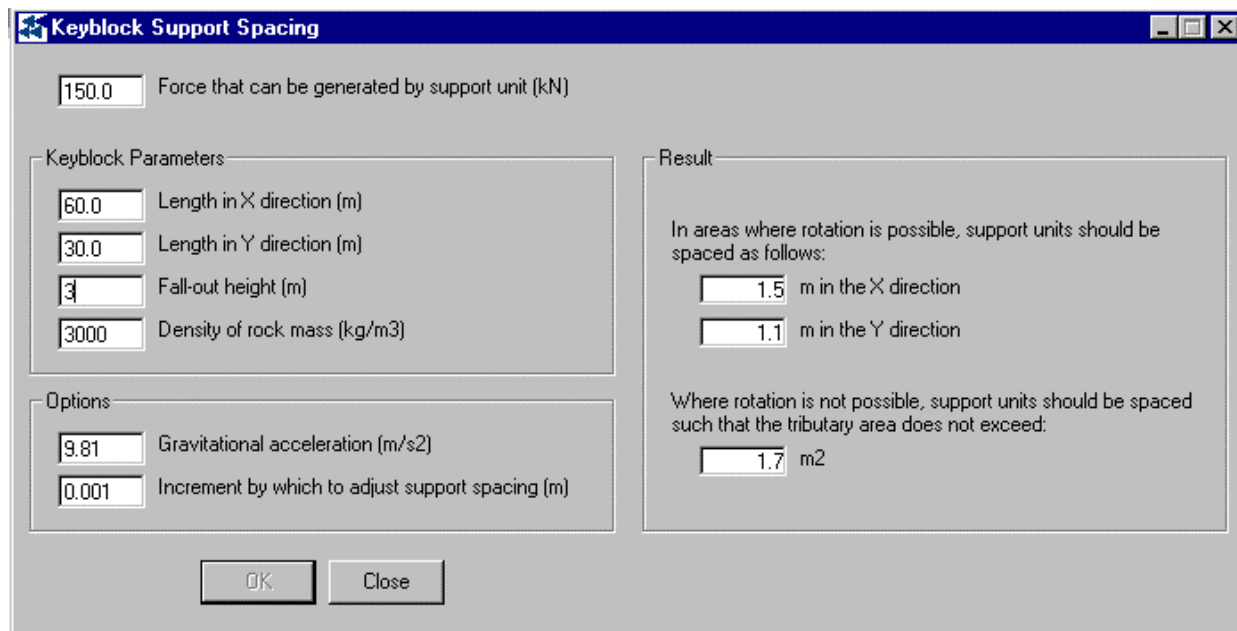
Figure 5.2.6   Support design example based on 150 kN props and a 60 m x 30 m x 3 m keyblock.

Figure 5.2.6 shows a second example based on a large unstable block. Note that in this case the support spacing for a rotating block (i.e. 1,5 m x 1,1 m in the x- and y-directions, respectively) implies a tributary area of 1,65 m^2, which approaches the tributary area for a non-rotating block (1,7 m^2). This assumes that no local closure occurs that exceeds the closure required to compress support units beyond their designed force/compression limit.

It is recommended that the Keyblock Support Spacing computer program be used to design appropriate support systems and spacing thereof in shallow / intermediate depth mines. The user is required to enter the support force and keyblock parameters. The spacing results are given for:

(i)   the case where block rotation is not likely (i.e. the maximum tributary area criterion is valid), and

(ii)   the case where block rotation is possible (i.e. reduced support spacing is required to account for the increased loading induced by block rotation).

The propensity for block rotation is determined from underground observations, previous rockfall back-analyses, and by making use of Figure 5.2.1.

5.3 Elongate performance under rotational and oblique loading conditions (main findings of Chapters 3 and 4)

Extensive laboratory and underground elongate compression tests led to an improved understanding of elongate performance under rotational and oblique loading conditions. The main findings are summarised below:

- It is preferable for elongates to be installed perpendicular to the dip of the strata. However, installation angles varying up to 25° do not significantly compromise the load-bearing capacity of the support unit. At angles exceeding 30° slip occurs between the timber and rock interface and the load-bearing capacity of the support unit is significantly reduced.

- The ends of timber elongates should be cut parallel to the loading surface, or suitably wedged to maximise the timber contact area with the foot- and hangingwall.

- Elongates subjected to simultaneous rotational and axial loading have reduced load carrying capacity. The reduction in capacity is relatively minor at angles of up to 5°. At rotation angles approaching 10° the load-bearing capacity is significantly compromised.

  It is thus important to design active support systems providing sufficient initial pre-stress such that any block rotation is prevented. Once block rotation commences the load capacity of support units is reduced, and the likelihood of structural failure of the support system is increased. The value of pre-stressing (preferably to 200 kN) and providing immediate active support is thus emphasised.

- Mine poles failing in the brushing mode offer improved yieldability compared to mine poles failing due to splitting or buckling. Brushing failure is thus the preferred failure mode. In mines where increased yieldability is required, it is preferable to use poles with an engineered brushing mechanism (e.g. profile props).

- The extensive laboratory and underground testing has led to an improved correlation between laboratory and underground compression test results. Laboratory test results can hence be used with confidence to estimate the actual underground performance of timber poles. Consequently an improved empirically based equation is proposed to relate laboratory test results (tested at comparatively fast compression rates) to the underground performance of timber elongates. A further empirical equation is proposed to adjust the stiffness of elongates tested in the laboratory to the expected stiffness of elongates underground. It is recommended that the improved correlation of laboratory to underground elongate performance be incorporated into the SDA II software.

- Creep tests were conducted to determine the load loss of pre-stressed mine poles. It was found that approximately 9 % of the pre-stressing load is 'lost' as a result of creep in the pre-stressing device only, and a further 6 % due to timber creep. The total creep results in a 15 % drop in the load over a period of six days.

A 15 % drop in load over a period of 6 days due to creep (i.e. no stope closure) is considered acceptable. Even small amounts of stope closure will rapidly re-generate the load loss and hence rock mass stability is maintained.

- Continuous underground closure and elongate load measurements indicate the sensitivity of mine pole performance to varying loading rate. This is unique underground data, which had not been measured before. The tests results show that immediately after the blast, the load transmitted by the mine pole increases commensurate with the increase in closure rate. Approximately 40 minutes after the blast the closure rate decreases and the mine pole load decreases correspondingly (in the tests conducted here the load increase is approximately 10 %).

- Underground factors, such as blast and scraper rope damage, can significantly compromise elongate performance and initiate premature failure. It is recommended that, during training programmes, emphasis be given to the importance of protecting the support units from blast damage (e.g. use of blast barricades) and the scraper (correct and accurate positioning of support units; correct scraper size; correct positioning of scraper rope snatch block).

- An important insight gained during this work is that the underground performance (i.e. peak load, extent of compression when the peak load is attained, yieldability) of mine poles varies significantly. Thus, when considering the mean load-bearing capacity of a number of mine poles installed in a stope, the average capacity is reduced compared to the peak load attained by individual support units. Note that this result should not be confused with the statistical analyses conducted to quantify the variability of support units. (see Section 4.2.2)

Figure 4.5.19 (reproduced here as Figure 5.3.1) and Figure 4.5.23 (reproduced here as Figure 5.3.2) show the mean underground performance of 140 mm and 170 mm diameter mine poles, respectively. Also shown are 90 % confidence curves for an average number (n) of support units, where $n = 1$, 3, 10 and 30. In a highly jointed, blocky environment the localised rock mass stability is dependent on only a few support units, i.e. $n = 1$ or 3. Hence the appropriate performance curves with $n = 1$ or 3 should be used. As is apparent from Figure 5.3.1, in these conditions, the use of a 140 mm diameter mine pole is not feasible, and 170 mm diameter mine poles should be used. In conditions with a comparatively continuous hangingwall, the rock mass stability is dependent on the average load-bearing capacity of a large number of support units (i.e. $n = 10$ to 30). The mine pole performance curves, which should be used in these conditions, are closer to the mean performance (see Figure 5.3.2). In these conditions, the use of both 140 mm and 170 mm mine poles is feasible. Choice of the mine pole type and spacing thereof depends, to a large extent, on the height of instability and possibility of block rotation (see Section 5.2).
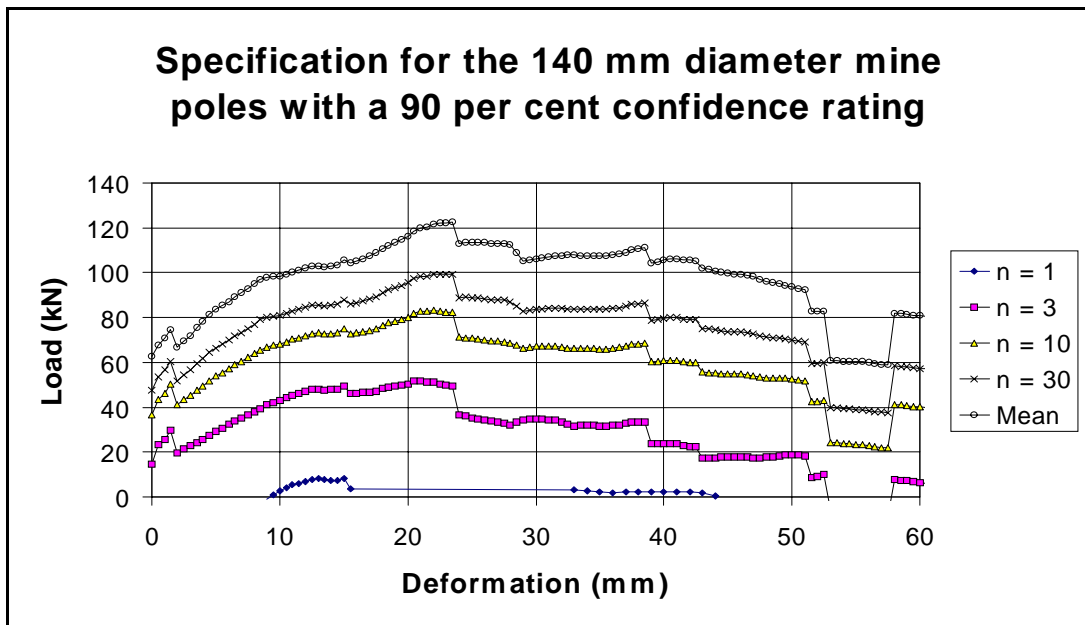
Figure 5.3.1 *Statistical results of the underground tests performed on 140 mm diameter mine poles.*
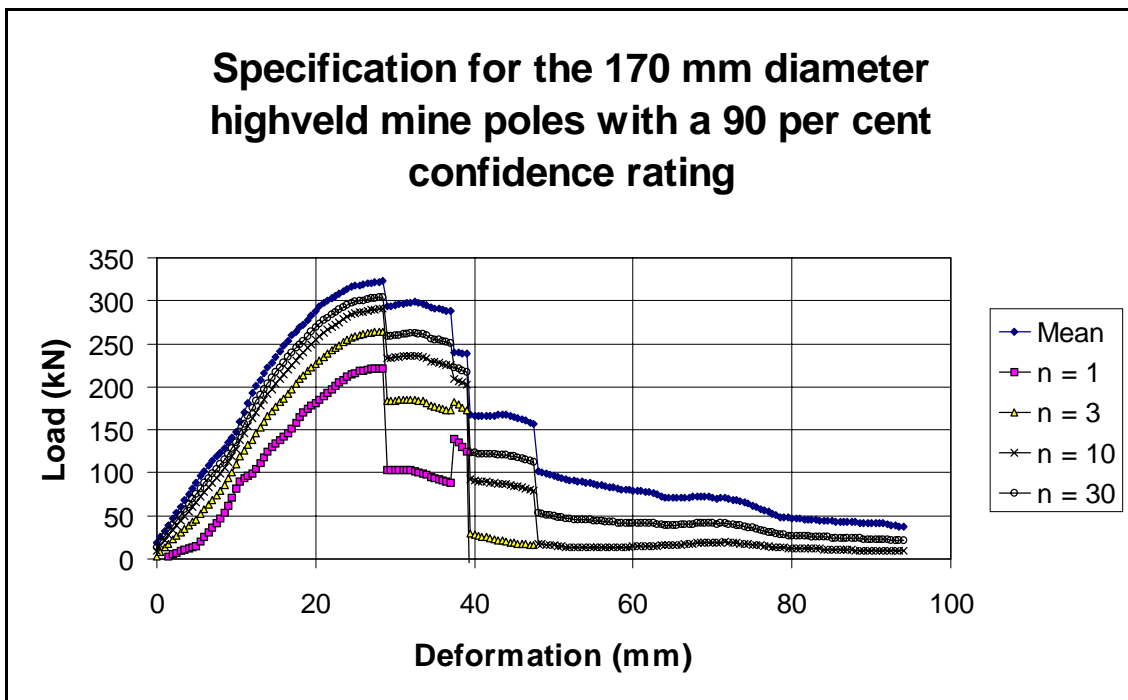
Figure 5.3.2 Statistical results of the underground tests performed on 170 mm diameter mine poles.

5.4 Conclusions

To summarise, in general elongate support is considered suitable for use in Bushveld mines. To ensure rock mass stability, however, the following factors need to be considered when designing support systems:

1. The rock engineer needs to determine if block rotation is likely (guidelines for determining if block rotation is possible are given in the report).

2. If block rotation is likely, the tributary area design methodology needs to be modified and the software developed as part of this project should be used to optimise support spacing. If block rotation is kinematically impossible, the standard tributary area method for support design is appropriate.

3. If block rotation is likely, the elongates should always be pre-stressed (preferably to 200 kN).

4. If the hangingwall is intensely jointed (i.e. between one and three support units per block) the appropriate performance curves need to be used (i.e. 90 % confidence curves and $n = 1$ or 3). In this case 140 mm diameter mine poles are not suitable, and larger diameter poles are required.

5. The stability of a comparatively continuous hangingwall can be maintained by designing support systems using the 90 % confidence elongate performance curves and $n = 10$ to 30 (depending on the number of support units, n, supporting each block). In this case 140 mm or 170 mm mine poles are suitable.

6 Video representation of elongate support interacting with rotating and obliquely moving blocks

6.1 Introduction

A video was produced, giving details of the salient findings of the project. It is recommended to distribute the video to the relevant rock mechanics practitioners on the platinum and shallow gold mines to increase the awareness of the hazard and special support requirements associated with hangingwall keyblocks with a propensity for rotation and oblique movement.

6.2 Description of video

An introduction to the video is footage of elongate support installation practices underground. This is followed by a brief overview of the description of conditions under which blocks can rotate and move obliquely. A description of the special test rig manufactured for this work to simulate oblique and rotational loading is given.

The effect of oblique loading, which occurs as a result of improper installation at an unfavourable angle, or due to unpredictable movement of the rock mass, is shown in the video on tests performed on mine poles and Profile Props.

In all, seven tests are presented in the video. These relate to oblique loading plate tests, rotating loading plate tests, loading of elongates installed obliquely and vertical loading of elongates. The load build-up and the response of the elongates to these loads are included in the representation. Also highlighted are the modes of failure normally associated with the above-mentioned types of loading conditions.

7 Review of principal findings and recommendations for further work

The present support design methodology commonly applied in South African platinum mines is based upon the tributary area concept. This simple concept takes care of the equilibrium requirements in a rudimentary sense, but it does not adequately address the fact that the rock being supported is likely to be discontinuous. Clearly, in these circumstances, the distribution of the support elements may be of paramount importance.

In a discontinuous, jointed rock mass, loose blocks can, under certain conditions, rotate and move obliquely, thereby subjecting elongate support elements to different loading conditions than those experienced under conventional axial loading. Since many panels of Bushveld and shallow gold mines are supported by elongates only, it is vital to understand and quantify the elongate interaction with rotating and obliquely moving blocks of rock. An assessment is required to determine if elongates are suitable and the optimum support type to stabilise such unstable blocks.

The aim of SIMRAC project GAP 613 is to evaluate the performance of elongate support units commonly used in platinum mines under various loading conditions. Five enabling outputs were defined to reach this objective:

EO1 Determine under which conditions it is kinematically possible for jointed blocks to rotate and move obliquely downwards.

EO2 Utilise CSIR loading presses to simulate loading conditions, which result from block rotation and oblique block movement.

EO3 Test and evaluate various elongates with off-centre loading to simulate block-rotation and oblique block movement.

EO4 Evaluate the suitability of elongate support systems for use in Bushveld mines.

EO5 Communicate test results and rotational/oblique movement of blocky rock masses by means of a video.

The five enabling outputs, as well as their associated principal findings, conclusions and recommendations for further work, are reviewed in Sections 7.1 to 7.5.

7.1 Analysis of keyblock kinematics

7.1.1 Summary

The objective of enabling output 1 is the quantification of the movement and degrees of freedom of jointed hangingwall blocks and how this influences the stability of standard and pre-stressed units. This is accomplished by conducting JBlock and analytical analyses and carrying out underground investigations to assess the potential for keyblocks to rotate.

The effects of block shape, support spacing and hangingwall jointing were investigated. Various failure modes of the support, including failure by rotation, fallout between support units and failure due to block weight, are considered. The probability of failure in all of these modes and for various safety factors is presented.

7.1.2 Principal findings and conclusions

Expected types of loading are identified through a keyblock analysis. The probabilities of block rotation for various block shapes, and for various support spacings are quantified using the JBlock program. This analysis demonstrates the conditions under which rotational movement of hangingwall blocks is possible, and outlines the implications of this type of movement in terms of support loading. In areas where rotational failure of keyblocks is possible, the resultant support force required to stabilise a keyblock is increased by a factor, k, with respect to the force required based purely on tributary area requirements.

It was found that the most significant factor contributing to failure of support units by rotation of keyblocks is the support spacing. The reason for this is that the centroid of the potentially rotating block and the resultant reaction force from the support units are brought closer together by increasing the support density. Increasing the support capacity may reduce the probability of failure slightly, but obviously has no effect on the relative positions of the keyblock centroid and the reaction force.

The probability of blocks failing by rotating out of the hangingwall of a stope depends on the shape of the block. Blocks with shallow dipping sides rotate more readily than blocks with steeply dipping sides.

A statistical analysis of keyblock rotation potential was conducted for typical Bushveld hangingwall jointing. For typical joint distributions in the Bushveld Complex, the near vertical joints do not represent a hazard in terms of block rotation. It is only when "dome" joints exist that rotation becomes possible. Analyses of keyblocks representing typical block size and shape distributions in Bushveld mines, which included dome joints, indicated that less than three per cent of the blocks that failed did so by the rotational mode.

The axial capacity of elongates will be reduced by the presence of bending moments. These bending moments can be caused by ride or off-centre loading of elongates.

Underground observations and instrumentation resulted in an improved understanding of block rotation mechanisms and the implications for support criteria.

Support elements should be installed as close to the face as possible, to provide for the unexpected development of horizontal extension fracturing in the hangingwall. Furthermore, the support system needs to be strong enough to cater for a cantilever that could develop between the face and the first line of support. Oblique loading of mine poles appears to occur during a FOG or where there are shallow dipping discontinuities within the hangingwall.

Closure rates could be used to warn of impending FOGs in susceptible areas, if panels are properly instrumented.

The importance of maintaining key-blocks in position is emphasised. Shallow dipping discontinuities and extension fractures in the immediate hangingwall significantly increase the risk of FOGs by forming plates (beams) bounded by these features (the existence of these planes are seldom known). Conditions leading to the formation of extension fracturing have been explored using ELFEN. The model predicted that multiple tension fractures could develop in the hangingwall if the panel mined into a zone of material with a higher modulus.

One of the main outcomes of this project is a proposed design tool to assist rock engineers on Bushveld and shallow gold mines in improving support design. Emphasis is placed on the estimation of optimised support spacing. The method for calculating support spacing is an extension of the tributary area concept. The design methodology has been coded as a computer program, and can easily be used by rock mechanics practitioners to optimise support spacing in geotechnical areas where keyblock rotation is likely.

7.1.3 Recommendations for further work

The presence of "dome joints" was included in the analysis, but it was determined that the statistical distribution and the analytical representation of these joints were not necessarily accurate. In light of this, it is recommended that a better understanding of the statistical distribution of dome joints be obtained, so that their hazard in terms of stability may be better evaluated. In addition, modification of the JBlock software is required to accurately represent the geometry of the dome joints, as this appears to be the major cause of actual rotational loading of supports in the Bushveld.

The flattening of joints as the stope face approaches potholes is important and requires further work to quantify the distribution and frequency of these features.

An important consideration in the quantification of "rotation" is the relative components of rotational and translational movement imposed on the support units. This may be expressed in terms of the length of the lever-arm (i.e. the distance between the support unit and the pivot point). The occurrence of lever-arm lengths should be statistically evaluated to ascertain the actual rotation of keyblocks.

It is recommended that the computer program, to estimate support spacing in geotechnical areas where keyblock rotation is likely, is distributed to the relevant rock mechanics practitioners on shallow gold and platinum mines.

7.2 Simulation of loading conditions resulting from block rotation and oblique block movement

1.1.1 Summary

The purpose of this enabling output is to simulate loading conditions that result from block rotation and oblique block movement. This is brought about by designing and manufacturing a loading device to simulate off-centre loading and bending moments induced by rotating and obliquely moving blocks. This device and CSIR loading presses were utilised to simulate the desired loading conditions during laboratory testing.

1.1.2 Principal findings and conclusions

It was found that the modified loading press met the requirements to simulate rotational and oblique loading of elongates. The press is equipped with measuring devices to record the load versus deformation behaviour of prop-type support units, and is a valuable research tool for future SIMRAC work to investigate and quantify prop failure mechanisms under non-axial loading conditions.

1.1.3 Recommendations for further work

It is recommended to maintain the press and continue the use thereof for the performance evaluation of elongates loaded under non-axial conditions.

7.3 Evaluation of timber elongate performance under oblique loading conditions

7.3.1 Summary

The objective of this enabling output is to evaluate the performance of timber elongates subjected to oblique loading conditions. This is achieved by conducting laboratory and underground tests, and reviewing relevant literature.

A literature review, covering failure modes and parameters that have a significant effect on timber elongates, and results processing and interpretation, was carried out.

Slow and rapid loading rate tests were performed on vertical and inclined elongates in the laboratory. Rotating plate tests and creep tests were also carried out. Underground testing was conducted to determine the effects of initial elongate shape, different hanging- and footwall conditions, pre-stressing and blast damage.

7.3.2 Principal findings and conclusions

Installing sticks at an oblique angle to the loading surface has little effect on the performance of the mine poles. Inclining the mine pole leads to more brushing/folding/yielding type failures, while inclining the one loading surface increases the incidence of buckling failures. Slipping off the loading surface occurs when the surface is inclined by more than 23^0.

A strategy was adopted by which one half of a stick was tested vertically, and the other at an angle. There is, however, no correlation between the performance of "twin" sticks.

The brushing and buckling failure mechanisms were identified and described in terms of load-displacement characteristics.

A number of laboratory tests were performed at loading rates similar to those encountered underground. These tests were conducted on mine poles with pre-stressing units attached. The mean load-displacement curves show an initial drop-off in load, associated with the behaviour of the pre-stressing pots.

Direct comparison of underground and laboratory test results indicate that the relationship proposed by Roberts *et al.* (1987) over-estimates the strength of mine poles installed *in situ*. An improved relationship, which better fits experimental data, is presented. Possible reasons for this discrepancy are inferred from one of the tests. It is noted that the frequency of measurement may have led to lower loads being recorded than actual. Uneven contact with the loading plate was also evident in the test.

A further attempt is made to correlate underground data and laboratory test results. The initial stiffnesses of the underground test specimens are lower than those of the laboratory test specimens, due to the soft loading conditions mentioned above. The equation relating loading rates is further modified to account for the discrepancy in initial stiffness.

Rotating plate tests are performed, showing a decrease in strength above rotation angles of 3°. The peak load is also realised at a higher displacement for the rotation tests, even in sticks, which fail ultimately by buckling.

Creep tests performed on mine poles with pre-stressing pots reveal a six per cent drop in capacity within the first five minutes after installation, and a 15 per cent drop in load, stabilising after six days.

A number of instrumented mine poles were installed at various angles at two locations underground. The installation angle has little effect on peak load, except where the units slip, i.e. where the angle is between 20^0 and 30^0. The observed failure mode of the mine pole is a more significant factor in determining the peak load. Brushing, buckling and slip are identified as the most common failure mechanisms. Brushing is the preferred failure mechanism as the displacements at failure and peak loads are higher than for buckling and slip.

The initial shape and condition of the timber, the profile of the loading surface and the presence of blast or scraper-rope damage are identified as important factors in determining the mode of

failure. The use of pre-stressing units has little effect on the performance characteristics of mine poles.

The effect of the blast on mine pole response is investigated. The time-dependent behaviour of the timber is demonstrated through time histories recorded during the blast.

The mean performance curves reflect a variation in the initial stiffness and the displacement at ultimate load. This results in a flat mean curve with a much lower ultimate strength than any individual unit. It is demonstrated statistically that the support density is once again crucial to the reliability of the support units.

7.3.3 Recommendations for further work

The aim of further laboratory investigations in this area should be to fully quantify and eliminate the discrepancies between underground measurements and downgraded laboratory results. As stated in Section 1.1.3, the factors resulting in "soft" loading of the elongates have been identified and may hence be quantified by performing the tests suggested.

While the current research has identified these components, and various correction factors have been suggested for the overall response, the quantification of these components should be undertaken to further enhance understanding of mine pole behaviour.

In addition, the effects of rotation at various lever-arm lengths should be ascertained, using the statistical distribution mentioned in section 7.1.3 to produce a test schedule. The effect of pure rotation without the influence of a translational component may also be determined by modifying the control programme for the press.

More underground instrumented tests are required to isolate the causes of the variability in response observed. The potential causes of variable mine pole performance are the performance of the pre-stressing unit, crushing of the footwall and uneven hangingwall contact. The following are proposed to quantify these contributions:

Performance of pre-stressing devices:

The performance of pre-stressing units may be checked in the laboratory. Pots should be installed on a rigid (steel) cylinder of the same diameter as a typical mine pole. The linear response of the steel should then be subtracted from the overall response. A number of tests should be performed to obtain a series of confidence curves for pot performance.

Footwall crushing:

The response of the footwall should be ascertained by underground experiments. The mine pole should once again be substituted by a steel cylinder. Other variables can be eliminated from the experiment by not using a pre-stressing unit, and by ensuring good contact with the hangingwall. The load-displacement characteristic of the footwall is obtained by removing the linear steel contribution from the overall response. Given the variability of the footwall condition,

a large number of tests should be performed and a statistical analysis executed to yield confidence curves.

Uneven hangingwall contact:

Uneven hangingwall contact, as stated above, can also be represented by a blocky hangingwall. The effect of uneven contact can hence be simulated in the laboratory by constructing artificial contact surfaces made up of blocks of a stiff material (steel). The size, evenness and profile of the surface should be varied to ascertain the bounds of this effect. A number of mine poles would have to be tested in order to eliminate the variability of the response of the timber units.

7.4 Evaluation of the suitability of elongate support systems for use in Bushveld mines

7.4.1 Summary

The purpose of this enabling output, is to evaluate the suitability of currently used elongate support systems for use in Bushveld mines, based on the outcomes of the tests and analyses conducted as part of this project.

7.4.2 Principal findings and conclusions

In general, elongate support is considered suitable for use in Bushveld mines. To ensure rock mass stability, however, the following factors need to be considered when designing support systems:

❖   The rock engineer needs to determine if block rotation is likely (guidelines for determining if block rotation is possible are given in the report).

❖   If block rotation is likely, the tributary area design methodology needs to be modified and the software developed as part of this project should be used to optimise support spacing. If block rotation is kinematically impossible, the standard tributary area method for support design is appropriate.

❖   If block rotation is likely, the elongates should always be pre-stressed (preferably to 200 kN).

❖   If the hangingwall is intensely jointed (i.e. between one and three support units per block) the appropriate performance curves need to be used (i.e. 90 % confidence curves and $n = 1$ or 3). In this case 170 mm (minimum) diameter mine poles are considered suitable.

- ❖ A comparatively continuous hangingwall can be supported by 90 % confidence performance curves and $n = 10$ to 30 (depending on the number of support units, n, supporting each block). In this case 140 mm or 170 mm mine poles are suitable.

7.4.3 Recommendations for further work

Further work is recommended to quantify the performance of timber, composite and cementitious packs as support in ground conditions where keyblock rotation and oblique movement thereof is likely. Currently little is known about the performance characteristics of non-axially loaded packs. It is anticipated that in these conditions packs are more prone to buckling-type failure. Hence the 2:1 height to width ratio rule of thumb typically applied by the industry might have to be modified, and a more conservative ratio of 1.5:1 to 1.8:1 might be necessary.

7.5 Communication of test results and rotational/oblique movement of blocky rockmasses by means of a video

7.5.1 Summary

The aim of this enabling output 5 is a means to visualise the interaction of elongate support with rotating and obliquely moving blocks. This is done by communicating test results and rotational/oblique block movement through a video.

7.5.2 Principal findings and conclusions

The video is found to be a suitable medium for distribution to the relevant rock mechanics practitioners on the platinum mines (and shallow gold mines) to increase the awareness of the hazard and support requirements associated with hangingwall keyblocks which are prone to rotation and oblique movement.

7.5.3 Recommendations for further work

It is recommended to widely distribute the video to platinum and shallow gold mines.

8   References

Bakker, D. 1993. Fall of ground accident statistics, Rock mechanics aspects of shallow to intermediate depth mines in the Bushveld Complex, SANGORM, Rustenburg.

Banks, C.H. 1976. The mechanical properties of South African timber, *South African Department of Forestry, Revised edition, Bulletin 48.*

Daehnke, A., Andersen, L.M., de Beer, D., Esterhuizen, G.S., Glisson, F.J., Grodner, M.W., Hagan, T.O., Jaku, E.P., Kuijpers, J.S., Kullmann, D.H., Peak, A.V., Piper, P.S., Quaye, G.B., Reddy, N., Roberts, M.K.C., Schweitzer, J.K., Stewart, R.D. & Wallmach, T. 1998. Stope face support systems, *SIMRAC GAP 330 final report.* CSIR. Division of Miningtek, Johannesburg. RSA.

Daehnke, A., Le Bron, K.B. & Van Zyl, M. 1999a. SIMRAC Final Project Report GAP 627. Preliminary investigation into the zone of support influence and stable span between support units, CSIR: Division of Mining Technology.

Daehnke, A., Salamon, M.D.G. & Roberts, M.K.C. 1999b. Investigating zones of support influence and quantifying stable hangingwall spans between support units. To be published in: *J. of South African Inst. of Mining and Metall.*

ELFEN 1999. Explicit formulation of finite/discrete element code. Rockfield, University of Swansea, Wales. UK.

Esterhuizen, G.S. 1996. JBlock user's manual and technical reference, Pretoria.

Esterhuizen, G.S. 1999. Analysis of keyblock rotation in Bushveld mines. Interim Report for SIMRAC Project GAP 613, The impact of soft loading conditions on the performance of elongate support elements, Colorado, USA, pp. 1 – 18.

Gere, J.M. & Timoschenko, S.P. 1994. Mechanics of Materials (Third SI Edition). London: Chapman & Hall.

Gerhards, C.C. 1982. Effect of moisture content and temperature on the mechanical properties of wood :an analysis of immediate effects, *Wood and Fibre Journal, January 1982, pp 5 – 26.*

Goodman, R.E. & Shi, G. 1985. Block theory and its application to rock engineering, Prentice Hall.

Lightfoot, N. 1997. *Support adjustment specification.* Internal report RE97. CSIR: Division of Mining Technology. Auckland Park, South Africa.

MINSIM-W 1997. Boundary element code for calculating elastic stress and displacements. CSIR: Division of Miningtek, Johannesburg: RSA.

Roark, R.J. & Young, W.C. (Fifth ed.) 1975. *Formulas for Stress and Strain.* Tokyo: Kosaido printing co.

Roberts, M.K.C., Jager, A.J. & Reimann, K. 1987. The performance characteristics of timber props. *Chamber of Mines Report no. 35/87.*

Roberts, M.K.C. 1995. Stope and gully support. *GAP032 SIMRAC Final Project Report*.

SABS 0163-1 1994. South African standard code of practice for the structural use of timber, Part 1: Limit-states design. Pretoria: SABS.

Turner, P. 1998. Personal communication. *CSIR Environmentek, P.O. Box 395 Pretoria, South Africa.*

Watson, B.P. 1999. Personal communication, CSIR: Division of Mining Technology.

Watson, B.P. & Acheampong, E. 1999. Influence of internal panel support systems on the stability of the panel hangingwall, *SIMRAC GAP 613 research report*. CSIR: Division of Miningtek, Johannesburg: RSA.

Watson, B.P. & Roberts, D. 1999. A new approach to designing safe panel spans on the Merensky Reef, *2nd Southern African Rock Engineering Symposium Proceeding.* : 324 - 330. Johannesburg: RSA.

York, G., Canbulat, I., Kabeya, K.K., Le Bron, K.B., Watson, B.P. & Williams, S.B. 1998. Develop guidelines for the design of pillar systems for shallow and intermediate depth, tabular, hard rock mines and provide a methodology for assessing hangingwall stability and support requirements for the panels between pillars, *SIMRAC GAP 334 final report.* CSIR. Division of Miningtek, Johannesburg. RSA.

Appendix

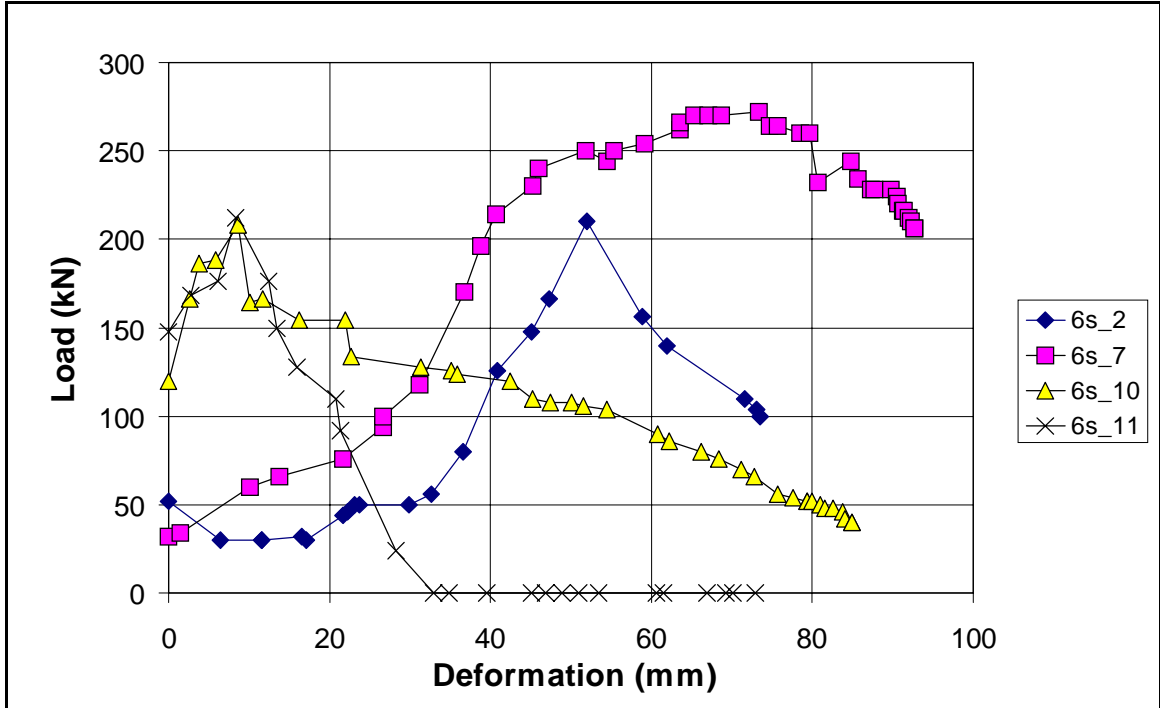Results of mine poles tested at various installation angles

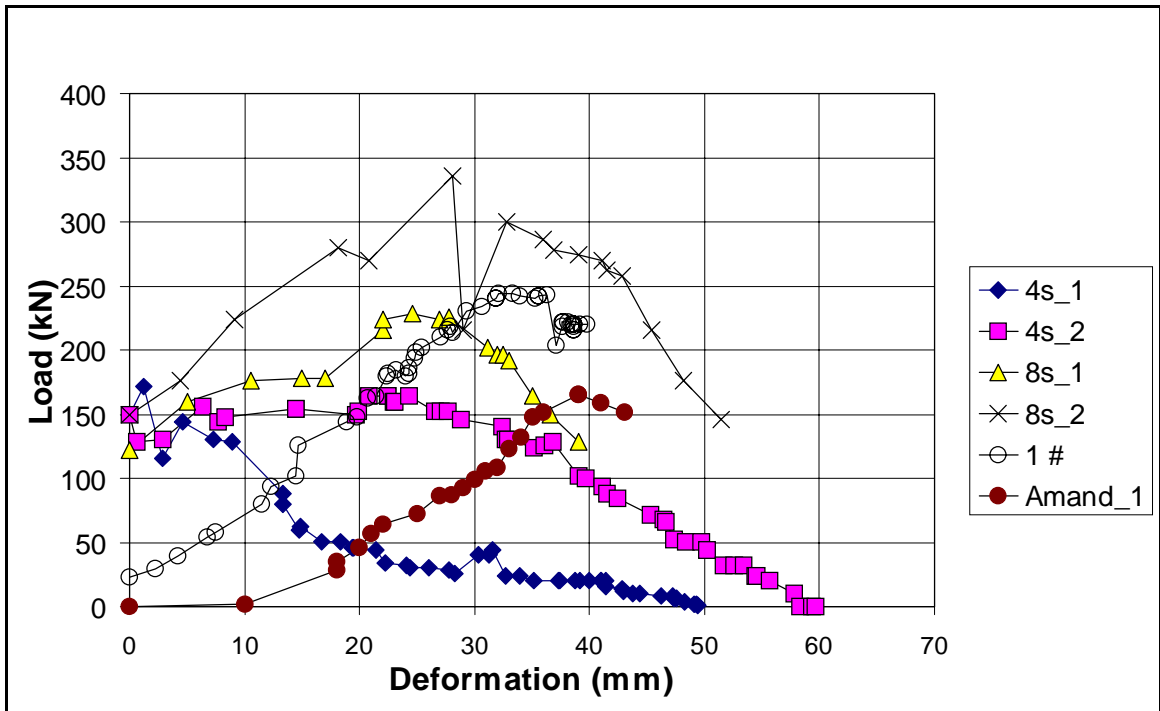***Figure A1.1   Results of mine poles installed vertically.***

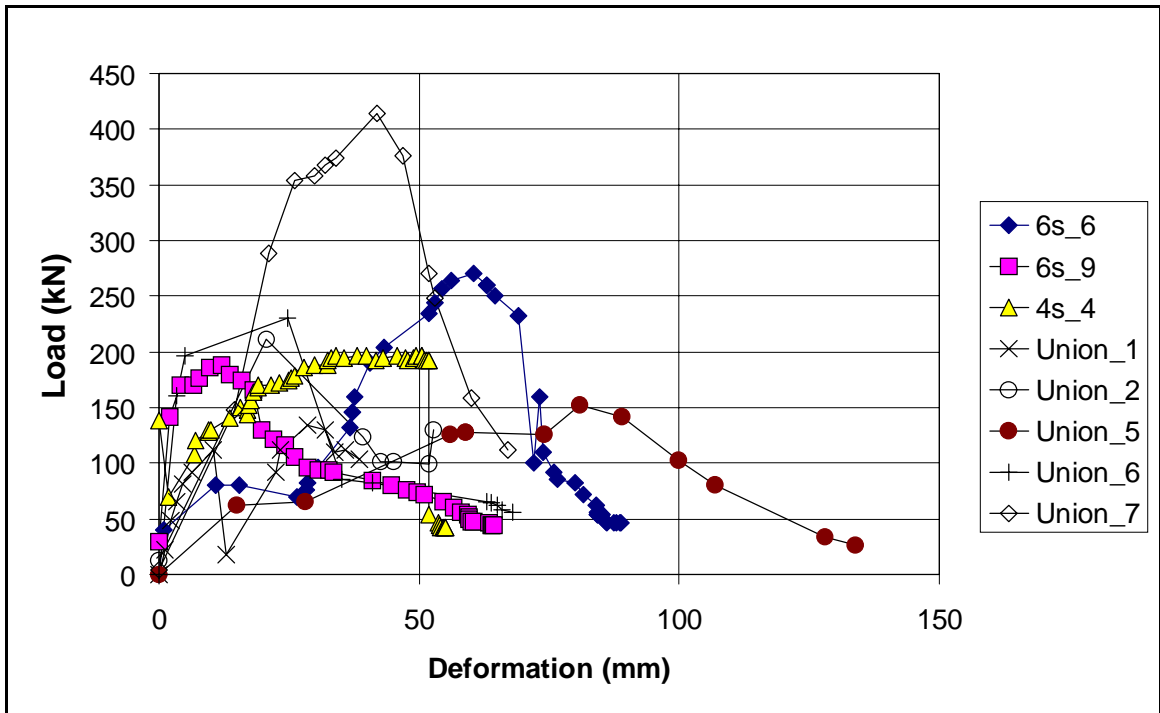***Figure A1.2   Results of mine poles installed at 10^0.***

Figure A1.3   *Results of mine poles installed at 20⁰.*
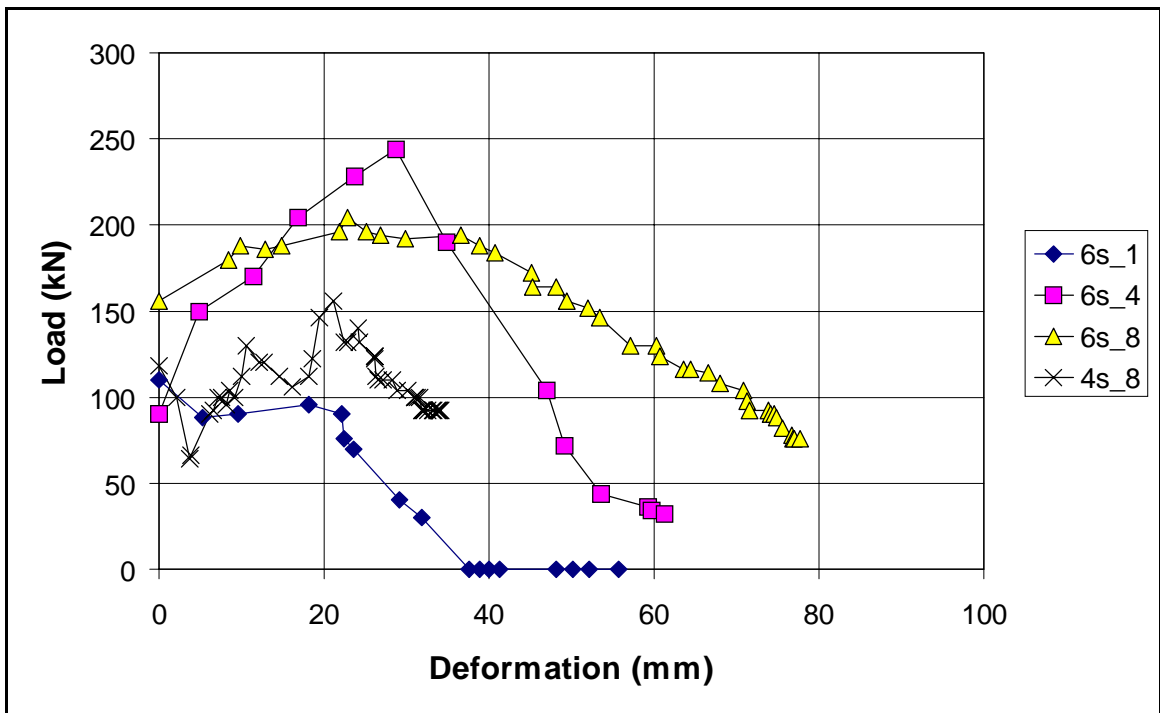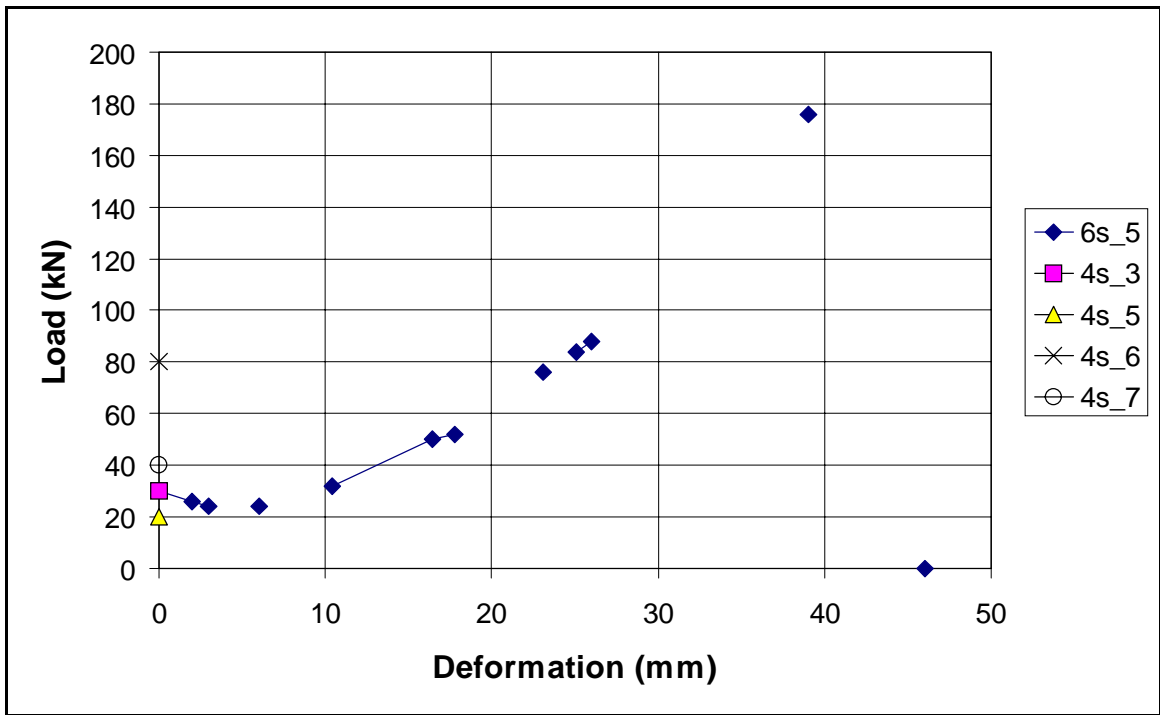

Figure A1.4   *Results of mine poles installed at 30⁰.*

Figure A1.5   Results of mine poles installed at 40⁰.